Energy-Efficient Distributed Multicast Beamforming Using Iterative Second-Order Cone Programming

Vom Fachbereich 18
Elektrotechnik und Informationstechnik
der Technischen Universität Darmstadt
zur Erlangung der Würde eines
Doktor-Ingenieurs (Dr.-Ing.)
genehmigte Dissertation

von
Dipl.-Ing. Nils Bornhorst
geboren am 8. Juli 1982 in Siegen, Deutschland.

Referent:	Prof. Dr.-Ing. Marius Pesavento
Korreferent:	Univ.-Prof. Dr.-Ing. Martin Haardt
Tag der Einreichung:	2. Oktober 2014
Tag der mündlichen Prüfung:	12. Dezember 2014

D 17
Darmstädter Dissertation
Darmstadt, 2015

To my father who passed away during my doctoral studies.

May he rest in peace.

Acknowledgments

First and foremost, I wholeheartedly thank my supervisor Prof. Dr.-Ing. Marius Pesavento for his support, guidance and the knowledge he has shared with me during my doctoral studies. I also sincerely thank Prof. Alex B. Gershman who started to supervise my thesis and facilitated a good start into my doctoral studies. Sadly, he passed away at the beginning of my doctoral studies. May he rest in peace.

I sincerely thank my co-supervisor Univ. Prof. Dr.-Ing. Martin Haardt for the interesting discussions and the helpful comments and suggestions. Further, I would like to thank Prof. Dr.-Ing. Anja Klein, Prof. Dr. rer. nat. Sebastian Schöps, and Prof. Dr.-Ing. Herbert De Gersem for their work as Board of Examiners.

Special thanks go to Marlis Gorecki, Florian Bahlke, Yong Cheng, Dana Ciochina, Ganapati Hegde, Ying Liu, Michael Muma, Fabio Nikolay, Pouyan Parvazi, Oscar Dario Ramos Cantor, Christian Steffens, Wassim Suleiman, Dima Taleb, Imran Wajid, Xin Wen, Yang Yang, Xin Zhang, and all my colleagues and former colleagues at Communication Systems Group at TU Darmstadt for their support and help and for providing a pleasant working environment.

I would also like to thank Juanshu Zhang and Florian Roemer from TU Ilmenau for the productive collaboration.

During my doctoral studies, I had the opportunity to supervise brilliant students whose efforts partly contributed to this thesis. I sincerely thank Parvaneh Davarmanesh, Fabio Nikolay, Max Polzin, Ghyslain Trésor Tsobgni, Nagasubramanian Visvanathan, and Tilman Wolfenstetter.

I would like to express my gratitude to my parents Anne Bornhorst-Kersting and Gerd Bornhorst for their unconditional love and support throughout my life and to my sister Dr. Sarah Bornhorst for her guidance as an older sister.

Finally, I am most grateful to Nadine Nixdorff for her love, encouragement, support, and joy.

Abstract

In multi-user (MU) downlink beamforming, a high spectral efficiency along with a low transmit power is achieved by separating multiple users in space rather than in time or frequency using spatially selective transmit beams. For streaming media applications, multi-group multicast (MGM) downlink beamforming is a promising approach to exploit the broadcasting property of the wireless medium to transmit the same information to a group of users. To limit inter-group interference, the individual streams intended for different multicast groups are spatially separated using MGM downlink beamforming. Spatially selective downlink beamforming requires the employment of an array of multiple antennas at the base station (BS). The hardware costs associated with the use of multiple antennas may be prohibitive in practice. A way to avoid the expensive employment of multiple antennas at the BS is to exploit user cooperation in wireless networks where multiple single-antenna users act as relays and take over the role of antenna elements in a virtual distributed antenna array.

In both downlink beamforming and distributed relay beamforming, several approaches to design the transmit beams exist. In many scenarios, minimizing the transmit power has a higher priority than maximizing throughput. This is the case, e.g., in downlink beamforming, when operators aim at reducing their operational expenditures and their carbon footprint, or in distributed beamforming when users are only willing to cooperate when the battery consumption of their devices is kept at a minimum level. Then, the transmit beams are designed as the solution of a quality-of-service-constrained (QoS-constrained) power minimization problem. The goal of this optimization approach is to minimize the total transmitted power (at the BS or at the relays) while guaranteeing a predefined QoS at the destination users. In many scenarios with a high relevance in practice such as MGM downlink beamforming and MU peer-to-peer (MUP2P) relay beamforming, the QoS-constrained power minimization problem is a nonconvex optimization problem which cannot be solved optimally in polynomial time. In state-of-the-art methods, the nonconvex problem is therefore approximated by a convex one which is easier to solve. As the number of users increases, however, these approximations become more and more inaccurate leading to severe performance degradation and problem infeasibility.

In this dissertation, we therefore propose a novel framework of iterative optimization schemes where a convex approximation of the original problem is successively improved. In each iteration of the proposed schemes, a convex approximation of the original problem is solved and then adapted to the solution obtained in this iteration. We prove that by this means, the approximate solution is improved from iteration to

iteration. In this way, an approximate solution which is much closer to the optimal solution of the original problem than in state-of-the-art methods is usually obtained. Moreover, the convex approximation may be infeasible in state-of-the-art methods even if the original problem is feasible. The proposed iterative scheme is therefore extended such that it can also be used to find a feasible initial approximation of the original problem. Simulations results reveal that in relay beamforming scenarios with a moderate to a large number of destination users, the proposed scheme substantially outperforms state-of-the-art methods in terms of total transmitted relay power and problem feasibility. In MGM downlink beamforming scenarios with a large number of users, the proposed technique achieves the same performance as the state-of-the-art methods at a substantially reduced computational complexity.

Several extensions of this basic iterative convex approximation technique are proposed in this dissertation: The feasibility search is extended to an admission control scheme where a minimum number of destination users is determined for which service has to be denied in case of shortage of spectral resources. Furthermore, a non-trivial extension of our iterative method is proposed to maintain its applicability in the case where only limited information about the state of the channels in the network is available. Finally, a complexity reduction is proposed to turn the proposed algorithms into computational efficient ones which are suitable for real time application in practice.

Due to its wide-ranging applicability, we also consider filter-and-forward (FF) relay beamforming where the relays are equipped with finite impulse response (FIR) filters and single-carrier (SC) transmission over frequency selective channels is performed. In this scenario, the signal received at the destination nodes is contaminated by inter-symbol interference (ISI). Using the FIR filters at the relays, the frequency selective channels are equalized to some extent such that the ISI at the destination nodes can be mitigated. In previous works, the FF relay networks have been assumed to be perfectly synchronized. Perfect timing synchronization is, however, not possible in MU FF relay networks as there exists no single point of reference. This synchronization issue has barely been addressed in the literature. In this dissertation, we consider FF beamforming in asynchronous MUP2P and MGM relay networks and extend the FF scheme by incorporating individual adaptive decoding delays at the destinations. Using these decoding delays, the destination users can individually adapt to the different link delays in the asynchronous network and thereby mitigate residual ISI. We again consider the QoS-constrained power minimization problem where now the filter coefficients at the relays, which are continuous variables, and the individual decoding delays at the destinations, which are discrete variables, are jointly optimized. This optimization problem is a nonconvex mixed-integer programming (MIP) problem which is generally hard to solve optimally. We propose (i) a customized branch-and-cut (BnC)

method yielding a lower bound on the total transmitted relay power as a benchmark and (ii) a low-complexity deflation algorithm providing an approximate solution for implementation in practice. The deflation method is based on the proposed iterative convex approximation approach mentioned above. Our simulation results show that the approximate solution obtained using the proposed deflation scheme is close to optimal and outperforms the solutions obtained by state-of-the-art schemes which do not make use of adaptive decoding delays.

Zusammenfassung

Mehrnutzer-Downlink-Beamforming (engl. *multi-user downlink beamforming*, MU downlink beamforming) erreicht eine hohe spektrale Effizienz bei gleichzeitig reduzierter Sendeleistung, indem mehrere Nutzer mit raumselektiven Sendebeams räumlich voneinander getrennt werden, anstatt sie im Zeit- oder Frequenzbereich voneinander zu trennen. Für Streaming-Medienanwendungen ist Mehrgruppen-Multicast-Downlink-Beamforming (engl. *multi-group multicast downlink beamforming*, MGM downlink beamforming) ein vielversprechender Ansatz, die Broadcasting-Eigenschaft des Mobilfunkkanals auszunutzen, um eine Gruppe von Nutzern mit der gleichen Information zu versorgen. Um Interferenz zwischen den Gruppen zu begrenzen, werden mittels MGM-Downlink-Beamforming die individuellen Streams, die für verschiedene Multicast-Gruppen vorgesehen sind, räumlich voneinander getrennt. Für Downlink-Beamforming ist es erforderlich, an der Basisstation (BS) ein Array von mehreren Antennen einzusetzen. Die dafür notwendige Hardware kann in der Praxis unerschwinglich sein. Eine Möglichkeit, den teuren Einsatz mehrerer Antennen an der BS zu umgehen, ist das Ausnutzen von Nutzerkooperation in drahtlosen Netzwerken. Dabei fungieren mehrere Nutzer, die jeweils nur mit einer einzigen Antenne ausgestattet sind, als Relays und übernehmen die Rolle von Antennenelementen in einem virtuellen und verteilten Antennen-Array.

Sowohl in Downlink-Beamforming als auch in verteiltem Relay-Beamforming existieren mehrere Ansätze, die Sendebeams zu entwerfen. In vielen Szenarien wird der Minimierung der Sendeleistung eine höhere Priorität eingeräumt als der Maximierung des Datendurchsatzes. Dies ist beispielsweise in Downlink-Beamforming der Fall, wenn die Mobilfunkanbieter ihre Betriebskosten und ihren CO2-Fußabdruck senken möchten. Ein anderes Beispiel ist, wenn in verteiltem Beamforming die Nutzer nur bereit sind zu kooperieren, sofern der Akkuverbrauch ihrer Geräte dabei minimal gehalten wird. In solchen Szenarien werden die Sendebeams als die Lösung eines Leistungsminimierungsproblems mit Quality-of-Service-Nebenbedingungen (QoS-Nebenbedingungen) entworfen. Ziel dieses Optimierungsansatzes ist es, die Gesamtsendeleistung (an der BS bzw. an den Relays) zu minimieren und gleichzeitig eine vordefinierte QoS an den Nutzern zu gewährleisten. In vielen Szenarien mit hoher praktischer Relevanz, wie beispielsweise MGM-Downlink-Beamforming oder MU-Peer-to-Peer-Relay-Beamforming (MUP2P-Relay-Beamforming), ist das Leistungsminimierungsproblem mit QoS-Nebenbedingungen ein nichtkonvexes Optimierungsproblem, dessen optimale Lösung nicht in polynomieller Zeit gefunden werden kann. In Verfahren, die dem Stand der Technik entsprechen, wird das nichtkonvexe Problem daher mit einem konvexen Problem approximiert, das sich einfacher lösen lässt. Mit einer

wachsenden Zahl an Nutzern werden diese Approximationen jedoch sehr ungenau, was zu erheblichen Einbußen in der Leistungsfähigkeit und Zulässigkeit der Verfahren führt.

In dieser Dissertation schlagen wir daher ein neues System von iterativen Optimierungsverfahren vor, bei denen eine konvexe Approximation des ursprünglichen Problems sukzessive verbessert wird. In jeder Iteration der vorgeschlagenen Verfahren wird eine konvexe Approximation des ursprünglichen Problems gelöst und anschließend an die in dieser Iteration ermittelte Lösung angepasst. Wir beweisen, dass auf diese Weise die angenäherte Lösung von Iteration zu Iteration verbessert wird. Eine angenäherte Lösung, die deutlich näher an der optimalen Lösung des ursprünglichen Problems ist als in Verfahren, die dem Stand der Technik entsprechen, wird dadurch ermittelt. Ferner kann die konvexe Approximation in Verfahren, die dem Stand der Technik entsprechen, unzulässig werden, selbst wenn das ursprüngliche Problem zulässig ist. Das vorgeschlagene iterative Verfahren wird daher derart erweitert, dass es auch eingesetzt werden kann, um eine zulässige Initialapproximation des ursprünglichen Problems zu finden. Simulationsergebnisse zeigen, dass das vorgeschlagene Verfahren in Relay-Beamforming-Szenarien mit einer mittleren bis großen Anzahl an Senkeknoten die Verfahren, die dem Stand der Technik entsprechen, deutlich übertrifft hinsichtlich Gesamtsendeleistung und Problemzulässigkeit. In MGM-Downlink-Beamforming-Szenarien mit einer großen Anzahl an Nutzern erzielt das vorgeschlagene Verfahren bei deutlich reduziertem Rechenaufwand die gleiche Leistungsfähigkeit wie die Verfahren, die dem Stand der Technik entsprechen.

Mehrere Erweiterungen dieser grundlegenden iterativen konvexen Approximationsmethode werden in dieser Dissertation vorgeschlagen: Die Zulässigkeitssuche wird zu einem Admission-Control-Verfahren erweitert. Dabei wird eine minimale Zahl an Nutzern ermittelt, denen der Dienst verwehrt werden muss, wenn es nicht möglich ist, alle Nutzer des Netzwerkes zu bedienen. Außerdem schlagen wir eine nicht-triviale Erweiterung unseres iterativen Verfahrens vor, um es auch in dem Fall anwenden zu können, wenn nur eingeschränkte Informationen über den Zustand der Kanäle des Netzwerkes vorhanden sind. Schließlich wird eine Verringerung des Rechenaufwands vorgeschlagen, um die vorgeschlagenen Algorithmen in recheneffiziente Algorithmen zu überführen, die für die praktische Anwendung in Echtzeit geeignet sind.

Wegen seiner weitreichenden Anwendbarkeit betrachten wir zudem Filter-and-Forward-Relay-Beamforming ((FF)-Relay-Beamforming). Dabei sind die Relays mit Finite-Impulse-Response-Filtern (FIR-Filtern) ausgestattet und es erfolgt Einträgerübertragung (engl. *single-carrier transmission*, SC transmission) über frequenzselektive Kanäle. In diesem Szenario ist das Signal, das die Senkeknoten empfangen, mit Intersymbolinterferenz (ISI) kontaminiert. Mittels der FIR-Filter an den Relays wird der

Einfluss der frequenzselektiven Kanäle bis zu einem gewissen Grad ausgeglichen, so dass die ISI an den Senkeknoten abgeschwächt werden kann. In vorherigen Arbeiten wurde angenommen, dass die FF-Relaynetzwerke perfekt synchronisiert sind. Perfekte zeitliche Synchronisierung ist jedoch in MU-FF-Relaynetzwerken nicht möglich, da kein gemeinsamer Bezugspunkt existiert. Dieser Synchronisierungsaspekt wurde in der Literatur bislang kaum berücksichtigt. In dieser Dissertation betrachten wir FF-Beamforming in asynchronen MUP2P- und MGM-Relaynetzwerken und erweitern das FF-Verfahren, indem wir individuelle adaptive Dekodierverzögerungen an den Senkeknoten einsetzen. Diese Dekodierverzögerungen können an den Senkeknoten individuell an die unterschiedlichen Verbindungsverzögerungen in dem asynchronen Netzwerk angepasst werden. Dadurch wird verbleibende ISI abgeschwächt. Wir betrachten wieder das Leistungsminimierungsproblem mit den QoS-Nebenbedingungen. Diesmal werden jedoch die Filterkoeffizienten an den Relayknoten, die kontinuierliche Variablen sind, und die individuellen Dekodierverzögerungen an den Senkeknoten, die diskrete Variablen sind, gemeinsam optimiert. Dieses Optimierungsproblem ist ein nichtkonvexes gemischt-ganzzahliges Programm (engl. *mixed-integer program*, MIP), dessen optimale Lösung sich im Allgemeinen nur schwer finden lässt. Wir schlagen zwei Lösungsansätze vor: (i) ein individuell angepasstes Branch-and-Cut-Verfahren (BnC-Verfahren), welches eine untere Grenze der Gesamtsendeleistung der Relays als Vergleichsgröße liefert, und (ii) einen Deflationsalgorithmus mit geringer Komplexität, der eine näherungsweise Lösung für die Implementierung in der Praxis bietet. Das Deflationsverfahren basiert auf dem vorgeschlagenen iterativen konvexen Approximationsansatz, der oben erwähnt wurde. Unsere Simulationsergebnisse zeigen, dass die mit dem vorgeschlagenen Deflationsverfahren erhaltene näherungsweise Lösung nah an der optimalen Lösung ist. Außerdem übertrifft das Ergebnis des Deflationsverfahrens die Lösungen von Verfahren, die dem Stand der Technik entsprechen und sich adaptive Dekodierverzögerungen nicht zunutze machen.

Mathematical Notation

$(\cdot)^T$	Transpose
$(\cdot)^H$	Hermitian (conjugate transpose)
$\mathrm{tr}(\cdot)$	Trace of a square matrix
$\mathrm{rank}(\cdot)$	Rank of a matrix
$\boldsymbol{A} \succeq 0$	$\boldsymbol{A}$ is positive semi-definite
$\mathrm{diag}\{\boldsymbol{a}\}$	A diagonal matrix containing the elements of vector $\boldsymbol{a}$ on its main diagonal
$\mathrm{diag}\{\boldsymbol{A}\}$	A vector whose elements are the elements on the main diagonal of square matrix $\boldsymbol{A}$
$\boldsymbol{I}_N$	$N \times N$ identity matrix
$\boldsymbol{e}_k$	kth column of $\boldsymbol{I}_N$
$\mathbf{1}$	Vector whose elements are all equal one
$\mathbf{0}$	Vector whose elements are all equal to zero
$\mathbf{0}_{N \times M}$	$N \times M$ matrix whose elements are all equal to zero
$\mathcal{P}\{\boldsymbol{A}\}$	Principal component (eigenvector) of matrix $\boldsymbol{A}$
$\mathcal{L}_{\max}\{\boldsymbol{A}\}$	Largest (principal) eigenvalue of matrix $\boldsymbol{A}$
$\|\cdot\|$	Euclidean (l-2) norm of a vector
$\otimes$	Kronecker product
$\mathrm{sinc}(\cdot)$	Sinc function
$\delta[\cdot]$	Kronecker delta function
j	$\sqrt{-1}$
$\mathrm{Re}\{\cdot\}$	Real part of a complex number
$\angle\{\cdot\}$	Phase of a complex number
$\mathrm{E}\{\cdot\}$	Statistical expectation

Contents

Chapter 1

Introduction

A noteworthy percentage of global greenhouse gas emissions is caused by the information and communications technology [9, 10]. Therefore, green communications has recently emerged as a very active field in the research community with the goal to find solutions for more energy-efficient communication technology [9, 10]. Cellular network operators have an additional economic incentive to employ energy-efficient infrastructure as a means to reduce their operational expenditures [9, 10]. On the other hand, the number of mobile subscribers has increased dramatically in recent years and a shift from voice services as the main service in cellular wireless networks to more data-intensive services such as web-browsing, audio- and video-streaming, has occurred. As a consequence, the mobile data traffic has been growing exponentially in recent years and it is expected that it will continue growing exponentially [11, 12]. However, since the spectrum is a scarce resource, the data rate cannot be increased by limitlessly increasing the bandwidth. Therefore, it is essential to develop more spectrum-efficient wireless technologies to meet the growing demand for higher data rates [11]. In wireless communication technology, both the energy efficiency and the spectral efficiency have to increase dramatically in order to achieve higher data rates at reduced energy consumption.

A promising approach to jointly achieve high energy efficiency and high spectral efficiency is the concept of digital downlink beamforming where the base station (BS) is equipped with multiple antenna elements [13–17]. In multi-user (MU) downlink beamforming, the signals to be transmitted via different antenna elements are processed in digital baseband to form a transmit beam towards the intended user which is adapted to the changing user locations. In this way, the energy is transmitted mainly into the desired direction, i.e., into the direction where the intended user is located, rather than transmitting the energy isotropically or with fixed beam patterns where the main portion of the energy is wasted by transmitting it into undesired directions. Furthermore, the co-channel interference caused to other users is suppressed. Superimposing multiple such beam patterns allows to separate users in space rather than in time or frequency [13,14]. This technique is referred to as space division multiple access and has the potential to substantially increase the spectral efficiency since multiple users can share common time and frequency resources [18]. It is already an integral part of modern cellular standards such as, e.g., Long-Term Evolution (LTE) and LTE-Advanced (LTE-A) [19].

Recently, there has been an increasing demand for multicast services, such as, e.g., audio- and video-streaming or mobile TV, where a common message is broadcasted to a group of multiple users. Now that multicast services are commonly used, a spectral and energy efficient transmission of multicast streams is of significant importance. In traditional wireless networks, these services have been enabled by multicast routing protocols at the network layer. In emerging wireless networks, however, the broadcasting property of the wireless channel can be exploited to achieve broadcasting and multicasting at the physical layer. Using multicast downlink beamforming, the transmission can be performed much more efficiently than in traditional television broadcasting networks [16, 17]. Multicast downlink beamforming is enabled by the use of antenna arrays and channel state information (CSI) at the BS which is envisaged in emerging wireless communication standards such as, e.g., Multimedia Broadcast Multicast Service (MBMS) in LTE-A. In multi-group multicast (MGM) downlink beamforming, multiple co-channel multicasting groups of multiple users are separated in space using a separate transmit beam for each multicasting group. Users within the same group intend to receive the same information stream. In contrast to conventional MU downlink beamforming, the signal transmitted to the users of the same group do not cause interference within this group. Co-channel interference is only caused in other groups. This, however, comes at the expense of less flexibility in the design in terms of degrees of freedom since multiple users share one common beam pattern.

The main disadvantage and impediment for the practical implementation of digital downlink beamforming is the necessity to employ multiple antennas, each with its own radio frequency (RF) chain, at the BS which may be prohibitively expensive. A promising approach to benefit from beamforming without the necessity to employ multiple antennas at the BS is to exploit user cooperation in wireless communications [21]: Multiple single-antenna users cooperate to form a virtual antenna array where each single-antenna user takes over the role of a virtual antenna element. Since the beamforming is accomplished in a distributed fashion, this is also referred to as distributed beamforming. User cooperation originally emerged from the idea of extending cell coverage: If due to, e.g., pathloss, a link between a BS and a distant user is weak, users located closer to the BS can assist to establish the communication link by means of signal relaying. With this technique, ad-hoc networks, which do not require any cellular infrastructure, become a feasible and attractive alternative; either for complementing cellular networks or even as a paradigm shift from cellular networks to ad-hoc decentralized networks. Among the various relaying protocols that have to date been proposed, the amplify-and-forward (AF) protocol is of a particular interest due to its simple implementation [21, 22]. It is also the protocol that paved the way to distributed beamforming. In AF relaying, the signal received at a relay is amplified,

phase adjusted, and forwarded to the destination. Several AF relay network scenarios have to date been investigated in the literature, e.g., the single-user (SU) relay network where a single source node transmits its information to a single destination node through multiple relay nodes [25, 26]. This network constellation is suitable for both the uplink and the downlink of a cellular network or in a decentralized network. In [27], the SU relay network has been extended to enable efficient bidirectional communication which is usually referred to as two-way relaying. The SU relay network has been generalized to the MU peer-to-peer (MUP2P) relay network where multiple source-destination pairs communicate with each other through multiple relays in [28]. In this thesis, the MUP2P relay network is further generalized to the MGM relay network where each source node may transmit its information to a group of multiple destination nodes. The MUP2P and the MGM relay network are more relevant in the context of decentralized networks rather than in the context of centralized cellular networks. While the former has been extended to two-way relaying in [29], the latter is designed for unidirectional communication since bidirectional communication is usually not required in multicasting scenarios. There are three fundamental differences between downlink beamforming and distributed beamforming. Firstly, in distributed beamforming, the relay noise is amplified and forwarded to the destinations while in downlink beamforming, noise is absent in the signal transmitted at the BS. Secondly, the relays do not exchange information about their received signals among each other while in downlink beamforming, the elements of the antenna array are all connected. Thirdly, the total transmitted power has to be split between source nodes and relays in distributed beamforming.

Several approaches to design the transmit beams exist in both downlink beamforming and distributed relay beamforming. In many applications, minimizing the energy consumption has a higher priority than maximizing throughput. This is the case, e.g., in distributed beamforming, when users are only willing to cooperate when the battery consumption of their devices is kept at a minimum level, or in downlink beamforming when operators aim at reducing their operational expenditures and their carbon footprint. Then, the transmit beams are designed as the solution of a quality-of-service-constrained (QoS-constrained) power minimization problem with the objective to minimize the total transmitted power (at the BS or at the relays) subject to the constraint that the QoS at the destination users does not fall below a predefined threshold. This problem exhibits a simple closed-form optimal solution in the case of SU relay beamforming [26]. It has been shown in [14] that in MU downlink beamforming, the power minimization problem can be reformulated as a convex second-order cone programming (SOCP) problem which can be efficiently solved using numerical interior-point methods [62]. In the broadcast (BC) downlink beamforming scenario, the MGM downlink

beamforming scenario, and the MUP2P relay beamforming scenario, however, the QoS-constrained power minimization problem is a non-deterministic polynomial time hard (NP-hard) nonconvex problem [16, 17, 28] which is generally hard to solve optimally. However, convex approximation approaches have been proposed in [16,17,28] where the originally nonconvex feasible set of the QoS-constrained power minimization problem is approximated by a convex set which contains the original feasible set as a subset. Hence, we refer to this approach as a convex outer approximation technique. The convex approximated problem is solved using efficient interior-point methods. The main drawback of this approach is that due to the convex outer approximation, the solution obtained by solving the approximated problem is often over optimistic in the sense that it does not correspond to a feasible solution of the original nonconvex problem. Therefore, randomization techniques have been proposed in [16, 17, 28] where multiple candidate solutions for the original problem are randomly generated from the optimal solution of the approximated problem. The candidate solution yielding the smallest transmitted power while satisfying all QoS constraints is selected as an approximate solution to the original problem. Note, however, that this approximate solution is generally only suboptimal for the original problem. Moreover, it may happen that an approximate solution which is feasible for the original problem cannot be obtained by randomization even if the original problem actually is feasible. As the number of destination nodes increases, the convex outer approximation becomes more and more inaccurate. As a consequence, the probability decreases that the randomization technique yields a feasible and close to optimal solution for the original problem.

For the MUP2P beamforming scenario, an alternative to the convex outer approximation scheme of [16, 17, 28] has been proposed in [30]: Rather than using a convex outer approximation, a convex inner approximation is proposed. The convex inner approximation consists in approximating the originally nonconvex feasible set of the QoS-constrained power minimization problem by a convex subset of the original feasible set. Hence, the solution of the approximated problem, provided that it exists, is always feasible for the original problem. As a consequence, randomization techniques are not required to obtain a feasible solution. With this property, the convex inner approximation approach has a significant advantage over the convex outer approximation approach. However, the convex inner approximation becomes very inaccurate when the number of source-destination pairs is moderate to large. This may yield an approximate solution which is far from optimal. Even if the original problem is feasible, the convex inner approximation may also become infeasible when the approximated feasible set shrinks to the empty set.

To overcome the problem of inaccurate convex outer or inner approximations, we propose a novel iterative approach in this thesis to approximately solve the QoS-

constrained power minimization problem for both the MGM downlink beamforming and the MGM relay beamforming scenarios. In every iteration of the proposed scheme, a convex inner approximation of the original nonconvex problem is solved and then adapted to the solution obtained in this iteration. We prove that by this means, the approximate solution is improved from iteration to iteration. An approximate solution which is much closer to the optimal solution of the original problem than in state-of-the-art methods is usually obtained in this way. In case of a moderate to a large number of users, the proposed iterative approximation approach substantially outperforms the convex outer approximation based methods of [16, 17, 28] and the non-iterative convex inner approximation scheme of [30]. Note that the convex outer approximation approach used in [16, 17, 28] is a universal approach to approximately solve nonconvex quadratically constrained quadratic programming (QCQP) problems which emerge in a variety of applications. To achieve improved performance, the proposed method is more customized to the specific problems we consider in this thesis. However, it can also be viewed as a universal approach to approximately solve a certain class of nonconvex QCQP problems in numerous applications beyond the ones considered in this thesis.

Note that a similar idea of successively improving a convex inner approximation of the original nonconvex problem has been proposed for a max-min fair relay beamforming problem in [45]. However, it has been published later than our original work [1] and a more straight-forward convex inner approximation than in our scheme is used: The nonconvex functions in the original problem are linearized to approximate them by convex functions yielding a convex QCQP problem. In each iteration of the scheme in [45], the nonconvex functions are linearized around the approximate solution of the previous iteration. This is a very general approach which is applicable to a variety of nonconvex problems. However, it is not customized to the specific problems considered in this thesis. In our approach, we instead use the convex inner approximation of [30] which is customized to the specific problems we consider. Moreover, the proposed adaptation of the convex inner approximation to the approximate solution of the previous iteration is more advanced and more customized to the specific problems than in the linearization approach of [45]. Thanks to the customization, the proposed method exhibits better convergence properties than the method of [45] applied to the specific problems considered in this thesis. The approximation of [30] yields a convex SOCP problem. Hence, we refer to the proposed scheme as the iterative SOCP method.

Note that the concept of distributed relay beamforming is fundamentally different from the concept of centralized relay beamforming. In centralized relay beamforming, the relay network contains only a single relay which is equipped with multiple antennas. The multiple-input-multiple-output (MIMO) relay has access to all the signals received

at each antenna and can process these received signals jointly [46–48]. Joint processing of the different received signals is not possible in distributed beamforming where each relay has only access to its own received signal. In a MUP2P relay network with a single MIMO relay, closed-form suboptimal approaches exist to design the beam patterns [4,47]. To the best of our knowledge, such closed-form suboptimal approaches do not exist for MUP2P relay networks where distributed beamforming with single-antenna relays is performed. The focus of this dissertation is on the latter case and hybrid forms, where the network contains multiple MIMO relays, are not considered either.

In most of the works in the literature on relay networks, either single-carrier (SC) transmission over frequency flat channels or orthogonal frequency division multiplexing (OFDM) transmission over frequency selective channels has been assumed, see, e.g., [25, 26, 28, 30, 49, 50]. Both assumptions, however, are likely to be unrealistic: The data-rate requirements of today's wireless services are usually too high for the former assumption to hold. On the other hand, power and cost limitations of mobile devices are incompatible with OFDM transmission where large and expensive highly linear power amplifiers are required. Hence, SC transmission over frequency selective channels is the most realistic scenario where the signal received at the destinations is contaminated with a substantial amount of inter-symbol interference (ISI). Therefore, it has been proposed in [51] and [52] to extend the simple AF relaying to a scheme where the relays are equipped with finite impulse response (FIR) filters. Using the FIR filters, the relays can pre-process their received signals before they forward it to the destinations. This is known as filter-and-forward (FF) relaying. The FIR filters allow the relays to equalize the channels to a certain extent and thereby to mitigate the ISI at the destinations nodes. Despite the use of FIR filters at the relays, however, residual ISI at the destination nodes usually remains. Note that the FF protocol enjoys a significantly lower computational complexity than OFDM-based relaying protocols for the following reason. The number of filter taps of the FIR filters employed at the relays in FF relaying can be much lower than the number of sub-carriers in OFDM-based schemes. The FF protocol can even be implemented in analogue domain using tunable analogue filters.

The earlier mentioned QoS-constrained power minimization problem can be adapted to the FF relaying scenario where the optimization variables are the FIR filter coefficients of the relays. The problem can be reformulated appropriately to exhibit a similar mathematical structure as the AF relaying problem. Thus, as in the AF relaying case, the QoS-constrained power minimization problem in the FF relaying case enjoys a simple closed-form solution in the SU scenario [52] while it is NP-hard and nonconvex in the MUP2P scenario which has been considered in [54]. In this thesis, we also consider the more general FF MGM scenario. The outer approximation and randomization

approach mentioned above and the proposed iterative inner approximation approach can be applied in the latter scenarios to approximately solve the problem.

In [55], it has been proposed to additionally perform equalization at the destination to further mitigate ISI in the SU scenario of [52]. Compared to the much simpler symbol-by-symbol decoding, the equalization scheme of [55] yields a significantly lower amount of ISI at the destination node. However, considerable complexity is added to the destination node if an equalizer is employed at this node. This is a crucial drawback of the scheme in [55]. Furthermore, a way to extend the equalization scheme of [55] to the MUP2P scenario of [54] has not yet been found.

In previous works, the FF relay networks are assumed to be perfectly synchronized in time. Perfect timing synchronization is achievable in the SU scenario of [52] since the different link delays from the source to the destination via the different relays can be compensated at the relays. In the MUP2P scenario of [54] and the more general FF MGM scenario, however, users experience different link delays not only with respect to different relays but also with respect to other users. Consequently, perfect timing synchronization is not achievable for all users simultaneously in the MUP2P and the MGM scenario. In this thesis, we therefore consider these relay network to be asynchronous.

In FF relaying, where SC transmission over frequency selective channels is performed, each sample of the received signal at a destination node taken at symbol rate consists of a superposition of delayed multipath copies of the symbols consecutively transmitted by the source(s). If no equalization filter is employed at the destinations, one of the symbols from the desired source in the above superposition is considered as the desired symbol while the other symbols of this source cause ISI. In this dissertation, we notice that the destination can decide which of these symbols to decode as the desired symbol, i.e., it can adaptively select an appropriate decoding delay. Flexible decoding delays are not used in state-of-the-art works: The same fixed decoding delay is selected for all destinations in [52] and [54] which only yields satisfactory results if the network is assumed to be perfectly synchronized. As mentioned earlier, perfect synchronization is not achievable in the MUP2P scenario of [54] and the MGM scenario and we consider the network to be asynchronous. In our scheme, part of the synchronization task is shifted from the relays to the destination nodes using individual adaptive decoding delays: We propose to optimize the individual decoding delays at the destinations such that each destination can decode the strongest symbol from the desired source in the received superposition and thereby effectively mitigate ISI. We formulate the problem of jointly optimizing the FIR filter coefficients at the relays and the adaptive decoding delays at the destinations. The approach proposed in this thesis to approximately

solve this problem is based on the proposed iterative convex approximation approach mentioned earlier. Note that the idea of an adaptive decoding delay at the destination in the SU FF relay network of [52] has independently been developed in [56] using a frequency domain approach. However, the scheme of [56] is restricted to a single decoding delay and can thus not be generalized to asynchronous MUP2P or MGM relay networks where an individual decoding delay is required for each destination node. Due to the synchronization issues mentioned above, individual adaptive decoding delays are more beneficial in MUP2P and MGM relay networks than in SU relay networks. The proposed schemes outperform state-of-the-art MUP2P FF beamforming schemes which do not make use of adaptive decoding delays.

1.1 Contributions and Thesis Overview

This dissertation is organized as follows. Before the main contributions are presented, the signal models are introduced in Chapters 2 and 3 and state-of-the-art methods are briefly described in Chapter 4. The main contributions are then presented in Chapters 5 to 9. A conclusion is given in Chapter 10.

In Chapter 2, the signal model of MGM downlink beamforming is introduced and the nonconvex NP-hard QoS-constrained power minimization problem is derived for this scenario according to [17]. The two special cases of MGM downlink beamforming, MU downlink beamforming [14] and BC downlink beamforming [16], are also briefly considered.

In Chapter 3, the signal models and problem statements for several relay beamforming scenarios are derived. We generalize the MUP2P relay network of [17] to the MGM relay network where each source node may transmit its information to a group of multiple destination nodes rather than to a single destination node only. Analogous to MGM downlink beamforming, the MGM relay network contains the MUP2P relay network and the BC relay network as special cases. Note that the BC relay network has not yet been considered in previous works. According to [52, 54], these scenarios are extended such that the relays are equipped with FIR filters to perform FF relaying rather than AF relaying. For all the distributed beamforming scenarios mentioned above, the signal models and the corresponding nonconvex NP-hard QoS-constrained power minimization problems are derived in Chapter 3 according to [17, 52, 54]. The QoS-constrained beamforming problems of all the considered relay network scenarios are combined in a generalized problem formulation.

The convex outer approximation approaches of [16, 17, 28] and the straight-forward iterative linearization approach of [45] are briefly described as state-of-the-art methods in Chapter 4.

In Chapter 5, the iterative convex inner approximation technique is proposed to approximately solve the generalized QoS-constrained power minimization problem which combines all the considered relay beamforming problems. To overcome the drawback of inaccurate convex approximations of the original nonconvex problem in state-of-the-art methods, we propose an iterative convex approximation technique where a convex inner approximation of the original problem is successively improved. In every iteration of the proposed scheme, a convex inner approximation of the original nonconvex problem is solved and then adapted to the solution obtained in this way. We show analytically that the approximate solution obtained in a given iteration of our algorithm is improved compared to that of the previous iteration proving a local convergence property of the proposed scheme. Even if the original problem is feasible, its convex inner approximation may be infeasible when it shrinks to the empty set. To overcome this drawback, an iterative feasibility search to obtain a feasible initial convex inner approximation of the original feasible set is also proposed. It is based on the same basic idea of successively improving the convex inner approximation. In the proposed feasibility search, however, the objective is not to minimize the total transmitted relay power. Instead, the objective is to minimize an indicator of how far the approximation is from being feasible. The basic idea of the proposed feasibility search is neither limited to the specific problems considered in this thesis nor to the specific iterative convex inner approximation schemes we propose in this thesis. It is applicable to any nonconvex problem which can be solved using an iterative convex approximation scheme that requires a feasible initial approximation. The proposed feasibility search is shown to be easily extendable to an admission control scheme where a minimum number of destination users is determined for which service has to be denied when serving all destination users in the network is infeasible. Our simulations reveal that the results of the proposed admission control scheme are close to those of an exhaustive search admission control scheme. We also propose a way to combine the outer and the inner approximation approaches by using the proposed scheme as a local refinement for the outer approximation approach. A detailed analytic complexity analysis comparing the computational complexities of the competing methods is provided as well. The simulation results demonstrate that the proposed method outperforms the state-of-the-art methods in terms of both, total transmitted relay power and feasibility when the number of destination users is moderate to large. The proposed combination of the outer approximation approach and the inner approximation approach achieves the best results which are near-optimal. The proposed iterative scheme is not limited to the

specific problems considered in this thesis. It can be viewed as a universal approach to approximately solve a certain class of nonconvex QCQP problems which emerge in a variety of applications.

In Chapter 6, the iterative convex inner approximation technique derived in Chapter 5 for relay beamforming scenarios is applied to the MGM downlink beamforming scenario of Chapter 2. The simulation results show that in this case, the performance improvements over the state-of-the-art methods in terms of total transmitted power and feasibility are less significant than in the relay beamforming scenarios. However, for scenarios with a large number of users, the proposed approach enjoys a substantially reduced computational complexity as compared to the state-of-the-art outer approximation techniques.

The proposed iterative scheme is only applicable under the assumption that instantaneous CSI is available at the BS or the processing node(s). The CSI is required to formulate the optimization problem. Instantaneous CSI, however, might be difficult to acquire since, e.g., in downlink beamforming with frequency division duplex, the users need to estimate the CSI and feed the estimates back to the BS. Especially in fast fading scenarios, where the instantaneous CSI quickly becomes outdated and has to be fed back frequently, the feedback of the CSI causes a significant signaling overhead. The second-order statistics of the CSI, however, usually evolve at a significantly lower rate than the corresponding instantaneous CSI. Hence, a more realistic assumption is that only second-order statistics of the CSI are available which requires significantly less signaling overhead [14, 26]. Therefore, a non-trivial extension of the iterative inner approximation scheme is proposed in Chapter 7 which establishes applicability of the latter scheme under the assumption that only statistical CSI is available. Our simulation results demonstrate that for scenarios with a realistic amount of scattering, the proposed extended iterative inner approximation scheme outperforms the existing outer approximation methods.

In each iteration of the schemes proposed in Chapters 5 and 6, a convex SOCP problem is solved to obtain an intermediate solution. The SOCP problem is solved using an interior-point method which is an iterative method itself. In Chapter 8, we notice that performing the iterations of the interior-point method to convergence is not required for the intermediate solutions which are anyway discarded. Performing only a single iteration of the interior-point method yields a sufficiently high accuracy for intermediate solutions. In Chapter 8, we therefore propose to reduce the computational complexity of the iterative SOCP scheme by performing only a single iteration of the interior-point method to obtain the intermediate solutions. Our simulation results show that the performance of the resulting efficient algorithm in terms of total transmitted power

and feasibility is almost the same as that of the original algorithm of Chapters 5 and 6. However, this performance is achieved at a significantly reduced computational complexity. This complexity reduction is not limited to the specific problems considered in this thesis. It can be universally applied to any scheme where a nonconvex problem is approximately solved via solving a sequence of convex problems which themselves are solved using interior-point methods.

For the FF MUP2P and MGM relay networks considered in previous chapters, perfect timing synchronization is not achievable in practice contrary to the assumptions in state-of-the-art works. In Chapter 9, we therefore consider asynchronous FF MUP2P and MGM relay networks. We propose to employ individual adaptive decoding delays at the destinations which are used to adapt to different link delays in the asynchronous networks. The problem of jointly optimizing the filter coefficients at the relays and the individual decoding delays at the destinations is considered. The selection of individual decoding delays at the destinations is modeled using integer (binary) decision variables while the filter coefficients at the relays are continuous optimization variables. Hence, the latter problem is a mixed-integer programming (MIP) problem. Even if the binary variables are relaxed to be continuous, the problem is nonconvex and NP-hard. This nonconvex MIP problem is thus generally hard to solve optimally. Our contribution in terms of approaching the optimal solution of this problem is twofold: (i) We propose a customized branch-and-cut (BnC) method yielding a lower bound on the total transmitted relay power. Its computation is affordable in simulations and it provides a valuable benchmark. (ii) For practical applications, we propose a low-complexity deflation algorithm providing an approximate solution. This deflation algorithm is based on the iterative convex inner approximation method of Chapter 5. Our simulation results demonstrate that the approximate solution obtained using the proposed scheme is close to the lower bound obtained by the BnC method and thus close to optimal. Furthermore, it outperforms the solutions obtained by the state-of-the-art schemes in [52, 54], which do not make use of adaptive decoding delays, in terms of both, total transmitted relay power and feasibility.

This dissertation is based on the following publications which have been published or submitted during the course of my doctoral studies:

Internationally refereed journal articles:

- N. Bornhorst and M. Pesavento, "Filter-and-forward beamforming with adaptive decoding delays in asynchronous multi-user relay networks," *Signal Process.*, vol. 109, pp. 132-147, April 2015.

- N. Bornhorst, M. Pesavento, and A. B. Gershman, "Distributed beamforming for multi-group multicasting relay networks," *IEEE Trans. Signal Process.*, vol. 60, no. 1, pp. 221-232, Jan. 2012.

Internationally refereed conference proceedings:

- N. Bornhorst and M. Pesavento, "Filter-and-forward beamforming in asynchronous relay networks," in *Proc. IEEE Int. Workshop on Signal Process. Advances in Wirel. Commun. (SPAWC)*, Darmstadt, Germany, pp. 375-379, June 2013.
- N. Bornhorst, P. Davarmanesh, M. Pesavento, "An extended interior-point method for transmit beamforming in multi-group multicasting," in *Proc. European Signal Process. Conf. (EUSIPCO)*, Bucharest, Romania, pp. 6-10, Aug. 2012.
- N. Bornhorst and M. Pesavento, "Beamforming for multi-group multicasting with statistical channel state information using second-order cone programming," in *Proc. IEEE Int. Conf. on Acoustics, Speech and Signal Process. (ICASSP)*, pp. 3237-3240, Kyoto, Japan, March 2012.
- J. Zhang, N. Bornhorst, F. Römer, M. Haardt, and M. Pesavento, "Optimal and suboptimal beamforming for multi-operator two-way relaying with a MIMO amplify-and-forward relay," in *Proc. IEEE/ITG Int. Workshop on Smart Antennas (WSA)*, pp. 307-311, Dresden, Germany, March 2012.
- N. Bornhorst and M. Pesavento, "An iterative convex approximation approach for transmit beamforming in multi-group multicasting," in *Proc. IEEE Int. Workshop on Signal Process. Advances in Wirel. Commun. (SPAWC)*, San Francisco, CA, USA, pp. 411-415, June 2011.
- N. Bornhorst, M. Pesavento, and A. B. Gershman, "Distributed beamforming for multiuser peer-to-peer and multi-group multicasting relay networks," in *Proc. IEEE Int. Conf. on Acoustics, Speech and Signal Process. (ICASSP)*, Prague, Czech Republic, pp. 2800-2803, May 2011.

1.2 Impact on Follow-up Research

Our works have inspired a range of follow-up research works: The iterative convex inner approximation approach proposed in our works has inspired a number of similar iterative convex approximation techniques for different optimization problems in [31–34].

Moreover, the good performance of alternatives to the outer approximation based approach with randomization has motivated others to develop further alternatives like the non-smooth optimization method of [35]. The basic idea of MUP2P relay beamforming has been extended in [36] to the case where the transmitted power of the source nodes, which is fixed in our works, and the beamforming weights at the relays are optimized jointly. An iterative feasibility search, which is inspired by the one proposed in our works, is used in [36] to obtain a feasible initialization for the iterative scheme proposed to approximately solve the joint optimization problem. The admission control scheme proposed in our works has motivated the authors in [37,38] to develop a novel admission control scheme where a dynamic QoS threshold serves as an implicit admission control mechanism. For the BC relay network, which has been considered in our works for the first time, a computationally efficient way of approximately solving the BC relay beamforming problem has been proposed in [39]. The same BC relay beamforming scenario has been generalized to the case where the nodes are equipped with multiple antennas in [40]. Furthermore, the dual-hop MGM relay beamforming network, which has first been considered in our works, has been generalized to a multi-hop MGM MIMO relay beamforming network in [41]. Finally, the detailed complexity analysis carried out in our work has been applied to the problems and methods considered in [42] to evaluate their worst-case complexities.

Chapter 2

Signal Model and Problem Formulations - Downlink Beamforming

2.1 Introduction

In traditional wireless networks, multicasting has been considered as a task performed by efficient routing protocols at the network layer to enable multicast services such as subscriber-based video streaming. In emerging wireless networks, however, this task can be shifted to the physical layer by exploiting the broadcasting property of the wireless medium. Future wireless communication standards such as MBMS in LTE-A, provide the use of antenna arrays and CSI at the transmitter enabling multicast transmit beamforming. In transmit beamforming, different weighted replicas of the signal are transmitted over multiple antennas. This strategy allows more sophisticated transmission than in traditional BC radio: Rather than radiating energy isotropically or with a fixed beam pattern, the transmitted energy can be steered with adaptive beam patterns towards the subscribers. In this way, the main portion of the energy is radiated into the desired directions increasing the energy efficiency of the transmission. Moreover, since the power is radiated in a spatially selective way, superimposing multiple beam patterns allows to multiplex different cochannel multicast groups in space rather than in time or frequency increasing the spectral efficiency of the system.

QoS-constrained downlink beamformer designs were first studied in [14, 16, 17]. In these designs, the goal is to minimize the total transmitted power while guaranteeing a minimum received signal-to-interference-plus-noise ratio (SINR) for each user. The MU downlink scenario, where K independent data streams are transmitted to K mobile users, was considered in [14]. It has been shown in [14] that the underlying optimization problem can be formulated as a convex SOCP problem in this case provided that instantaneous CSI is available at the transmitter. The BC scenario, also referred to as the single-group multicasting scenario, where the same stream is transmitted to M mobile users, has been studied in [16]. The QoS-constrained downlink beamformer design yields a NP-hard optimization problem in this case. In [17], the MU downlink and the BC scenario are combined in the more general MGM scenario and the QoS-constrained downlink beamformer design problem has been studied for this scenario. The QoS-constrained beamforming problem is an NP-hard optimization problem in this case too as we will see in the present chapter.

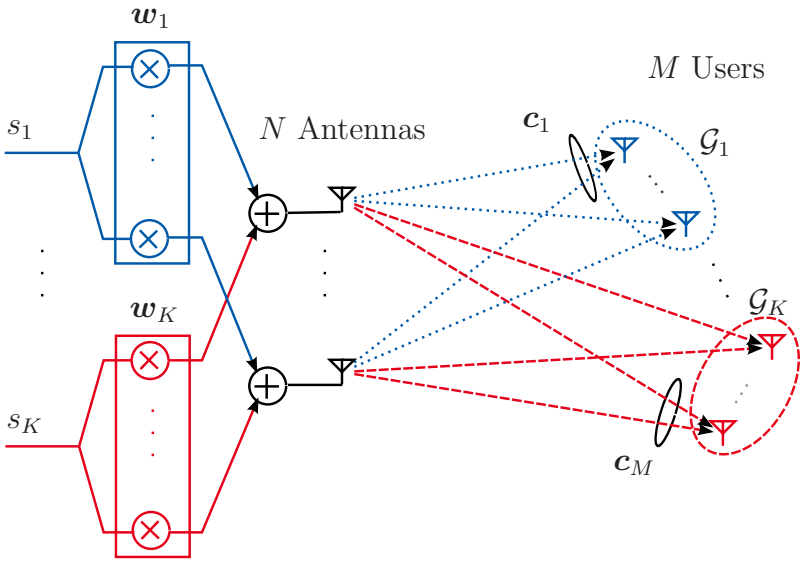

Figure 2.1. MGM downlink beamforming scenario.

We briefly derive the signal model and the original NP-hard problem formulation of the MGM downlink beamforming scenario in this chapter. Further, we consider the problem formulations of the two special cases of this scenario, BC downlink beamforming and MU downlink beamforming. The purpose of this chapter is to lay the foundation for later chapters by introducing the signal model and problem formulations. It does not contain own contributions.

2.2 MGM Downlink Beamforming

Let us consider a traditional downlink beamforming scenario where a BS is equipped with an antenna array comprising several antenna elements. The antenna array enables the BS to efficiently transmit data streams to single antenna users. In particular, we consider the wireless MGM scenario of [17] shown in Fig. 2.1 where a single BS equipped with an array of N antenna elements transmits information symbols to M single-antenna mobile users. We consider $1 \leq K \leq M$ multicast groups, $\{\mathcal{G}_1, \ldots, \mathcal{G}_K\}$, where $\mathcal{G}_k$ denotes the set of indices of the users intended to receive the message of multicasting stream k, and $k \in \mathcal{K}$ where $\mathcal{K} \triangleq \{1, \ldots, K\}$. We assume that each user receives only a single stream and hence, the multicasting groups are disjoint, i.e., $\mathcal{G}_k \cap \mathcal{G}_l = \emptyset$, for $l \neq k$ and $\cup_k \mathcal{G}_k = \mathcal{M}$ where $\mathcal{M} \triangleq \{1, \ldots, M\}$.

Let $\boldsymbol{w}_k^* \triangleq [w_{k,1}^*, \ldots, w_{k,N}^*]^T$ be the beamforming vector comprising the complex weighting coefficients applied to the N transmitting antenna elements to form a beam towards

the kth multicast group. To transmit the K information symbols to the K different multicast groups simultaneously, the BS superimposes the K information symbols weighted with the K beamforming weight vectors and transmits the following signal

$$\boldsymbol{x} = \sum_{k=1}^{K} \boldsymbol{w}_k^* s_k \tag{2.1}$$

where $\boldsymbol{x} \triangleq [x_1, \ldots, x_N]^T$ and s_k is the complex information symbol for the kth multicast group. We assume frequency flat fading as in [17]. This is a reasonable assumption since frequency flat channels occur, e.g., in OFDM used in the downlink in Long-Term Evolution (LTE). The signal received at the mth mobile user is then given by

$$y_m = \boldsymbol{x}^T \boldsymbol{c}_m + \nu_m = \sum_{k=1}^{K} \boldsymbol{w}_k^H \boldsymbol{c}_m s_k + \nu_m = \underbrace{\boldsymbol{w}_d^H \boldsymbol{c}_m s_d}_{y_{\mathrm{S},m}} + \underbrace{\sum_{k \neq d} \boldsymbol{w}_k^H \boldsymbol{c}_m s_k}_{y_{\mathrm{I},m}} + \nu_m \tag{2.2}$$

where $\boldsymbol{c}_m \triangleq [c_{m,1}, \ldots, c_{m,N}]^T$, $c_{m,n}$ is the complex channel coefficient corresponding to the frequency flat channel between the nth antenna element of the transmitting antenna array and the mth user, and $y_{\mathrm{S},m}$, $y_{\mathrm{I},m}$, and ν_m are the desired signal, the interference, and the noise components at the mth user, respectively.

Similar to [17], we formulate the multicast beamformer design as the problem of minimizing the total power radiated at the transmitting antenna array subject to individual QoS constraints at the receivers. Several quantities are usually included in the QoS such as, e.g., the latency. In the context of beamforming, however, the focus is on the SINR as a measure for the QoS. The QoS constraints then guarantee that the SINR at each user is kept above a predefined QoS threshold. The optimization problem can be formulated as

$$\min_{\{\boldsymbol{w}_k\}_{k=1}^K} \quad P_{\mathrm{T}} \tag{2.3a}$$

$$\text{subject to} \quad \mathrm{SINR}_m \geq \gamma_m, \ \forall m \in \mathcal{G}_d, \ \forall d \in \mathcal{K} \tag{2.3b}$$

where γ_m is the SINR threshold at the mth receiver, P_{T} is the total power radiated by the transmitting antenna array, and SINR_m is the SINR at the mth receiver defined as

$$\mathrm{SINR}_m \triangleq \frac{\mathrm{E}\left\{|y_{\mathrm{S},m}|^2\right\}}{\mathrm{E}\left\{|y_{\mathrm{I},m}|^2\right\} + \mathrm{E}\left\{|\nu_m|^2\right\}}. \tag{2.4}$$

As in [17], we assume throughout the thesis that the information symbols of the different multicast groups are zero-mean with unit variance and mutually uncorrelated. Then, P_{T} can be expressed as

$$P_{\mathrm{T}} = \sum_{n=1}^{N} \mathrm{E}\{|x_n|^2\} = \sum_{n=1}^{N} \sum_{k=1}^{K} |w_{k,n}|^2 \mathrm{E}\{|s_k|^2\} = \sum_{k=1}^{K} \|\boldsymbol{w}_k\|^2. \tag{2.5}$$

From (2.2), we now derive expressions for the desired signal power, the interference power, and the noise power in (2.4). When the channel vector is known at the BS, i.e., instantaneous CSI is available, the desired signal power at the mth receiver can be expressed as

$$\begin{aligned}\mathrm{E}\left\{|y_{\mathrm{S},m}|^2\right\} &= \mathrm{E}\left\{|s_d|^2\right\}\mathrm{E}\left\{(\boldsymbol{w}_d^H\boldsymbol{c}_m)(\boldsymbol{w}_d^H\boldsymbol{c}_m)^H\right\} \\ &= \boldsymbol{w}_d^H\mathrm{E}\left\{\boldsymbol{c}_m\boldsymbol{c}_m^H\right\}\boldsymbol{w}_d = \boldsymbol{w}_d^H\boldsymbol{c}_m\boldsymbol{c}_m^H\boldsymbol{w}_d = \boldsymbol{w}_d^H\boldsymbol{C}_m\boldsymbol{w}_d \end{aligned} \tag{2.6}$$

where

$$\boldsymbol{C}_m \triangleq \boldsymbol{c}_m\boldsymbol{c}_m^H. \tag{2.7}$$

The interference power at the mth user is given by

$$\mathrm{E}\left\{|y_{\mathrm{I},m}|^2\right\} = \sum_{k\neq d}\mathrm{E}\left\{|s_k|^2\right\}\mathrm{E}\left\{(\boldsymbol{w}_k^H\boldsymbol{c}_m)(\boldsymbol{w}_k^H\boldsymbol{c}_m)^H\right\} = \sum_{k\neq d}\boldsymbol{w}_k^H\boldsymbol{c}_m\boldsymbol{c}_m^H\boldsymbol{w}_k = \sum_{k\neq d}\boldsymbol{w}_k^H\boldsymbol{C}_m\boldsymbol{w}_k. \tag{2.8}$$

Using (2.4)-(2.6) and (2.8), problem (2.3) can be written as

$$\min_{\{\boldsymbol{w}_k\}_{k=1}^K} \quad \sum_{k=1}^K \|\boldsymbol{w}_k\|^2 \tag{2.9a}$$

$$\text{s.t.} \quad \frac{\boldsymbol{w}_d^H\boldsymbol{C}_m\boldsymbol{w}_d}{\sum_{k\neq d}\boldsymbol{w}_k^H\boldsymbol{C}_m\boldsymbol{w}_k + \sigma_m^2} \geq \gamma_m,\ \forall m \in \mathcal{G}_d,\ \forall d, k \in \mathcal{K} \tag{2.9b}$$

where $\sigma_m^2 = \mathrm{E}\{|\nu_m|^2\}$ is the noise power at the mth receiver. Problem (2.9) is non-convex and not solvable in polynomial time, i.e., it is NP-hard. This has been pointed out in [17] and we show the reason for this phenomenon later.

We assume that the CSI in terms of the instantaneous channel vectors $\{\boldsymbol{c}_m\}_{m=1}^M$ and the receiver noise powers $\{\sigma_m^2\}_{m=1}^M$ are known at the transmitter. This assumption holds in two cases: The first case is a time division duplex system where channel reciprocity can be exploited to estimate the instantaneous downlink channels from the uplink. In the second case, each user estimates its channel vector $\boldsymbol{c}_m$ and its noise power σ_m^2 and feeds the estimates back to the BS via a feedback link in frequency division duplex systems [14]. Using the instantaneous CSI, problem (2.9) can be solved at the BS such that the resulting beamforming vectors $\{\boldsymbol{w}_k\}_{k=1}^K$ are available at the BS.

Let us now discuss two special cases which are contained in the MGM beamforming problem (2.9), the MU downlink beamforming problem and the single-group multicast or BC downlink beamforming problem.

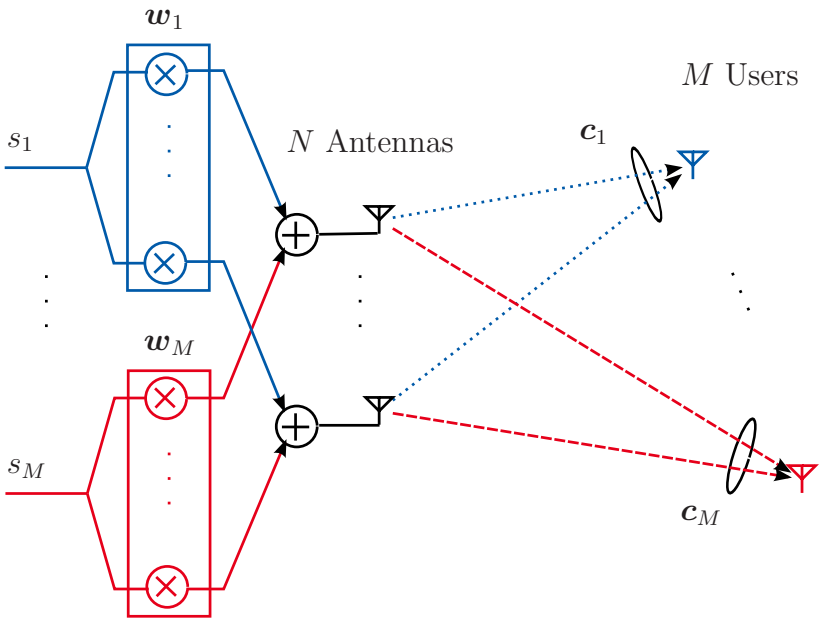

Figure 2.2. MU downlink beamforming scenario.

2.2.1 Special Case 1: MU Downlink Beamforming

The first special case that is contained in the MGM beamforming problem (2.9) is the MU downlink beamforming problem that is shown in Fig. 2.2 and has been considered in [14]. It can be interpreted as a MGM beamforming scenario where each multicast group contains only a single user, i.e., $\mathcal{G}_k = k,\ \forall k \in \mathcal{K}$. Thus, the only difference between the MGM beamforming problem and the MU downlink beamforming problem is the indexing:

$$\min_{\{\boldsymbol{w}_k\}_{k=1}^K} \quad \sum_{k=1}^{K} \|\boldsymbol{w}_k\|^2 \tag{2.10a}$$

$$\text{s.t.} \quad \frac{\boldsymbol{w}_d^H \boldsymbol{C}_d \boldsymbol{w}_d}{\sum_{k\neq d} \boldsymbol{w}_k^H \boldsymbol{C}_d \boldsymbol{w}_k + \sigma_d^2} \geq \gamma_d,\ \forall d, k \in \mathcal{K}. \tag{2.10b}$$

It has been shown in [14] that problem (2.10) can be equivalently reformulated as a convex SOCP problem solvable by interior-point methods [62]. Let us briefly revisit the SOCP reformulation here. In [14], the rank-one property of the matrix $\boldsymbol{C}_k$ is exploited to rewrite the kth QoS constraint in problem (2.10) as

$$|\boldsymbol{w}_d^H \boldsymbol{c}_d| \geq \sqrt{\gamma_d \left(\sum_{k\neq d} \boldsymbol{w}_k^H \boldsymbol{C}_d \boldsymbol{w}_k + \sigma_d^2 \right)}. \tag{2.11}$$

By introducing the new matrix and vector

$$\boldsymbol{\mathcal{H}}_k \triangleq \begin{bmatrix} \sigma_k^2 & \mathbf{0}^T \\ \mathbf{0} & (\boldsymbol{I} - \mathrm{diag}\{\boldsymbol{e}_k\}) \otimes \boldsymbol{C}_k \end{bmatrix}^{1/2}, \ \forall k \in \mathcal{K},$$
$$\boldsymbol{w}_{\mathrm{all}} \triangleq [1, \boldsymbol{w}_1^T, \ldots, \boldsymbol{w}_K^T]^T,$$

the constraint in (2.11) can be further rewritten as

$$|\boldsymbol{w}_d^H \boldsymbol{c}_d| \geq \sqrt{\gamma_d} \|\boldsymbol{\mathcal{H}}_d \boldsymbol{w}_{\mathrm{all}}\|. \tag{2.12}$$

Note that the original problem (2.10) is independent of a multiplication of each $\boldsymbol{w}_k$ by a rotation factor $\exp(j\varphi_k)$. In other words, the phase φ_k of the optimal solution $\boldsymbol{w}_{k,\mathrm{opt}}$ can be chosen arbitrarily without changing the optimality property of $\boldsymbol{w}_{k,\mathrm{opt}}$. Hence, we can replace the magnitude in the left-hand side of each QoS constraint (2.12) by the real-part since, using φ_k, $\forall k \in \mathcal{K}$, each inner product $\boldsymbol{w}_k^H \boldsymbol{c}_k$, $\forall k \in \mathcal{K}$ can always be rotated onto the positive real axis where the real-part is equal to the magnitude. Thus, we can equivalently rewrite problem (2.10) as

$$\min_{t \in \mathbb{R},\, \boldsymbol{w}_{\mathrm{all}} \in \mathbb{C}^{KN+1}} \quad t \tag{2.13a}$$
$$\text{s.t.} \quad \|\boldsymbol{w}_{\mathrm{all}}\| \leq t \tag{2.13b}$$
$$\sqrt{\gamma_d} \|\boldsymbol{\mathcal{H}}_d \boldsymbol{w}_{\mathrm{all}}\| \leq \mathrm{Re}\{\boldsymbol{w}_d^H \boldsymbol{c}_d\}, \ \forall d \in \mathcal{K}, \tag{2.13c}$$
$$w_{\mathrm{all},1} = 1 \tag{2.13d}$$

which is a convex SOCP problem [62].

2.2.2 Special Case 2: BC Downlink Beamforming

Let us now consider the second special case contained in the MGM beamforming problem (2.9), the BC downlink beamforming problem where only a single multicast group is present, i.e., $K = 1$. This scenario is displayed in Fig. 2.3 and has first been investigated in [16]. Since only a single stream is transmitted to a single group of users, there is no interference in this scenario, and problem (2.9) becomes

$$\min_{\boldsymbol{w}_1} \quad \|\boldsymbol{w}_1\|^2 \tag{2.14a}$$
$$\text{s.t.} \quad \boldsymbol{w}_1^H \boldsymbol{C}_m \boldsymbol{w}_1 \geq \gamma_m \sigma_m^2, \ \forall m \in \{1, \ldots, M\}. \tag{2.14b}$$

It has been shown in [16] that problem (2.14) is nonconvex and NP-hard for the following reason. Each of the QoS constraints in (2.14b) describes a super-level set of a quadratic function [62]. Such a set is only convex if the quadratic function is concave, i.e., if the matrix $\boldsymbol{C}_m$ is negative semi-definite. However, $\boldsymbol{C}_m$ is positive semi-definite making the problem nonconvex and NP-hard. The non-convexity and NP-hardness of problem (2.14) implies non-convexity and NP-hardness of the more general problem (2.9) as well [17].

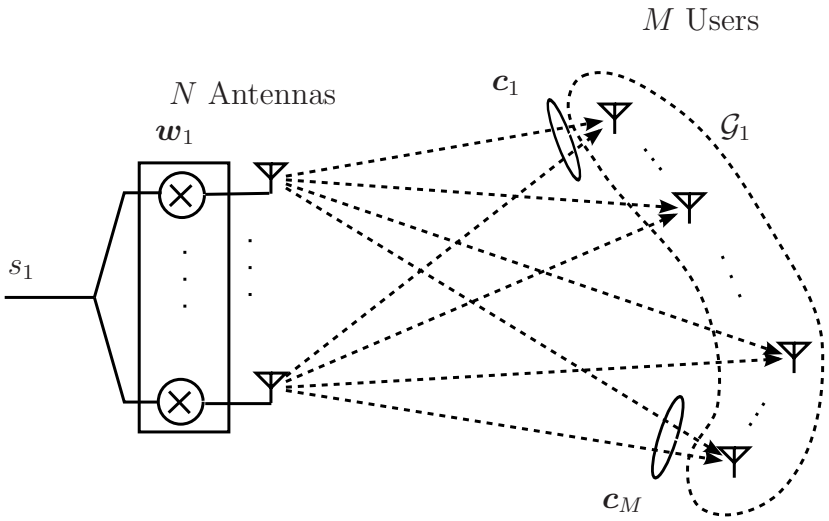

Figure 2.3. BC downlink beamforming scenario.

2.3 Statistical CSI

The availability of instantaneous CSI in terms of the channel vectors $\{\boldsymbol{c}_m\}_{m=1}^M$ at the BS is assumed in the previous section. Instantaneous CSI, however, might be difficult to acquire since, e.g., in frequency division duplex systems, the users need to estimate the channel vectors $\{\boldsymbol{c}_m\}_{m=1}^M$ and feed the estimates back to the BS. The feedback of the CSI causes a significant signaling overhead especially in fast fading scenarios where the instantaneous CSI quickly becomes outdated and has to be fed back frequently. The second-order statistics of the channels, however, usually evolve at a significantly lower rate than the corresponding instantaneous channel realizations. Therefore, beamformer designs based on channel covariance matrices are associated with a significantly reduced signaling overhead [14]. Hence, let us now assume that only second-order statistics of the CSI in terms of the covariance matrices of the channel vectors are available at the BS as in [14]. Under this assumption, the expectation with respect to the channel vectors does not vanish in the previous derivations and thus, e.g., in (2.6), the second last equality does not hold. Instead, we need to redefine the matrix $\boldsymbol{C}_m$ as

$$\boldsymbol{C}_m \triangleq \mathrm{E}\left\{\boldsymbol{c}_m \boldsymbol{c}_m^H\right\}. \tag{2.15}$$

Note that the matrix $\boldsymbol{C}_m$, which is a rank-one matrix in case of instantaneous CSI, is of higher rank when only second-order statistics of the CSI are assumed to be available. Further note that the MGM beamforming problem (2.9) remains the same in this case whereas $\boldsymbol{C}_m$ is defined as in (2.15).

Chapter 3

Signal Model and Problem Formulations - Distributed Beamforming

3.1 Introduction

The transmit beamforming schemes of the previous chapter have a main drawback: Implementing arrays with multiple antennas may be impractical for most devices; not only for small mobile terminals with strong requirements on size, weight, cost and complexity, but also for BSs if a separate RF chain is required for each antenna as in digital beamforming.

A promising approach that enables to benefit from spatial diversity or beamforming gains without the necessity of employing multiple antennas in a single device is user cooperation in wireless communication networks which has recently attracted much attention in the research community [21, 22]. The idea in user cooperative schemes is that users mutually assist each other in transmitting their data through the network by means of signal relaying from the transmitter to the receiver via multiple channel paths. Various relaying protocols have been proposed so far among which the most popular ones are AF [21, 22], decode-and-forward [22], compress-and-forward [23], and coded cooperation [24].

Due to its simple implementation, the AF protocol is of a particular interest [21, 22]. It has opened up the concept of distributed beamforming where each of the cooperating single-antenna users takes over the role of one element in a virtual antenna array. Recently, distributed beamforming approaches have been proposed for a number of relay network scenarios [25, 26, 28, 30]. The simplest relay network scenario is the single user relay network where a single source sends its information to a single destination through several relays. It has been studied in [25] and [26]. This network has been extended from the single source-destination pair to multiple source-destination pairs in [28] and [30] yielding a MUP2P relay network (see Fig. 3.2).

Similar to the generalization of MU downlink beamforming to downlink beamforming for MGM in [17], we generalize the concept of MUP2P relay networks to that of MGM relay networks in this chapter (see Fig. 3.1). In MGM relay networks, each source may broadcast a message to a group of multiple destination users rather than only

to a single user as in the MUP2P relay network. Like in downlink beamforming, this new extension is relevant, e.g., for the transmission of streaming media. Analogous to downlink beamforming, the MGM relay network includes the BC relay network as an important special case when $K = 1$ and only a single group of destination users is present (see Fig. 3.3). It is worth noting that distributed network beamforming differs from the traditional "centralized" transmit beamforming in that in the distributed setting, each relay antenna only knows its own received signal and is not able to share it with other relays [15]. In traditional transmit beamforming, on the contrary, all the information about the transmitted signals is available at each array antenna. As a consequence, in the traditional "centralized" transmit beamforming of Chapter 2, each signal intended for a particular multicast group of destination users is transmitted with its own weight vector. In contrast, in distributed multicast beamforming, only one weight vector can be used to transmit all the relay received signals to the multiple groups of destination users [15].

In this chapter, analogous to Chapter 2, we consider the problem of minimizing the total transmitted relay power subject to receiver QoS constraints. In the context of relay networks, this is a common way of formulating distributed beamformer design problems [26, 28, 30]. In the MUP2P relay network case, the resulting optimization problem is non-convex and NP-hard and cannot be solved optimally in polynomial time [28]. In this chapter, we show that the MGM generalization of network beamforming yields a QoS-constrained power minimization problem whose mathematical structure is very similar to that of the latter problem in MUP2P networks. The non-convex NP-hard property is thus inherited from the MUP2P beamforming problem. However, efficiently solvable convex approximations of the underlying non-convex problem are presented in the subsequent chapters.

As it has been made clear above, beamforming for AF relaying has been extensively studied in the context of SC transmission over frequency flat channels (see, e.g., [25, 26, 28, 30]). However, these schemes are not directly applicable in many practical situations since the bandwidth of modern wireless standards is usually too high for SC transmission over frequency flat channels as, e.g., in LTE and LTE-A where the signal bandwidth can be up to 20 MHz and more. Therefore, AF relaying techniques for OFDM transmission over frequency selective channels have been investigated in, e.g., [49] and [50]. Due to its high peak-to-average power ratio, OFDM requires highly linear power amplifiers. This makes the use of OFDM impractical in many relay networks, e.g., when the relays are mobile terminals or sensors in a sensor network which both need to be small, simple and power efficient; three properties which highly linear power amplifiers generally lack. Due to these restrictions, OFDM is, e.g., not used in the uplink of LTE. To enable high data rate transmission without OFDM, the FF

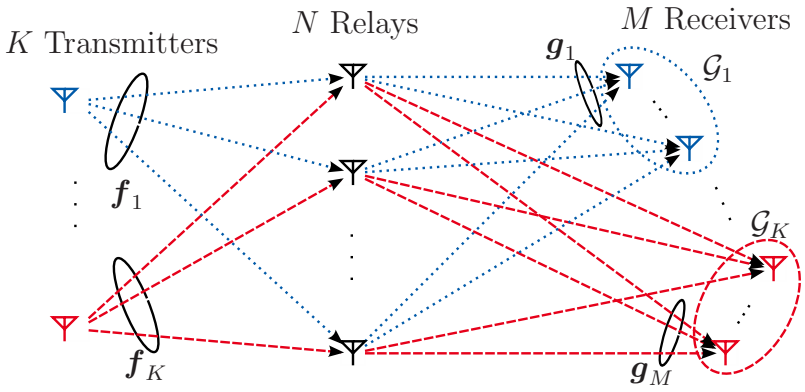

Figure 3.1. MGM wireless relay network.

beamforming protocol has therefore been introduced in [51] and [52] and extended to two-way relaying in [53]. In FF beamforming, the individual relays are equipped with FIR filters to mitigate the effect of ISI in SC transmission over frequency selective channels in addition to achieving a beamforming gain. As a first step towards FF beamforming, the authors in [51] and [52] have focused on a SU scenario. FF beamforming has then been extended to a MUP2P scenario in [54]. In all above references, a simple symbol-by-symbol decoder is employed at the destinations.

In this chapter, we derive the signal model and consider the QoS-constrained power minimization problem in the context of MGM relay networks with both frequency flat channels and AF relays on the one hand and with frequency selective channels and FF relays on the other hand. We show that a generalized problem formulation exists that combines the QoS-constrained power minimization problems of both the AF scenario and the FF scenario. Similar to the previous chapter, the purpose of this chapter is to lay the foundation for later chapters by introducing the signal model and problem formulations. The own contribution in this chapter is the generalization of the MUP2P relay networks to MGM relay networks.

3.2 MGM Relay Network with AF Beamforming

Let us consider a wireless relay network consisting of K transmitters (source nodes), N relays and M receivers (destination users), with $K \leq M$, as illustrated in Fig. 3.1. Each node in this network is equipped with a single antenna and can be viewed, for example, as a mobile user or a sensor node in a sensor network. All nodes in the network operate in a common frequency band. We assume that, due to severe path loss and signal fading, no direct links between the source and destination nodes are available. However, the

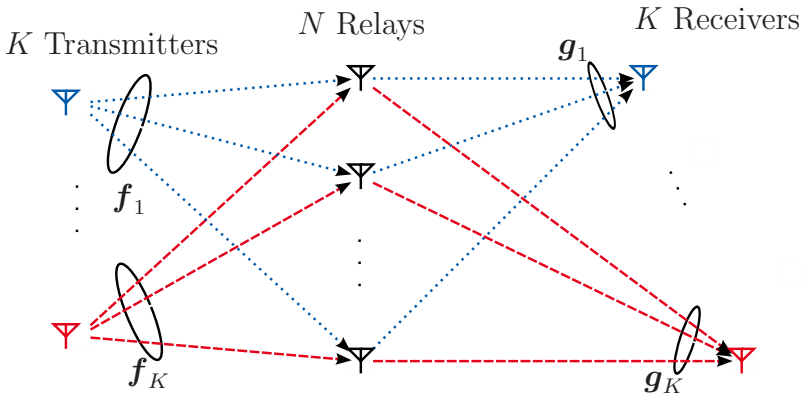

Figure 3.2. MUP2P wireless relay network.

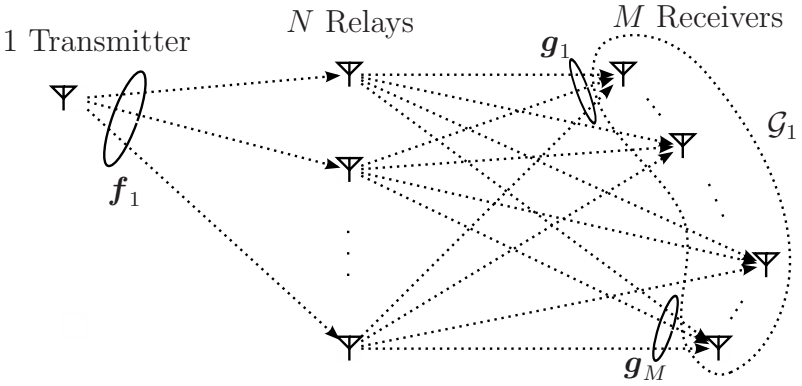

Figure 3.3. BC wireless relay network.

relay nodes help to establish the communication link by forwarding the messages of the source nodes to the destination nodes. Similar to the MGM downlink beamforming scenario of the previous chapter, each source serves one out of K disjoint multicast groups, $\{\mathcal{G}_1, \ldots, \mathcal{G}_K\}$, where $\mathcal{G}_k$ is the set of indices of the destination users intended to receive the message of the kth transmitter. The properties of $\mathcal{G}_k$ are identical to those of $\mathcal{G}_k$ of the previous chapter. Analogous to the MGM downlink beamforming scenarios, two special cases are included in this model, the MUP2P relay network of [28] and [30] for $K = M$ and the BC relay network for $K = 1$. These two special cases are depicted in Figs. 3.2 and 3.3, respectively. In the MUP2P scenario, each source transmits its information to a single destination only, while in the BC scenario, there is only a single source which broadcasts its information to all destination nodes.

In this section, we consider the two-step AF protocol [22], where in the first step, all transmitters broadcast their signals to the relays, and in the second step, each relay forwards an amplified and phase-adjusted version of its received signal to the

destinations. The received signals at the relays can be written as

$$\boldsymbol{r} = \sum_{k=1}^{K} \boldsymbol{f}_k s_k + \boldsymbol{\eta} \tag{3.1}$$

where $\boldsymbol{\eta} \triangleq [\eta_1, \ldots, \eta_N]^T$ is the relay noise vector, s_k is the complex information symbol transmitted by the kth source node, $\boldsymbol{f}_k \triangleq [f_{k,1}, \ldots, f_{k,N}]^T$, $f_{k,n}$ is the complex channel gain between the kth source node and the nth relay, $\boldsymbol{r} \triangleq [r_1, \ldots, r_N]^T$, and r_n is the signal observed at the nth relay. In the second step, the nth relay multiplies its received signal r_n by a complex weighting coefficient w_n^* and transmits the resulting signal x_n to the destination users. The multiplication by w_n^* is performed in digital baseband. The vector of signals transmitted by the relays can be written as

$$\boldsymbol{x} = \boldsymbol{W}^H \boldsymbol{r} \tag{3.2}$$

where $\boldsymbol{x} = [x_1, \ldots, x_N]^T$, $\boldsymbol{W} \triangleq \mathrm{diag}\{\boldsymbol{w}\}$, and $\boldsymbol{w} \triangleq [w_1, \ldots, w_N]^T$. Let the channel coefficient between the nth relay and the mth destination be denoted as $g_{m,n}$ and let $\boldsymbol{g}_m \triangleq [g_{m,1}, \ldots, g_{m,N}]^T$. Further, assume that the mth destination node belongs to multicast group $\mathcal{G}_d$ (i.e., $m \in \mathcal{G}_d$). Using (3.1) and (3.2), we can express the signal received at the mth destination node as

$$\begin{aligned} y_m &= \boldsymbol{g}_m^T \boldsymbol{x} + \nu_m = \boldsymbol{g}_m^T (\boldsymbol{W}^H \sum_{k=1}^{K} \boldsymbol{f}_k s_k + \boldsymbol{W}^H \boldsymbol{\eta}) + \nu_m \\ &= \underbrace{\boldsymbol{w}^H \boldsymbol{G}_m \boldsymbol{f}_d s_d}_{y_{\mathrm{S},m}} + \underbrace{\boldsymbol{w}^H \boldsymbol{G}_m \sum_{k \neq d} \boldsymbol{f}_k s_k}_{y_{\mathrm{I},m}} + \underbrace{\boldsymbol{w}^H \boldsymbol{G}_m \boldsymbol{\eta} + \nu_m}_{y_{\mathrm{N},m}} \end{aligned} \tag{3.3}$$

where $\boldsymbol{G}_m = \mathrm{diag}\{\boldsymbol{g}_m\}$, ν_m is the noise at the mth receiver, and $y_{\mathrm{S},m}$, $y_{\mathrm{I},m}$, and $y_{\mathrm{N},m}$ are the desired signal, the interference and the total noise components at the mth receiver, respectively.

The following common assumptions are used throughout the thesis [28], [30]:

A1: The symbols of different transmitters are zero-mean and mutually uncorrelated.

A2: The relay noise is spatially white and, for the sake of notational simplicity, all relays are assumed to have the same noise power. Note that our approach can be straightforwardly extended to the case where the latter assumption is relaxed.

A3: The information symbols, the relay noises and the receiver noises are mutually statistically independent.

A4: The kth source uses its maximum power P_k to transmit its symbol s_k, i.e., $\mathrm{E}\{|s_k|^2\} = P_k$.

Similar to Chapter 2 and as , e.g., in [28], we formulate the network beamformer design as the problem of minimizing the total power transmitted by the relays subject to QoS constraints. These constraints guarantee that the SINR at the receivers does not fall below certain QoS thresholds denoted by $\gamma_1, \ldots, \gamma_M$. Therefore, the goal is to solve the following optimization problem:

$$\min_{\boldsymbol{w}} \quad P_{\mathrm{T}} \tag{3.4a}$$

$$\text{subject to} \quad \mathrm{SINR}_m \geq \gamma_m, \ \forall m \in \mathcal{G}_d, \ \forall d \in \mathcal{K} \tag{3.4b}$$

where $\mathcal{K} = \{1, \ldots, K\}$ and SINR_m is the SINR at the mth receiver defined as

$$\mathrm{SINR}_m \triangleq \frac{\mathrm{E}\{|y_{\mathrm{S},m}|^2\}}{\mathrm{E}\{|y_{\mathrm{I},m}|^2\} + \mathrm{E}\{|y_{\mathrm{N},m}|^2\}}. \tag{3.5}$$

In (3.4), P_{T} is the total transmitted relay power given by

$$P_{\mathrm{T}} = \sum_{n=1}^{N} \mathrm{E}\left\{|x_n|^2\right\} = \sum_{n=1}^{N} |w_n|^2 \mathrm{E}\left\{|r_n|^2\right\} = \sum_{n=1}^{N} |w_n|^2 [\boldsymbol{R}_r]_{n,n} = \boldsymbol{w}^H \boldsymbol{D} \boldsymbol{w} \tag{3.6}$$

where $\boldsymbol{R}_r \triangleq \mathrm{E}\left\{\boldsymbol{r}\boldsymbol{r}^H\right\}$ is the correlation matrix of the relay received signals, $\boldsymbol{D}$ is the diagonal matrix with

$$[\boldsymbol{D}]_{n,n} = [\boldsymbol{R}_r]_{n,n} \tag{3.7}$$

and $[\boldsymbol{A}]_{n,n}$ denotes the nth diagonal entry of matrix $\boldsymbol{A}$. Using (3.1) and assumptions A1-A4, this correlation matrix can be written as

$$\boldsymbol{R}_r = \mathrm{E}\left\{ \left(\sum_{k=1}^{K} \boldsymbol{f}_k s_k + \boldsymbol{\eta} \right) \left(\sum_{k=1}^{K} \boldsymbol{f}_k s_k + \boldsymbol{\eta} \right)^H \right\} = \sum_{k=1}^{K} P_k \boldsymbol{f}_k \boldsymbol{f}_k^H + \sigma_\eta^2 \boldsymbol{I} \tag{3.8}$$

where σ_η^2 is the variance of the relay noise.

From (3.3), we next derive expressions for the desired signal power, the interference power, and the total noise power in (3.5). With assumptions A3 and A4, the desired signal power at the mth receiver is given by

$$\begin{aligned} \mathrm{E}\left\{|y_{\mathrm{S},m}|^2\right\} &= \mathrm{E}\left\{|s_d|^2\right\} \mathrm{E}\left\{(\boldsymbol{w}^H \boldsymbol{G}_m \boldsymbol{f}_d)(\boldsymbol{w}^H \boldsymbol{G}_m \boldsymbol{f}_d)^H\right\} \\ &= P_d \boldsymbol{w}^H \mathrm{E}\left\{\boldsymbol{h}_{d,m} \boldsymbol{h}_{d,m}^H\right\} \boldsymbol{w} = P_d \boldsymbol{w}^H \boldsymbol{h}_{d,m} \boldsymbol{h}_{d,m}^H \boldsymbol{w} = \boldsymbol{w}^H \boldsymbol{R}_{d,m} \boldsymbol{w} \end{aligned} \tag{3.9}$$

where $\boldsymbol{h}_{d,m} \triangleq \boldsymbol{G}_m \boldsymbol{f}_d$ and

$$\boldsymbol{R}_{d,m} \triangleq P_d \boldsymbol{h}_{d,m} \boldsymbol{h}_{d,m}^H. \tag{3.10}$$

Using assumptions A1, A3 and A4, the interference power at the mth receiver can be expressed as

$$\begin{aligned}\mathrm{E}\left\{|y_{\mathrm{I},m}|^2\right\} &= \boldsymbol{w}^H\left(\sum_{k\neq d}\mathrm{E}\left\{|s_k|^2\right\}\mathrm{E}\left\{(\boldsymbol{G}_m\boldsymbol{f}_k)(\boldsymbol{G}_m\boldsymbol{f}_k)^H\right\}\right)\boldsymbol{w}\\ &= \boldsymbol{w}^H\left(\sum_{k\neq d}P_k\boldsymbol{h}_{k,m}\boldsymbol{h}_{k,m}^H\right)\boldsymbol{w} = \boldsymbol{w}^H\boldsymbol{Q}_{\mathrm{I},m}\boldsymbol{w}\end{aligned} \tag{3.11}$$

where $\boldsymbol{h}_{k,m} \triangleq \boldsymbol{G}_m\boldsymbol{f}_k$ and $\boldsymbol{Q}_{\mathrm{I},m} \triangleq \sum_{k\neq d}P_k\boldsymbol{h}_{k,m}\boldsymbol{h}_{k,m}^H$. Finally, using assumptions A2 and A3, the total noise power at the mth receiver can be written as

$$\begin{aligned}\mathrm{E}\left\{|y_{\mathrm{N},m}|^2\right\} &= \mathrm{E}\left\{\boldsymbol{\eta}^H\boldsymbol{G}_m^H\boldsymbol{w}\boldsymbol{w}^H\boldsymbol{G}_m\boldsymbol{\eta}\right\} + \mathrm{E}\left\{|\nu_m|^2\right\}\\ &= \mathrm{tr}\left\{\mathrm{E}\left\{\boldsymbol{\eta}\boldsymbol{\eta}^H\right\}\mathrm{E}\left\{\boldsymbol{G}_m^H\boldsymbol{w}\boldsymbol{w}^H\boldsymbol{G}_m\right\}\right\} + \sigma_\nu^2\\ &= \sigma_\eta^2\boldsymbol{w}^H\boldsymbol{G}_m\boldsymbol{G}_m^H\boldsymbol{w} + \sigma_\nu^2 = \boldsymbol{w}^H\tilde{\boldsymbol{Q}}_{\mathrm{N},m}\boldsymbol{w} + \sigma_\nu^2\end{aligned} \tag{3.12}$$

where $\tilde{\boldsymbol{Q}}_{\mathrm{N},m}$ is the diagonal matrix with $[\tilde{\boldsymbol{Q}}_{\mathrm{N},m}]_{n,n} = \sigma_\eta^2[\boldsymbol{g}_m\boldsymbol{g}_m^H]_{n,n}$.

With (3.5), (3.6), and (3.9)-(3.12), the optimization problem in (3.4) can be written as

$$\min_{\boldsymbol{w}} \ \boldsymbol{w}^H\boldsymbol{D}\boldsymbol{w} \tag{3.13a}$$

$$\text{s.t.} \ \frac{\boldsymbol{w}^H\boldsymbol{R}_{d,m}\boldsymbol{w}}{\boldsymbol{w}^H(\boldsymbol{Q}_{\mathrm{I},m}+\tilde{\boldsymbol{Q}}_{\mathrm{N},m})\boldsymbol{w}+\sigma_\nu^2} \geq \gamma_m, \ \forall m \in \mathcal{G}_d, \ \forall d \in \mathcal{K}. \tag{3.13b}$$

3.2.1 Special Case 1: MUP2P Relay Network

As mentioned before, the MGM relay network contains the MUP2P relay network, that has been considered in [28] and [30] and is shown in Fig. 3.2, as a special case. It can be viewed as a MGM relay network where each multicast group contains only a single user. Hence, the QoS-constrained power minimization problem corresponding to the MUP2P relay network differs from problem (3.13) only in the indexing:

$$\min_{\boldsymbol{w}} \ \boldsymbol{w}^H\boldsymbol{D}\boldsymbol{w} \tag{3.14a}$$

$$\text{s.t.} \ \frac{\boldsymbol{w}^H\boldsymbol{R}_{d,d}\boldsymbol{w}}{\boldsymbol{w}^H(\boldsymbol{Q}_{\mathrm{I},m}+\tilde{\boldsymbol{Q}}_{\mathrm{N},m})\boldsymbol{w}+\sigma_\nu^2} \geq \gamma_d, \ \forall d \in \mathcal{K}. \tag{3.14b}$$

3.2.2 Special Case 2: BC Relay Network

The second special case contained in the MGM relay network is the BC relay network shown in Fig. 3.3. It can be interpreted as a single-group multicasting relay network where all destination nodes belong to the same single multicast group. Thus, again, the QoS-constrained power minimization problem corresponding to the BC relay network differs from problem (3.13) only in the indexing:

$$\min_{\boldsymbol{w}} \ \boldsymbol{w}^H \boldsymbol{D} \boldsymbol{w} \tag{3.15a}$$

$$\text{s.t.} \ \ \frac{\boldsymbol{w}^H \boldsymbol{R}_{1,m} \boldsymbol{w}}{\boldsymbol{w}^H (\boldsymbol{Q}_{\mathrm{I},m} + \tilde{\boldsymbol{Q}}_{\mathrm{N},m}) \boldsymbol{w} + \sigma_\nu^2} \geq \gamma_m, \ \forall m \in \mathcal{G}_1. \tag{3.15b}$$

3.3 Filter-and-Forward Beamforming

Let us now consider the more realistic signal model where the channels between the nodes in the network are subject to frequency selective fading causing ISI. We assume that in this case, the relays operate according to the FF protocol of [51] and [52] instead of the AF protocol. Recall that according to the AF protocol, the relays only apply a single weighting coefficient. According to the FF protocol, each relay filters its received signal using an FIR filter with adaptive filter coefficients and forwards the result to the destination nodes. This procedure is illustrated in Fig. 3.4 for a MUP2P relay network. The FIR filters at the relays are used in such a way that they have an equalizing effect on the overall channel between the sources and the destinations and mitigate the effect of ISI at the destination nodes. Compared to the considerations in the previous sections, we thus need to replace the frequency flat channel coefficients by frequency selective channel impulse responses (CIRs) and the single weighting coefficients at the relays by FIR filters. Let us now extend the signal model derived in the previous sections to the case where FF beamforming is performed.

Like in [52–56], we assume that the source-to-relay and the relay-to-destination CIRs can be modeled as FIR filters. Then, the vector $\boldsymbol{r}[n] = [r_1[n], \ldots, r_N[n]]^T$ of (3.1) containing the signals received by the relay nodes at sampling time n becomes

$$\boldsymbol{r}[n] = \sum_{k=1}^{K} \sum_{l=0}^{L_f - 1} \boldsymbol{f}_k[l] s_k[n-l] + \boldsymbol{\eta}[n] \tag{3.16}$$

where $s_k[n]$ is the complex information symbol transmitted by the kth source at time n, L_f is the length of the source-to-relay CIRs, $\boldsymbol{f}_k[l] \triangleq [f_{k,1}[l], \ldots, f_{k,N}[l]]^T$ is the $N \times 1$

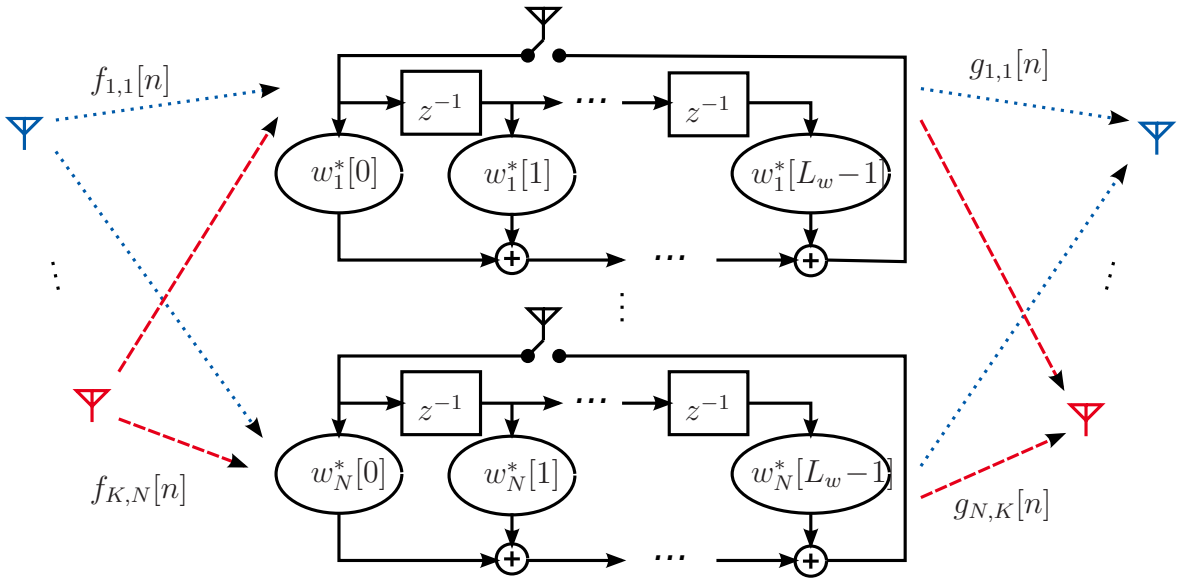

Figure 3.4. FF wireless relay network.

complex vector of lth effective filter taps of the channels between the kth source and the relays, and $\boldsymbol{\eta}[n] \triangleq [\eta_1[n], \ldots, \eta_N[n]]^T$ is the $N \times 1$ complex relay noise vector. Note that we now have to take into account the sampling time n which we could omit in (3.1). In (3.16), the summation over l represents the convolution between the signal transmitted by the kth source and the CIRs of the backward channels. The vector of signals transmitted by the relay nodes, i.e., (3.2), becomes

$$\boldsymbol{x}[n] = \sum_{l=0}^{L_w-1} \boldsymbol{W}^H[l]\boldsymbol{r}[n-l] \tag{3.17}$$

where $\boldsymbol{W}[l] \triangleq \text{diag}\{[w_1[l], \ldots, w_N[l]]\}$ and $w_i[l]$ is the lth complex valued effective filter tap of the FIR filter of length L_w employed at the ith relay. In the FF case, the signal received at the kth destination, i.e., (3.3), reads

$$y_m[n] = \sum_{l=0}^{L_g-1} \boldsymbol{g}_m^T[l]\boldsymbol{x}[n-l] + \nu_m[n] \tag{3.18}$$

where L_g is the length of the relay-to-destination CIRs, $\boldsymbol{g}_m[l] \triangleq [g_{m,1}[l], \ldots, g_{m,N}[l]]^T$, $g_{m,i}[l]$ is the lth complex valued effective filter tap of the channels between the ith relay and the mth destination, and $\nu_m[n]$ is the complex noise at the mth destination. Inserting (3.16) and (3.17) into (3.18) and following the derivations in [52], the latter

equation can be written as

$$y_m[n] = \boldsymbol{w}^H \boldsymbol{\mathcal{G}}_m \sum_{k=1}^{K} \boldsymbol{F}_k \boldsymbol{s}_k[n] + \boldsymbol{w}^H \boldsymbol{\mathcal{G}}_m \breve{\boldsymbol{I}} \breve{\boldsymbol{\eta}}[n] + \nu_m[n] \tag{3.19a}$$

where

$$\boldsymbol{s}_k[n] \triangleq [s_k[n], \ldots, s_k[n - L_f - L_w - L_g + 3]]^T \tag{3.19b}$$

$$\breve{\boldsymbol{\eta}}[n] \triangleq [\boldsymbol{\eta}^T[n], \ldots, \boldsymbol{\eta}^T[n - L_w - L_g + 2]]^T \tag{3.19c}$$

$$\boldsymbol{w} \triangleq [\boldsymbol{w}^T[0], \ldots, \boldsymbol{w}^T[L_w - 1]]^T \tag{3.19d}$$

$$\boldsymbol{w}[l] \triangleq \mathrm{diag}\{\boldsymbol{W}[l]\} \tag{3.19e}$$

$$\boldsymbol{\mathcal{G}}_m \triangleq [\boldsymbol{I}_{L_w} \otimes \mathrm{diag}\{\boldsymbol{g}_m[0]\}, \ldots, \boldsymbol{I}_{L_w} \otimes \mathrm{diag}\{\boldsymbol{g}_m[L_g - 1]\}] \tag{3.19f}$$

$$\boldsymbol{F}_k \triangleq [\boldsymbol{\mathcal{F}}_{k,0}^T, \ldots, \boldsymbol{\mathcal{F}}_{k,L_g-1}^T]^T \tag{3.19g}$$

$$\boldsymbol{\mathcal{F}}_{k,l} \triangleq [\boldsymbol{0}_{NL_w \times l}, \boldsymbol{\mathcal{F}}_k, \boldsymbol{0}_{NL_w \times (L_g-1-l)}] \tag{3.19h}$$

$$\boldsymbol{\mathcal{F}}_k \triangleq [\breve{\boldsymbol{F}}_{k,0}^T, \ldots, \breve{\boldsymbol{F}}_{k,L_w-1}^T]^T \tag{3.19i}$$

$$\breve{\boldsymbol{F}}_{k,l} \triangleq [\boldsymbol{0}_{N \times l}, \breve{\boldsymbol{F}}_k, \boldsymbol{0}_{N \times (L_w-1-l)}] \tag{3.19j}$$

$$\breve{\boldsymbol{F}}_k \triangleq [\boldsymbol{f}_k[0], \ldots, \boldsymbol{f}_k[L_f - 1]] \tag{3.19k}$$

$$\breve{\boldsymbol{I}} \triangleq [\breve{\boldsymbol{I}}_0^T, \ldots, \breve{\boldsymbol{I}}_{L_g-1}^T]^T \tag{3.19l}$$

$$\breve{\boldsymbol{I}}_l \triangleq [\boldsymbol{0}_{NL_w \times Nl}, \boldsymbol{I}_{NL_w}, \boldsymbol{0}_{NL_w \times N(L_g-1-l)}]. \tag{3.19m}$$

We observe from (3.19) that, due to multipath propagation and FIR filtering at the relays, the signal $y_m[n]$ received at the mth destination at time n depends on the symbol transmitted from the dth source at time n as well as symbols transmitted in previous time slots. We remark that an arbitrary element of $\boldsymbol{s}_d[n]$, say $s_d[n - l_m]$, can be selected as the desired symbol for the mth destination where l_m can be different for each destination. In Chapter 9, we optimize the selection of the desired symbol at the destinations, i.e., we optimize individual adaptive decoding delays at the destinations. For now, however, let us assume as in [51–54] that the decoding delays are not adaptive and that the center element of $\boldsymbol{s}_d[n]$ is selected as the desired symbol for all destinations as in [54]. Thus, $l_m \triangleq \lfloor (L_f + L_w + L_g - 2)/2 \rfloor$, $\forall m \in \{1, \ldots, M\}$ where l_m is the decoding delay employed at the mth destination. In this dissertation, like in [52, 54, 56], we consider a simple symbol-by-symbol decoder rather than the more complex equalizer receiver considered in [55] which requires block processing of the received symbols. Thus, we consider all remaining entries of $\boldsymbol{s}_d[n]$ as ISI.

Let the convolution matrix corresponding to the CIR of the combined (source-to-relay and relay-to-destination) channel be denoted as $\boldsymbol{H}_{d,m} \triangleq \boldsymbol{\mathcal{G}}_m \boldsymbol{F}_d$. Further, let us define $\boldsymbol{\vartheta}_{d,m,l_m}$ as the (l_m+1)th column of $\boldsymbol{H}_{d,m}$ and let $\bar{\boldsymbol{H}}_{m,l_m,1}$ and $\bar{\boldsymbol{H}}_{m,l_m,2}$ denote the residues

of $\boldsymbol{H}_{d,m}$ so that $\boldsymbol{H}_{d,m} = [\bar{\boldsymbol{H}}_{d,m,l_m,1}, \boldsymbol{\vartheta}_{d,m,l_m}, \bar{\boldsymbol{H}}_{d,m,l_m,2}]$. Then, (3.19) can be written as

$$\begin{aligned} y_m[n] &= \boldsymbol{w}^H [\bar{\boldsymbol{H}}_{d,m,l_m,1}, \boldsymbol{\vartheta}_{d,m,l_m}, \bar{\boldsymbol{H}}_{d,m,l_m,2}] \begin{bmatrix} \bar{\boldsymbol{s}}_{d,l_m,1}[n] \\ s_d[n-l_m] \\ \bar{\boldsymbol{s}}_{d,l_m,2}[n] \end{bmatrix} \\ &\quad + \sum_{k=1,k\neq d}^{K} \boldsymbol{w}^H \boldsymbol{\mathcal{G}}_m \boldsymbol{F}_k \boldsymbol{s}_k[n] + \boldsymbol{w}^H \boldsymbol{\mathcal{G}}_m \breve{\boldsymbol{I}} \breve{\boldsymbol{\eta}}[n] + \nu_m[n] \\ &= y_{\mathrm{S},m}[n] + y_{\mathrm{ISI},m}[n] + y_{\mathrm{MUI},m}[n] + y_{\mathrm{N},m}[n] \end{aligned} \tag{3.20}$$

where

$$\begin{aligned} \bar{\boldsymbol{s}}_{d,l_m,1}[n] &\triangleq [s_d[n], \ldots, s_d[n-l_m+1]]^T \\ \bar{\boldsymbol{s}}_{d,l_m,2}[n] &\triangleq [s_d[n-l_m-1], \ldots, s_d[n-L_f-L_w-L_g+3]]^T \end{aligned}$$

and

$$y_{\mathrm{S},m}[n] \triangleq \boldsymbol{w}^H \boldsymbol{\vartheta}_{d,m,l_m} s_d[n-l_m] \tag{3.21a}$$

$$y_{\mathrm{ISI},m}[n] \triangleq \boldsymbol{w}^H \bar{\boldsymbol{H}}_{d,m,l_m} \bar{\boldsymbol{s}}_{d,l_m}[n] \tag{3.21b}$$

$$y_{\mathrm{MUI},m}[n] \triangleq \sum_{k=1,k\neq d}^{K} \boldsymbol{w}^H \boldsymbol{\mathcal{G}}_m \boldsymbol{F}_k \boldsymbol{s}_k[n] \tag{3.21c}$$

$$y_{\mathrm{N},m}[n] \triangleq \boldsymbol{w}^H \boldsymbol{\mathcal{G}}_m \breve{\boldsymbol{I}} \breve{\boldsymbol{\eta}}[n] + \nu_m[n] \tag{3.21d}$$

represent the desired symbol, ISI, multi-user interference (MUI), and noise components at the mth destination, respectively. In (3.21b), $\bar{\boldsymbol{H}}_{d,m,l_m} \triangleq [\bar{\boldsymbol{H}}_{d,m,l_m,1}, \bar{\boldsymbol{H}}_{d,m,l_m,2}]$ and $\bar{\boldsymbol{s}}_{d,m,l_m}[n] \triangleq [\bar{\boldsymbol{s}}^T_{d,m,l_m,1}[n], \bar{\boldsymbol{s}}^T_{d,m,l_m,2}[n]]^T$.

Our goal is again to solve the QoS-constrained power minimization problem of (3.4) where, however, we have to adapt the definitions of P_{T} and SINR_m to the FF scenario which we do next. It has been shown in [52] and [54] that under the assumptions A1 and A2,

$$P_{\mathrm{T}} = \sum_{i=1}^{N} p_i = \sum_{i=1}^{N} \mathrm{E}\{|x_i[n]|^2\} = \boldsymbol{w}^H \boldsymbol{D} \boldsymbol{w} \tag{3.22}$$

where

$$\boldsymbol{D} \triangleq \sum_{i=1}^{N} \boldsymbol{D}_i, \tag{3.23a}$$

$$\boldsymbol{D}_i \triangleq \sum_{k=1}^{K} P_k (\boldsymbol{I}_{L_w} \otimes \boldsymbol{E}_i) \boldsymbol{\mathcal{F}}_k \boldsymbol{\mathcal{F}}_k^H (\boldsymbol{I}_{L_w} \otimes \boldsymbol{E}_i)^H + \sigma_\eta^2 (\boldsymbol{I}_{L_w} \otimes \boldsymbol{E}_i)(\boldsymbol{I}_{L_w} \otimes \boldsymbol{E}_i)^H, \tag{3.23b}$$

$\boldsymbol{E}_i \triangleq \mathrm{diag}\{\boldsymbol{e}_i\}$, and $\boldsymbol{e}_i$ is the ith column of $\boldsymbol{I}_N$. The SINR at the mth destination can be written as

$$\mathrm{SINR}_m = \frac{\mathrm{E}\{|y_{\mathrm{S},m}[n]|^2\}}{\mathrm{E}\{|y_{\mathrm{ISI},m}[n]|^2\} + \mathrm{E}\{|y_{\mathrm{MUI},m}[n]|^2\} + \mathrm{E}\{|y_{\mathrm{N},m}[n]|^2\}} \tag{3.24}$$

Making use of (3.21a), we obtain that

$$\begin{aligned} \mathrm{E}\{|y_{\mathrm{S},m}[n]|^2\} &= \mathrm{E}\{\boldsymbol{w}^H \boldsymbol{\vartheta}_{d,m,l_m} s_d[n-l_m] s_d^*[n-l_m] \boldsymbol{\vartheta}_{d,m,l_m}^H \boldsymbol{w}\} \\ &= \boldsymbol{w}^H \boldsymbol{R}_{d,m} \boldsymbol{w} \end{aligned} \tag{3.25}$$

where

$$\boldsymbol{R}_{d,m} \triangleq P_d \boldsymbol{\vartheta}_{d,m,l_m} \boldsymbol{\vartheta}_{d,m,l_m}^H. \tag{3.26}$$

Similarly, using (3.21b)-(3.21d) and following the derivations in [52], we obtain

$$\mathrm{E}\{|y_{\mathrm{ISI},m}[n]|^2\} = \boldsymbol{w}^H \boldsymbol{Q}_{\mathrm{ISI},d,m} \boldsymbol{w} \tag{3.27a}$$

$$\mathrm{E}\{|y_{\mathrm{MUI},m}[n]|^2\} = \boldsymbol{w}^H \boldsymbol{Q}_{\mathrm{MUI},m} \boldsymbol{w} \tag{3.27b}$$

$$\mathrm{E}\{|y_{\mathrm{N},m}[n]|^2\} = \boldsymbol{w}^H \boldsymbol{Q}_{\mathrm{N},m} \boldsymbol{w} + \sigma_\nu^2 \tag{3.27c}$$

where

$$\boldsymbol{Q}_{\mathrm{ISI},d,m} \triangleq P_d \bar{\boldsymbol{H}}_{d,m,l_m} \bar{\boldsymbol{H}}_{d,m,l_m}^H \tag{3.28a}$$

$$\boldsymbol{Q}_{\mathrm{MUI},m} \triangleq \sum_{k=1,k\neq d}^{K} P_k \boldsymbol{\mathcal{G}}_m \boldsymbol{F}_k \boldsymbol{F}_k^H \boldsymbol{\mathcal{G}}_m^H \tag{3.28b}$$

$$\boldsymbol{Q}_{\mathrm{N},m} \triangleq \sigma_\eta^2 \boldsymbol{\mathcal{G}}_m \breve{\boldsymbol{I}} \breve{\boldsymbol{I}}^H \boldsymbol{\mathcal{G}}_m^H. \tag{3.28c}$$

Inserting (3.22)-(3.27) into problem (3.4), the latter problem becomes

$$\min_{\boldsymbol{w}} \ \boldsymbol{w}^H \boldsymbol{D} \boldsymbol{w} \tag{3.29a}$$

$$\text{s.t.} \ \frac{\boldsymbol{w}^H \boldsymbol{R}_{d,m} \boldsymbol{w}}{\boldsymbol{w}^H (\boldsymbol{Q}_{\mathrm{ISI},d,m} + \boldsymbol{Q}_{\mathrm{MUI},m} + \boldsymbol{Q}_{\mathrm{N},m}) \boldsymbol{w} + \sigma_\nu^2} \geq \gamma_m, \ \forall m \in \mathcal{G}_d, \ \forall d \in \mathcal{K}. \tag{3.29b}$$

In spite of the different nature of the FF protocol as compared to the AF protocol, problem (3.29) looks surprisingly similar to problem (3.13) from a mathematical point of view. There are only two main differences: Firstly, the optimization variable of (3.29) exhibits a larger dimension than that of (3.13) since it comprises multiple FIR filter coefficients per relay rather than only a single weighting coefficient. Secondly, problem (3.29) exhibits $\boldsymbol{w}^H \boldsymbol{Q}_{\mathrm{ISI},d,m} \boldsymbol{w}$ as an additional interference term accounting for ISI. However, problems (3.13) and (3.29) mathematically belong to the same class of nonconvex problems. Therefore, we now combine all problems derived in this chapter in one common generalized problem formulation.

3.4 Generalized Problem Formulation

Problems (3.13), (3.14), (3.15), and (3.29) can be combined in the following common generalized problem

$$\min_{\boldsymbol{w}} \ \boldsymbol{w}^H \boldsymbol{D} \boldsymbol{w} \tag{3.30a}$$

$$\text{s.t.} \ \ \frac{\boldsymbol{w}^H \boldsymbol{R}_{d,m} \boldsymbol{w}}{\boldsymbol{w}^H \boldsymbol{Q}_m \boldsymbol{w} + \sigma_\nu^2} \geq \gamma_m, \ \forall m \in \mathcal{G}_d, \ \forall d \in \mathcal{K}. \tag{3.30b}$$

where, depending on whether the AF or the FF protocol is considered, $\boldsymbol{w} \in \{\mathbb{C}^N\}$ or $\boldsymbol{w} \in \{\mathbb{C}^{L_w N}\}$, $\boldsymbol{D}$ is either defined as in (3.7) or in (3.23), $\boldsymbol{R}_{d,m}$ is either defined as in (3.10) or in (3.26), and $\boldsymbol{Q}_m$ is either defined as

$$\boldsymbol{Q}_m \triangleq \boldsymbol{Q}_{\mathrm{I},m} + \tilde{\boldsymbol{Q}}_{\mathrm{N},m} \tag{3.31}$$

or as

$$\boldsymbol{Q}_m \triangleq \boldsymbol{Q}_{\mathrm{ISI},d,m} + \boldsymbol{Q}_{\mathrm{MUI},m} + \boldsymbol{Q}_{\mathrm{N},m}. \tag{3.32}$$

The MUP2P beamforming problem (3.14), which has been considered in [28] and [30], has been shown to be generally non-convex in [28]. The same holds true for the more general problem (3.30): Since $\boldsymbol{w}^H \boldsymbol{Q}_m \boldsymbol{w} + \sigma_\nu^2 \geq 0$, problem (3.30) is equivalent to

$$\min_{\boldsymbol{w}} \ \boldsymbol{w}^H \boldsymbol{D} \boldsymbol{w} \tag{3.33a}$$

$$\text{s.t.} \ \ \boldsymbol{w}^H \boldsymbol{T}_{d,m} \boldsymbol{w} \geq \gamma_m \sigma_\nu^2, \ \forall m \in \mathcal{G}_d, \ \forall d \in \mathcal{K} \tag{3.33b}$$

where $\boldsymbol{T}_{d,m} \triangleq (\boldsymbol{R}_{d,m} - \gamma_m \boldsymbol{Q}_m)$. Each QoS constraint in (3.33) describes a super-level set of a quadratic function [62]. As mentioned earlier, such a set is only convex if the quadratic function is concave and, hence, negative semi-definiteness of the matrices $\boldsymbol{T}_{d,m}, \ \forall m \in \mathcal{G}_d, \ \forall d \in \mathcal{K}$ is required for problem (3.33) to be convex. We remark that in this case, the feasible set is empty as $\boldsymbol{w}^H \boldsymbol{T}_{d,m} \boldsymbol{w} \leq 0, \ \forall m \in \mathcal{G}_d, \ \forall d \in \mathcal{K}$, and for all $\boldsymbol{w}$. As a consequence, problem (3.30) is non-convex and NP-hard. However, problem (3.30) can be solved approximately. In Chapter 4, we briefly revisit state-of-the-art methods, which have been proposed to obtain such an approximate solution using an outer approximation of the feasible set, while in Chapter 5, we propose a novel method based on inner approximations of the feasible set to obtain an approximate solution.

Note that in practice, the relays can be hand-held devices of mobile users with a limited battery lifetime. These users may not be interested in assisting transmission if the power consumption of their devices is too high. Then, it may not be sufficient to minimize the total transmitted relay power. In addition, the individual transmitted relay powers have to be kept below certain thresholds. According to [30], this can be

accomplished by adding individual power constraints to problem (3.30). In the AF relaying case, the power transmitted by the ith relay can be written as

$$p_i = \mathrm{E}\left\{|x_i|^2\right\} = |w_i|^2 \mathrm{E}\left\{|r_i|^2\right\} = \boldsymbol{w}^H \boldsymbol{D}_i \boldsymbol{w}$$

where

$$\boldsymbol{D}_i \triangleq \boldsymbol{E}_i \boldsymbol{D}. \tag{3.34}$$

It has been shown in [52] that the power of the ith relay in the FF relaying case can be written as

$$p_i = \mathrm{E}\{|x_i[n]|^2\} = \boldsymbol{w}^H \boldsymbol{D}_i \boldsymbol{w}.$$

where $\boldsymbol{D}_i$ is defined as in (3.23b). Let $\mathcal{I}$ stand for the set of indexes of relays for which an individual power constraint is required. Such a constraints for each relay in $\mathcal{I}$ can then be added to problem (3.30) as follows

$$\begin{aligned} \min_{\boldsymbol{w}} \quad & \boldsymbol{w}^H \boldsymbol{D} \boldsymbol{w} && \text{(3.35a)} \\ \text{s.t.} \quad & \boldsymbol{w}^H \boldsymbol{D}_i \boldsymbol{w} \leq p_{i,\max}, \ \forall i \in \mathcal{I}, && \text{(3.35b)} \\ & (3.30b) && \text{(3.35c)} \end{aligned}$$

where the maximum power at which the ith relay is allowed to transmit is denoted by $p_{i,\max}$ and $\boldsymbol{D}_i$ is either defined as in (3.34) or as in (3.23b). In this thesis, we have only considered the case where $\mathcal{I} = \emptyset$. However, as the constraints in (3.35b) are convex constraints, all concepts presented in this dissertation are straightforwardly extendable to the general case of arbitrary $\mathcal{I}$.

Following, e.g., [25, 28, 30, 53], we assume availability of the instantaneous CSI (i.e., the channel vectors $\boldsymbol{f}_k$ and $\boldsymbol{g}_m$ in case of AF relaying or $\boldsymbol{f}_k[n]$ and $\boldsymbol{g}_m[n]$ in case of FF relaying) of the whole network at the processing nodes. For example, this CSI may be available at the relays which are then able to compute their weighting coefficients themselves. Since we aim to optimize all the relay weights jointly, each relay has to compute all the weights and then use its own one. Thus, the relays are not able to share the computational load in this kind of distributed processing. It may also be possible that this CSI is available at a single processing node which computes the relay weights and distributes them to the relays. Note that despite such kind of centralized processing, the beamforming scheme can be regarded as a distributed one since the relays do not process their received signals jointly. Therefore, it should not be confused with the case of a single relay equipped with N antennas (see, e.g., [48] and [46]) which is fundamentally different since the multi-antenna relay has access to all the signals received at each antenna. In the next section, we address difficulties to acquire the CSI of the whole network at the processing node(s) in practice.

3.5 Statistical CSI

In the previous sections, the availability of instantaneous CSI of the whole relay network at one or more processing nodes in the network is assumed. However, instantaneous CSI is even more difficult to acquire in relay networks than in the cellular downlink scenario of Chapter 2: At each node in the network, the instantaneous channels corresponding to that node need to be estimated and the resulting estimates have to be transmitted to the processing node(s). Furthermore, if the beamforming or FIR filter coefficients are computed at a single central processing node, this node has to inform the relays about the beamforming coefficients or FIR filter coefficients to use. This may cause a prohibitive signaling overhead especially in fast fading scenarios. Like in the cellular downlink scenario, the second-order statistics of the channels, however, usually evolve at a significantly lower rate than the corresponding instantaneous channel realizations. Therefore, like conventional downlink beamformer designs, distributed beamformer designs based on statistical CSI are associated with a significantly reduced signaling overhead [26] and, similar to Section 2.3, we now assume that only statistical CSI is available at the processing node(s) as in [26]. Again, we need to redefine matrices: $\boldsymbol{D}$, $\boldsymbol{R}_{d,m}$, $\boldsymbol{Q}_{\mathrm{I},m}$, $\tilde{\boldsymbol{Q}}_{\mathrm{N},m}$, $\boldsymbol{Q}_{\mathrm{ISI},d,m}$, $\boldsymbol{Q}_{\mathrm{MUI},m}$, and $\boldsymbol{Q}_{\mathrm{N},m}$ have to be redefined as follows.

$\boldsymbol{D}$ is the diagonal matrix with $[\boldsymbol{D}]_{n,n} = [\boldsymbol{R}_r]_{n,n}$ and $\boldsymbol{R}_r$ is defined as $\boldsymbol{R}_r \triangleq \sum_{k=1}^{K} P_k \mathrm{E}\left\{\boldsymbol{f}_k \boldsymbol{f}_k^H\right\} + \sigma_\eta^2 \boldsymbol{I}$, $\boldsymbol{R}_{d,m} \triangleq P_d \mathrm{E}\left\{\boldsymbol{h}_{d,m}\boldsymbol{h}_{d,m}^H\right\}$, $\boldsymbol{Q}_{\mathrm{I},m} \triangleq \sum_{k\neq d} P_k \mathrm{E}\left\{\boldsymbol{h}_{k,m}\boldsymbol{h}_{k,m}^H\right\}$, and $\tilde{\boldsymbol{Q}}_{\mathrm{N},m}$ is the diagonal matrix with $[\tilde{\boldsymbol{Q}}_{\mathrm{N},m}]_{n,n} \triangleq \sigma_\eta^2 \left[\mathrm{E}\left\{\boldsymbol{g}_m \boldsymbol{g}_m^H\right\}\right]_{n,n}$. In case of FF relaying,

$$\boldsymbol{D}_i \triangleq \sum_{k=1}^{K} P_k (\boldsymbol{I}_{L_w} \otimes \boldsymbol{E}_i) \mathrm{E}\left\{\boldsymbol{\mathcal{F}}_k \boldsymbol{\mathcal{F}}_k^H\right\} (\boldsymbol{I}_{L_w} \otimes \boldsymbol{E}_i)^H + \sigma_\eta^2 (\boldsymbol{I}_{L_w} \otimes \boldsymbol{E}_i)(\boldsymbol{I}_{L_w} \otimes \boldsymbol{E}_i)^H,$$

$\boldsymbol{R}_{d,m} \triangleq P_d \mathrm{E}\left\{\boldsymbol{\vartheta}_{d,m,l_m} \boldsymbol{\vartheta}_{d,m,l_m}^H\right\}$, $\boldsymbol{Q}_{\mathrm{ISI},d,m} \triangleq P_d \mathrm{E}\left\{\bar{\boldsymbol{H}}_{d,m,l_m} \bar{\boldsymbol{H}}_{d,m,l_m}^H\right\}$, $\boldsymbol{Q}_{\mathrm{MUI},m} \triangleq \sum_{k=1,k\neq d}^{K} P_k \mathrm{E}\left\{\boldsymbol{\mathcal{G}}_m \boldsymbol{F}_k \boldsymbol{F}_k^H \boldsymbol{\mathcal{G}}_m^H\right\}$, and $\boldsymbol{Q}_{\mathrm{N},m} \triangleq \sigma_\eta^2 \mathrm{E}\left\{\boldsymbol{\mathcal{G}}_m \breve{\boldsymbol{I}} \breve{\boldsymbol{I}}^H \boldsymbol{\mathcal{G}}_m^H\right\}$. Note that, similar to Section 2.3, the matrix $\boldsymbol{R}_{d,m}$ is of higher rank in case of statistical CSI. Further note that the general problem (3.30) remains the same in this case where, however, the definitions of the involved matrices change as described above.

Chapter 4

State-of-the-Art Methods

4.1 Introduction

As mentioned in the previous chapters, problems (2.9), (2.14), (3.30), (3.14), and (3.15) are nonconvex and NP-hard. However, efficiently solvable convex approximations of the underlying nonconvex problems have been proposed in [16, 17, 28, 52]. These approximations are based on a semi-definite relaxation (SDR) where the originally nonconvex feasible set is approximated by a convex one which contains the original feasible set as a subset, i.e., a convex outer approximation is used. In this way, the originally nonconvex optimization problem is approximated by a semi-definite programming (SDP) problem which is efficiently solvable using interior-point methods [62]. Due to the relaxation involved, the optimal solution of the SDP is not necessarily feasible for the original problem. In [16,17,28,52], randomization techniques are therefore used where multiple candidate beamforming vectors are generated from the optimal solution of the SDP problem. The candidate beamforming vector yielding the best approximate solution for the original problem is then used as the final beamforming vector. Note, however, that a feasible solution for the original problem cannot always be obtained in this way and that the obtained solution is generally suboptimal for the original problem. These SDR-based techniques shall be briefly introduced in this chapter. Due to the slightly simpler mathematical structure of problem (3.30) as compared to problem (2.9), we start with the distributed beamforming scenario and the downlink beamforming counterpart will be discussed afterwards.

An iterative linearization approach has been proposed in [45] as an alternative to the SDR-based approach for a max-min fair relay beamforming problem. In the approach of [54], the nonconvex functions in the original problem are linearized to approximate them by convex functions yielding a convex QCQP problem. In each iteration of the approach of [45], the nonconvex functions are linearized around the approximate solution of the previous iteration. In this chapter, we briefly describe this approach applied to the QoS-constrained power minimization problem. The iterative linearization approach of [45] is described using the example of distributed beamforming. We do not describe this approach for downlink beamforming as it is very similar in the latter case.

4.2 SDR-Based Approach - Distributed Beamforming

According to [28], we can introduce the new optimization variable $\boldsymbol{X} \triangleq \boldsymbol{w}\boldsymbol{w}^H$ and rewrite problem (3.33) as

$$\min_{\boldsymbol{X}} \ \mathrm{tr}(\boldsymbol{D}\boldsymbol{X}) \tag{4.1a}$$

$$\text{s.t.} \ \ \mathrm{tr}(\boldsymbol{T}_{d,m}\boldsymbol{X}) \geq \gamma_m \sigma_\nu^2, \ \forall m \in \mathcal{G}_d, \ \forall d \in \mathcal{K} \tag{4.1b}$$

$$\boldsymbol{X} \succeq 0, \quad \mathrm{rank}(\boldsymbol{X}) = 1. \tag{4.1c}$$

This problem can be relaxed by dropping the last non-convex rank-one constraint $\mathrm{rank}(\boldsymbol{X}) = 1$. This leads to the following convex SDP problem solvable by interior-point methods [62]:

$$\min_{\boldsymbol{X}} \ \mathrm{tr}(\boldsymbol{D}\boldsymbol{X}) \tag{4.2a}$$

$$\text{s.t.} \ \ \mathrm{tr}(\boldsymbol{T}_{d,m}\boldsymbol{X}) \geq \gamma_m \sigma_\nu^2, \ \forall m \in \mathcal{G}_d, \ \forall d \in \mathcal{K} \tag{4.2b}$$

$$\boldsymbol{X} \succeq 0. \tag{4.2c}$$

Obviously, if the solution matrix $\boldsymbol{X}_{\mathrm{opt}}$ of problem (4.2) is rank-one, it is also optimal for the original non-relaxed problem (4.1) and the solution of problem (3.30) can be obtained from the principal component of $\boldsymbol{X}_{\mathrm{opt}}$. Due to the relaxation, $\boldsymbol{X}_{\mathrm{opt}}$ generally will not be rank-one which is commonly observed in multicast beamforming scenarios. In this case, the so-called randomization techniques are discussed in [16,28] that can be used to obtain an approximate solution for the original problem (3.30). Basically, these techniques randomly generate multiple candidate beamforming vectors from $\boldsymbol{X}_{\mathrm{opt}}$ and then scale them such that the QoS constraint of problem (3.30), which is most difficult to satisfy, is satisfied with equality. This guarantees that, for a particular candidate, all QoS constraints are satisfied with the least possible total transmitted relay power. The scaled candidate yielding the smallest objective value for problem (3.30) is then chosen as a proper sub-optimal solution. However, in the case when $\boldsymbol{X}_{\mathrm{opt}}$ is far from being rank-one, e.g., if more than one of its eigenvalues are significantly large, it may turn out that none of the generated candidates is feasible after scaling. Then, such a sub-optimal solution cannot be found via randomization. Note that this approach is applicable independent of the rank of the matrix $\boldsymbol{R}_{d,m}$ in (3.30), i.e., it is applicable to both instantaneous and statistical CSI.

A byproduct of the SDR approach is the total transmitted relay power corresponding to the solution $\boldsymbol{X}_{\mathrm{opt}}$ of the relaxed problem (4.2). Due to the relaxation, $\boldsymbol{X}_{\mathrm{opt}}$ provides

a lower bound on the transmitted power and it is thus a valuable benchmark which we display in our simulations. Note that this lower bound is generally non-achievable as the solution $\boldsymbol{X}_{\text{opt}}$ usually lies outside the feasible set of the original problem (3.30).

For a better comprehension of the effects of SNR and randomization, let us have a look at the schematic visualization in Fig. 4.1. The large light gray area illustrates the original, nonconvex feasible set. The larger and darker gray area depicts the convex outer approximation of the original feasible set which is obtained by relaxing the original feasible set using the SDR. The grid of dashed circles represents the level curves of the objective function. The smaller the radius of a level curve, the smaller the value of the objective function. Hence, the upper vertex of the original feasible set is the global optimum of the original problem while the lower vertex is only a local optimum. The optimal solution $\boldsymbol{X}_{\text{opt}}$ of problem (4.2) is indicated by a dot that is located at the point within the outer approximation of the feasible set where the objective function is smallest. As we can see, it is located outside the original feasible set. Using the randomization technique, candidate beamforming vectors in the vicinity of $\boldsymbol{X}_{\text{opt}}$ are generated. Two of them are shown in Fig. 4.1. They may not yet be located inside the original feasible set either. Therefore, they are scaled such that they just satisfy the QoS constraints of the original problem and as a consequence, are inside (at the border of) the original feasible set. The scaling is indicated by arrows. Finally, the scaled candidate yielding the smallest objective value is chosen as an approximate solution for the original problem. In this example, it is the upper left candidate. In practice, of course, a lot more random candidate vectors are generated, usually several hundred.

4.3 SDR-Based Approach - Downlink Beamforming

In MGM downlink beamforming, the state-of-the-art SDR-based method is very similar to the one described in the previous section especially in the spacial case of BC downlink beamforming. Let us therefore consider the special case of BC downlink beamforming first.

4.3.1 Special Case 2: BC Downlink Beamforming

For the BC downlink beamforming problem, a SDR approach has been proposed in [16]. It can be derived in the same way as the SDR approach of the previous section:

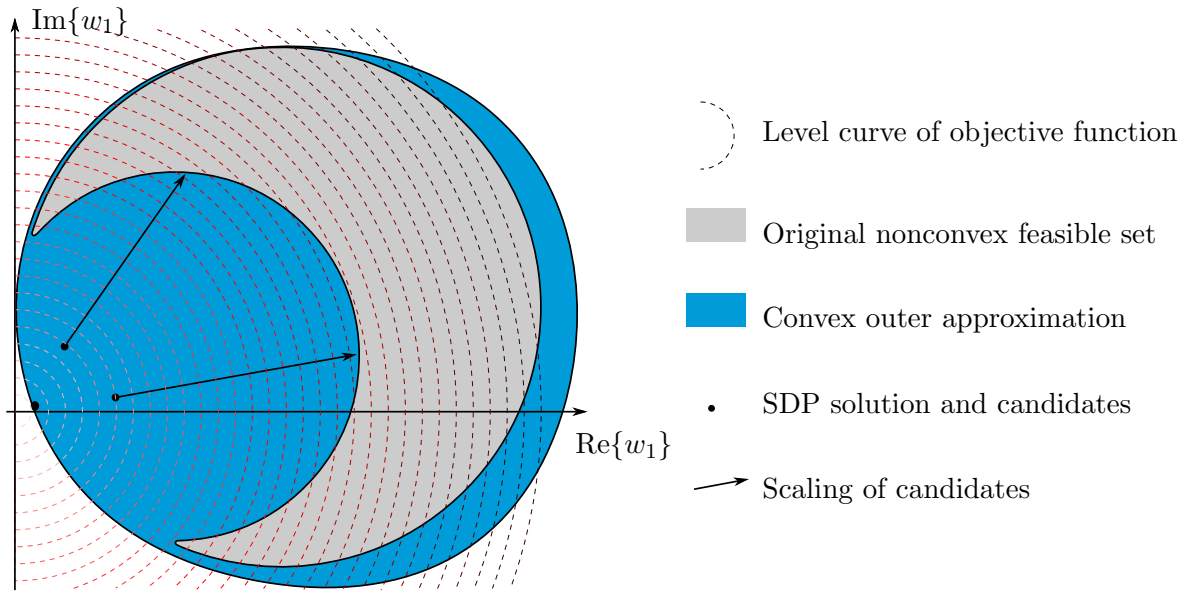

Figure 4.1. Visualization of the state-of-the-art SDR-based approach with randomization.

Introducing the new optimization variable $\boldsymbol{X}_1 \triangleq \boldsymbol{w}_1\boldsymbol{w}_1^H$ and following the derivations of the previous section, problem (2.14) can be approximated by the following convex SDP

$$\min_{\boldsymbol{X}_1} \ \operatorname{tr}(\boldsymbol{X}_1) \tag{4.3a}$$

$$\text{s.t.} \ \ \operatorname{tr}(\boldsymbol{C}_m\boldsymbol{X}_1) \geq \gamma_m\sigma_m^2, \ \forall m \in \{1,\ldots,M\} \tag{4.3b}$$

$$\boldsymbol{X}_1 \succeq 0. \tag{4.3c}$$

From the optimal solution of problem (4.3), a feasible solution for the original problem (2.14) can be obtained using a randomization technique and scaling the candidate beamforming vectors such that they satisfy the QoS constraints in problem (2.14) exactly as described in the previous section [16]. Again, $\operatorname{tr}(\boldsymbol{X}_{1,\text{opt}})$ provides a lower bound on the total transmitted power which we use as a benchmark in our simulations.

4.3.2 MGM Downlink Beamforming

Let us now briefly revisit the SDR approach for the more general MGM downlink beamforming problem (2.9) as proposed in [17]. Different from problems (3.30) and (2.14), problem (2.9) exhibits multiple beamforming vectors, one for each multicast group. Hence, in this case, multiple new optimization variables $\{\boldsymbol{X}_k \triangleq \boldsymbol{w}_k\boldsymbol{w}_k^H\}_{k=1}^K$

need to be introduced. However, the derivations are again similar to those in the previous section yielding the following convex SDP approximation of problem (2.9)

$$\min_{\{\boldsymbol{X}\}_{k=1}^{K}} \quad \sum_{k=1}^{K} \mathrm{tr}(\boldsymbol{X}_k) \tag{4.4a}$$

$$\text{s.t.} \quad \mathrm{tr}(\boldsymbol{C}_m \boldsymbol{X}_d) - \gamma_m \sum_{k \neq d} \mathrm{tr}(\boldsymbol{C}_m \boldsymbol{X}_k) \geq \gamma_m \sigma_m^2, \ \forall m \in \mathcal{G}_d, \ \forall d, k \in \mathcal{K}, \tag{4.4b}$$

$$\boldsymbol{X}_k \succeq 0, \ \forall k \in \mathcal{K}. \tag{4.4c}$$

After solving problem (4.4), a randomization technique is applied in the approach proposed in [17] as well. However, there is a main difference when it comes to scaling the power of the candidate beamforming vectors to satisfy the QoS constraints of the original problem (2.9): The candidate beamforming vectors cannot simply be scaled since boosting the beamforming vector of one group also increases the interference caused to users in other groups. Therefore, rather than scaling, it is required to solve the following MGM power control problem

$$\min_{\{P_k\}_{k=1}^{K}} \quad \sum_{k=1}^{K} \beta_k P_k \tag{4.5a}$$

$$\text{s.t.} \quad \frac{\varrho_{d,m} P_d}{\sum_{k \neq d} \varrho_{k,m} P_k + \sigma_m^2} \geq \gamma_m, \ \forall m \in \mathcal{G}_d, \ \forall d, k \in \mathcal{K}, \tag{4.5b}$$

$$P_k \geq 0, \ \forall k \in \mathcal{K} \tag{4.5c}$$

where $\beta_k \triangleq \|\boldsymbol{w}_k^{(l)}\|^2$, $\varrho_{k,m} \triangleq \boldsymbol{w}_k^{(l)H} \boldsymbol{C}_m \boldsymbol{w}_k^{(l)}$, and $\boldsymbol{w}_k^{(l)}$ is the current candidate beamforming vector. This problem can be rewritten as the following linear programming (LP) problem

$$\min_{\{P_k\}_{k=1}^{K}} \quad \sum_{k=1}^{K} \beta_k P_k \tag{4.6a}$$

$$\text{s.t.} \quad \varrho_{d,m} P_d - \gamma_m \sum_{k \neq d} \varrho_{k,m} P_k \geq \gamma_m \sigma_m^2, \ \forall m \in \mathcal{G}_d, \ \forall d, k \in \mathcal{K}, \tag{4.6b}$$

$$P_k \geq 0, \ \forall k \in \mathcal{K}. \tag{4.6c}$$

The scaled candidate beamforming vectors are then given by $\left\{ \sqrt{P_k^{(l)}} \boldsymbol{w}_k^{(l)} \right\}_{k=1}^{K}$ where $\{P_k^{(l)}\}_{k=1}^{K}$ is the optimal solution of problem (4.6).

Similar to the previous SDP problems, we use $\sum_{k=1}^{K} \mathrm{tr}(\boldsymbol{X}_{k,\mathrm{opt}})$ as a lower bound on the total transmitted power to benchmark the evaluated methods in our simulations.

4.3.3 Special Case 1: MU Downlink Beamforming

As mentioned above, problem (2.10) can be reformulated as an equivalent convex SOCP problem. This is not possible in case of statistical CSI where the matrix $\boldsymbol{C}_k$ is of higher rank. In this case, we resort to the SDR approach described above. Hence, problem (4.4) is solved where $\mathcal{G}_k = \{k\},\ \forall k$. However, it has been shown in [14] that in this particular case, if problem (4.4) is feasible, it has at least one optimal solution with $\text{rank}(\boldsymbol{X}_k) = 1, \forall k \in \mathcal{K}$. Due to the rank-one property, this solution is also an optimal solution for the original problem (2.10).

4.4 Iterative Linearization Approach

The original QoS constraint (3.30b) of the generalized distributed beamforming power minimization problem can be rewritten as

$$\gamma_m \boldsymbol{w}^H \boldsymbol{Q}_m \boldsymbol{w} + \gamma_m \sigma_\nu^2 - \boldsymbol{w}^H \boldsymbol{R}_{d,m} \boldsymbol{w} \leq 0 \tag{4.7}$$

which defines the sublevel set of the function on the left-hand side of the inequality. If this function was convex, the sublevel set would be a convex set. Since the involved matrices in (4.7) are all positive semi-definite, the term $\gamma_m \boldsymbol{w}^H \boldsymbol{Q}_m \boldsymbol{w} + \gamma_m \sigma_\nu^2$ corresponds to a convex function while the term $-\boldsymbol{w}^H \boldsymbol{R}_{d,m} \boldsymbol{w}$ describes a concave function. The sublevel set described by (4.7) is hence nonconvex. However, it can be approximated by a convex sublevel set via linearizing the concave function $-\boldsymbol{w}^H \boldsymbol{R}_{d,m} \boldsymbol{w}$. In [45], this is achieved as follows. Firstly, $\boldsymbol{w}$ is replaced by $\boldsymbol{w}_{\text{opt}}^{(i)} + \Delta\boldsymbol{w}$ where $\boldsymbol{w}_{\text{opt}}^{(i)}$ is the constant around which the concave function is linearized and $\Delta\boldsymbol{w}$ is the new optimization variable. Then, the nonlinear terms are neglected as follows

$$\begin{aligned} & - (\boldsymbol{w}_{\text{opt}}^{(i)} + \Delta\boldsymbol{w})^H \boldsymbol{R}_{d,m} (\boldsymbol{w}_{\text{opt}}^{(i)} + \Delta\boldsymbol{w}) \\ = & - \boldsymbol{w}_{\text{opt}}^{(i)H} \boldsymbol{R}_{d,m} \boldsymbol{w}_{\text{opt}}^{(i)} - 2\text{Re}\{\Delta\boldsymbol{w} \boldsymbol{R}_{d,m} \boldsymbol{w}_{\text{opt}}^{(i)}\} - \Delta\boldsymbol{w}^H \boldsymbol{R}_{d,m} \Delta\boldsymbol{w} \\ \leq & - \boldsymbol{w}_{\text{opt}}^{(i)H} \boldsymbol{R}_{d,m} \boldsymbol{w}_{\text{opt}}^{(i)} - 2\text{Re}\{\Delta\boldsymbol{w} \boldsymbol{R}_{d,m} \boldsymbol{w}_{\text{opt}}^{(i)}\}. \end{aligned} \tag{4.8}$$

Using the linearization in (4.8), the original problem (3.30) can be approximated by the following convex QCQP

$$\min_{\Delta\boldsymbol{w}} \ (\boldsymbol{w}_{\text{opt}}^{(i)} + \Delta\boldsymbol{w})^H \boldsymbol{D} (\boldsymbol{w}_{\text{opt}}^{(i)} + \Delta\boldsymbol{w}) \tag{4.9a}$$

$$\begin{aligned} \text{s.t.} \ & \gamma_m (\boldsymbol{w}_{\text{opt}}^{(i)} + \Delta\boldsymbol{w})^H \boldsymbol{Q}_m (\boldsymbol{w}_{\text{opt}}^{(i)} + \Delta\boldsymbol{w}) + \gamma_m \sigma_\nu^2 \\ & - \boldsymbol{w}_{\text{opt}}^{(i)H} \boldsymbol{R}_{d,m} \boldsymbol{w}_{\text{opt}}^{(i)} - 2\text{Re}\{\Delta\boldsymbol{w} \boldsymbol{R}_{d,m} \boldsymbol{w}_{\text{opt}}^{(i)}\} \leq 0, \ \forall m \in \mathcal{G}_d, \ \forall d \in \mathcal{K}. \end{aligned} \tag{4.9b}$$

In [45], an iterative linearization approach is then proposed where in each iteration, problem (4.9) is solved. The new constant around which the concave function is linearized in the next iteration is defined as $\boldsymbol{w}_{\text{opt}}^{(i+1)} \triangleq \boldsymbol{w}_{\text{opt}}^{(i)} + \Delta\boldsymbol{w}_{\text{opt}}^{(i)}$ where $\Delta\boldsymbol{w}_{\text{opt}}^{(i)}$ is the optimal solution of problem (4.9) obtained in the ith iteration. In [45], it is proven that in this way, the approximate solution is improved from one iteration to the next. Note that an initial $\boldsymbol{w}_{\text{opt}}^{(1)}$ which is feasible for the original problem (3.30b) is required for the iterative approach of [45]. We refer to [45] for more details.

Chapter 5

Proposed Iterative SOCP Approach - Distributed Beamforming

5.1 Introduction

When the number of destination nodes in the relay networks introduced in Chapter 3 is large, the number of constraints in the optimization problem (3.30) is large and the convex outer approximations proposed in [28, 54] may become rather inaccurate. As a consequence, the solution of the approximated problem (4.2) can be far from the optimal solution of the original problem (3.30). In this case, the candidate beamforming vectors generated from the solution of the relaxed problem (4.2) by randomization and scaling may be far from the optimal beamforming vector. It may even happen that after scaling, none of the generated candidates can become feasible for the original problem (3.30).

In [30], it has been proposed to use a convex inner approximation of the feasible set of the original problem (3.30) rather than the convex outer approximation of [28,54]. The convex inner approximation yields a convex SOCP problem whose solution, provided it exists, is always feasible for the original problem. Hence, the randomization technique is not required. However, the convex inner approximation suffers from the same problems as the convex outer approximation approach: The approximation may become rather inaccurate in case of a large number of destination nodes. As a consequence, the solution of the approximated problem may be far from the optimal solution of the original problem or it may become infeasible even when the original problem still remains feasible.

To overcome the difficulties of the state-of-the-art approaches, we propose an iterative procedure in this chapter where in each iteration, the convex inner approximation of [30] is applied to the original problem to obtain a convex SOCP problem. The convex inner approximation is then successively improved by adapting the approximation of the next iteration to the solution obtained in the current iteration. We prove that in each iteration of our method, the approximate solution obtained by solving the SOCP problem is improved relative to the approximate solution obtained in the previous iteration. Further, we use the same iterative concept to compute a feasible initial approximation for the first iteration. Then, it is shown that this iterative feasibility

search can be extended to an admission control procedure similar to that used in [63]. Moreover, we provide a way to use the proposed algorithm as a local refinement for the SDR approach. The complexity of all competing methods is analyzed and compared to each other in detail as well. Simulation results reveal that our method outperforms the approaches of [28,30,54] in terms of both the transmitted power and problem feasibility when the number of destination nodes is moderate to large. Note that a large number of destination nodes is common, especially in MGM networks.

This chapter is based on my original work that has been published in [1, 3].

5.2 Convex Inner Approximation of the Feasible Set

An alternative to the convex outer approximation of the SDR approach consists in exploiting the rank-one property of the matrix $\boldsymbol{R}_{d,m} = P_d \boldsymbol{h}_{d,m} \boldsymbol{h}_{d,m}^H$ (in case of instantaneous CSI) and approximating problem (3.30) by a SOCP problem using an inner approximation of the feasible set [30]. Towards this end, the QoS constraints of problem (3.30) are rewritten as

$$\frac{\sqrt{P_d}|\boldsymbol{w}^H \boldsymbol{h}_{d,m}|}{\sqrt{\boldsymbol{w}^H \boldsymbol{Q}_m \boldsymbol{w} + \sigma_\nu^2}} \geq \sqrt{\gamma_m},\ \forall m \in \mathcal{G}_d,\ \forall d \in \mathcal{K}. \tag{5.1}$$

By introducing [30]

$$\boldsymbol{U}_m \triangleq \begin{bmatrix} \sigma_\nu^2 & \boldsymbol{0}^T \\ \boldsymbol{0} & \boldsymbol{Q}_m \end{bmatrix}^{1/2}, \qquad \tilde{\boldsymbol{w}} \triangleq [1, \boldsymbol{w}^T]^T, \qquad \tilde{\boldsymbol{h}}_{d,m} \triangleq [0, \boldsymbol{h}_{d,m}^T]^T,$$

the QoS constraints in (5.1) are further rewritten as

$$|\tilde{\boldsymbol{w}}^H \tilde{\boldsymbol{h}}_{d,m}| \geq \sqrt{\gamma_m / P_d} \|\boldsymbol{U}_m \tilde{\boldsymbol{w}}\|,\ \forall m \in \mathcal{G}_d,\ \forall d \in \mathcal{K}. \tag{5.2}$$

With the conservative approximation [30]

$$|\tilde{\boldsymbol{w}}^H \tilde{\boldsymbol{h}}_{d,m}| \geq \mathrm{Re}\{\tilde{\boldsymbol{w}}^H \tilde{\boldsymbol{h}}_{d,m}\}, \tag{5.3}$$

we strengthen the non-convex constraints in (5.2) as

$$\mathrm{Re}\{\tilde{\boldsymbol{w}}^H \tilde{\boldsymbol{h}}_{d,m}\} \geq \sqrt{\gamma_m / P_d} \|\boldsymbol{U}_m \tilde{\boldsymbol{w}}\|,\ \forall m \in \mathcal{G}_d,\ \forall d \in \mathcal{K}. \tag{5.4}$$

The inequalities (5.4) describe second-order cone constraints that are generally convex. Introducing the auxiliary variable t and the matrix

$$\boldsymbol{V} \triangleq \begin{bmatrix} 0 & \boldsymbol{0}^T \\ \boldsymbol{0} & \boldsymbol{D} \end{bmatrix}^{1/2}, \tag{5.5}$$

problem (3.30) can be approximated by the following convex SOCP problem [30]:

$$\min_{t,\tilde{\boldsymbol{w}}} \; t \tag{5.6a}$$

$$\text{s.t.} \; \|\boldsymbol{V}\tilde{\boldsymbol{w}}\| \leq t \tag{5.6b}$$

$$\sqrt{\gamma_m/P_d}\|\boldsymbol{U}_m\tilde{\boldsymbol{w}}\| \leq \mathrm{Re}\{\tilde{\boldsymbol{w}}^H\tilde{\boldsymbol{h}}_{d,m}\}, \; \forall m \in \mathcal{G}_d, \; \forall d \in \mathcal{K} \tag{5.6c}$$

$$\tilde{w}_1 = 1. \tag{5.6d}$$

As a property of SOCP, problem (5.6) can be efficiently solved in polynomial time using interior-point methods [62].

Note that (5.3) is satisfied with equality if and only if $\tilde{\boldsymbol{w}}^H\tilde{\boldsymbol{h}}_{d,m}$ are real and positive $\forall m \in \mathcal{G}_d, \; \forall d \in \mathcal{K}$. Thus, replacing (5.2) by (5.4) yields a restricted convex feasible set which is a subset of the original feasible set of problem (3.30). Consequently, such a strengthening of the QoS constraints guarantees that if the solution of (5.6) exists, it is always feasible for (3.30). However, drawbacks of this approach are that the solution of (5.6) may not be optimal for (3.30) and that it may turn an originally feasible problem into an infeasible one when the restricted feasible set shrinks to the empty set. Note that the concept of the SDR approach of [28] is opposite in the sense that the approximated feasible set contains the original feasible set as a subset. In the next sections, we propose an iterative method which overcomes the drawbacks of the SOCP approach of [30] and offers substantial advantages over the SDR approach of [28].

5.3 Iterative QoS-Constrained Power Minimization

Note that problem (3.30) is independent of a multiplication of $\boldsymbol{w}$ by a rotation factor $\exp(j\varphi)$ where $j \triangleq \sqrt{-1}$. In the single destination user case ($M = K = 1$), one can choose this rotation factor such that $\tilde{\boldsymbol{w}}^H\tilde{\boldsymbol{h}}_{1,1}$ becomes real-valued and non-negative [30]. Inequality (5.3) holds with equality in this case and as a consequence, replacing (5.2) by (5.4) does not involve any restriction of the feasible set. Hence, in this simple case, the solution of problem (5.6) is optimal for the original problem (3.30). However, in the MU case ($M > 1$), it is generally not possible to make all $\tilde{\boldsymbol{w}}^H\tilde{\boldsymbol{h}}_{d,m}, \; \forall m \in \mathcal{G}_d, \; \forall d \in \mathcal{K}$ real-valued and non-negative using the phase rotation of $\boldsymbol{w}$ described above. The reason is that one common $\boldsymbol{w}$ needs to be shared by multiple users which reduces the degrees of freedom.

Note, however, that the left-hand side of each QoS constraint in (5.4) depends on a different channel vector $\tilde{\boldsymbol{h}}_{d,m}$ which we can rotate instead. Generally, physical channel

Initialization: $\tilde{\boldsymbol{h}}_{d,m}^{(1)} = \tilde{\boldsymbol{h}}_{d,m},\ \forall m \in \mathcal{G}_d,\ \forall d \in \mathcal{K}$
for $i = 1, \ldots, I$
Solve problem (5.6) with $\tilde{\boldsymbol{h}}_{d,m} = \tilde{\boldsymbol{h}}_{d,m}^{(i)}$.
Perform the rotation of (5.7) with $\alpha_{d,m}^{(i)} = \angle(\tilde{\boldsymbol{w}}_{\text{opt}}^{(i)H} \tilde{\boldsymbol{h}}_{d,m}^{(i)})$.
end

Table 5.1. Proposed iterative procedure

coefficients are given through observation and, therefore, we cannot anyhow change or rotate them. However, from (3.30), it can be observed that the original problem remains invariant to such a channel which can be used in a "virtual" sense, just to modify the mathematical approximation (5.6) of the original problem (3.30). The idea proposed in this chapter is to iteratively rotate the channel vectors to successively improve the approximation in (5.4).

Let us define the channel rotation recursion as

$$\tilde{\boldsymbol{h}}_{d,m}^{(i+1)} \triangleq \tilde{\boldsymbol{h}}_{d,m}^{(i)} \exp\left(-j\alpha_{d,m}^{(i)}\right),\ \forall m \in \mathcal{G}_d,\ \forall d \in \mathcal{K} \tag{5.7}$$

where $\alpha_{d,m}^{(i)} \in [0, 2\pi)$ describes the rotation in the ith iteration and $\tilde{\boldsymbol{w}}_{\text{opt}}^{(i)}$ denotes the solution of (5.6) for $\tilde{\boldsymbol{h}}_{d,m} = \tilde{\boldsymbol{h}}_{d,m}^{(i)}$ in the ith iteration. Note again that any rotation of the channel vectors according to (5.7) does not affect the original problem (3.30) since the rotation factor $\exp(-j\alpha_{d,m}^{(i)})$ cancels out in its QoS constraints (5.2). However, such rotations changes the convex approximation of the QoS constraints. The rotation in (5.7) can thus be used to improve the approximation of the original QoS constraints in the vicinity of the current solution $\tilde{\boldsymbol{w}}_{\text{opt}}^{(i)}$ which makes it possible to find a better solution $\tilde{\boldsymbol{w}}_{\text{opt}}^{(i+1)}$ in the next iteration as we show later. Recall that the approximation consists in replacing (5.2) by (5.4). Hence, choosing $\alpha_{d,m}^{(i)} = \angle(\tilde{\boldsymbol{w}}_{\text{opt}}^{(i)H} \tilde{\boldsymbol{h}}_{d,m}^{(i)})$, i.e., rotating $\tilde{\boldsymbol{w}}_{\text{opt}}^{(i)H} \tilde{\boldsymbol{h}}_{d,m}^{(i)}$ onto the positive real axis, optimizes the approximation around $\tilde{\boldsymbol{w}}_{\text{opt}}^{(i)}$ since then

$$|\tilde{\boldsymbol{w}}_{\text{opt}}^{(i)H} \tilde{\boldsymbol{h}}_{d,m}| = \text{Re}\left\{\tilde{\boldsymbol{w}}_{\text{opt}}^{(i)H} \tilde{\boldsymbol{h}}_{d,m}^{(i)} \exp\left(-j\alpha_{d,m}^{(i)}\right)\right\} \tag{5.8a}$$

$$= \text{Re}\left\{\tilde{\boldsymbol{w}}_{\text{opt}}^{(i)H} \tilde{\boldsymbol{h}}_{d,m}^{(i+1)}\right\} \geq \text{Re}\left\{\tilde{\boldsymbol{w}}_{\text{opt}}^{(i)H} \tilde{\boldsymbol{h}}_{d,m}^{(i)}\right\} \tag{5.8b}$$

where equality holds in (5.8b) if and only if $\alpha_{d,m}^{(i)} = 0$. We initialize our iterative scheme with $\tilde{\boldsymbol{h}}_{d,m}^{(1)} = \tilde{\boldsymbol{h}}_{d,m}$. With I denoting the maximum number of iterations, the algorithm is summarized in Table 5.1.

Lemma 1: The proposed algorithm of Table 5.1 yields an improved solution in iteration $(i+1)$ compared to that of iteration i as long as $\alpha_{d,m}^{(i)} \neq 0$ for all active QoS constraints (5.6c) in iteration i.

Proof of Lemma 1: We first show by contradiction that at the optimum of (5.6), at least one QoS constraint is active, i.e., satisfied with equality. Let no QoS constraint be active at the solution $\tilde{\boldsymbol{w}}_{\text{opt}}$ of (5.6). Note that the QoS constraints (5.4) are equivalent to

$$\frac{\text{Re}\left\{\boldsymbol{w}^H \boldsymbol{h}_{d,m}\right\}}{\sqrt{\boldsymbol{w}^H \boldsymbol{Q}_m \boldsymbol{w} + \sigma_\nu^2}} \geq \sqrt{\gamma_m / P_d},\ \forall m \in \mathcal{G}_d,\ \forall d \in \mathcal{K}. \tag{5.9}$$

Since the left-hand sides of the inequalities in (5.9) are monotonically increasing functions of a scaling factor of $\boldsymbol{w}$, $\boldsymbol{w}_{\text{opt}}$ could be scaled down until at least one QoS constraint is active and the remaining QoS constraints remain inactive. This, however, reduces the objective function contradicting the optimal of $\tilde{\boldsymbol{w}}_{\text{opt}}$. We proceed with our proof using contradiction again. Let us assume that in some iteration $(i+1)$, the solution of (5.6) is the same as that in the previous iteration i, i.e., $\tilde{\boldsymbol{w}}_{\text{opt}}^{(i+1)} = \tilde{\boldsymbol{w}}_{\text{opt}}^{(i)}$. Let us further assume that $\alpha_{d,m}^{(i)} \neq 0$ for all active QoS constraints in iteration i. Then, (5.8b) implies that for these constraints, the left-hand sides of (5.4) in iteration $(i+1)$ are greater than those in iteration i while the right-hand sides remain the same. Thus, all the (strengthened) QoS constraints in (5.6) are inactive, contradicting optimality of $\tilde{\boldsymbol{w}}_{\text{opt}}^{(i+1)} = \tilde{\boldsymbol{w}}_{\text{opt}}^{(i)}$ for (5.6) in iteration $(i+1)$. Further, since $\tilde{\boldsymbol{w}}_{\text{opt}}^{(i)}$ is feasible for (5.6) in iteration $(i+1)$, we can conclude that the objective value must decrease monotonically with the iterations as long as $\alpha_{d,m}^{(i)} \neq 0$ for all active QoS in the current iteration i. □

Note, however, that in general, there is no guarantee that the algorithm converges to the global optimum of problem (3.30).

We remark that two similar approximation approaches have been proposed in [64] and [65]. In [64], a joint beamforming and power control problem for a BC channel with a multi-antenna relay and a multi-antenna BS has been considered while the authors in [65] have considered the same MUP2P relay beamforming scenario as in this thesis where, however, the relays have multiple antennas. The idea in the latter two references is to approximate the original problem by a SOCP problem and to find the rotation angles which optimize the SOCP approximation when applied to the channel vectors. In this respect, both approaches are similar to the approach proposed in this thesis. However, the method proposed in [64] corresponds to an exhaustive search for these optimal rotation angles and is thus highly demanding since a SOCP problem has to be solved for each possible set of rotated channel vectors. The scheme proposed in [65] exhibits a reduced computational complexity relative to the method in [64]: A nested bisection search is proposed in the former reference reducing the number of SOCP problems which have to be solved. Due to the nested nature of the bisection search, however, the number of SOCP problems that need to be solved grows exponentially with the number of source-destination pairs K and is thus still prohibitively high. Our method is more sophisticated and exhibits a much

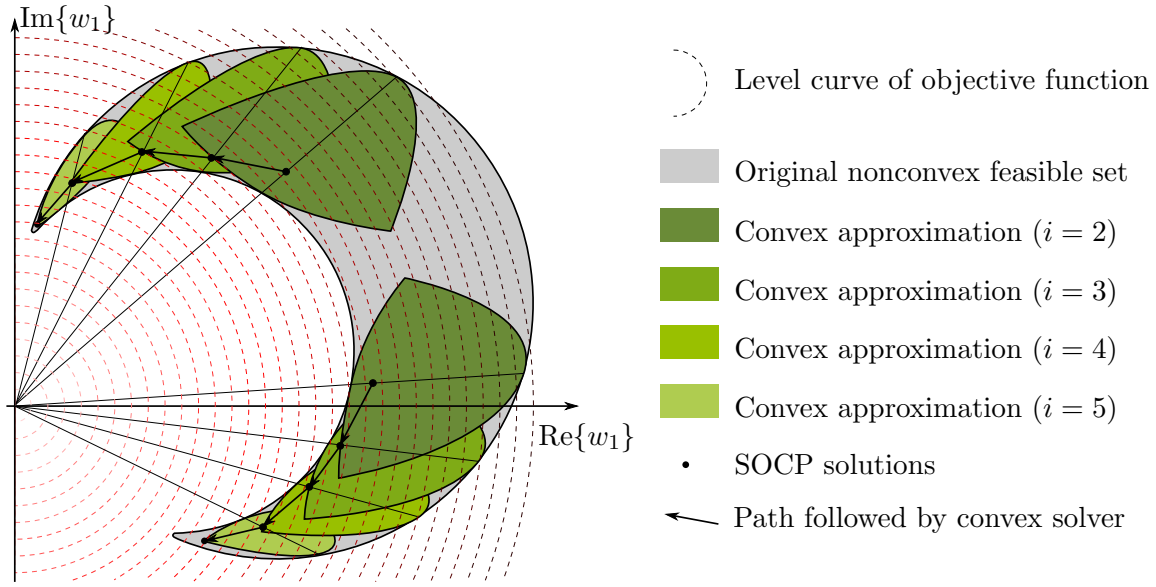

Figure 5.1. Visualization of the proposed iterative SOCP approach.

lower computational complexity than the schemes of the latter two references since it aims at finding the optimal rotation angles recursively in only a few iterations instead of performing demanding exhaustive or nested bisection searches. Note that the work of [65] has been extended in [44] where, in addition to the nested bisection search, the same iterative algorithm for finding close to optimal rotation angles as proposed in this thesis has been used. However, [44] has been published later than our original works [1] and [3]. Moreover, the powerful iterative feasibility search, which makes the iterative SOCP approach applicable in difficult situations where it is not trivial to find a feasible SOCP approximation of the original problem, has not been proposed in [44].

For a better comprehension of the proposed algorithm, it is advantageous to illustrate how the convex inner approximation of the originally nonconvex feasible set is adapted to the solution $\boldsymbol{w}_{\text{opt}}^{(i)}$ in the current iteration and how this improves the approximate solution. For simplicity, let us consider the case where $\boldsymbol{w} = [w_1,\ w_2]^T$ (note that we consider $\boldsymbol{w}$ rather than $\tilde{\boldsymbol{w}}$) and display only its first component $w_1 \in \mathbb{C}$ in the complex plane while treating its second component $w_2 \in \mathbb{C}$ as constant. We assume for convenience that this fixed w_2 is optimal for the original problem and for the approximated problem in each considered iteration. Further, assume that $\boldsymbol{D} = \boldsymbol{I}$ in (3.30), i.e., the optimization problem (3.30) consists in reducing the norm of $\boldsymbol{w}$ as far as the feasible set allows.

The illustration under these assumptions is shown in Fig. 5.1 for $M = 2$ QoS constraints. The large light gray area depicts the original, nonconvex feasible set. The

smaller and darker gray areas illustrate its convex approximations in three consecutive iterations of two possible situations. The approximated feasible set in a particular iteration is depicted darker than that of the next iteration and is overlapping with it. For both possibilities, the darkest approximated set corresponds to the second iteration and the subsequent sets to the third and the fourth iteration, respectively. The approximation in the first iteration is not shown. Depending on the initial approximation in the first iteration, the proposed algorithm may converge to different solutions. Two possible scenarios are depicted in Fig. 5.1. The grid of dashed circles around the origin of the coordinate system helps to evaluate the norm and thus the objective value of each point. It reveals that the upper vertex of the original feasible set is the global optimum of the original problem while the lower vertex is only a local optimum. The optimal points $\boldsymbol{w}_{\text{opt}}^{(i)}$ in iterations one to four are indicated as dots that are connected with arrows. Further, the set of positively scaled versions of $\boldsymbol{w}_{\text{opt}}^{(i)}$ in the ith is represented by a straight line passing through the origin of the coordinate system and the corresponding dot. Note that (5.8a) not only holds for $\tilde{\boldsymbol{w}}_{\text{opt}}^{(i)}$ (and equivalently for $\boldsymbol{w}_{\text{opt}}^{(i)}$) but also for all these positively scaled versions of $\boldsymbol{w}_{\text{opt}}^{(i)}$. Hence on the straight line depicting positively scaled $\boldsymbol{w}_{\text{opt}}^{(i)}$ in the ith iteration, the boundaries of the original set and those of the approximated set in the $(i+1)$th iteration coincide. The more we deviate from this straight line, the more the approximation deviates from the original feasible set. According to (5.3), the approximated feasible set is always located in the interior of the original feasible set. In each iteration, the interior-point algorithm yields $\boldsymbol{w}$ with the smallest norm in the approximated feasible set. The arrows pointing from $\boldsymbol{w}_{\text{opt}}^{(i)}$ to $\boldsymbol{w}_{\text{opt}}^{(i+1)}$ illustrate the search. We observe that, depending on the outcome of the first iteration, the algorithm converges to the local optimum of the original problem or to the global one.

5.4 Iterative Feasibility Search

The proposed iterative algorithm relies on the assumption that (5.6) is feasible. As mentioned earlier, this assumption may not be valid even if the original problem (3.30) is feasible. However, if problem (5.6) is infeasible for initialization $\tilde{\boldsymbol{h}}_{d,m}^{(1)} = \tilde{\boldsymbol{h}}_{d,m}$, there may exist initial rotations of the channel vectors for which (5.6) becomes feasible. These can be obtained from a reformulation of (5.6) as an optimization problem, where an infeasibility indicator is minimized, and applying the same concept of successively rotating the channel vectors. It is clear from the discussion in the previous section that once a set of rotated channel vectors is found for which problem (5.6) is feasible, then it remains feasible in all iterations of the algorithm described in Table 5.1.

Inspired by the phase I method for obtaining a feasible starting point in interior-point methods as described in [62], Chapter 11.4.1, we introduce the real-valued and non-negative variable z_m which can be interpreted as a measure of how far the mth QoS constraint in (5.6) is from being satisfied. Together with the vector $\boldsymbol{z} = [z_1, \ldots, z_M]^T$ we can then formulate the following optimization problem [62]

$$\min_{\boldsymbol{z},\tilde{\boldsymbol{w}}} \mathbf{1}^T\boldsymbol{z} \tag{5.10a}$$

$$\text{s.t. } \sqrt{\gamma_m/P_d}\|\boldsymbol{U}_m\tilde{\boldsymbol{w}}\| - \mathrm{Re}\{\tilde{\boldsymbol{w}}^H\tilde{\boldsymbol{h}}_{d,m}\} \leq z_m,\ \forall m \in \mathcal{G}_d,\ \forall d \in \mathcal{K} \tag{5.10b}$$

$$z_m \geq 0,\ \forall m \in \mathcal{G}_d,\ \forall d \in \mathcal{K} \tag{5.10c}$$

$$\tilde{w}_1 = 1 \tag{5.10d}$$

The SOCP problem (5.10) with optimal solution $\boldsymbol{z}_{\text{opt}}$ and $\tilde{\boldsymbol{w}}_{\text{opt}}$ is always feasible, i.e., a solution always exists. Note that the closer the optimal value $\mathbf{1}^T\boldsymbol{z}_{\text{opt}}$ is to zero, the closer is the solution $\tilde{\boldsymbol{w}}_{\text{opt}}$ of (5.10) to being feasible for (5.6). A component $z_m = 0$ indicates that the mth QoS constraint in (5.6) is satisfied whereas $z_m > 0$ indicates the contrary. Hence, all QoS constraints are satisfied and $\tilde{\boldsymbol{w}}_{\text{opt}}$ is a feasible point of (5.6) if and only if $\mathbf{1}^T\boldsymbol{z}_{\text{opt}} = 0$. However, if $\mathbf{1}^T\boldsymbol{z}_{\text{opt}} > 0$, then (5.6) is infeasible. In this case, we propose to apply the same concept as described in the previous section, i.e., to successively rotate the channel vectors and thereby successively improve the approximation of problem (5.10). Hence, we perform the iterative procedure described in Table 5.1 where, however, we replace problem (5.6) by (5.10).

Let us refer to the optimal value $\mathbf{1}^T\boldsymbol{z}_{\text{opt}}^{(i+1)}$ of problem (5.10) in the $(i+1)$th iteration as the *infeasibility indicator*.

Lemma 2: The proposed scheme yields a reduced infeasibility indicator in the $(i+1)$th iteration relative to that of the ith iteration as long as $\alpha_{d,m}^{(i)} \neq 0$ and $[\boldsymbol{z}_{\text{opt}}^{(i)}]_m > 0$ for at least one pair d, m in iteration i. Thus, the algorithm converges locally.

Proof of Lemma 2: This local convergence property can be proved using arguments similar to that of the previous section: Again, assume that $\tilde{\boldsymbol{w}}_{\text{opt}}^{(i+1)} = \tilde{\boldsymbol{w}}_{\text{opt}}^{(i)}$. Further, assume that $\alpha_{d,m}^{(i)} \neq 0$ and $[\boldsymbol{z}_{\text{opt}}^{(i)}]_m > 0$ for at least one pair d, m in iteration i. Then, we see from (5.8b) and (5.10) that $\mathbf{1}^T\boldsymbol{z}_{\text{opt}}^{(i+1)} < \mathbf{1}^T\boldsymbol{z}_{\text{opt}}^{(i)}$. □

Thus, the infeasibility indicator decreases monotonically with the iterations as long as $\alpha_{d,m}^{(i)} \neq 0$ and $[\boldsymbol{z}_{\text{opt}}^{(i)}]_m > 0$ for at least one pair d, m in the current iteration i until either $\mathbf{1}^T\boldsymbol{z}_{\text{opt}}^{(i)} = 0$ or $\alpha_{d,m}^{(i)} = 0\ \forall m \in \mathcal{G}_d,\ \forall d \in \mathcal{K}$. If in some iteration i, $\alpha_{d,m}^{(i)} = 0\ \forall m \in \mathcal{G}_d,\ \forall d \in \mathcal{K}$ but still $\mathbf{1}^T\boldsymbol{z}_{\text{opt}}^{(i)} > 0$, no feasible approximation of problem (3.30) can be found with this method. Otherwise, once the stopping criterion $\mathbf{1}^T\boldsymbol{z}_{\text{opt}}^{(i)} = 0$ is reached, a feasible

Initialization: $\mathcal{M} := \{1, \ldots, M\}$
while $\mathbf{1}^T \boldsymbol{z}_{\text{opt}}^{(I)} > 0$
1) Perform the iterative algorithm of Table 5.1 for problem (5.10) considering all users in $\mathcal{M}$.
2) $\mathcal{M} := \mathcal{M} \setminus m$ where m corresponds to the largest $[\boldsymbol{z}_{\text{opt}}^{(I)}]_m$.
end

Table 5.2. Admission control procedure

approximation of problem (3.30) is found. Then, we can proceed with the iterative procedure of Table 5.1 applied to problem (5.6) using the previously obtained set of rotated channel vectors as feasible initializations.

The proposed iterative feasibility search is a powerful tool since its basic idea can be applied to any iterative convex inner approximation method to obtain a feasible initial approximation.

5.5 Incorporation Into Admission Control

One of the advantages of the feasibility search proposed in the previous section is that it can easily be incorporated into an admission control (AC) procedure similar to the one of [63]. Consider the case when, after I iterations, no feasible SOCP approximation of (3.30) could be found. The larger the mth element of the final solution of (5.10), $\boldsymbol{z}_{\text{opt}}^{(I)}$, the larger the gap between the target SINR of the mth user and the SINR that could actually be achieved for that user. Therefore, we propose to deny service to the user corresponding to the largest $[\boldsymbol{z}_{\text{opt}}^{(I)}]_m$, since its QoS requirement is hardest to satisfy, and resume the feasibility search algorithm with the set of remaining users. For the reduced set of users, the probability that a feasible approximation can be found is increased. This procedure can then be repeated until such a feasible approximation is found. The AC procedure is summarized in Table 5.2.

5.6 SOCP as a Local Refinement for SDP

In the previous sections, we have used the original channel vectors to initialize the proposed method. However, the solution to the SDP problem (4.2) may provide a better initialization. That is, we can combine the SDP method with our method. In

other words, the proposed method can be used as a sort of refinement for the solution of the SDP problem (4.2).

Recall that problem (4.2) is a relaxed version of (3.30) and yields the solution $\boldsymbol{X}_{\text{opt}}$ which is not rank-one in general. As mentioned above, the principal eigenvector of $\boldsymbol{X}_{\text{opt}}$ (which we denote as $\boldsymbol{w}_{\text{p}}$) may not be feasible for (3.30). However, it is always feasible for (5.10). Hence, we can use $\boldsymbol{w}_{\text{p}}$ to compute a reasonable initialization for the feasibility search as follows:

$$\boldsymbol{h}_{d,m}^{(1)} \triangleq \boldsymbol{h}_{d,m} \exp\left(-j\alpha_{d,m}^{(1)}\right),\ \forall m \in \mathcal{G}_d,\ \forall d \in \mathcal{K} \tag{5.11}$$

where

$$\alpha_{d,m}^{(1)} = \angle(\boldsymbol{w}_{\text{p}}^H \boldsymbol{h}_{d,m}),\ \forall m \in \mathcal{G}_d,\ \forall d \in \mathcal{K}. \tag{5.12}$$

We thus adapt this approximation of the feasible set to $\boldsymbol{w}_{\text{p}}$. This is reasonable since $\boldsymbol{w}_{\text{p}}$ might be already close to the global optimum of (3.30), even if it is infeasible for (3.30). Our simulation results show that this is in fact a very good initialization.

5.7 Complexity Analysis

In this section, we compare the computational complexity of our iterative SOCP method to that of the non-iterative version of [30] and the SDP method of [28]. To indicate the computational complexity, the worst-case complexity in terms of floating-point operations (FLOPs) is used where a FLOP represents either a complex addition or a complex multiplication. The SOCP problem (5.6), which has to be solved only once in the non-iterative SOCP approach, has to be solved in each iteration of our method. In the SDP method, the SDP problem (4.2) has to be solved once. It has been shown in [66] that problem (5.6) can be solved most efficiently using the primal-dual interior-point method with the worst-case complexity of $\mathcal{O}(N^3M^{1.5})$. To evaluate the complexity of problem (4.2), we rewrite it as follows.

Let us introduce slack variables to turn the inequality constraints into equalities, i.e., rewrite (4.2) as

$$\min_{\boldsymbol{X},\boldsymbol{\rho}}\ \operatorname{tr}(\boldsymbol{D}\boldsymbol{X}) \tag{5.13a}$$

$$\text{s.t.}\ \ \operatorname{tr}(\boldsymbol{T}_{d,m}\boldsymbol{X}) - \rho_m = \theta_m,\ \forall m \in \mathcal{G}_d,\ \forall d \in \mathcal{K} \tag{5.13b}$$

$$\boldsymbol{X} \succeq 0 \tag{5.13c}$$

$$\rho_m \geq 0,\ m = 1, \ldots, M \tag{5.13d}$$

where $\boldsymbol{\rho} \triangleq [\rho_1, \ldots, \rho_M]^T$ and $\theta_m \triangleq \gamma_m \sigma_\nu^2$. Introducing

$$\tilde{\boldsymbol{X}} \triangleq \begin{bmatrix} \operatorname{diag}\{\boldsymbol{\rho}\} & \mathbf{0}^T \\ \mathbf{0} & \boldsymbol{X} \end{bmatrix}$$
$$\tilde{\boldsymbol{D}} \triangleq \begin{bmatrix} \operatorname{diag}\{\mathbf{0}\} & \mathbf{0}^T \\ \mathbf{0} & \boldsymbol{D} \end{bmatrix}$$
$$\tilde{\boldsymbol{T}}_{d,m} \triangleq \begin{bmatrix} \operatorname{diag}\{-\boldsymbol{e}_m\} & \mathbf{0}^T \\ \mathbf{0} & \boldsymbol{T}_{d,m} \end{bmatrix},$$

we can reformulate problem (4.2) as

$$\max_{\tilde{\boldsymbol{X}}} \quad -\operatorname{tr}(\tilde{\boldsymbol{D}}\tilde{\boldsymbol{X}}) \tag{5.14a}$$
$$\text{s.t.} \quad \operatorname{tr}(\tilde{\boldsymbol{T}}_{d,m}\tilde{\boldsymbol{X}}) = \theta_m, \ \forall m \in \mathcal{G}_d, \ \forall d \in \mathcal{K} \tag{5.14b}$$
$$\tilde{\boldsymbol{X}} \succeq 0. \tag{5.14c}$$

According to [67], problem (5.14) can be interpreted as the dual problem to the following primal standard SDP problem:

$$\min_{\boldsymbol{\lambda}} \quad \boldsymbol{\theta}^T \boldsymbol{\lambda} \tag{5.15a}$$
$$\text{s.t.} \quad \tilde{\boldsymbol{D}} + \sum_{m=1}^{M} \lambda_m \tilde{\boldsymbol{T}}_{d,m} \succeq 0 \tag{5.15b}$$

where $\boldsymbol{\lambda} \triangleq [\lambda_1, \ldots, \lambda_M]^T$, $\boldsymbol{\theta} \triangleq [\theta_1, \ldots, \theta_M]^T$ and the block diagonal structure of $\tilde{\boldsymbol{X}}$ has been inherited from that in $\tilde{\boldsymbol{D}} + \sum_{m=1}^{M} \lambda_m \tilde{\boldsymbol{T}}_{d,m}$. It has been shown in [67] that problem (5.15) can be solved efficiently using the primal-dual interior-point method with the worst-case complexity of $\mathcal{O}(M^2(N+M)^{2.5})$. As described in [67], the primal-dual interior-point method solves the primal and the dual problems jointly. Therefore, we can consider $\mathcal{O}(M^2(N+M)^{2.5})$ as the worst-case complexity of solving problem (4.2).

In our method, the SOCP problem (5.6) with a complexity of $\mathcal{O}(N^3 M^{1.5})$ has to be solved in each of (at most) $2I$ iterations. The overall complexity of our method is, hence, at most $\mathcal{O}(IN^3M^{1.5})$ and can be traded off against performance by choosing I. The increase in complexity by I relative to the non-iterative method can be reduced as follows. We can use the solution in the current iteration $\tilde{\boldsymbol{w}}_{\text{opt}}^{(i)}$ as a starting point for the next iteration as a much better starting point than an arbitrary one. Because of this, fewer iterations of the interior-point method are required to find the solution for the current iteration.

The increase/decrease in complexity of the SDP method compared to one iteration of our method is roughly $\mathcal{O}(M^3N^{-3} + M^{0.5}N^{-0.5})$. Hence, as the ratio M/N increases, the complexity of our method decreases relative to that of the SDP method and vice versa. Additionally, our method is also better in performance as the ratio M/N increases.

5.8 Simulation Results

Throughout the simulations of this chapter, we assume that the relay and receiver noise powers are equal to each other and that the power of each source is 10 dB above the noise power. In addition, we assume equal SINR thresholds at the destination receivers and flat-fading Rayleigh channels with unit variance. A total of 5000 randomization vectors were generated for each SDP-based solution, see [16]. First of all, two versions of our approach (both without the AC step) are compared to the state-of-the-art methods. The first version corresponds to our iterative SOCP approach as described in Sections 5.3 and 5.4 with $I_1 = 5$ iterations. The second version corresponds to our approach with $I_2 = 1$ iteration used as a local refinement for the solution of the SDP problem (4.2) as described in Section 5.6. For all the cases we consider, the second version with just a single iteration ($I_2 = 1$) of both the feasibility search and the power minimization outperforms the first version with $I_1 = 5$ iterations. The state-of-the-art methods we consider are the non-iterative SOCP method of [30], the SDR-based approach with randomization of [16, 17, 28] described in Chapter 4, and the iterative linearization approach of [45] described in Chapter 4. In order to find a feasible starting point $\boldsymbol{w}_{\text{opt}}^{(1)}$ for the scheme of [45], the basic idea of the feasibility search of Section 5.4 has to be applied to the approach of [45]. Thus, when we refer to the method of [45] in the simulations, we actually mean a combination of the approach of [45] and our iterative feasibility search. Since the proposed iterative scheme is more customized to the problems considered in this thesis than the approach of [45], our simulations have revealed that the method of [45] converges more slowly than our iterative SOCP method. Therefore, we always show two results of the method of [45]: Firstly, we show the results of the method of [45] after the maximum number of iterations I which are required for our iterative SOCP method to converge. In this case, the complexity of the two methods is similar as in every iteration of the method of [45], a quadratically constrained quadratic program is solved which exhibits a similar worst-case complexity as the SOCP problem solved in every iteration of our method. Note that usually, $I = 5$ or $I = 3$. Due to its smaller convergence speed, convergence is usually not achieved for the method of [45] after I iterations. Therefore, we show secondly the result of the method of [45] after a maximum of 10 iterations after which convergence is usually achieved. This also holds for the remainder of the thesis. All results of this part of the simulations are averaged over 300 Monte Carlo runs. We then investigate the AC procedure of Section 5.5. Finally, we compare the performances of the proposed methods and the state-of-the-art methods in a FF relay network scenario with frequency selective channels.

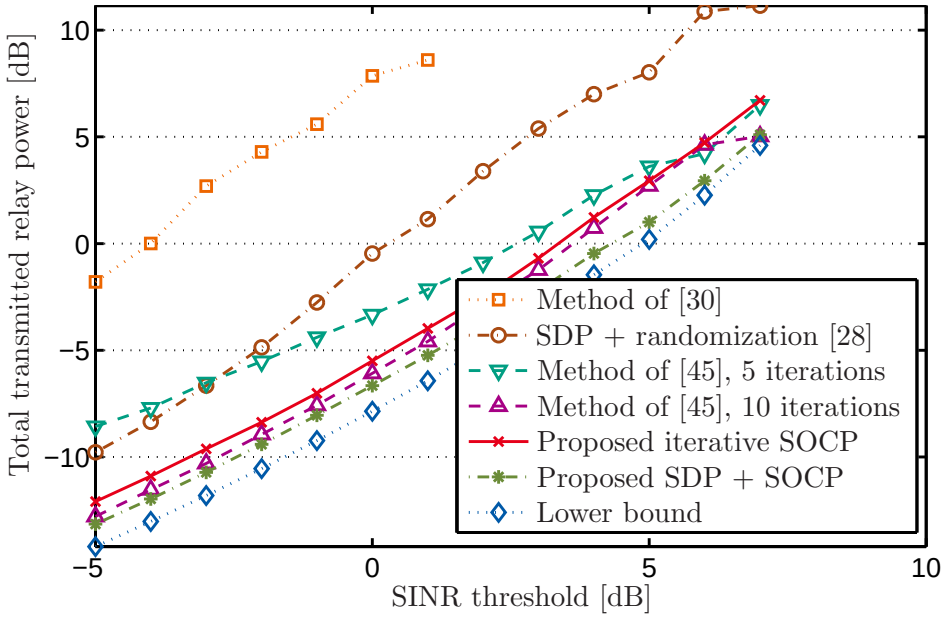

Figure 5.2. Total transmitted relay power versus SINR threshold. $K = 2$, $N = 16$, $M = 20$.

5.8.1 AF Relay Networks with Frequency Flat Channels

Let us first study a simple MGM scenario with $K = 2$ source nodes (and, hence, $K = 2$ multicast groups), $N = 16$ relays and $M = 20$ destination users where each multicast group contains the same number of users. In Fig. 5.2, the total transmitted relay power P_{T} versus the minimal SINR required at the destinations is displayed. To be specific, the power on the vertical axis is the summation of all the powers transmitted at the relays related to the transmitted power of the source nodes in dB, i.e., $10\log_{10}(P_{\mathrm{T}}/P_k)$ where P_k is the same for all source nodes. Fig. 5.2 reveals that the proposed iterative SOCP technique significantly improves the performance of the non-iterative SOCP approach of [30] and substantially outperforms the SDR approach of [28]. Furthermore, the proposed iterative SOCP method clearly outperforms the method of [45] when the same number of iterations is used for both methods. After convergence, the method of [45] yields a slightly reduced total transmitted relay power as compared to the proposed iterative scheme. In the scheme of [45], however, convergence is reached after a significantly larger number of iterations than in our method. The comparison of the proposed iterative SOCP method to the method of [45] yields similar conclusions in the remainder of the thesis. The best results which are very close to the lower bound are achieved by using the proposed technique as a local refinement for the SDR approach.

Fig. 5.3 depicts the percentage of feasible Monte Carlo runs versus the SINR threshold for all the methods tested. In the latter figure, problem (4.2) provides an upper bound

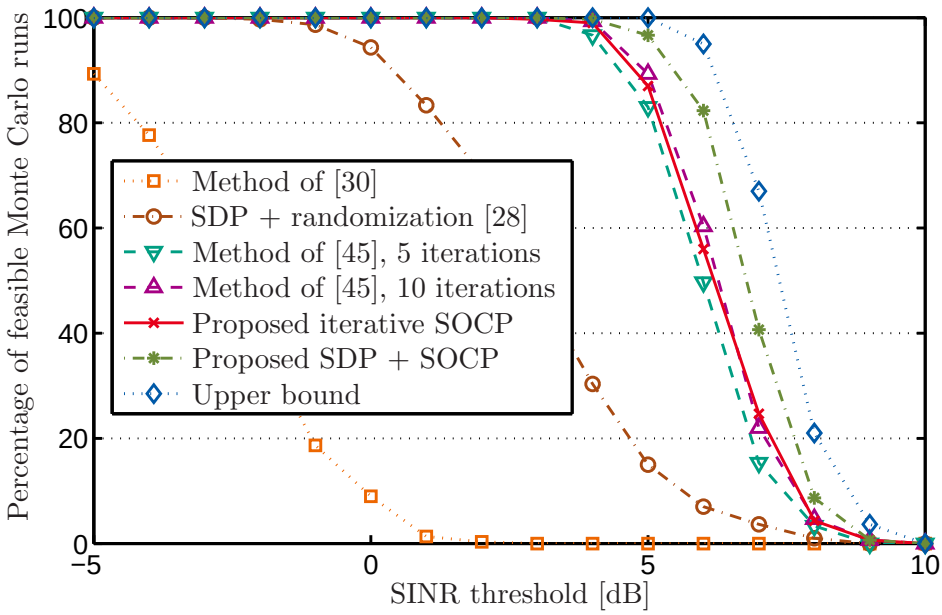

Figure 5.3. Percentage of feasible Monte Carlo runs versus SINR threshold. $K = 2$, $N = 16$, $M = 20$.

since even if the original problem (3.30) is infeasible, a feasible solution may be found for problem (4.2) due to the relaxation. None of the methods can thus achieve a larger number of feasible Monte Carlo runs than the solution of problem (4.2). It can be observed that the proposed approach achieves a much higher probability of problem feasibility as compared to the methods [28] and [30]. The results closest to the upper bound are achieved when using the proposed method as a local refinement for the SDR approach.

Next, we investigate the BC scenario of Section 3.2.2, i.e., the special case where only one single multicast group served by $K = 1$ source is present. In addition to the single source, the network consists of $N = 10$ relays and $M = 20$ destinations. The results are shown in Figs. 5.4 and 5.5 which are similar in their displayed curves to Figs. 5.2 and 5.3, respectively, of the MGM scenario of the previous example. From Figs. 5.4 and 5.5, we conclude that the performance gain of our methods compared to the SDR-based method with randomization is less significant in the BC scenario while the performance degradation of the method of [30] with respect to the other approaches is even more pronounced. The relaxed problem is always feasible in this case and also all methods tested exhibit a very high probability of being feasible except the method of [30].

Let us now study the second special case, the MUP2P scenario of Section 3.2.1. We consider a network of $N = 20$ relays and $K = M = 12$ source-destination pairs. The results are depicted in Figs. 5.6 and 5.7. The performance of the approach of [30]

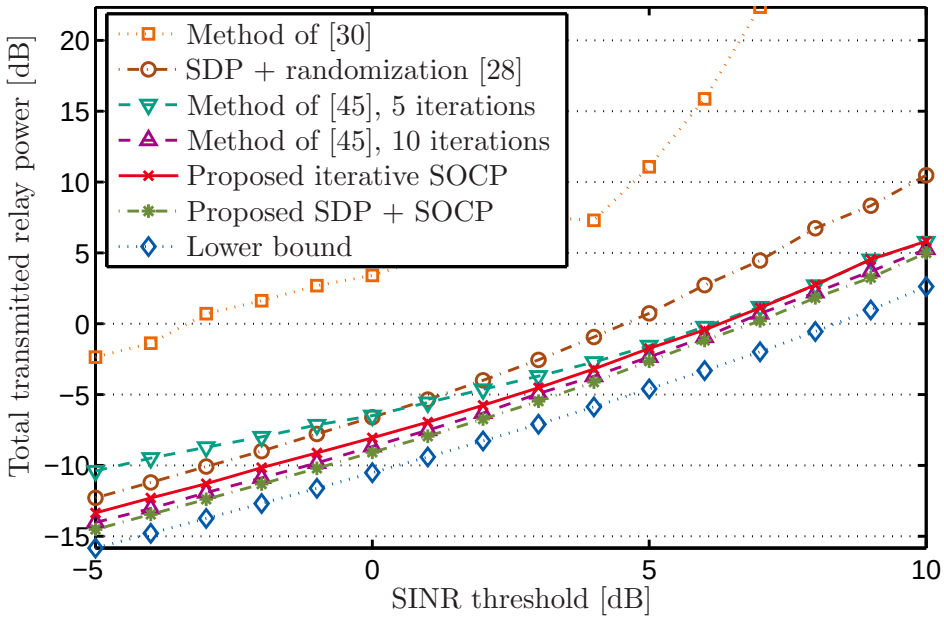

Figure 5.4. Total transmitted relay power versus SINR threshold. $K = 1$, $N = 10$, $M = 20$.

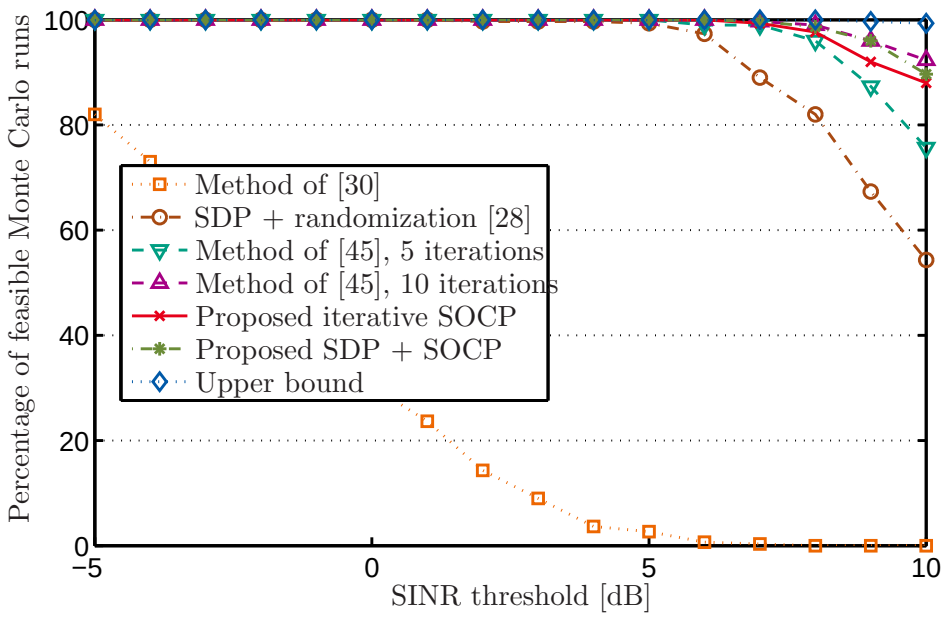

Figure 5.5. Percentage of feasible Monte Carlo runs versus SINR threshold. $K = 1$, $N = 10$, $M = 20$.

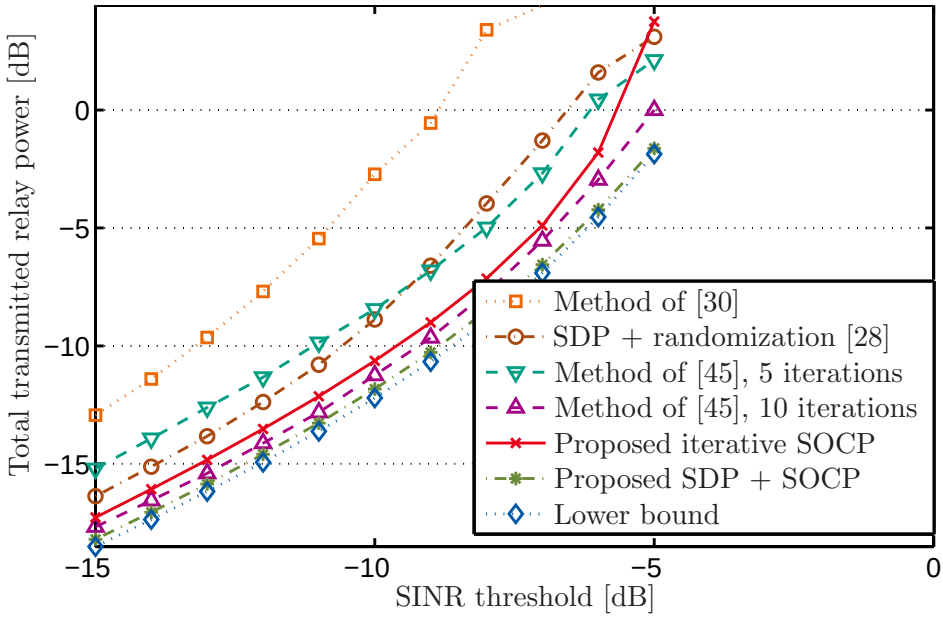

Figure 5.6. Total transmitted relay power versus SINR threshold. $K = 12$, $N = 20$, $M = 12$.

is closer to that of the other approaches in this scenario than in the MGM and the BC scenario. However, the iterative version still provides a substantial performance improvement over the state-of-the-art techniques. The proposed combination of the SDR-based approach and the iterative SOCP scheme as a local refinement almost reaches the lower/upper bound and can therefore be considered as nearly optimal in this case. Due to the large number of interfering sources, the original problem becomes infeasible if the SINR threshold exceeds -4 dB. Due to the poor performance of the method of [30], which always yields the worst results, we no longer show its results in the figures for the remainder of the thesis.

Next, we investigate the impact of the number of destination nodes on the performance of the competing schemes. Figs. 5.8 and 5.9 show the total transmitted relay power and the percentage of feasible Monte Carlo runs, respectively, versus the number of destination nodes for a MGM relay network with $K = 3$ source nodes, $N = 16$ relay nodes and an SINR threshold of $\gamma_m = 2$ dB for all destination nodes. The figures demonstrate that the iterative approximation methods clearly outperform the SDR-based method for a moderate to a large number of destination nodes.

We finally study the performance of the AC extension to our algorithm proposed in Section 5.5. A scenario with $K = 3$ sources, $N = 6$ relays and $M = 6$ destinations is considered where the multicast groups contain the same number of receivers. In the AC scheme of Section 5.5, a particular (largest cardinality) subset of users is determined

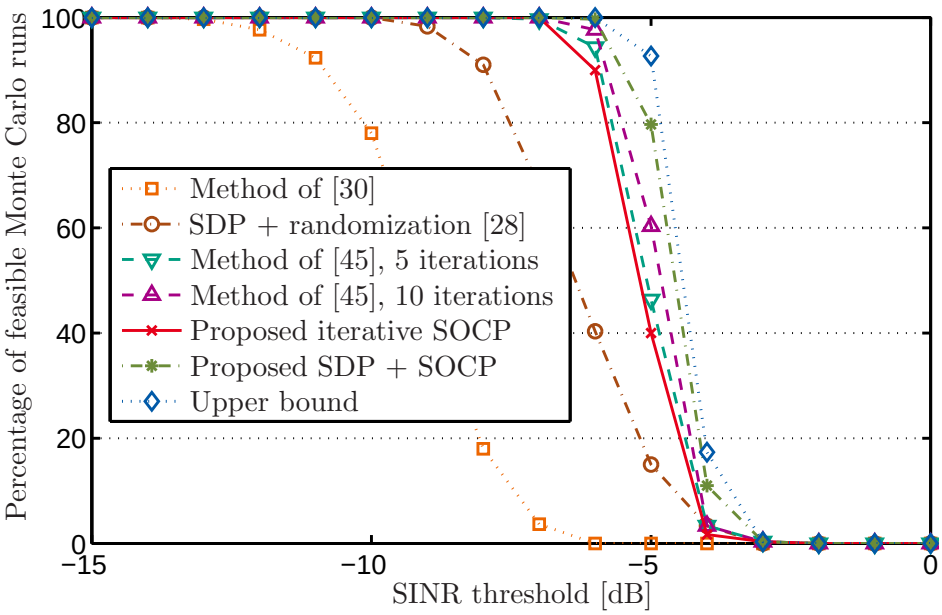

Figure 5.7. Percentage of feasible Monte Carlo runs versus SINR threshold. $K = 12$, $N = 20$, $M = 12$.

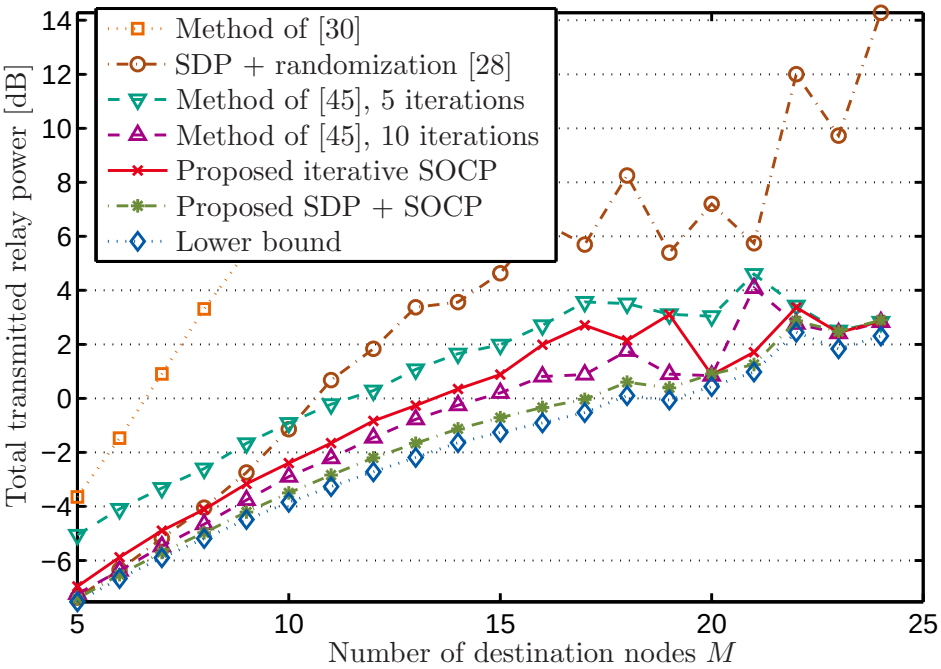

Figure 5.8. AF relay beamforming. Total transmitted relay power versus M. $K = 3$, $N = 16$.

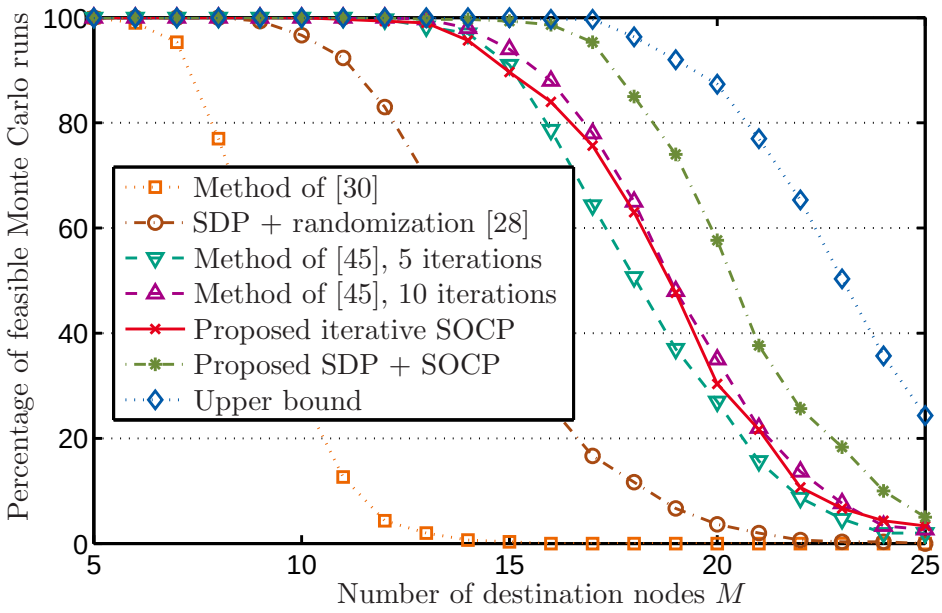

Figure 5.9. AF relay beamforming. Percentage of feasible Monte Carlo runs versus M. $K = 3$, $N = 16$.

for which a feasible approximation can be found using the iterative SOCP method. It is not guaranteed that the determined subset of users is optimal in the sense that the number of served users is maximized. As a benchmark (but prohibitively expensive) approach, the optimal subset of users can be found by an exhaustive search where the iterative SOCP method is applied to every possible subset of users. The subset with the maximum number of users for which a feasible approximate solution can be found is then chosen as the optimal subset. In the case of two or more subsets with the same maximum number of users, the one yielding the smallest total transmitted relay power is selected. Since such an exhaustive search is very time-consuming and the number of possible subsets increases exponentially with the number of destinations, we limit the number of receivers to $M = 6$ and average over only 100 Monte Carlo runs. Fig. 5.10 depicts the number of users that are excluded from the network on average by the compared AC algorithms. The corresponding total transmitted relay power required to satisfy the QoS constraints of the remaining (non-excluded) users is shown in Fig. 5.11 for the two AC schemes. It follows from Fig. 5.10 that the average number of excluded users slightly increases with the SINR threshold. We can observe that without AC, communication would already have been disabled for the whole network at an SINR threshold of around 3 dB on average as no feasible solution would have been found. However, at this SINR threshold, the AC algorithms have to exclude only one destination user from the network to restore its functioning. It can be observed from Fig. 5.11 that the total transmitted relay power corresponding to the exhaustive

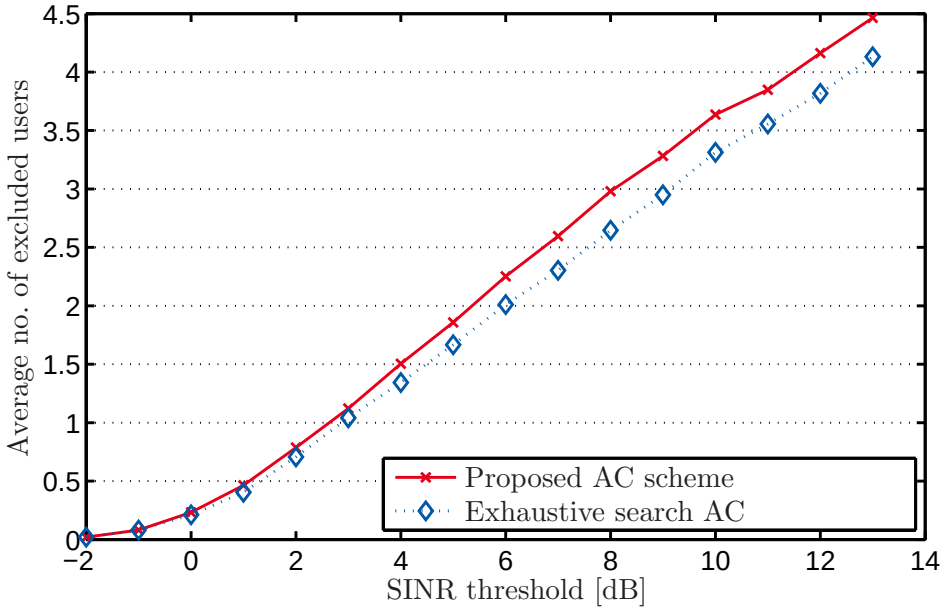

Figure 5.10. AC: Average number of excluded users versus SINR threshold.

search is sometimes greater than that corresponding to the proposed AC scheme. This happens when the optimal subset comprises more users than the subset determined by the proposed AC procedure. Figs. 5.10 and 5.11 demonstrate that the results of the proposed AC scheme are always close to those of the AC scheme based on exhaustive search.

5.8.2 FF Relay Networks with Frequency Selective Channels

Let us now investigate the performance of the proposed schemes and the state-of-the-art methods when applied to the FF relay networks with frequency selective channels of Section 3.3. We model the FIR filter coefficients of the CIRs as in [52–56], i.e., the FIR filter coefficients are modeled as independent quasi-static Rayleigh fading following the exponential power delay profile $p[n] = \frac{1}{\sigma_t} \sum_{l=0}^{L_x-1} e^{-n/\sigma_t} \delta[n-l]$ where σ_t characterizes the delay spread and $L_x \in \{L_f, L_g\}$. We consider a MGM relay network with $K = 3$ source nodes, $N = 16$ relay nodes, and $5 \leq M \leq 20$ destination nodes, choose $L_f = L_w = L_g = 5$, and set the SINR threshold to $\gamma_m = -7$ dB $\forall m \in \mathcal{M}$.

Figs. 5.12 and 5.13 display the total transmitted relay power and the percentage of feasible Monte Carlo runs, respectively, versus the number of destination nodes. It is clear from the latter two figures that the proposed methods outperform the existing SDR-based method in the FF relaying scenario as well.

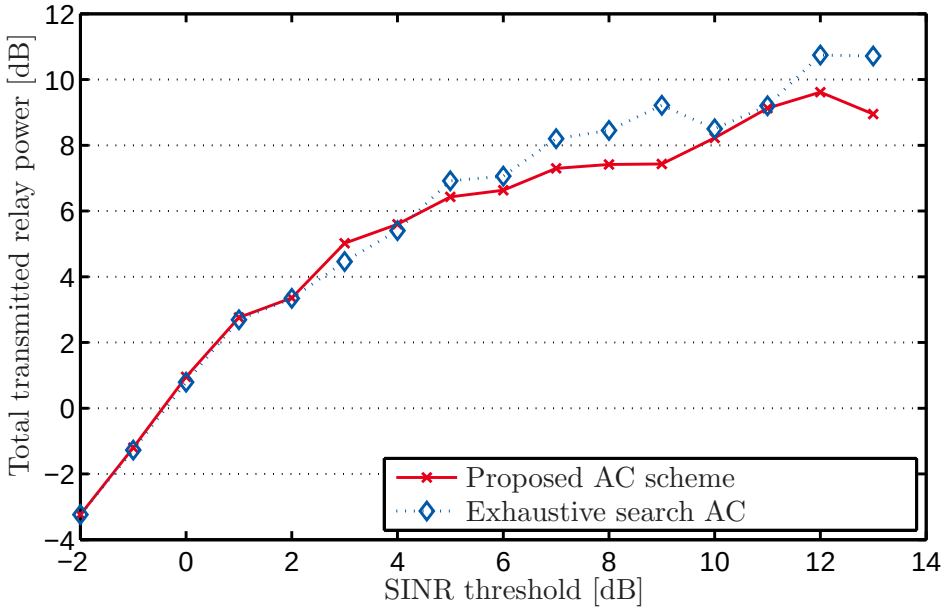

Figure 5.11. Total transmitted relay power versus SINR threshold with AC.

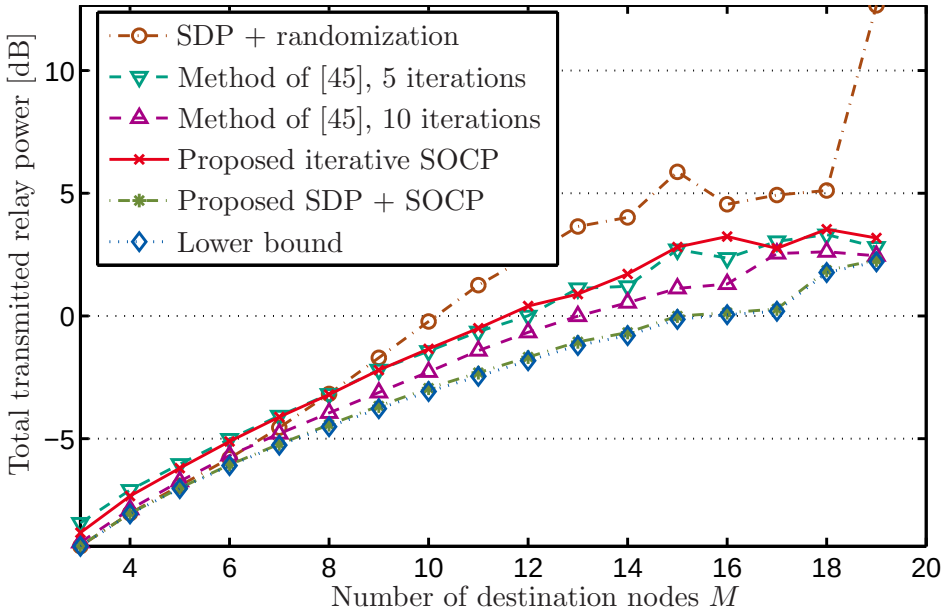

Figure 5.12. FF relay beamforming. Total transmitted relay power versus M. $K = 3$, $N = 16$.

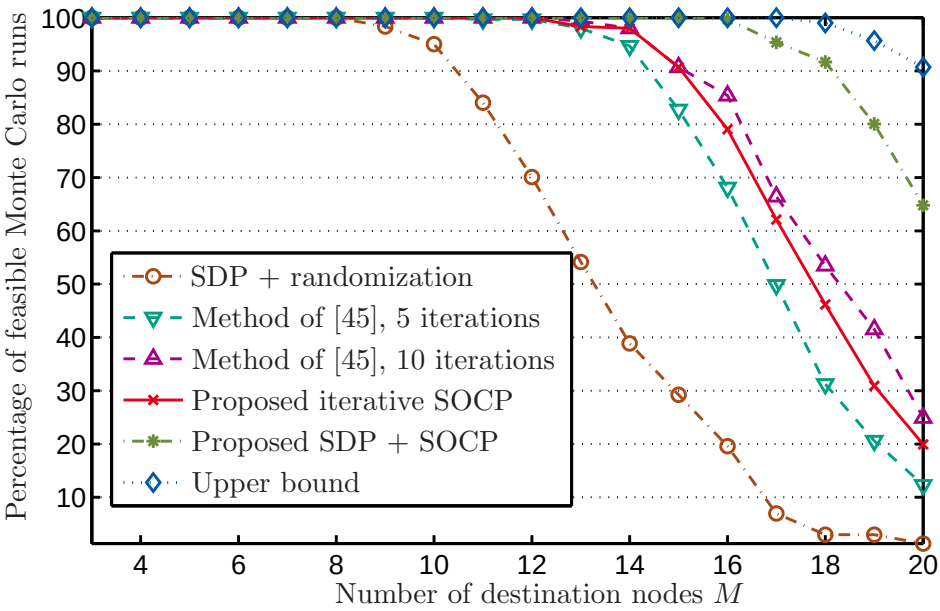

Figure 5.13. FF relay beamforming. Percentage of feasible Monte Carlo runs versus M. $K = 3$, $N = 16$.

5.9 Summary

In this chapter, we have proposed an iterative SOCP method where in each iteration, a convex SOCP approximation of the original problem is solved in polynomial time and the approximation is adapted to the solution obtained by this means. We have shown analytically that the approximate solution is thereby improved from iteration to iteration. To avoid infeasibility of the convex SOCP approximation, we have proposed an iterative feasibility search with which a feasible initial SOCP approximation of the original problem can be obtained in most cases. The feasibility search has also been embedded into an admission control scheme. Furthermore, we have shown that the proposed technique can also be used as a local refinement for the solution obtained with the SDP method of [28]. The worst-case computational complexities of the competing techniques have been discussed analytically. We were able to conclude that, as the number of destination nodes increases, the complexity of our iterative method decreases relative to that of the SDP method of [28]. In our numerical simulations, we have demonstrated that when the number of destination users in the considered relay beamforming networks is moderate to large, the proposed iterative SOCP technique outperforms state-of-the-art schemes in terms of both total transmitted relay power and feasibility. Using the proposed method as a local refinement for the solution of the SDP problem is associated with the highest computational complexity of all methods considered. However, our simulation results have shown that the latter combination

of the two approaches yields the best results which are very close to the lower bound. and thus near-optimal. Our simulation results have also shown that using the proposed method as a local refinement for the solution of the SDP problem yields the best results which are very close to the lower bound and thus near-optimal. Of course, the latter combination of the two approaches is associated with the highest computational complexity. However, if this complexity is affordable, a near-optimal solution can be achieved. The variety of relay beamforming problems to which the proposed iterative method has been applied demonstrates that it is a powerful tool which is widely applicable. In the next chapter, we show that with a few modifications, it is also applicable to the more traditional downlink beamforming in MGM scenarios.

Chapter 6

Proposed Iterative SOCP Approach - Downlink Beamforming

6.1 Introduction

In this chapter, we apply the proposed iterative SOCP approach to the MGM downlink beamforming problem (2.9). From a mathematical perspective, the only significant difference between problem (3.30) and problem (2.9) is that the latter problem exhibits multiple beamforming vectors (one for each multicast group) while in the former problem, only a single beamforming vector is shared by all multicast groups. Since we consider MGM, each beamforming vector in problem (2.9) is, however, still shared as a common beamforming vector by multiple users. As a consequence, the proposed iterative SOCP approach can be applied to problem (2.9), too. Towards this end, only a few modifications for the iterative SOCP scheme are required which shall be explained in this chapter.

Recall that the SDR approach of [17] described in Section 4.3 requires randomization and costly power control, i.e., solving an instance of problem (4.6) for each generated candidate. The property of our iterative SOCP method, that the convex inner approximation yields a SOCP problem whose solution, provided it exists, is always feasible for the original problem (2.9), is preserved when applying it to MGM downlink beamforming. Hence, randomization and costly power control is avoided in our method. Recall that in the special case of a single multicast group, i.e., in the BC case of Section 2.2.2, the power control required for the SDR approach is simpler than in the general case of MGM downlink beamforming since it can be obtained by simple scaling. A simplification in the BC case is available for our method as well: We show that in the BC case, the SOCP problem in our method can be further simplified to a quadratic programming (QP) problem. Our simulation results show that in terms of transmitted power and feasibility, the performance of the proposed method is very similar to that of the SDR-based approach. In terms of computational complexity, the proposed method outperforms the SDR-based approach when the number of users is large.

This chapter is based on my original work that has been published in [2].

6.2 Convex Inner Approximation of the Feasible Set

For the general MGM downlink beamforming problem (2.9), the derivation of the convex inner approximation of the feasible set is similar to that of the equivalent reformulation of the MU downlink beamforming problem (2.10) as a convex SOCP problem: First, we exploit the rank-one property of the matrix $\boldsymbol{C}_m$ (in case of instantaneous CSI) to rewrite the QoS constraints in problem (2.9) as

$$|\boldsymbol{w}_d^H \boldsymbol{c}_m| \geq \sqrt{\gamma_m \left(\sum_{k \neq d} \boldsymbol{w}_k^H \boldsymbol{C}_m \boldsymbol{w}_k + \sigma_m^2 \right)}. \tag{6.1}$$

By introducing the new matrix and vector

$$\begin{aligned} \boldsymbol{\mathcal{H}}_{d,m} &\triangleq \begin{bmatrix} \sigma_m^2 & \boldsymbol{0}^T \\ \boldsymbol{0} & (\boldsymbol{I} - \operatorname{diag}\{\boldsymbol{e}_d\}) \otimes \boldsymbol{C}_m \end{bmatrix}^{1/2}, \ \forall m \in \mathcal{G}_d, \ \forall d \in \mathcal{K}, \\ \boldsymbol{w}_{\text{all}} &\triangleq [1, \boldsymbol{w}_1^T, \ldots, \boldsymbol{w}_K^T]^T, \end{aligned}$$

we further rewrite the constraint in (6.1) as

$$|\boldsymbol{w}_d^H \boldsymbol{c}_m| \geq \sqrt{\gamma_m} \|\boldsymbol{\mathcal{H}}_{d,m} \boldsymbol{w}_{\text{all}}\|. \tag{6.2}$$

Recall that in the special case of MU downlink beamforming, one can argue that the phase φ_d of each beamforming vector $\boldsymbol{w}_d$ can be chosen such that the inner product $\boldsymbol{w}_d^H \boldsymbol{c}_d$ becomes real-valued and non-negative for all QoS constraints simultaneously (see Section 2.2.1). This is not possible in the general case of MGM downlink beamforming due to the following reason: In the MU downlink scenario, each beamforming vector $\boldsymbol{w}_d$ is associated with a single QoS constraint while in the MGM downlink scenario, a common beamforming vector $\boldsymbol{w}_d$ is shared by multiple users associated with the same multicast group. As a consequence, an equivalent SOCP reformulation as in the MU downlink case does not exist for the MGM downlink beamforming problem (2.9). However, we can approximate the original problem (2.9) by a SOCP problem and successively improve this approximation much like in the previous chapter. Using the same conservative approximation as in the previous chapter, i.e., approximating the magnitude in the left-hand side of inequality (6.2) by the real-part, we obtain the following convex SOCP approximation of the original non-convex problem (2.9)

$$\begin{aligned} \min_{t \in \mathbb{R},\, \boldsymbol{w}_{\text{all}} \in \mathbb{C}^{KN+1}} \quad & t && \text{(6.3a)} \\ \text{s.t.} \quad & \|\boldsymbol{w}_{\text{all}}\| \leq t && \text{(6.3b)} \\ & \sqrt{\gamma_m} \|\boldsymbol{\mathcal{H}}_{d,m} \boldsymbol{w}_{\text{all}}\| \leq \operatorname{Re}\{\boldsymbol{w}_d^H \boldsymbol{c}_m\}, \ \forall m \in \mathcal{G}_d, \forall d \in \mathcal{K}, && \text{(6.3c)} \\ & w_{\text{all},1} = 1. && \text{(6.3d)} \end{aligned}$$

Initialization: $\boldsymbol{c}_m^{(1)} = \boldsymbol{c}_m,\ \forall m \in \mathcal{G}_d,\ \forall d \in \mathcal{K}$
for $i = 1, \ldots, I$
Solve problem (6.3) with $\boldsymbol{c}_m = \boldsymbol{c}_m^{(i)}$.
Perform the rotation of (6.4) where $\alpha_{d,m}^{(i)}$ is obtained as in (6.5).
end

Table 6.1. Proposed iterative procedure

6.3 Iterative QoS-Constrained Power Minimization

The iterative SOCP algorithm for the MGM downlink beamforming scenario is very similar to the iterative SOCP algorithm for the distributed beamforming scenario described in Chapter 5: The channel rotation recursion is defined as

$$\boldsymbol{c}_m^{(i+1)} \triangleq \boldsymbol{c}_m^{(i)} \exp\left(-j\alpha_{d,m}^{(i)}\right),\ \forall m \in \mathcal{G}_d,\ \forall d \in \mathcal{K} \tag{6.4}$$

where $\alpha_{d,m}^{(i)}$ is chosen as

$$\alpha_{d,m}^{(i)} = \angle(\boldsymbol{w}_{d,\text{opt}}^{(i)H} \boldsymbol{c}_m^{(i)}) \tag{6.5}$$

and $\boldsymbol{w}_{d,\text{opt}}^{(i)}$ is the optimal solution of problem (6.3) for $\boldsymbol{c}_m = \boldsymbol{c}_m^{(i)}$ obtained in the ith iteration. The choice of $\alpha_{d,m}^{(i)}$ according to (6.5) optimizes the SOC approximation of the feasible set of problem (2.9) in the vicinity of $\boldsymbol{w}_{d,\text{opt}}^{(i)}$ since

$$|\boldsymbol{w}_{d,\text{opt}}^{(i)H} \boldsymbol{c}_m| = \text{Re}\left\{\boldsymbol{w}_{d,\text{opt}}^{(i)H} \boldsymbol{c}_m^{(i)} \exp\left(-j\alpha_{d,m}^{(i)}\right)\right\} \tag{6.6a}$$

$$= \text{Re}\left\{\boldsymbol{w}_{d,\text{opt}}^{(i)H} \boldsymbol{c}_m^{(i+1)}\right\} \geq \text{Re}\left\{\boldsymbol{w}_{d,\text{opt}}^{(i)H} \boldsymbol{c}_m^{(i)}\right\} \tag{6.6b}$$

where equality holds in (6.6b) if and only if $\alpha_{d,m}^{(i)} = 0$. The algorithm is summarized in Table 6.1.

Lemma 3: The method of Table 6.1 yields an improved solution in iteration $(i+1)$ relative to that of iteration i as long as $\alpha_{d,m}^{(i)} \neq 0$ holds for all active constraints in at least one multicast group in iteration i.

Proof of Lemma 3: Lemma 3 can be proved by contradiction. Towards this end, we assume that in some iteration $(i+1)$, the solution of (6.3) is the same as that in the previous iteration i, i.e., $\{\boldsymbol{w}_{k,\text{opt}}^{(i+1)}\}_{k=1}^K = \{\boldsymbol{w}_{k,\text{opt}}^{(i)}\}_{k=1}^K$. Note that at optimum of (6.3), at least one QoS constraint per group will be active, i.e., satisfied with equality. Let us further assume that $\alpha_{d,m}^{(i)} \neq 0$ holds for all active constraints in at least one multicast group $\mathcal{G}_d$ in iteration i. Then, (6.6b) reveals that for these constraints, the

right-hand parts of the approximated QoS constraints in problem (6.3) in iteration $(i+1)$ are greater than those in iteration i whereas the left-hand parts remain the same. Hence, the dth beamformer, $\boldsymbol{w}_{d,\text{opt}}^{(i+1)}$, can be scaled down while still satisfying all QoS constraints of the dth multicast group and thereby contradicting optimality of $\boldsymbol{w}_{d,\text{opt}}^{(i+1)} = \boldsymbol{w}_{d,\text{opt}}^{(i)}$ for (6.3) in iteration $(i+1)$. We conclude that the objective value must decrease monotonically with the iterations as long as $\alpha_{d,m}^{(i)} \neq 0$ holds for all active constraints in at least one multicast group in iteration i. □

Note, however, that in general, there is no guarantee that the algorithm converges to the global optimum of problem (2.9).

6.4 Iterative Feasibility Search

The feasibility search is also very similar to the one proposed in Section 5.4: Problem (6.3) is modified in the same way as problem (5.6) is modified in Section 5.4 such that we obtain the following optimization problem

$$\min_{\boldsymbol{z}\in\mathbb{R}^M,\, \boldsymbol{w}_{\text{all}}\in\mathbb{C}^{KN}} \quad \mathbf{1}^T\boldsymbol{z} \tag{6.7a}$$

$$\text{s.t.} \quad \sqrt{\gamma_m}\|\boldsymbol{\mathcal{H}}_{d,m}\boldsymbol{w}_{\text{all}}\| - \text{Re}\{\boldsymbol{w}_d^H\boldsymbol{c}_m\} \leq z_m,\ \forall m \in \mathcal{G}_d, \forall d \in \mathcal{K}, \tag{6.7b}$$

$$z_m \geq 0,\ \forall m \in \mathcal{G}_d,\ \forall d \in \mathcal{K} \tag{6.7c}$$

$$w_{\text{all},1} = 1. \tag{6.7d}$$

To find feasible initial rotations of the channel vectors, the algorithm of Table 6.1 is performed where we replace problem (6.3) by problem (6.7).

Lemma 4: The proposed scheme yields a reduced infeasibility indicator in the $(i+1)$th iteration relative to that of the ith iteration as long as $\alpha_{d,m}^{(i)} \neq 0$ and $[\boldsymbol{z}_{\text{opt}}^{(i)}]_m > 0$ for at least one pair d, m in iteration i.

Proof of Lemma 4: Lemma 4 can be proved in the same way Lemma 2 has been proved: Again, assume that $\boldsymbol{w}_{d,\text{opt}}^{(i+1)} = \boldsymbol{w}_{d,\text{opt}}^{(i)}$. Further, assume that $\alpha_{d,m}^{(i)} \neq 0$ and $[\boldsymbol{z}_{\text{opt}}^{(i)}]_m > 0$ for at least one pair d, m in iteration i. Then, we see from (6.6b) and (6.7) that $\mathbf{1}^T\boldsymbol{z}_{\text{opt}}^{(i+1)} < \mathbf{1}^T\boldsymbol{z}_{\text{opt}}^{(i)}$. □

Note that this feasibility search can straightforwardly be extended to the admission control procedure of Section 5.5. The extension is identical to the one proposed in Section 5.5.

6.5 SOCP as a Local Refinement for SDP

In the case of MGM downlink beamforming, the iterative SOCP scheme can be used as a local refinement for the SDR approach of Section 4.3. This is very similar to the approach described in Section 5.6: We solve the SDP problem (4.4) to obtain its optimal solution $\{\boldsymbol{X}_{k,\mathrm{opt}}\}_{k=1}^{K}$ and, for each k, we compute the principal component $\boldsymbol{w}_{k,\mathrm{p}}$ of the matrix $\boldsymbol{X}_{k,\mathrm{opt}}$. Then, we use the following initial rotation of the channel vectors for the feasibility search:

$$\boldsymbol{c}_m^{(1)} \triangleq \boldsymbol{c}_m \exp\left(-j\alpha_{k,m}^{(1)}\right),\ \forall m \in \mathcal{G}_k,\ \forall k \in \mathcal{K} \tag{6.8}$$

where

$$\alpha_{k,m}^{(1)} = \boldsymbol{w}_{k,\mathrm{p}}^H \boldsymbol{c}_m,\ \forall m \in \mathcal{G}_k,\ \forall k \in \mathcal{K}. \tag{6.9}$$

6.6 Special Case 2: BC Downlink Beamforming

Recall that the computational complexity of the SDR-based scheme is lower in the BC downlink case than in the MGM downlink case since in the former case, it is not required to solve the LP problem (4.6) for each candidate beamforming vector. Similarly, the iterative convex inner approximation method proposed in this thesis enjoys a lower computational complexity in the BC case as compared to the MGM case for the following reason. In the special case of BC downlink beamforming, the convex inner approximation of Section 6.2 yields an even simpler optimization problem than the SOCP problem (6.3) as we show next. Exploiting the rank-one property of matrix $\boldsymbol{C}_m$ (in case of instantaneous CSI), the mth QoS constraint of the BC downlink beamforming problem (2.14) can be rewritten as

$$|\boldsymbol{w}_1^H \boldsymbol{c}_m| \geq \sqrt{\gamma_m \sigma_m^2}. \tag{6.10}$$

Approximating the magnitude in the left-hand side of inequality (6.10) by the real-part, we obtain the following convex approximation of problem (2.14)

$$\min_{\boldsymbol{w}_1 \in \mathbb{C}^N} \quad \|\boldsymbol{w}_1\|^2 \tag{6.11a}$$

$$\text{s.t.} \quad \mathrm{Re}\{\boldsymbol{w}_1^H \boldsymbol{c}_m\} \geq \sqrt{\gamma_m \sigma_m^2},\ \forall m \in \{1, \ldots, M\}. \tag{6.11b}$$

This problem is a convex (linearly constrained) QP problem whose complexity is even less than that of problem (6.3). Obviously, the concept of successively improving the approximation via the channel rotations as described in Sections 6.3 and 6.4 can straightforwardly be applied to problem (6.11) as well.

6.7 Complexity Analysis

Similar to Section 5.7, we now compare the computational complexity of the proposed sequential inner approximation technique to that of the SDR-based scheme of [16, 17] for the downlink beamforming scenarios.

According to [66], the SOCP problem (6.3) can be solved with a worst-case complexity of $\mathcal{O}(K^3N^3M^{1.5})$ using primal-dual interior point methods. In the proposed iterative method, this complexity scales linearly with the number of required iterations I yielding an overall complexity of the proposed iterative method of $\mathcal{O}(IK^3N^3M^{1.5})$.

The SDP problem (4.4) exhibits the same mathematical structure as the SDP problem (4.2) apart from the fact that in the latter problem, only a single matrix $\boldsymbol{X}$ is optimized while the former problem exhibits multiple optimization matrices $\boldsymbol{X}_k$. Thus, in terms of dimensions, the two problems only differ in the dimension of the optimization variable. Hence, from the worst-case complexity of problem (4.2) as derived in Section 5.7, we conclude that the SDP problem (4.4) can be solved with a worst-case complexity of $\mathcal{O}(M^2(KN+M)^{2.5})$. In the MGM downlink beamforming scenario, it is required to additionally solve one LP problem (4.6) for each candidate beamforming vector obtained by randomization. Let N_{rand} stand for the number of generated candidate vectors of which, according to [17], a few hundred are usually required. Then, the overall computational complexity of the SDR-based approach is that of the SDP problem (4.4) along with N_{rand} times that of the LP problem (4.6) which can be solved with a worst-case complexity of $\mathcal{O}(K^{3.5}+MK^{3.5})$ using interior-point methods [17]. Hence, the overall complexity of the SDR-based approach is $\mathcal{O}(M^2(KN+M)^{2.5}) + \mathcal{O}(N_{\text{rand}}(K^{3.5}+MK^{3.5}))$.

We conclude that with an increasing number of users M, the computational complexity of the proposed method decreases relative to that of the SDR-based scheme.

6.8 Simulation Results

Throughout the simulations in this chapter, we assume frequency flat Rayleigh-fading channels with unit variance and, without loss of generality, equal noise powers and SINR thresholds at the users. For our algorithm, we have chosen the maximum number of iterations as $I = 3$ and for the SDR-based approach, 100 candidate vectors have been generated. All results are averaged over 300 Monte Carlo runs. We consider two

different scenarios, a MGM scenario with $K = 3$ multicast groups of similar size, $N = 6$ antennas at the transmitter and $M = 16$ users, and a BC scenario with $K = 1$ multicast group, $N = 6$ antennas at the transmitter and $M = 20$ users. We do not consider Special Case 1 of Section 2.2.1 since an optimal solution can be obtained for the MU downlink beamforming problem and our proposed algorithm is not required in this scenario.

Let us first consider the MGM scenario. Figs. 6.1 and 6.2 show the total power radiated at the transmitter and the percentage of feasible Monte Carlo runs, respectively, versus the SINR threshold at the users for the MGM downlink beamforming scenario. For the BC downlink beamforming scenario, the total transmitted power versus the signal-to-noise ratio (SNR) threshold is shown in Fig. 6.3. The corresponding percentage of feasible Monte Carlo runs is not shown since the BC downlink beamforming problem (2.14) is always feasible. We can observe that the performance improvements of the proposed methods compared to state-of-the-art methods are less pronounced in the traditional downlink beamforming scenarios than in relay beamforming. However, in the MGM scenario, the result of the proposed combination of the SDP and the SOCP approach virtually reaches the lower bound and is thus virtually optimal. Furthermore, recall that the proposed iterative method enjoys a lower computational complexity than the SDR-based approach in case of a moderate to a large number of users. In MGM and BC scenarios with a large number of users, the proposed method is therefore superior to the one of [16, 17] in terms of computational complexity.

6.9 Summary

In this chapter, we have shown that with some modifications, the proposed iterative SOCP technique is also applicable to downlink beamforming in MGM and BC scenarios. All the concepts proposed in the previous chapter have been adopted for MGM downlink beamforming in this chapter, i.e., the iterative power minimization, the iterative feasibility search with the extension to admission control, and the combination of the proposed method and the SDR-based approach of [16, 17]. It has been shown that in MGM scenarios with a large number of users, the complexity reduction that can be achieved using our iterative method rather than the SDR-based approach is even more pronounced than in the previous chapter. This is due to the fact that solving additional power control problems, whose complexity increases with the number of users, is required in the method [17]. We have shown that in the special case of BC downlink beamforming, our iterative SOCP scheme is simplified to an iterative QP

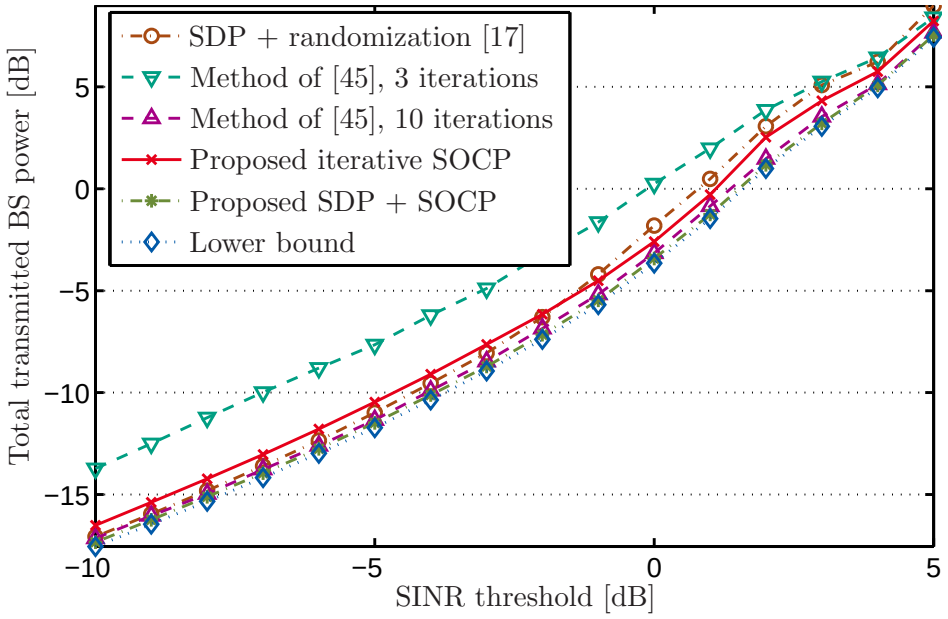

Figure 6.1. Downlink Beamforming. Total transmitted power versus SINR threshold. $K = 3$, $N = 6$, $M = 16$.

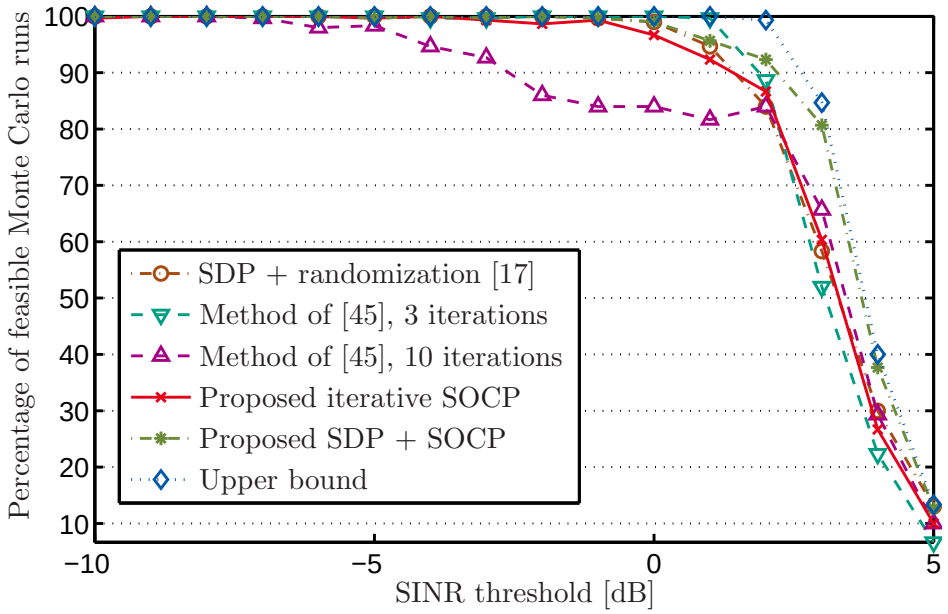

Figure 6.2. Downlink Beamforming. Percentage of feasible Monte Carlo runs versus SINR threshold. $K = 3$, $N = 6$, $M = 16$.

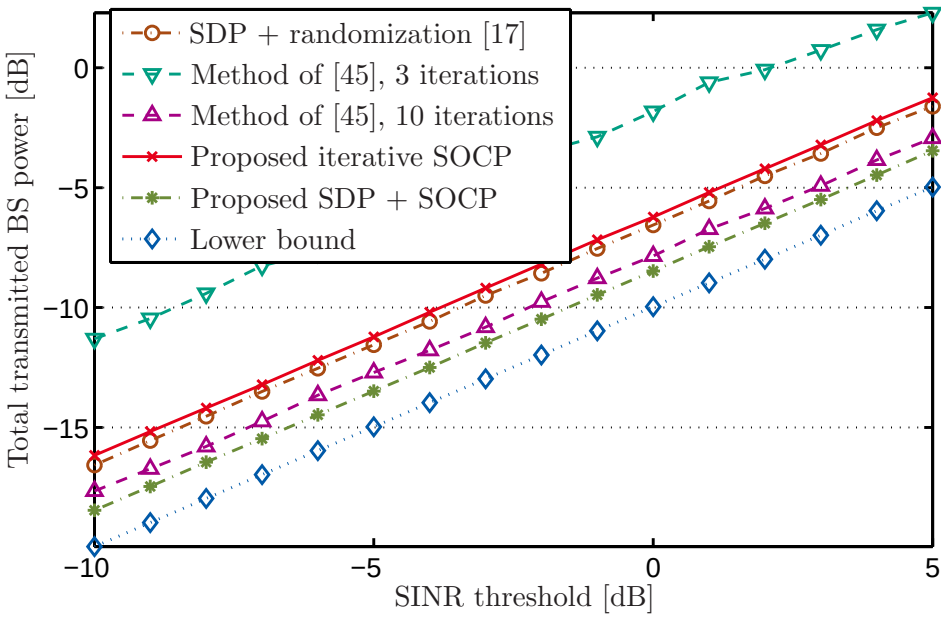

Figure 6.3. Downlink Beamforming. Total transmitted power versus SNR threshold. $K = 1$, $N = 6$, $M = 20$.

scheme whose complexity is even less than that of the former scheme. Our simulation results have revealed that the performance of the proposed method in terms of total transmitted relay power and feasibility is very similar to that achieved with the SDR-based approach of [16, 17]. However, this similar performance is achieved at a significantly reduced computational complexity when the number of users is moderate to large. In the MGM scenario, using the proposed method as a local refinement for the SDP solution is virtually optimal in our simulations.

Chapter 7

Proposed Iterative SOCP Approach for Statistical CSI

7.1 Introduction

As shown in Chapters 5 and 6, the iterative SOCP technique proposed in the latter chapters offers various advantages over the SDR approach of [28], [54], and [17]. However, the iterative SOCP scheme suffers from the following major shortcoming as compared to the SDR approach. The two competing techniques have different requirements on the availability of CSI at the transmitter or the processing node(s). The SDR technique is applicable in both cases, with instantaneous CSI as well as in the case when only statistical CSI in the form of channel covariance matrices are available at the transmitter or the processing node(s). The iterative SOCP scheme can only be applied in the former case. As explained in Sections 2.3 and 3.5, the acquisition of instantaneous CSI is, however, often associated with a prohibitive signaling overhead. Beamformer designs based on channel covariance matrices are therefore used to significantly reduce the signaling overhead.

In this chapter, we propose a non-trivial extension of the iterative SOCP method proposed in Chapters 5 and 6 to the case when statistical CSI is available at the transmitter or the processing node(s). In our extension, the aforementioned advantages of the iterative SOCP technique over the SDR technique are preserved. After the extension, e.g., the approximation of the feasible set is still a convex inner approximation such that the use of randomization techniques, and costly power control in case of MGM downlink beamforming, is avoided. As in Chapters 5 and 6, we approximate the original problem by a convex SOCP problem and successively improve the approximate solution. Simply using the principal component of the channel covariance matrix to formulate the SOCP approximation would be a trivial way to keep the method of Chapters 5 and 6 applicable. However, this approximation is poor if the covariance matrix is of higher rank and yields unsatisfactory beamforming results in the latter case. Therefore, we propose a more sophisticated approximation of the covariance matrix based on the l_1-norm approximation of the Euclidean norm that enables the use of all eigenvectors in the optimization procedure. As in Chapters 5 and 6, we prove that the approximate solution obtained by our algorithm is improved from iteration to

iteration. Our simulation results reveal that the performance advantages of the iterative SOCP approach over the SDR approach are preserved in the proposed extension, i.e., the iterative SOCP scheme for statistical CSI outperforms the SDR scheme for a moderate to a large number of users.

This chapter is based on my original work that has been published in [5].

7.2 Iterative QoS-Constrained Power Minimization

Let us consider statistical CSI and define the matrix $\boldsymbol{R}_{d,m}$ as in Section 3.5, i.e., $\boldsymbol{R}_{d,m} \triangleq P_d \mathrm{E}\left\{\boldsymbol{h}_{d,m}\boldsymbol{h}_{d,m}^H\right\}$ which is generally not rank-one. Hence, we can no longer exploit the rank-one property of $\boldsymbol{R}_{d,m}$ as defined in Chapter 5, i.e., $\boldsymbol{R}_{d,m} \triangleq P_d \boldsymbol{h}_{d,m}\boldsymbol{h}_{d,m}^H$. Thus, we need to rewrite (5.2) as follows.

$$\sqrt{\boldsymbol{w}^H \boldsymbol{R}_{d,m} \boldsymbol{w}} \geq \sqrt{\gamma_m} \|\boldsymbol{U}_m \tilde{\boldsymbol{w}}\|, \ \forall m \in \mathcal{G}_d, \ \forall d \in \mathcal{K} \tag{7.1}$$

As in Section 5.2, in order to find a second-order cone approximation of the constraint in (7.1), its left-hand side needs to be linearized. In the linearization proposed below, we exploit the fact that the l_1-norm of a vector $\boldsymbol{a} = [a_1, \ldots, a_N]^T$ is a lower approximation of the corresponding Euclidean norm such that

$$\sqrt{\sum_{n=1}^{N} |a_n|^2} \geq \frac{1}{\sqrt{N}} \sum_{n=1}^{N} |a_n|. \tag{7.2}$$

Note that in (7.2), equality holds if and only if all elements of $\boldsymbol{a}$ have the same magnitude. Further, note that inequality (7.2) still holds if we use only a subset of the elements in $\boldsymbol{a}$ for the approximation, i.e.,

$$\sqrt{\sum_{n=1}^{N} |a_n|^2} \geq \sqrt{\sum_{n \in \bar{\mathcal{N}}} |a_n|^2} \geq \frac{1}{\sqrt{\bar{N}}} \sum_{n \in \bar{\mathcal{N}}} |a_n| \tag{7.3}$$

where the index set $\bar{\mathcal{N}}$ is defined as a subset of the original set $\mathcal{N}$, i.e., $\bar{\mathcal{N}} \subseteq \mathcal{N} = \{1, \ldots, N\}$ and $\bar{N} = |\bar{\mathcal{N}}|$. To show that an appropriate choice of the index set can improve the approximation, let us consider the specific example of $|a_1| = 0$ and $|a_2| = \cdots = |a_N| > 0$ in which the approximation in (7.2) is not tight. However, if we define the subset $\bar{\mathcal{N}} = \{2, \ldots, N\}$, the inequalities in (7.3) are satisfied with equality. With these observations, we next derive the proposed linearization of the left-hand side of (7.1).

For simplicity of notation, the indices d and m in $\boldsymbol{R}_{d,m}$ are omitted in the following discussion. Making use of the eigenvalue decomposition of the channel covariance matrix given by $\boldsymbol{R} = \sum_{n=1}^{N} \lambda_n \boldsymbol{v}_n \boldsymbol{v}_n^H$, the left-hand side of inequality (7.1) can be rewritten as

$$\sqrt{\sum_{n=1}^{N} \lambda_n \boldsymbol{w}^H \boldsymbol{v}_n \boldsymbol{v}_n^H \boldsymbol{w}} = \sqrt{\sum_{n=1}^{N} |\sqrt{\lambda_n} \boldsymbol{w}^H \boldsymbol{v}_n|^2} \geq \frac{1}{\sqrt{\bar{N}}} \sum_{n \in \bar{\mathcal{N}}} \sqrt{\lambda_n} |\boldsymbol{w}^H \boldsymbol{v}_n| \tag{7.4}$$

where λ_n and $\boldsymbol{v}_n$ denote the nth eigenvalue and eigenvector of $\boldsymbol{R}$, respectively, and $\bar{\mathcal{N}}$ can be any subset of $\mathcal{N}$. Note that (7.3) has been used to obtain the approximation in (7.4). The final step in our linearization is similar to the approach in Section 5.2, i.e., it consists in approximating the magnitude of a complex scalar by its real-part, hence,

$$\frac{1}{\sqrt{\bar{N}}} \sum_{n \in \bar{\mathcal{N}}} \sqrt{\lambda_n} |\boldsymbol{w}^H \boldsymbol{v}_n| \geq \frac{1}{\sqrt{\bar{N}}} \sum_{n \in \bar{\mathcal{N}}} \sqrt{\lambda_n} \mathrm{Re}\{\boldsymbol{w}^H \boldsymbol{v}_n\}. \tag{7.5}$$

Note that, similar to the observation in Section 5.3, the left-hand side of (7.5) is independent of a multiplication of each $\boldsymbol{v}_n$ by a rotation factor $\exp(-j\alpha_n)$, where α_n is the corresponding rotation angle. However, this multiplication changes the right-hand side of (7.5) and can be used in the same way as in Section 5.3 to improve the approximation. Thus, we generalize the approximation (7.5) by replacing $\boldsymbol{v}_n$ with $\bar{\boldsymbol{v}}_n = \boldsymbol{v}_n \exp(-j\alpha_n)$.

The linearization steps in (7.4) and (7.5) can be summarize as follows

$$\sqrt{\boldsymbol{w}^H \boldsymbol{R} \boldsymbol{w}} \geq \frac{1}{\sqrt{\bar{N}}} \sum_{n \in \bar{\mathcal{N}}} \sqrt{\lambda_n} \mathrm{Re}\{\boldsymbol{w}^H \bar{\boldsymbol{v}}_n\} \tag{7.6}$$

where $\bar{\mathcal{N}} \subseteq \mathcal{N}$ and $\bar{\boldsymbol{v}}_n = \boldsymbol{v}_n \exp(-j\alpha_n)$. Let us next approximate the original non-convex problem (3.30) by the following convex SOCP problem

$$\begin{aligned}
\min_{t, \tilde{\boldsymbol{w}}} \quad & t && \text{(7.7a)}\\
\text{s.t.} \quad & \|\boldsymbol{V} \tilde{\boldsymbol{w}}\| \leq t, && \text{(7.7b)}\\
& \frac{1}{\sqrt{\bar{N}_{d,m}}} \sum_{n \in \bar{\mathcal{N}}_{d,m}} \sqrt{\lambda_{d,m,n}} \mathrm{Re}\{\boldsymbol{w}^H \bar{\boldsymbol{v}}_{d,m,n}\} \geq \sqrt{\gamma_m} \|\boldsymbol{U}_m \tilde{\boldsymbol{w}}\|, \ \forall m \in \mathcal{G}_d, \ \forall d \in \mathcal{K}, && \text{(7.7c)}\\
& \tilde{w}_1 = 1 && \text{(7.7d)}
\end{aligned}$$

where $\bar{\mathcal{N}}_{d,m} \subseteq \mathcal{N}_{d,m}$, $\bar{\boldsymbol{v}}_{d,m,n} = \boldsymbol{v}_{d,m,n} \exp(-j\alpha_{d,m,n})$, and the indices d and m have been reinstalled. Like problem (5.6), problem (7.7) can be solved efficiently using interior-point methods [62]. Note that there are more degrees of freedom in parameterizing this approximation than in that of (5.6): In addition to the rotation angles $\alpha_{d,m,n}$, we can choose the subsets $\bar{\mathcal{N}}_{d,m}$. Thus, the goal is to find those $\bar{\mathcal{N}}_{d,m}$ and $\alpha_{d,m,n}$ which yield

the best approximate solution. Similar to the idea in Chapter 5, we propose to pursue this goal using an iterative algorithm where the SOCP approximation is successively improved.

Let $\boldsymbol{w}_{\text{opt}}^{(i)}$ denote the solution to the SOCP problem (7.7) for $\bar{\mathcal{N}}_{d,m} = \bar{\mathcal{N}}_{d,m}^{(i)}$ and $\bar{\boldsymbol{v}}_{d,m,n} = \bar{\boldsymbol{v}}_{d,m,n}^{(i)}$ in the ith iteration of our algorithm. Similar to the update in Section 5.3, we can then find $\bar{\mathcal{N}}_{d,m}^{(i+1)}$ and $\bar{\boldsymbol{v}}_{d,m,n}^{(i+1)}$ of the next iteration such that the approximation in the next iteration is optimized around $\boldsymbol{w}_{\text{opt}}^{(i)}$ of the current iteration. This makes it possible to find an improved solution $\boldsymbol{w}_{\text{opt}}^{(i+1)}$ in the next iteration which we show below. Therefore, the idea is to maximize the right-hand side of (7.6) for the current $\boldsymbol{w} = \boldsymbol{w}_{\text{opt}}^{(i)}$ of the ith iteration through the choice of $\bar{\mathcal{N}}_{d,m}^{(i+1)}$ and $\bar{\boldsymbol{v}}_{d,m,n}^{(i+1)}$ in order to make the approximation as tight as possible. Instead of finding the optimal $\bar{\mathcal{N}}_{d,m}^{(i+1)}$ using an exhaustive search, let us search more efficiently for an optimal $\bar{N}_{d,m}^{(i+1)} = |\bar{\mathcal{N}}_{d,m}^{(i+1)}|$ using the following approach. For $\boldsymbol{w} = \boldsymbol{w}_{\text{opt}}^{(i)}$, we sort the eigenvalues and eigenvectors such that the summands in the left-hand side of the inequality in (7.4) are arranged in descending order, i.e., $\lambda_{m,\kappa_1}|\boldsymbol{w}_{\text{opt}}^{(i)H}\boldsymbol{v}_{m,\kappa_1}|^2 \geq \ldots \geq \lambda_{m,\kappa_N}|\boldsymbol{w}_{\text{opt}}^{(i)H}\boldsymbol{v}_{m,\kappa_N}|^2$ where $\kappa_n \in \{1,\ldots,N\}$ and $\cup_n \kappa_n = \{1,\ldots,N\}$. Then, we choose $\bar{N}_{d,m}^{(i+1)}$ according to

$$\bar{N}_{d,m}^{(i+1)} = \underset{\bar{N}_{d,m}}{\operatorname{argmax}} \frac{1}{\sqrt{\bar{N}_{d,m}}} \sum_{n=1}^{\bar{N}_{d,m}} \sqrt{\lambda_{m,\kappa_n}} |\boldsymbol{w}_{\text{opt}}^{(i)H} \bar{\boldsymbol{v}}_{m,\kappa_n}^{(i)}| \tag{7.8}$$

so that the approximation in (7.4) becomes closest to the Euclidean norm. In this way, an exhaustive search is only required to obtain the optimal $\bar{N}_{d,m}$ in (7.8). An exhaustive search over all possible $\bar{\mathcal{N}}_{d,m}$, for which a substantially larger number of possible combinations exist than for $\bar{N}_{d,m}$, is avoided. The optimal $\bar{\mathcal{N}}_{d,m}^{(i+1)}$ can then be obtained from the optimal $\bar{N}_{d,m}^{(i+1)}$ by considering the above ordering. After computing the optimal index set $\bar{\mathcal{N}}_{d,m}^{(i+1)}$, the optimal rotation angles $\alpha_{d,m,n}^{(i)}$ associated with the beamforming vector $\boldsymbol{w}_{\text{opt}}^{(i)}$ obtained in the ith iteration are computed similar to those in Section 5.3, i.e.,

$$\bar{\boldsymbol{v}}_{d,m,n}^{(i+1)} = \bar{\boldsymbol{v}}_{d,m,n}^{(i)} \exp\left(-j\alpha_{d,m,n}^{(i)}\right) \tag{7.9}$$

where $\alpha_{d,m,n}^{(i)} = \angle(\boldsymbol{w}_{\text{opt}}^{(i)H}\bar{\boldsymbol{v}}_{d,m,n}^{(i)})$. For the proposed algorithm summarized in Table 7.1, the following lemma, which guarantees the convergence to a local optimum of the original problem (3.30) with $\boldsymbol{R}_{d,m} = P_d \mathrm{E}\left\{\boldsymbol{h}_{d,m}\boldsymbol{h}_{d,m}^H\right\}$, applies.

Lemma 5: The iterative procedure summarized in Table 7.1 yields an improved approximate solution in each iteration until the active QoS constraints (7.7c) remain unchanged in consecutive iterations.

Proof of Lemma 5: Let us first proof that for $\boldsymbol{w} = \boldsymbol{w}_{\text{opt}}^{(i)}$, the left-hand sides of the QoS constraints (7.7c) in iteration $(i+1)$ are greater or equal to the corresponding left-hand

Initialization: $\bar{\mathcal{N}}_{d,m}^{(1)} = p_{d,m},\ \bar{\boldsymbol{v}}_{d,m,n}^{(1)} = \boldsymbol{v}_{d,m,n}$
for $i = 1, \ldots, I$
Solve problem (7.7) with $\bar{\mathcal{N}}_{d,m} = \bar{\mathcal{N}}_{d,m}^{(i)}$ and $\bar{\boldsymbol{v}}_{d,m,n} = \bar{\boldsymbol{v}}_{d,m,n}^{(i)}$.
Perform the rotation of (7.9) with $\alpha_{d,m,n}^{(i)} = \angle(\boldsymbol{w}_{\text{opt}}^{(i)H} \bar{\boldsymbol{v}}_{d,m,n}^{(i)})$.
Find $\bar{\mathcal{N}}_{d,m}^{(i+1)}$ according to (7.8).
end

Table 7.1. Proposed iterative procedure for statistical CSI

sides in iteration i.

$$\frac{1}{\sqrt{\bar{N}_{d,m}^{(i+1)}}} \sum_{n \in \bar{\mathcal{N}}_{d,m}^{(i+1)}} \sqrt{\lambda_{d,m,n}} \text{Re}\left\{ \boldsymbol{w}_{\text{opt}}^{(i)H} \bar{\boldsymbol{v}}_{d,m,n}^{(i+1)} \right\} \tag{7.10a}$$

$$= \frac{1}{\sqrt{\bar{N}_{d,m}^{(i+1)}}} \sum_{n \in \bar{\mathcal{N}}_{d,m}^{(i+1)}} \sqrt{\lambda_{d,m,n}} |\boldsymbol{w}_{\text{opt}}^{(i)H} \boldsymbol{v}_{d,m,n}| \tag{7.10b}$$

$$\geq \frac{1}{\sqrt{\bar{N}_{d,m}^{(i)}}} \sum_{n \in \bar{\mathcal{N}}_{d,m}^{(i)}} \sqrt{\lambda_{d,m,n}} |\boldsymbol{w}_{\text{opt}}^{(i)H} \boldsymbol{v}_{d,m,n}| \tag{7.10c}$$

$$\geq \frac{1}{\sqrt{\bar{N}_{d,m}^{(i)}}} \sum_{n \in \bar{\mathcal{N}}_{d,m}^{(i)}} \sqrt{\lambda_{d,m,n}} \text{Re}\left\{ \boldsymbol{w}_{\text{opt}}^{(i)H} \bar{\boldsymbol{v}}_{d,m,n}^{(i)} \right\}. \tag{7.10d}$$

We proceed proving Lemma 5 by contradiction as follows. Assume that the solution in iteration $(i+1)$ is the same as that in the previous iteration i, i.e., $\boldsymbol{w}_{\text{opt}}^{(i+1)} = \boldsymbol{w}_{\text{opt}}^{(i)}$. Assume further that the approximation of all active QoS constraints, i.e., (7.7c), changes from iteration i to iteration $(i+1)$. Then, we can observe from inequality (7.10) and the QoS constraints (7.7c) that the solution in iteration $(i+1)$ can be scaled down, still satisfying all QoS constraints. This contradicts optimality of $\boldsymbol{w}_{\text{opt}}^{(i+1)} = \boldsymbol{w}_{\text{opt}}^{(i)}$ and we conclude that $\|\boldsymbol{w}_{\text{opt}}^{(i+1)}\|_2 < \|\boldsymbol{w}_{\text{opt}}^{(i)}\|_2$ in this case. □

Our algorithm is initialized with the unrotated principal component of each channel covariance matrix, i.e., we choose $\bar{\mathcal{N}}_{d,m}^{(1)} = p_{d,m}$ and $\bar{\boldsymbol{v}}_{d,m,n}^{(1)} = \boldsymbol{v}_{d,m,n}$ where $p_{d,m}$ denotes the index corresponding to the principal component of $\boldsymbol{R}_{d,m}$. The iterative scheme is summarized in Table 7.1 where I stands for the total number of iterations.

7.3 Iterative Feasibility Search

Like in the iterative SOCP method for instantaneous CSI described in Chapter 5, the SOCP problem in (7.7) might not be feasible when initialized as in Table 5.1.

However, the iterative feasibility search proposed in Section 5.4 can straightforwardly be extended to find an initial approximation of the QoS constraints for which problem (7.7) becomes feasible. The only difference to the iterative feasibility search of Section 5.4 is that, rather than updating the rotation angles of the instantaneous channel vectors, the rotation angles of the eigenvectors of the channel covariance matrices and the subsets of these eigenvectors need to be updated in each iteration. Thus, the iterative procedure described in Table 7.1 is performed where, however, problem (7.7) is replaced by the following problem

$$\min_{\boldsymbol{z},\tilde{\boldsymbol{w}}} \ \mathbf{1}^T\boldsymbol{z} \tag{7.11a}$$

$$\text{s.t.} \ \sqrt{\gamma_m}\|\boldsymbol{U}_m\tilde{\boldsymbol{w}}\| - \frac{1}{\sqrt{\bar{N}_{d,m}}}\sum_{n\in\bar{\mathcal{N}}_{d,m}}\sqrt{\lambda_{d,m,n}}\mathrm{Re}\{\boldsymbol{w}^H\bar{\boldsymbol{v}}_{d,m,n}\} \leq z_m,$$

$$\forall m \in \mathcal{G}_d, \ \forall d \in \mathcal{K}, \tag{7.11b}$$

$$z_m \geq 0, \ \forall m \in \mathcal{G}_d, \ \forall d \in \mathcal{K}, \tag{7.11c}$$

$$\tilde{w}_1 = 1. \tag{7.11d}$$

Lemma 6: The proposed feasibility search yields a reduced infeasibility indicator in the $(i+1)$th iteration relative to that of the ith iteration until the active approximated QoS constraints (7.7c) remain unchanged in consecutive iterations. Thus, the algorithm converges locally.

Proof of Lemma 6: The proof is similar to the proof of Lemma 2 and that of Lemma 5: Assume that the solution in iteration $(i+1)$ is the same as that in the previous iteration, i.e., $\boldsymbol{w}_{\text{opt}}^{(i+1)} = \boldsymbol{w}_{\text{opt}}^{(i)}$. Assume further that all active approximated QoS constraints (7.7c) change from iteration i to iteration $(i+1)$. Then, we can observe from inequality (7.10) and (7.11) that $\mathbf{1}^T\boldsymbol{z}_{\text{opt}}^{(i+1)} < \mathbf{1}^T\boldsymbol{z}_{\text{opt}}^{(i)}$. □

The resulting sets of eigenvectors and rotation angles are used to initialize the iterative QoS constrained power minimization procedure of Table 7.1. Note that the feasibility search described in this section can straightforwardly be extended to the admission control scheme proposed in Section 5.5.

7.4 MGM Downlink Beamforming

The extension of the iterative SOCP scheme to statistical CSI, which has been described above for distributed relay beamforming, can straightforwardly be applied to MGM

downlink beamforming. The algorithm for MGM downlink beamforming is very similar to that in Table 7.1 and only a few modifications are required in Table 7.1 to adapt the algorithm to MGM downlink beamforming: Problem (7.7) has to be replaced by the following problem

$$\begin{aligned}
\min_{t,\boldsymbol{w}_{\text{all}}} \quad & t && \text{(7.12a)}\\
\text{s.t.} \quad & \|\boldsymbol{w}_{\text{all}}\| \leq t, && \text{(7.12b)}\\
& \frac{1}{\sqrt{\bar{N}_m}} \sum_{n\in\bar{\mathcal{N}}_m} \sqrt{\lambda_{m,n}}\text{Re}\{\boldsymbol{w}_d^H \bar{\boldsymbol{u}}_{m,n}\} \geq \sqrt{\gamma_m}\|\boldsymbol{\mathcal{H}}_{d,m}\boldsymbol{w}_{\text{all}}\|, \\
& \forall m \in \mathcal{G}_d,\ \forall d \in \mathcal{K}, && \text{(7.12c)}\\
& w_{\text{all},1} = 1 && \text{(7.12d)}
\end{aligned}$$

where $\boldsymbol{u}_{m,n}$ is defined as the nth eigenvector of the channel covariance matrix $\boldsymbol{C}_m$. Further, we need to replace $\boldsymbol{w}_{\text{opt}}^{(i)}$ by $\boldsymbol{w}_{d,\text{opt}}^{(i)}$ and $\boldsymbol{v}_{d,m,n}$ by $\boldsymbol{u}_{m,n}$ everywhere and the rotation angle $\alpha_{d,m,n}^{(i)} = \angle(\boldsymbol{w}_{d,\text{opt}}^{(i)H}\bar{\boldsymbol{u}}_{m,n}^{(i)})$, $\forall m \in \mathcal{G}_d$, $\forall d \in \mathcal{K}$, has to be used when performing the rotation of (7.9). The local convergence property of the algorithm in the MGM downlink case can be proved using the same arguments as in the proof of Lemma 5. Furthermore, the iterative feasibility search of Section 7.3 can straightforwardly be applied to the MGM downlink case.

7.5 Simulation Results

We demonstrate the performance of the proposed extension of our iterative SOCP algorithm to statistical CSI using the examples of MGM relay beamforming and MGM downlink beamforming. Of course, it can also straightforwardly be applied to, e.g., FF beamforming. However, this is beyond the scope of this thesis and we focus on the former two examples.

For the relay beamforming and the downlink beamforming scenarios, let us consider different channel models. For the former case, we consider the channel model of [26] where the channel covariance matrices of a flat fading Rician channel are calculated which are briefly described next.

7.5.1 MGM Relay Beamforming

Let us assume the channel coefficients f_i and g_j to be independent from each other for any i and j. We further assume that the channel coefficients are given by

$$f_i = \bar{f}_i + \tilde{f}_i$$

where $\bar{f}_i$ denotes the mean of f_i, i.e., the Rician line-of-sight component, and $\tilde{f}_i$ denotes a zero-mean random variable that corresponds to the Rayleigh scattering component. $\tilde{f}_i$ and $\tilde{f}_j$ are assumed to be independent for $i \neq j$. For each f_i, let us choose $\bar{f}_i = e^{j\theta_i}/\sqrt{1+\beta_f}$ and $\mathrm{var}(\tilde{f}_i) = \beta_f/(1+\beta_f)$ where θ_i is a random variable distributed uniformly on the interval $[0, 2\pi]$ and β_f denotes a parameter that can be used to vary the level of scattering and, hence, the level of uncertainty in the channel coefficient f_i. The forward channel coefficients g_i are modeled accordingly. For this channel modeling, the (i,j)th entry of the matrix $\boldsymbol{R}_{d,m}$ is given by

$$[\boldsymbol{R}]_{i,j} = P_d \left(\bar{f}_i \bar{f}_j^* + \frac{\beta_f}{1+\beta_f}\delta_{ij} \right) \left(\bar{g}_i \bar{g}_j^* + \frac{\beta_f}{1+\beta_f}\delta_{ij} \right).$$

As mentioned earlier, the approach of Chapters 5 and 6 can be made applicable to statistical CSI via approximating $\boldsymbol{R}_{d,m}$ or $\boldsymbol{C}_m$ by its principal component. This is the trivial way of keeping the latter approach applicable for statistical CSI which is, however, usually inferior to the approach presented in this chapter. It corresponds to a less sophisticated version of the proposed method where, instead of choosing the optimal subset $\bar{\mathcal{N}}_m^{(i+1)}$ according to (7.8), only the principal eigenvector is chosen in every iteration, i.e., $\bar{\mathcal{N}}_{d,m}^{(i)} = p_{d,m}$, $i = 1, \ldots, I$. In this scenario, however, it turned out that it is more beneficial to use the above trivial extension rather than the more sophisticated extension of this chapter as long as a feasible solution can be obtained using the trivial extension. As soon as a feasible solution can no longer be obtained in this way, we switch to the method proposed in this chapter where the probability, that a feasible solution can be found, is much higher. We also compare the results of the method proposed in this chapter to the less sophisticated method where the principal eigenvector is chosen in every iteration which we refer to as the method of Chapter 5.

Let us consider a MUP2P relay beamforming network with $K = M = 10$ source-destination pairs and $N = 20$ relays. The SINR threshold γ_k is set to -10dB for all destinations and all other settings are the same as in Section 5.8. Figs. 7.1 and 7.2 depict the total transmitted relay power and the percentage of feasible Monte Carlo runs, respectively, versus the scattering parameter α, which is varied from -10 dB to 10 dB, for all the methods tested. We can observe that the number of feasible Monte Carlo runs corresponding to our iterative SOCP scheme could be substantially increased using the extension proposed in this chapter. However, the good performance in terms of feasibility of the competing schemes could not be reached for a scattering parameter of $\alpha \geq 6$ dB. However, such high scattering is usually unrealistic. In terms of total transmitted relay power, the performance of the proposed scheme slightly outperforms the SDR-based approach for a realistic amount of scattering. Only for unrealistically high scattering, the performance is worse than that of the SDR-based approach.

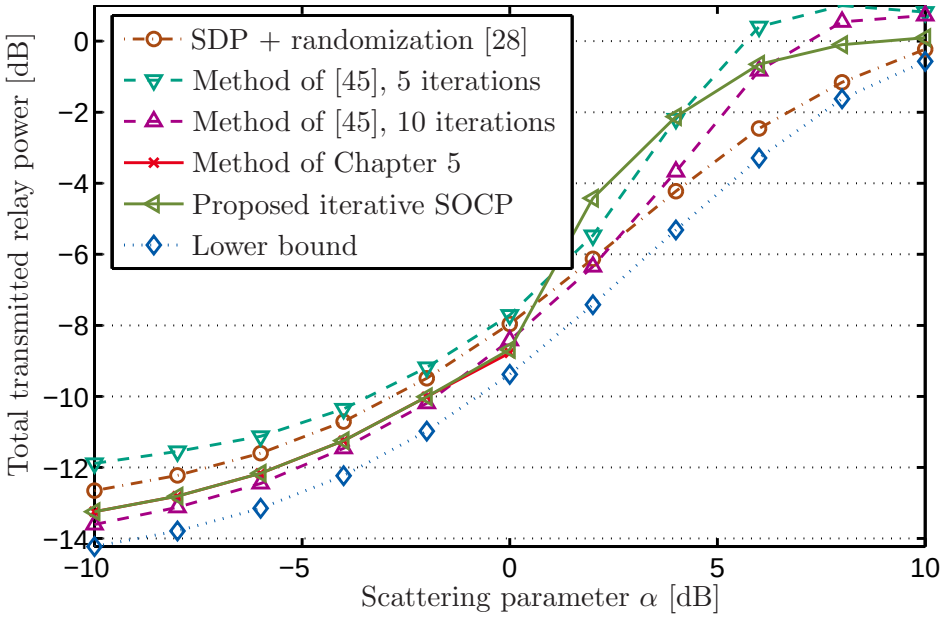

Figure 7.1. Relay beamforming with statistical CSI. Total transmitted relay power versus α. $K = M = 10$, $N = 20$.

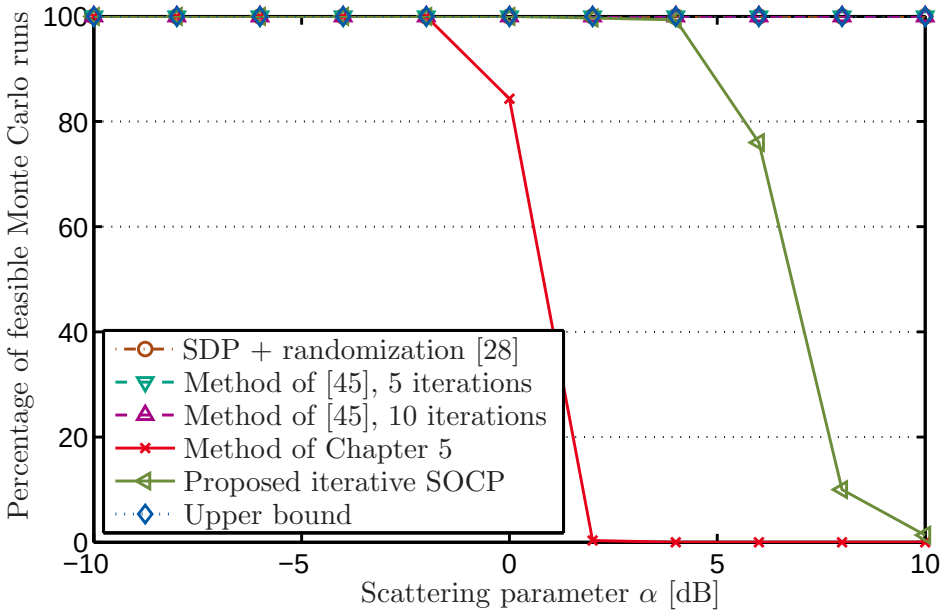

Figure 7.2. Relay beamforming with statistical CSI. Percentage of feasible Monte Carlo runs versus α. $K = M = 10$, $N = 20$.

7.5.2 MGM Downlink Beamforming

In this subsection, let us consider the following scenario similar to the one in [13]. $M = 16$ users are located in angular directions distributed uniformly on the interval $[0°, 360°]$. The users are partitioned into $K = 3$ spatially separated multicasting groups of similar size. As in previous simulation setups, a transmit antenna array with $N = 6$ elements is considered. Furthermore, we consider a uniform linear array with an element spacing of half a wavelength. Then, according to [13], the channel covariance matrix can be approximated by

$$[\boldsymbol{C}(\theta, \sigma_\theta)]_{k,l} = \exp(j\pi(k-l)\sin\theta)\exp\left(-\frac{(\pi(k-l)\sigma_\theta\cos\theta)^2}{2}\right)$$

where the index m of $\boldsymbol{C}_m$ has been omitted for simplicity of notation and θ and σ_θ denote the angular direction of the user and the spread angle, respectively. The spread angle models local scattering at the mobile terminal. Note that for a BS, e.g., on a rooftop, significantly less local scattering can be assumed making this a realistic model. The larger the spread angle, the larger the number of local scatterers by which the users are surrounded and the higher the rank of the corresponding channel covariance matrix $\boldsymbol{C}$. If $\sigma_\theta = 0$, $\boldsymbol{C}$ is rank-one. Thus, while the parameter controlling the level of scattering is β_f in the previous subsection, it is σ_θ in this channel model.

Different from the previous subsection, our studies have revealed that in the above scenario, the more sophisticated extension of our iterative method to statistical CSI that is proposed in this chapter always yields better results than the trivial extension of using the principal eigenvector of the covariance matrix in each iteration, no matter whether the iterative method with the trivial extension yields a feasible solution or not. Similar to the previous subsection, the results of the iterative method with the trivial extension, referred to as the method of Chapter 6, is also shown. 300 candidate vectors are generated in the randomization procedure of the method in [17] while in the proposed iterative methods, a maximum of only $I = 3$ iterations are used.

Fig. 7.3 displays the total transmitted BS power obtained by the competing methods versus the spread angle which is varied from 0° to 20°. For this range of spread angles, all the methods almost always yield feasible solutions. Therefore, the percentage of feasible Monte Carlo runs is not shown. Clearly from Fig. 7.3, for small spread angles, the method of Chapter 6 and the proposed method have the same performance. The reason is that in this region, the optimal subset contains only the principal eigenvector in every iteration of the proposed method. As the spread angle is further increased, the curves deviate, revealing superior performance of the proposed method. Further, we

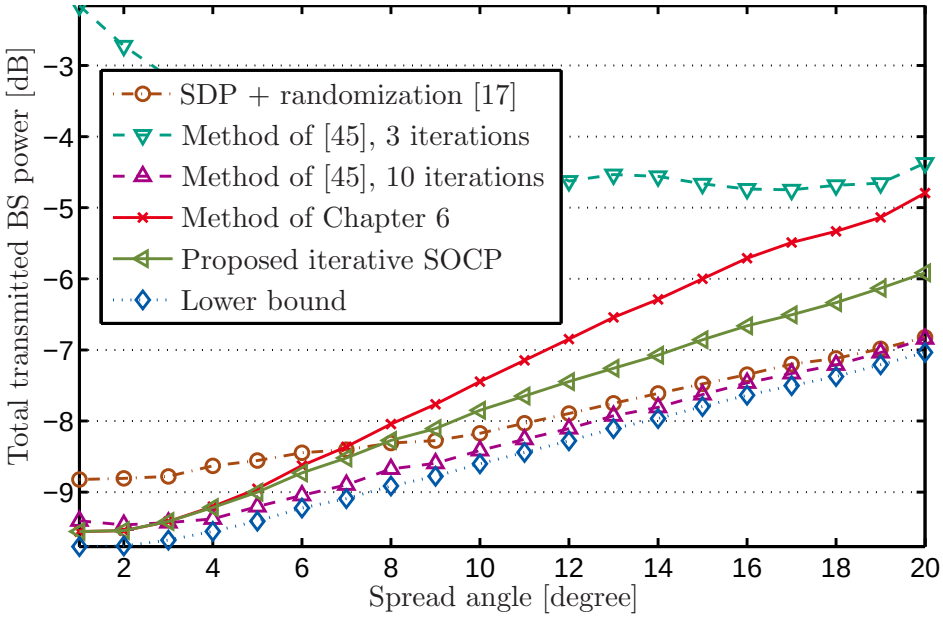

Figure 7.3. Downlink beamforming with statistical CSI. Total transmitted power versus σ_θ. $K = 3$, $N = 6$, $M = 16$.

can observe that, for the wide range of spread angles between 0° and 7°, our method clearly outperforms the method of [17]. Angles beyond 7° correspond to unrealistically strong scattering in the vicinity of the users. The performance of the method of [45] is ambivalent: For the same maximum number of iterations as used for our method, it performs clearly worse than our method while at convergence, after a maximum of 10 iterations, it clearly outperforms all other methods and is close to optimal.

7.6 Summary

In this chapter, we have proposed a non-trivial extension for our iterative SOCP technique to the case where only statistical CSI in terms of the channel covariance matrices is available at the BS or at the processing node(s). The extension consists in performing an eigenvalue decomposition on the channel covariance matrix followed by an l_1-norm approximation of the euclidean norm such that the original QoS-constrained power minimization problem can still be approximated by a convex SOCP problem when the channel vectors are replaced by the channel covariance matrices. In addition to the channel rotations of Chapters 5 and 6, we have adapted the selection of a subset of the eigenvectors of the channel covariance matrices to the solution of the current iteration. We have observed that the extended iterative SOCP algorithm of this chapter enjoys all the benefits of the original iterative SOCP scheme of Chapters 5 and 6.

Our simulation results have revealed that for a realistic amount of scattering, the proposed extended iterative SOCP method outperforms the state-of-the-art SDR-based approaches in terms of total transmitted power.

Chapter 8

Extended Interior-Point Method with Reduced Complexity

8.1 Introduction

In each iteration of the algorithms proposed in Chapters 5-7, the optimal solution of the SOCP problem (5.6), (6.3), (7.7), or (7.12) is obtained with high accuracy using interior-point methods [62]. However, the feasible set of the SOCP problem is updated in the next iteration and a new solution has to be computed. Hence, a high accuracy of these intermediate solutions is not required and rather a waste of computational effort. In this chapter, we therefore propose intermediate solutions which are only suboptimal for the SOCP problems to reduce the computational complexity of the schemes in Chapters 5-7. The interior-point method used to solve the SOCP problem is an iterative algorithm itself. The suboptimal intermediate solutions can thus be obtained by performing only a single iteration of the interior-point method. In other words, rather than solving the exact SOCP problem, we solve only an approximation of the SOCP problem which requires less computational effort. When the updates of the feasible set become negligible, we successively increase the approximation accuracy similar to the traditional interior-point methods to compute the final optimal beamforming vector with sufficiently high accuracy. The barrier method is used as a simple and illustrative example of an interior-point method to demonstrate our idea. However, our idea is applicable for other interior-point methods as well, e.g., for the more efficient primal-dual interior-point methods [62]. Our simulation results reveal that the scheme proposed in this chapter achieves the same performance in terms of transmitted power and feasibility as the algorithm proposed in Chapters 5 and 6 at a substantially reduced computational complexity. Thus, there is no price we have to pay for the complexity reduction proposed in this chapter.

The proposed complexity reduction for our algorithm is derived using the example of the distributed beamforming scenario of Chapter 3 and is then applied to the MGM downlink beamforming scenario of Chapter 2.

This chapter is based on my original work that has been published in [6].

8.2 Iterative QoS-Constrained Power Minimization

In the iterative method proposed in Chapter 5, a sequence of optimization problems (5.6) has to be solved and as a consequence, the complexity of this method is unnecessarily high for the following reason. In each iteration, the SOCP problem (5.6) is solved using an interior-point method which is an iterative method itself. To make them distinguishable, let us refer to the iterations of successive channel rotations indexed by (i) in (5.7) as *outer iterations* and to those of the interior-point method as *inner iterations*. In a particular outer iteration, performing inner iterations to convergence yields the optimal solution of the SOCP problem (5.6). However, as the feasible set is then updated in the next outer iteration, it is not necessary to perform the inner iterations to convergence. Therefore, the idea presented in this chapter is to avoid this unnecessarily high accuracy of intermediate solutions and obtain solutions which are only suboptimal for problem (5.6). This can be achieved by performing only a single inner iteration per outer iteration which corresponds to solving an approximation of the SOCP problem (5.6) rather than problem (5.6) itself. This reduces the computational complexity of the iterative method in Chapter 5. Note that, since only a single inner iteration per outer iteration is performed rather than performing multiple inner iterations per outer iteration, the two-time-scale algorithm is transformed into a one-time-scale algorithm.

Our idea is explained considering the example of the barrier method [62] as a particular interior-point method which is most straight-forward. We note, however, that our idea can be applied to other interior-point methods as well. Let us first briefly review the concept of the barrier method. A common tool to solve convex problems, such as equality-constrained convex problems, is Newton's method [62]. However, convex problems with inequality constraints cannot directly be solved using this method. Therefore, in the barrier method, the solution to an inequality-constrained convex problem is obtained by solving a sequence of equality-constrained convex problems, each of which is solved using Newton's method. Towards this end, the original inequality constrained convex problem, in our case problem (5.6), is approximated by a convex problem without inequality constraints as shown next. Following the derivation of the barrier method in [62], we incorporate the inequality constraints of problem (5.6) into the objective function using the indicator function $I_-(u)$ as follows

$$\min_{\tilde{\boldsymbol{w}}} \quad \|\boldsymbol{V}\tilde{\boldsymbol{w}}\| + \sum_{d=1}^{K} \sum_{m\in\mathcal{G}_d} I_- \Big(\sqrt{\gamma_m/P_d}\|\boldsymbol{U}_m\tilde{\boldsymbol{w}}\| - \mathrm{Re}\{\tilde{\boldsymbol{w}}^H\tilde{\boldsymbol{h}}_{d,m}\}\Big) \tag{8.1a}$$

$$\text{s.t.} \quad \tilde{w}_1 = 1 \tag{8.1b}$$

where the indicator function for non-positive reals $I_-(u)$ is defined as

$$I_-(u) = \begin{cases} 0 & u \leq 0 \\ \infty & u > 0. \end{cases}$$

If at a given point, the eliminated inequality constraints are satisfied, the indicator function has no effect. However, if these constraints are violated, the indicator function is equal to infinity and as a consequence, an infinite penalty is added to the objective function. This prevents that any infeasible point will be considered as a solution for problem (8.1) [62]. Thus, problem (8.1) is equivalent to problem (5.6), i.e., problem (5.6) is turned into an equivalent equality-constrained problem. However, the objective function of problem (8.1) is non-differentiable. Accordingly, Newton's method, which requires twice differentiable functions, cannot be applied directly. To overcome this problem, we use the idea of the barrier method to approximate the indicator function with a differentiable function. Here, we use the logarithmic barrier function as an approximation [62]. Using the generalized logarithm for the second-order cone [62], the approximation of the indicator function in problem (8.1), can be defined as [62]

$$\hat{I}_-(\boldsymbol{w}) = -\left(\frac{1}{\kappa}\right) \log\left(\left(\operatorname{Re}\{\tilde{\boldsymbol{w}}^H \tilde{\boldsymbol{h}}_{d,m}\}\right)^2 - \frac{\gamma_m}{P_d}\|\boldsymbol{U}_m \tilde{\boldsymbol{w}}\|^2\right)$$

which is twice differentiable and where the parameter κ controls the accuracy of the approximation. That is, the larger the value of κ, the closer is the logarithmic approximation to the original indicator function I_-. Substituting the original with the approximated indicator function in problem (8.1), one obtains the following approximation [62]

$$\min_{\tilde{\boldsymbol{w}}} \quad \kappa\|\boldsymbol{V}\tilde{\boldsymbol{w}}\|^2 + \phi(\tilde{\boldsymbol{w}}) \qquad \text{s.t.} \quad \tilde{w}_1 = 1. \tag{8.2}$$

The function $\phi(\tilde{\boldsymbol{w}})$ denotes the logarithmic barrier for the SOCP problem (5.6) and is defined as

$$\phi(\tilde{\boldsymbol{w}}) = -\sum_{d=1}^{K} \sum_{m \in \mathcal{G}_d} \log\left(\left(\operatorname{Re}\{\tilde{\boldsymbol{w}}^H \tilde{\boldsymbol{h}}_{d,m}\}\right)^2 - \frac{\gamma_m}{P_d}\|\boldsymbol{U}_m \tilde{\boldsymbol{w}}\|^2\right). \tag{8.3}$$

Problem (8.2) is an approximation of the original SOCP problem (5.6). The function in (8.3) is convex (which is not obvious but has been shown in [62] for SOCPs in general) and thus, problem (8.2) is convex. The domain of problem (8.2) is equal to the feasible set of problem (5.6). To achieve a near-optimal approximate solution, the parameter κ has to be chosen large. However, problem (8.2) is difficult to solve via Newton's method for a large value of κ except when the starting point is chosen close to the optimum of (8.2) (see [62]). Therefore, an iterative approach is used in the barrier method where in each iteration, problem (8.2) is solved for a particular value of κ. In the first iteration, κ is chosen small and it is then increased in every iteration

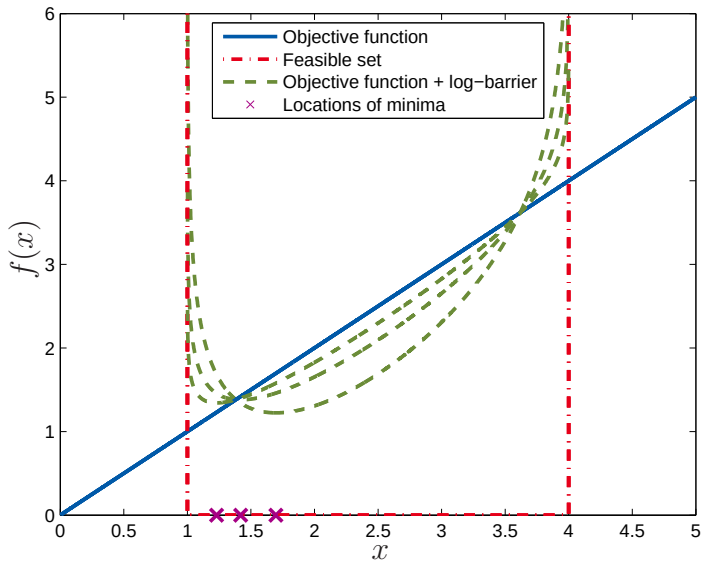

Figure 8.1. Illustration of the Barrier Method.

where the solution obtained in the current iteration serves as the starting point in the next iteration. This iterative scheme terminates when the solution to problem (5.6) is approximated with sufficiently high accuracy.

Let us briefly illustrate the barrier method using a simple example. Fig. 8.1 depicts the objective function and the feasible set of the simple optimization problem

$$\min_{x\in\mathbb{R}} x \quad \text{s.t.} \quad x \geq 1, \quad x \leq 4. \tag{8.4}$$

The linear objective function is depicted by a solid line and the feasible set is the interval between the two vertical dash-dotted lines each of which corresponds to one inequality constraint. These two vertical lines together with the horizontal dash-dotted line may also be interpreted as the superposition of the two indicator functions corresponding to the two inequality constraints. Approximations of this problem using the logarithmic barrier are depicted by dashed lines for three values of the accuracy parameter, $\kappa \in \{1, 2, 4\}$. The approximation for $\kappa = 1$ exhibits the smoothest curvature while the approximation for $\kappa = 4$ is most accurate. The location of the minimum of each approximation is depicted by a cross. We can see from the figure that the optimal solution of the approximated problem approaches the optimal solution of the original problem as the parameter κ is increased.

As mentioned earlier, the high accuracy achieved by successively increasing the accuracy parameter κ is not required for intermediate solutions of the iterative method of

Section 5.3. Therefore, we propose to use only the first iteration of the barrier method to obtain an approximate solution to problem (5.6). This corresponds to combining the barrier method with the iterative scheme of Section 5.3 as follows. In each iteration of the proposed method, rather than solving problem (5.6) using an interior-point method, we solve problem (8.2) for a small κ which can be done more efficiently using Newton's method. Instead of increasing κ in each iteration as in the interior-point method, we perform the rotation of (5.7) and keep κ fixed as long as the rotation is significant. As soon as the rotations become negligible (i.e., as soon as $\max_m\{|\alpha_m^{(i)}|\} < \epsilon$, for some small ϵ), the feasible set only changes marginally and we can start increasing κ in every iteration like in traditional interior-point methods. This guarantees that, once a good approximation of the feasible set has been found, the final weight vector is obtained with sufficiently high accuracy. As in the traditional barrier method, the solution obtained in a given iteration with Newton's method always serves as the starting point for Newton's method in the subsequent iteration. This ensures that Newton's method converges even for large values of κ. This procedure is repeated for a fixed number of iterations I. As in the iterative method proposed in Section 5.3, in this method, the initial channel vector is assumed to be equal to the original channel vector, i.e., $\tilde{\boldsymbol{h}}_{d,m}^{(1)} = \tilde{\boldsymbol{h}}_{d,m}$. The proposed iterative method is summarized in Table 8.1 where $\mu > 1$.

Initialization: $\tilde{\boldsymbol{h}}_{d,m}^{(1)} = \tilde{\boldsymbol{h}}_{d,m}, \quad \kappa^{(1)} > 0.$
for $i = 1 \ldots I$
  Solve problem (8.2) with $\tilde{\boldsymbol{h}}_{d,m} = \tilde{\boldsymbol{h}}_{d,m}^{(i)}$ and $\kappa = \kappa^{(i)}$.
  Perform the rotation of (5.7) with $\alpha_{d,m}^{(i)} = \angle\left(\tilde{\boldsymbol{w}}_{\text{opt}}^{(i)H}\tilde{\boldsymbol{h}}_{d,m}^{(i)}\right)$.
  if $\max_m\{|\alpha_m^{(i)}|\} < \epsilon$ **then**
    $\kappa^{(i+1)} = \mu \cdot \kappa^{(i)}$
  else
    $\kappa^{(i+1)} = \kappa^{(i)}$
  end if
end

Table 8.1. Proposed Extended Interior-Point Method

For a better comprehension of the algorithm in Table 8.1, let us visualize this algorithm as we have visualized the algorithm in Section 5.3. We consider the same simple example which we have also considered in Section 5.3 to illustrate the iterative SOCP algorithm. The visualization is shown in Fig. 8.2 which is similar to Fig. 5.1 in Section 5.3. The difference between the two figures can be described as follows. Recall that in the algorithm of Section 5.3, in each outer iteration, the point yielding the minimum objective value inside the approximated feasible set is obtained by performing multiple inner iterations. Then, the approximation of the feasible set is adapted

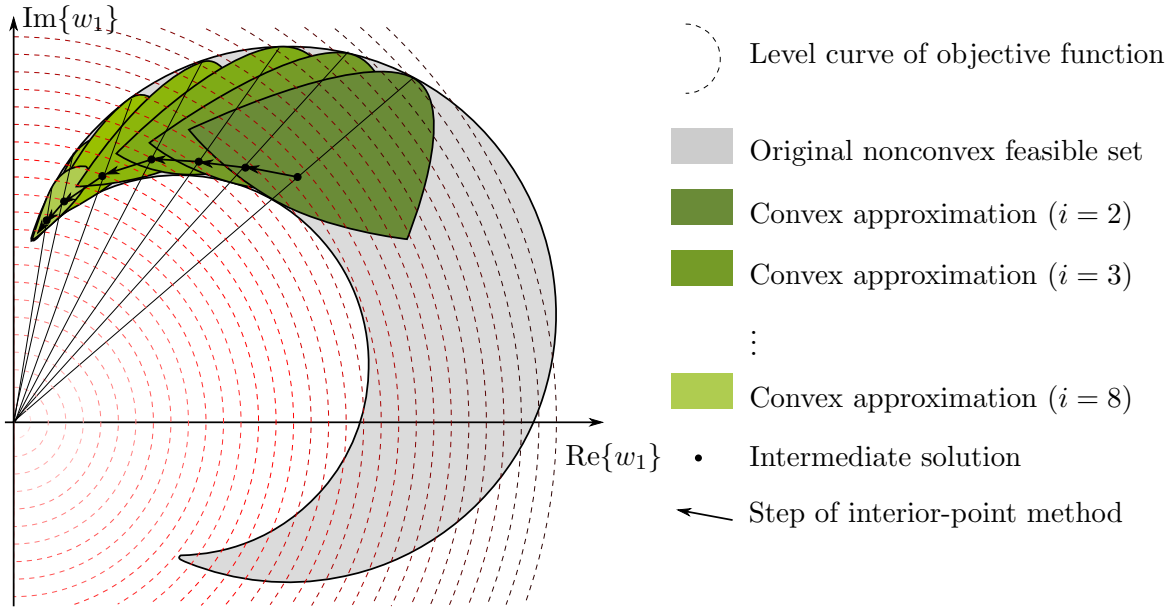

Figure 8.2. Visualization of the proposed extended interior-point method.

to this point. In Fig. 8.2, only a single step towards the optimal point within the current approximation of the feasible set is taken by performing only a single inner iteration. Then, the approximation of the feasible set is already updated. These steps, which are indicated by arrows in Fig. 8.2, are obviously smaller than those taken in Fig. 5.1. However, they are computed with a significantly lower computational complexity. Thus, although more iterations of the one-time-scale algorithm are required to find the local optimum than outer iterations of the two-time-scale algorithm, the total computational complexity of the one-time-scale algorithm is much less than that of the two-time-scale algorithm.

As we show in our simulations in Section 8.6, the method in Table 8.1 achieves the same performance as the method in Table 5.1. However, this is achieved at a significantly reduced computational cost since most of the inner iterations have been eliminated.

Note that in this dissertation, we have focused on the logarithmic barrier method for simplicity. However, the idea presented here can also be applied to all other interior-point methods which are based on the concept of successively increasing an accuracy parameter κ. The more sophisticated primal-dual interior-point methods [62] belong to this class of interior-point methods.

8.3 Iterative Feasibility Search

Recall that for the original channel vectors $\tilde{\boldsymbol{h}}_{d,m}$, problem (5.6) may be infeasible even if problem (3.13) is feasible. Obviously, this infeasibility is then inherited by problem (8.2) as well: If problem (5.6) is infeasible, the domain of problem (8.2) is empty. To mitigate this drawback, the same concept of iterative feasibility search that is used in Section 5.4 can be applied to the more efficient method: Instead of solving (5.10) in every iteration, we again reduce the unnecessarily high accuracy of intermediate solutions by applying the same idea used for the approximation of problem (5.6) to problem (5.10). Thus, we use the indicator function to incorporate the inequality constraints into the objective function and then approximate the indicator function. This yields an approximated version of (5.10) in the following form [62]

$$\min_{\boldsymbol{z},\tilde{\boldsymbol{w}}} \quad \kappa \mathbf{1}^T \boldsymbol{z} + \psi\left(\tilde{\boldsymbol{w}}, \boldsymbol{z}\right) \qquad \text{s.t.} \quad \tilde{w}_1 = 1 \tag{8.5}$$

where ψ denotes the logarithmic barrier for the SOCP problem (5.10) and is defined as

$$\psi\left(\tilde{\boldsymbol{w}}, \boldsymbol{z}\right) = -\sum_{d=1}^{K} \sum_{m \in \mathcal{G}_d} \left[\log\left(\left(z_m + \mathrm{Re}\{\tilde{\boldsymbol{w}}^H \tilde{\boldsymbol{h}}_{d,m}\} \right)^2 - \frac{\gamma_m}{P_d} \|\boldsymbol{U}_m \tilde{\boldsymbol{w}}\|^2 \right) + \log(z_m) \right]. \tag{8.6}$$

Replacing problem (5.10) with problem (8.5) in the iterative feasibility search of Section 5.4, we obtain the computationally more efficient feasibility search of Table 8.1 where problem (8.2) is replaced by problem (8.5). In the feasibility search in Section 5.4, the infeasibility indicator $\mathbf{1}^T \boldsymbol{z}$ is reduced in every iteration. This applies for the proposed algorithm as well. When $\mathbf{1}^T \boldsymbol{z} = 0$, a feasible initial rotation has been found and one can proceed with the algorithm in Table 8.1 performed on problem (8.2) using this initial rotation.

8.4 Complexity Analysis

As mentioned in Section 5.7, the SOCP problem (5.6) can be solved with a worst-case complexity of $\mathcal{O}(N^3 M^{1.5})$ using primal-dual interior-point methods. The terms $\mathcal{O}(N^3 M)$ and $\mathcal{O}(\sqrt{M})$ correspond to the complexity per iteration and the number of iterations required in the interior-point method, respectively [66]. For the complexity analysis, let us assume that the idea presented in this chapter is applied to the more efficient primal-dual interior point methods for which the worst-case complexities have been derived in [66]. Then, the complexity per iteration of the efficient extended

interior-point method proposed in this chapter is the same, i.e., $\mathcal{O}(N^3M)$. The number of required iterations of the proposed efficient method is slightly larger than $\mathcal{O}(\sqrt{M})$ since in addition to increasing the parameter κ at the end of the proposed algorithm, the feasible sets are updated before increasing κ. If we assume I_1 significant updates of the feasible set during which κ is kept fixed, the proposed method requires $I_1+\mathcal{O}(\sqrt{M})$ iterations with a complexity of $\mathcal{O}(N^3M)$. In the method of Section 5.3, problem (5.6) is solved about I_1 times to achieve the same performance. Hence, it requires $I_1 \cdot \mathcal{O}(\sqrt{M})$ iterations with the per-iteration complexity of the proposed efficient method which results in a higher overall computational complexity: The overall complexity of the method of Section 5.3 amounts to $\mathcal{O}(I_1N^3M^{1.5})$ while the overall complexity of the efficient method proposed in this chapter amounts to only $\mathcal{O}((I_1+\sqrt{M})N^3M)$.

8.5 MGM Downlink Beamforming

The complexity reduction via the transformation of the two-time-scale algorithm into a one-time-scale algorithm can straightforwardly be applied to the MGM downlink scenario as well. Only a few modifications are required in Table 8.1 for the adaptation of the algorithm to the MGM downlink beamforming case: Problem (8.2) has to be replaced by the following problem

$$\min_{\boldsymbol{w}_{\text{all}}} \quad \kappa\|\boldsymbol{w}_{\text{all}}\|^2 + \phi\left(\boldsymbol{w}_{\text{all}}\right) \qquad \text{s.t.} \quad w_{\text{all},1} = 1 \tag{8.7}$$

where the function $\phi\left(\boldsymbol{w}_{\text{all}}\right)$ has to be redefined as

$$\phi\left(\boldsymbol{w}_{\text{all}}\right) = -\sum_{d=1}^{K}\sum_{m\in\mathcal{G}_d} \log\Big(\left(\text{Re}\{\boldsymbol{w}_d^H\boldsymbol{h}_m\}\right)^2 - \gamma_m\|\boldsymbol{\mathcal{H}}_{d,m}\boldsymbol{w}_{\text{all}}\|^2\Big). \tag{8.8}$$

Furthermore, we need to replace $\tilde{\boldsymbol{h}}_{d,m}$ by $\boldsymbol{c}_m$ in Table 8.1 and (5.7) and use the rotation angle $\alpha_{d,m}^{(i)} = \angle\left(\boldsymbol{w}_{d,\text{opt}}^{(i)H}\boldsymbol{c}_m^{(i)}\right)$ in (5.7). In the iterative feasibility search of Section 8.3, the problem (8.5) has to be modified accordingly and the complexity reduction that can be achieved in case of MGM downlink beamforming is the same as that given in Section 8.4 for distributed relay beamforming.

8.6 Simulation Results

Let us consider the MUP2P relay network studied in the simulations of Chapter 5 and the MGM downlink beamforming scenario of the numerical simulations of the previous

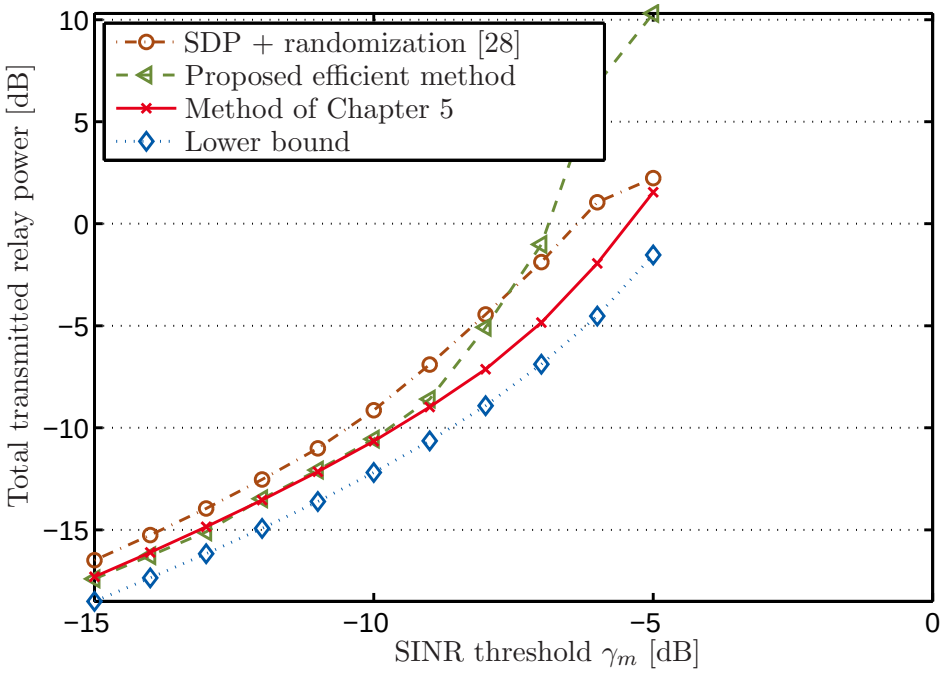

Figure 8.3. AF relay beamforming. Total transmitted relay power versus SINR threshold. $K = M = 12$, $N = 20$.

Chapter to exemplarily demonstrate the performance of the efficient method proposed in this chapter. For the original iterative SOCP method of Chapters 5 and 6, we have chosen the maximum number of iterations as $I_1 = 5$ and $I_1 = 3$, respectively, and for the efficient method proposed in this chapter as $I_2 = 10$. We set the parameters of the proposed efficient method to $\kappa^{(1)} = 0.1$, $\mu = 8$ and $\epsilon = 30°$. All results (apart from the runtime results) are averaged over 300 Monte Carlo runs.

Figs. 8.3 and 8.4 display the total transmitted relay power and the percentage of feasible Monte Carlo runs, respectively, versus the SINR threshold for the MGM relay beamforming case while Figs. 8.5 and 8.6 depict the corresponding values for the MGM downlink beamforming scenario. We observe from these figures that the performance of the method proposed in this chapter is very similar to the performance of the method of Chapters 5 and 6. However, this performance is achieved at a substantially reduced computational complexity.

In order to complement our theoretical complexity analysis, we compare the runtimes of the different methods observed during the simulations. For the MGM downlink beamforming scenario, the runtime of each of the competing methods for approximately solving an exemplary instance of problem (2.9) is provided in Table 8.2. The proposed method clearly outperforms the state-of-the-art methods and the method of Chapters 5 and 6 in terms of runtime.

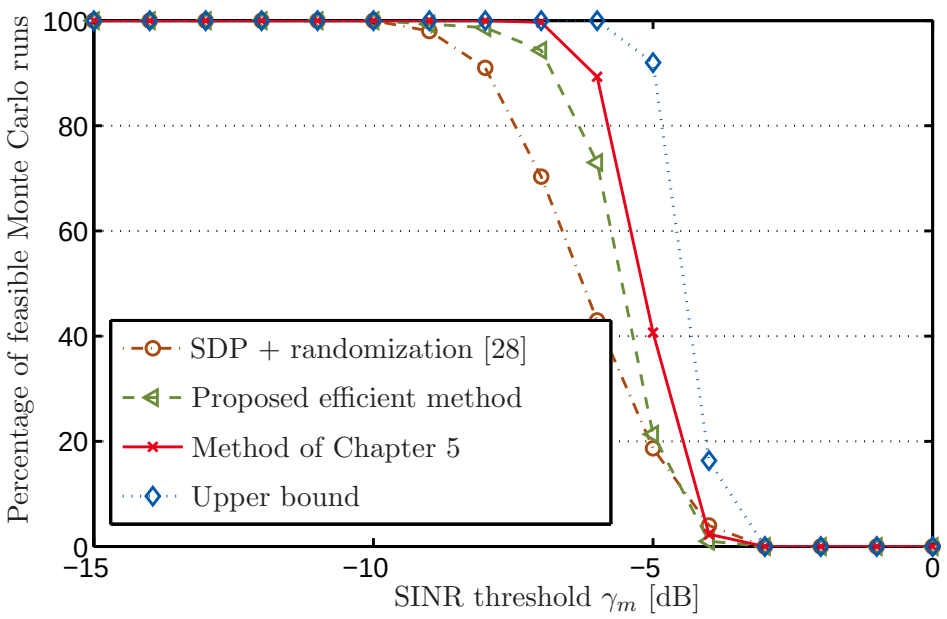

Figure 8.4. AF relay beamforming. Percentage of feasible Monte Carlo runs versus SINR threshold. $K = M = 12$, $N = 20$.

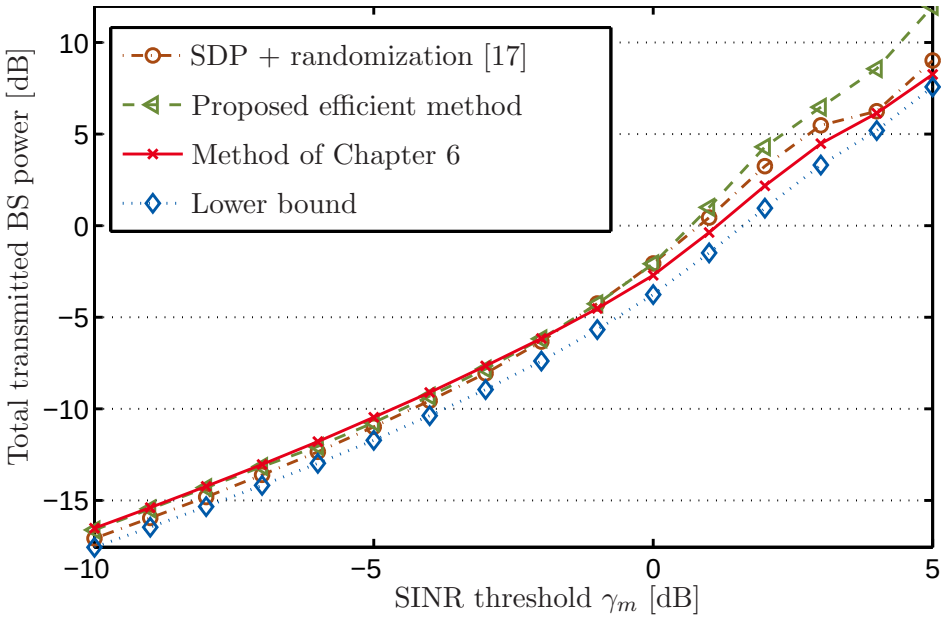

Figure 8.5. Downlink Beamforming. Total transmitted power versus SINR threshold. $K = 3$, $N = 6$, $M = 16$. With efficient method.

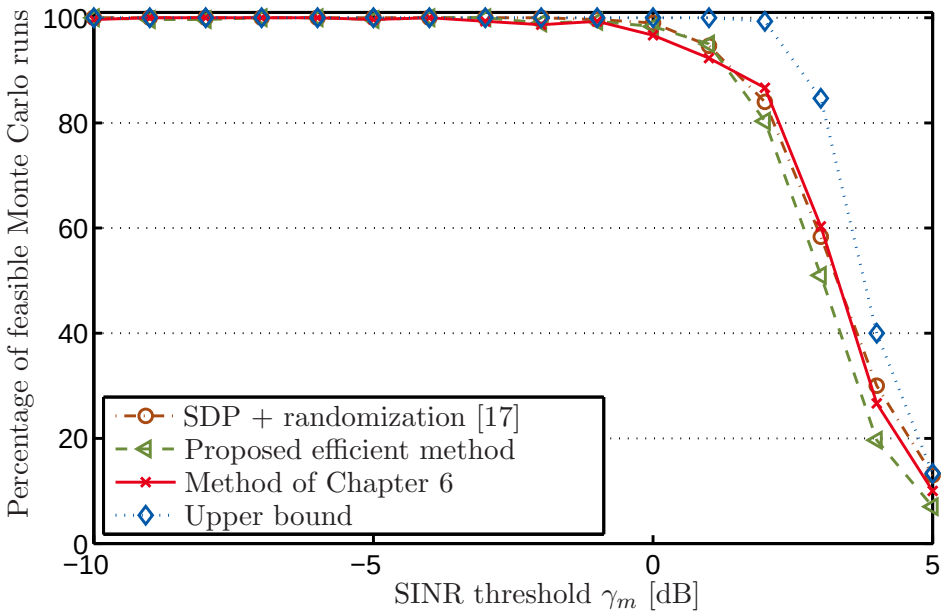

Figure 8.6. Downlink Beamforming. Percentage of feasible Monte Carlo runs versus SINR threshold. $K = 3$, $N = 6$, $M = 16$. With efficient method.

Method of [17]	Method of Chapters 5 and 6	Method proposed in this chapter
1.691	0.447	0.217

Table 8.2. Comparison of runtime in seconds

8.7 Summary

In this chapter, we have proposed a complexity reduction for our iterative SOCP scheme. The complexity reduction has been achieved by performing only a single iteration of the interior-point method used to solve the SOCP problem in each iteration of our iterative scheme rather than performing the interior-point method to convergence. In this way, we were able to save a significant amount of superfluous computations which arise from unnecessarily accurate intermediate solutions. From a different perspective, updating the approximated feasible set has been incorporated into the iterations of the interior-point method yielding a low-complexity one time scale algorithm. Our simulation results have shown that the good performance in terms of total transmitted power and feasibility of the iterative SOCP scheme of the previous chapters could be maintained while halving its required runtime.

Chapter 9

FF Beamforming with Adaptive Decoding Delays in Asynchronous MU Relay Networks

9.1 Introduction

In this chapter, we turn our attention to the FF relay beamforming scenario again. Recall that the signal received at a destination node in the FF relay network with frequency selective channels of Section 3.3 contains a significant amount of ISI. To mitigate the ISI in the SU scenario of [52], where $K = M = 1$, the authors in [55] have proposed to additionally perform linear equalization or decision feedback equalization at the destination. The FIR filter coefficients at the relays that maximize the SINR at the output of the equalizer subject to relay power constraints are obtained using a gradient algorithm. Block processing of the received symbols required for channel equalization significantly improves the SINR performance compared to much simpler symbol-by-symbol decoding. However, it also adds considerable complexity to the destination node which is a crucial drawback of the scheme in [55]. Furthermore, to the best of our knowledge, a way to extend the method in [55] to the MUP2P or the MGM relay network of Chapter 3 has not yet been found.

In the FF beamforming scenario, where SC transmission over frequency selective channels is performed, each sample of the received signal taken at symbol rate at a destination node consists of a superposition of delayed multipath copies of consecutive symbols that are transmitted by both, the desired source and the undesired sources. The symbols from the undesired sources cause MUI. If no equalization filter is employed at the destinations, one of the symbols from the desired source in the above superposition is considered as the desired symbol while the other symbols of this source cause ISI. In this chapter, we notice that the destination can decide which of the symbols from the desired source in the received superposition to decode as the desired symbol and which to treat as ISI. In other words, each destination can adaptively select an appropriate decoding delay. In [56], a similar idea has individually been developed using a frequency domain approach that, however, is restricted to SU relay networks. Previous works do not make use of flexible decoding delays: In [52] and [54], the same fixed decoding delay is selected for all destinations (cf. Section 3.3) which only yields satisfactory results if the network is perfectly synchronized.

In [56], it has been proposed for the perfectly synchronized SU scenario of [52] to jointly optimize the adaptive decoding delay at the destination and the FIR filter coefficients at the relays. It has been shown in the latter reference that a simple closed-form solution of this joint optimization problem exists in the SU case which is, however, restricted to SU relay networks. To the best of our knowledge, the scheme of [56] cannot easily be generalized to MUP2P or MGM relay networks.

In this chapter, we propose a scheme enabling adaptive decoding delays for MUP2P and MGM relay networks using a time-domain approach and a MIP framework. In a MUP2P or MGM scenario, the use of adaptive decoding delays offers dramatic performance improvements for the following reason. In the SU scenario of [52], the different link delays from the source to the destination via the different relays can be compensated at the relays. Hence, perfect synchronization is achievable for this scenario. In a practical MUP2P or MGM scenario, however, users not only experience different link delays with respect to different relays but also with respect to other users. As a consequence, synchronization is only possible for one source-destination pair at a time but not for more than one such pair simultaneously. Thus, perfect synchronization cannot be achieved in the MUP2P network of [28], [3], and [54]. In this case, it is not appropriate to select equal decoding delays for all users that are constant over all channel realizations. In our scheme, we essentially shift part of the synchronization task from the relays to the destinations: We propose to optimize the individual decoding delays at the destinations such that each destination can decode the symbol of the desired source that exhibits the highest SINR in the received superposition and effectively mitigate ISI. Since different decoding delays can be selected for different users, an additional degree of freedom in multiplexing the users is provided. Taking a slightly different perspective, in contrast to the approach of [54], where users are only separated in frequency and space domain via a combination of filtering and beamforming, in our proposed scheme, users are additionally separated in time domain via flexible decoding delays and thus, part of the MUI is implicitly mitigated.

We again consider the problem of minimizing the total power transmitted at the relays subject to a QoS constraint at each destination. Since part of the optimization variables, i.e., the FIR filter coefficients, are continuous and others, i.e., the decoding delays, are integer, the problem represents a MIP problem. Recall from Chapter 3 that even if the integer decoding delays are fixed, the latter problem is nonconvex and NP-hard in general. This is fundamentally different from the SU case where the optimization problem exhibits a simple closed-form solution. Commercial BnC solvers like CPLEX [57] can only solve mixed-integer linear programming problems and mixed-integer SOCP (MISOCP) problems but not the nonconvex MIP problem we consider.

Therefore, we propose a customized BnC method yielding a lower bound on the required total transmitted relay power. It is based on MIP and two particular relaxations of the original problem, a continuous relaxation (see, e.g., [58]) and the SDR described in Chapter 4. To reduce the computational complexity of the BnC method, we propose a preprocessing stage which substantially reduces the number of possible combinations of the integer variables. The computational complexity of the BnC method is prohibitive for on-line implementation but it provides a very valuable benchmark to assess the performance of the suboptimal fast algorithms. For practical implementation, we propose a deflation method with a much lower computational complexity than the BnC procedure to approximately solve the problem. We also provide a way to reduce the computational complexity of the deflation method without sacrificing performance.

In our simulations, we test the proposed schemes with two different channel models: with asynchronous versions of the simple model considered in Section 5.8.2, [52–56], and of the widely accepted spatial channel model extended (SCME) [59], [60] commonly used for simulation-based evaluation of Beyond-3G (third generation) systems. Our simulations demonstrate significant performance improvements of the proposed methods compared to the approaches of [52] and [54] in the asynchronous MUP2P relay network for both channel models.

This chapter is based on my original work that has been submitted in [8] and my original work that has been published in [7].

9.2 Signal Model and Problem Formulation

We again consider the FF relay networks of Section 3.3. Recall that in the latter section, the decoding delay l_m has been considered to be fixed, i.e., non-adaptive, and identical for all destinations. Further recall that, however, an arbitrary element of $\boldsymbol{s}_d[n]$, say $s_d[n-l_m]$, can be selected as the desired symbol for the mth destination where l_m can be different for each destination. In this chapter, we make use of this fact and consider l_m, $\forall m \in \{1,\ldots,M\}$ to be a variable rather than a constant. Therefore, we denote the desired signal component and the ISI component in (3.21a) and (3.21b) by $y_{\mathrm{S},m,l_m}[n]$ and $y_{\mathrm{ISI},m,l_m}[n]$, respectively. Similarly, we denote $\boldsymbol{Q}_{\mathrm{ISI},d,m}$ by $\boldsymbol{Q}_{\mathrm{ISI},d,m,l_m}$ in (3.28b). We propose to adapt the selection of the index l_m of the desired symbol at the destinations to the channel realizations, i.e., to employ an adaptive decoding delay at the destinations. In this way, the decoding delay of each destination can be individually adapted to the overall CIRs corresponding to that destination. Our goal is

to jointly optimize the adaptive decoding delays at the destinations and the FIR filter coefficients at the relays. The joint optimization problem will be derived next.

We again consider the QoS-constrained power minimization problem. In this chapter, we formulate this problem using a MIP framework by introducing binary variables $\{a_{m,l_m}, \forall l_m \in \mathcal{L}_m, \forall m \in \mathcal{M}\}$, where $\mathcal{L}_m \triangleq \{0, \ldots, L-1\}$, $L \triangleq L_f + L_w + L_g - 2$, and $\mathcal{M} \triangleq \{1, \ldots, M\}$, to model the selection of a decoding delay as follows. $a_{m,l_m} = 1$ and $a_{m,\tilde{l_m}} = 0,\ \forall \tilde{l_m} \neq l_m \in \mathcal{L}_m$, if $s_d[n - l_m]$ is selected as the desired symbol at the mth destination. Then, we can formulate the QoS-constrained power minimization problem as

$$\begin{aligned}
\min_{\boldsymbol{w}, \{a_{m,l_m}\}} \quad & P_{\mathrm{T}} && \text{(9.1a)}\\
\text{s.t.} \quad & \mathrm{SINR}_{m,l_m} \geq a_{m,l_m}\gamma_m,\ \forall l_m \in \mathcal{L}_m,\ \forall m \in \mathcal{M}, && \text{(9.1b)}\\
& a_{m,l_m} \in \{0,1\},\ \forall l_m \in \mathcal{L}_m,\ \forall m \in \mathcal{M}, && \text{(9.1c)}\\
& \sum_{l_m=0}^{L-1} a_{m,l_m} = 1,\ \forall m \in \mathcal{M} && \text{(9.1d)}
\end{aligned}$$

where P_{T} is the total transmitted relay power given by (3.22), SINR_{m,l_m} denotes the SINR at the mth destination for the decoding delay l_m, and the binary variables are used to switch the SINR constraints on or off. The constraints in (9.1d) represent multiple choice constraints which guarantee that a single SINR constraint per destination is activated, i.e., a single decoding delay is selected per destination. Using the derivations of Section 3.3 with the slightly new notation introduced above, problem (9.1) can be reformulated as the following nonconvex MIP problem

$$\begin{aligned}
\min_{\boldsymbol{w}, \{a_{m,l_m}\}} \quad & \boldsymbol{w}^H \boldsymbol{D} \boldsymbol{w} && \text{(9.2a)}\\
\text{s.t.} \quad & \frac{P_d |\boldsymbol{w}^H \boldsymbol{\vartheta}_{d,m,l_m}|^2}{\boldsymbol{w}^H (\boldsymbol{Q}_{\mathrm{ISI},d,m,l_m} + \boldsymbol{Q}_{\mathrm{MUI},m} + \boldsymbol{Q}_{\mathrm{N},m}) \boldsymbol{w} + \sigma_\nu^2} \geq a_{m,l_m}\gamma_m, && \text{(9.2b)}\\
& \forall l_m \in \mathcal{L}_m,\ \forall m \in \mathcal{G}_d,\ \forall d \in \mathcal{K},\ (9.1c),\ (9.1d).
\end{aligned}$$

To simplify problem (9.2), let us introduce

$$\begin{aligned}
\tilde{\boldsymbol{w}} \triangleq \boldsymbol{D}^{1/2}\boldsymbol{w}, \qquad \tilde{\boldsymbol{\vartheta}}_{d,m,l_m} \triangleq \boldsymbol{D}^{-1/2}\boldsymbol{\vartheta}_{d,m,l_m},\\
\tilde{\boldsymbol{Q}}_{d,m,l_m} \triangleq \boldsymbol{D}^{-1/2}(\boldsymbol{Q}_{\mathrm{ISI},d,m,l_m} + \boldsymbol{Q}_{\mathrm{MUI},m} + \boldsymbol{Q}_{\mathrm{N},m})\boldsymbol{D}^{-1/2},
\end{aligned}$$

and rewrite it as

$$\begin{aligned}
\min_{\tilde{\boldsymbol{w}},\{a_{m,l_m}\}} \quad & \|\tilde{\boldsymbol{w}}\|^2 && \text{(9.3a)}\\
\text{s.t.} \quad & |\tilde{\boldsymbol{w}}^H \tilde{\boldsymbol{\vartheta}}_{d,m,l_m}|^2 \geq \\
& a_{m,l_m} \frac{\gamma_m}{P_d} (\tilde{\boldsymbol{w}}^H \tilde{\boldsymbol{Q}}_{d,m,l_m} \tilde{\boldsymbol{w}} + \sigma_\nu^2),\ \forall l_m \in \mathcal{L}_m, \forall m \in \mathcal{G}_d,\ \forall d \in \mathcal{K}, && \text{(9.3b)}\\
& (9.1c),\ (9.1d). && \text{(9.3c)}
\end{aligned}$$

Problem (9.3) is a nonlinear MIP problem which is NP-hard and, to the best of our knowledge, there is no method to compute a globally optimal solution in affordable time. Therefore, we propose a BnC method for obtaining a lower bound on the optimal value of problem (9.3) in Section 9.3. Although affordable in simulations to compute a lower bound as a valuable benchmark, the complexity of the BnC method is generally too high for implementation in practical systems. Therefore, we propose a deflation scheme to obtain an approximately optimal solution of problem (9.3) with a much lower computational complexity in Section 9.4.

9.3 Proposed BnC Method

Due to the multiple choice constraint (9.1d), problem (9.3) exhibits a combinatorial part. The most straightforward way to solve a combinatorial problem is to run an exhaustive search where all possible combinations are evaluated. In most cases, however, an exhaustive search is prohibitively expensive in terms of computational complexity. A standard way to reduce the number of combinations that need to be evaluated is to use a BnC procedure [58]. In the BnC method, a binary search tree consisting of nodes is constructed where each node corresponds to a particular subset of binary variables fixed at particular values. Then, an intelligent search is performed on the tree such that only a fraction of the nodes have to be visited. For relatively simple MIP problems like mixed-integer linear programming problems and MISOCP problems, BnC-based commercial solvers like CPLEX [57] exist. The MISOCP problem for instance can be solved by CPLEX as the original MISOCP problem becomes a convex SOCP problem after the binary variables are relaxed to be continuous. To the best of our knowledge, however, no reformulation of problem (9.3) exists such that it becomes a convex problem after the continuous relaxation. Thus, commercial solvers like CPLEX cannot be applied to solve problem (9.3). As we show later, we instead further relax the continuous relaxation of problem (9.3) to obtain a convex SDP problem approximation. We then apply a customized BnC procedure to obtain a lower bound on the optimal value

of problem (9.3). Note that customization of the general BnC framework is of critical importance and that the contribution of this dissertation is not to apply the well known BnC procedure but rather to customize the BnC procedure for the particular problem under consideration.

For a general BnC framework, an upper and a lower bound on the optimal value of the original MIP problem is required for every combination of every subset of the binary variables [58]. However, in our customized BnC procedure, we only use a separate lower bound for every combination of every subset of the binary variables and a single upper bound as we explain later. The single upper bound, that is derived in Section 9.3.3, is simply a suboptimal solution of problem (9.3) and hence, an upper bound on the optimal value of the general problem (9.3), i.e., not for a particular combination of a subset of binary variables. Let us now explain how to obtain lower bounds on the optimal value of problem (9.3).

9.3.1 Derivation of the Proposed Lower Bounds

To this end, we separate the binary and the continuous variables in the same way as in [61], i.e., we reformulate problem (9.3) as

$$\begin{aligned}
\min_{\tilde{\boldsymbol{w}},\{a_{m,l_m}\}} \quad & \|\tilde{\boldsymbol{w}}\|^2 && \text{(9.4a)}\\
\text{s.t.} \quad & |\tilde{\boldsymbol{w}}^H\tilde{\boldsymbol{\vartheta}}_{d,m,l_m}|^2 + (1-a_{m,l_m})B_{m,l_m} \geq \\
& \frac{\gamma_m}{P_d}(\tilde{\boldsymbol{w}}^H\tilde{\boldsymbol{Q}}_{d,m,l_m}\tilde{\boldsymbol{w}} + \sigma_\nu^2),\ \forall l_m \in \mathcal{L}_m, \forall m \in \mathcal{G}_d, \forall d \in \mathcal{K}, && \text{(9.4b)}\\
& \|\tilde{\boldsymbol{w}}\|^2 \leq P_{\text{UB}}, && \text{(9.4c)}\\
& a_{m,l_m} \in \{0,1\},\ \forall l_m \in \mathcal{L}_m, \forall m \in \mathcal{M}, && \text{(9.4d)}\\
& \sum_{l_m=0}^{L-1} a_{m,l_m} = 1,\ \forall m \in \mathcal{M} && \text{(9.4e)}
\end{aligned}$$

where B_{m,l_m} is an upper bound on the right-hand side of inequality (9.4b) and P_{UB} is an upper bound on the optimal value of problem (9.3). The constraints in (9.4b) and (9.3b) are equivalent: Due to the upper bound B_{m,l_m}, the constraint (9.4b) is automatically satisfied when $a_{m.l_m} = 0$ which also holds for the constraint (9.3b). On the other hand, when $a_{m.l_m} = 1$, the upper bound B_{m,l_m} disappears and the constraint (9.4b) is the same as the constraint (9.3b) for $a_{m.l_m} = 1$. Note that the original problem formulation (9.3) is bilinear in the binary optimization variables whereas problem (9.4) is linear in these variables. Thus, although problem (9.4) is an exact reformulation

of problem (9.3), the former problem is easier to solve than the latter. We define the constant B_{m,l_m} as follows

$$\begin{aligned} B_{m,l_m} &\triangleq \max_{\|\tilde{\boldsymbol{w}}\|^2 \leq P_{\mathrm{UB}}} \frac{\gamma_m}{P_d}(\tilde{\boldsymbol{w}}^H \tilde{\boldsymbol{Q}}_{d,m,l_m} \tilde{\boldsymbol{w}} + \sigma_\nu^2) \\ &= \frac{\gamma_m}{P_d}(P_{\mathrm{UB}} \mathcal{P}\{\tilde{\boldsymbol{Q}}_{d,m,l_m}\}^H \tilde{\boldsymbol{Q}}_{d,m,l_m} \mathcal{P}\{\tilde{\boldsymbol{Q}}_{d,m,l_m}\} + \sigma_\nu^2) \\ &= \frac{\gamma_m}{P_d}(P_{\mathrm{UB}} \mathcal{L}_{\max}\{\tilde{\boldsymbol{Q}}_{d,m,l_m}\} + \sigma_\nu^2) \end{aligned} \tag{9.5}$$

where we use the upper bound on the optimal value of problem (9.3) that will be derived in Section 9.3.3, as P_{UB}. This follows from the observation that at optimum, the total transmitted relay power is less than or equal to its upper bound. Note that we have added the power constraint (9.4c) to guarantee that B_{m,l_m} is an upper bound on the right-hand side of inequality (9.4b). Although the constraint (9.4c) is redundant for the original version of problem (9.4), it becomes relevant in Section 9.3.2 when some of its binary variables are fixed: Solving problem (9.4) with fixed binary variables generally only yields a suboptimal solution for problem (9.4) and thus, without the constraint (9.4c), the total transmitted relay power can exceed P_{UB} when some of the binary variables are fixed.

Let us relax the binary variables $\{a_{m,l_m}, \forall l_m \in \mathcal{L}_m, \forall m \in \mathcal{M}\}$, originally defined on the discrete set $\{0,1\}$, to be continuous and confined in the closed interval $[0,1]$. This is well known in the context of MIP as the continuous relaxation approach [58]. In this way, problem (9.4) is approximated by a continuous problem which provides a lower bound on the optimal value of problems (9.3) and (9.4). To tighten this lower bound, we add constraints (9.6b) to problem (9.4) as in [61]:

$$\min_{\tilde{\boldsymbol{w}}, \{a_{m,l_m}\}} \ \|\tilde{\boldsymbol{w}}\|^2 \tag{9.6a}$$

$$\text{s.t. } |\tilde{\boldsymbol{w}}^H \tilde{\boldsymbol{\vartheta}}_{d,m,l_m}|^2 \geq a_{m,l_m} \frac{\gamma_m}{P_d} \sigma_\nu^2, \ \forall l_m \in \mathcal{L}_m, \forall m \in \mathcal{G}_d, \forall d \in \mathcal{K} \tag{9.6b}$$

$$(9.4b), \ (9.4c), \ (9.4d), \ (9.4e). \tag{9.6c}$$

Comparing the constraints in (9.4b) to the added constraints in (9.6b), which are often referred to as cuts, reveals that the latter constraints are always satisfied when the variables $\{a_{m,l_m}, \forall l_m \in \mathcal{L}_m, \forall m \in \mathcal{M}\}$ are binary. Hence, problem (9.6) is equivalent to problems (9.3) and (9.4). However, the cuts reduce the feasible set of the associated continuous relaxation. Consequently, the continuous relaxation of problem (9.6) yields a tighter lower bound on the optimal value of problem (9.3) than the continuous relaxation of problem (9.4).

Problems (9.4) and (9.6) are turned into continuous problems using the continuous relaxation. However, they remain nonconvex after the continuous relaxation which is

fundamentally different from problems considered in other works like, e.g., [61] where the problem becomes convex after the continuous relaxation. As mentioned earlier, problem (9.6) can thus not be handled by any available solver. Therefore, we propose to apply the SDR described in Chapter 4 to the continuously relaxed version of problem (9.6) to approximate it by a convex SDP problem. Like in Chapter 4, we introduce the new optimization variable $\boldsymbol{X} \triangleq \tilde{\boldsymbol{w}}\tilde{\boldsymbol{w}}^H$ and reformulate the continuously relaxed version of problem (9.6) as

$$\min_{\boldsymbol{X},\{a_{m,l_m}\}} \quad \mathrm{tr}(\boldsymbol{X}) \tag{9.7a}$$

$$\text{s.t.} \quad \mathrm{tr}(\tilde{\boldsymbol{\vartheta}}_{d,m,l_m}\tilde{\boldsymbol{\vartheta}}_{d,m,l_m}^H\boldsymbol{X}) + (1-a_{m,l_m})B_{m,l_m} \geq \frac{\gamma_m}{P_d}(\mathrm{tr}(\tilde{\boldsymbol{Q}}_{d,m,l_m}\boldsymbol{X}) + \sigma_\nu^2),\ \forall l_m \in \mathcal{L}_m, \forall m \in \mathcal{G}_d, \forall d \in \mathcal{K}, \tag{9.7b}$$

$$\mathrm{tr}(\tilde{\boldsymbol{\vartheta}}_{d,m,l_m}\tilde{\boldsymbol{\vartheta}}_{d,m,l_m}^H\boldsymbol{X}) \geq a_{m,l_m}\frac{\gamma_m}{P_d}\sigma_\nu^2,\ \forall l_m \in \mathcal{L}_m, \forall m \in \mathcal{G}_d, \forall d \in \mathcal{K}, \tag{9.7c}$$

$$\mathrm{tr}(\boldsymbol{X}) \leq P_{\mathrm{UB}}, \tag{9.7d}$$

$$0 \leq a_{m,l_m} \leq 1,\ \forall l_m \in \mathcal{L}_m, \forall m \in \mathcal{M}, \tag{9.7e}$$

$$\sum_{l_m=0}^{L-1} a_{m,l_m} = 1,\ \forall m \in \mathcal{M}, \tag{9.7f}$$

$$\boldsymbol{X} \succeq 0, \tag{9.7g}$$

$$\mathrm{rank}(\boldsymbol{X}) = 1. \tag{9.7h}$$

Recall that the SDR consists in dropping the nonconvex rank-one constraint (9.7h) (see Chapter 4) which yields the following problem

$$\min_{\boldsymbol{X},\{a_{m,l_m}\}} \mathrm{tr}(\boldsymbol{X}) \tag{9.8a}$$

$$\text{s.t. } (9.7b) - (9.7g). \tag{9.8b}$$

Problem (9.8) is a convex SDP problem which can be solved by interior-point methods [62]. Since two relaxations are involved, the continuous relaxation and the SDR, it provides a lower bound for the original, non-relaxed problem (9.3). If one or more of the binary variables in problem (9.8) are fixed at zero or one, problem (9.8) provides a lower bound for the original problem for these variables fixed. Note that if a binary variable of the mth destination is fixed at one, all remaining binary variables of the mth destination must be equal to zero according to the multiple choice constraint (9.4e).

9.3.2 Proposed Branching Procedure

The strategy we propose for our BnC procedure is to successively fix subsets of binary variables, solve problem (9.8) for each of these subsets to obtain a lower bound for the

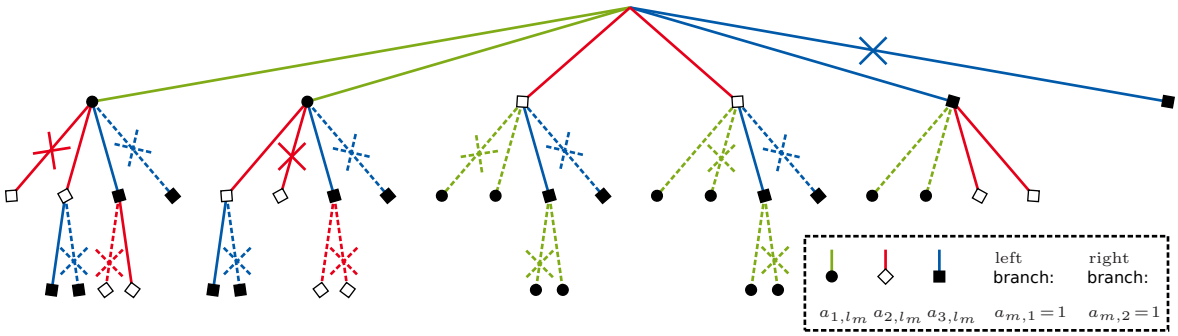

Figure 9.1. Branching tree of the proposed BnC method for $M = 3$ and $L = 2$.

original problem (9.3) for each of these subsets, and compare these lower bounds to the upper bound P_{UB} for the original problem (9.3) where the binary variables are not fixed. P_{UB} will be derived in Section 9.3.3. If the lower bound corresponding to the current set of fixed binary variables is greater than the upper bound, the current set of fixed binary variables can be discarded as a candidate for the optimum combination of binary variables.

Our BnC method is carried out using the following hierarchical procedure. On the first level, which is at the top of the hierarchy, one by one, each binary variable is fixed to one. Each time, only a single binary variable corresponding to a single destination is fixed to one. On the second level, two of the binary variables are fixed to one, i.e., the decoding delays of two destinations are fixed. All remaining possible combinations of two binary variables fixed to one are tested. On the third level, three are fixed, and so on. Once enough combinations of binary variables have been eliminated, problem (9.8) is solved for the remaining combinations of all binary variables fixed and the smallest lower bound is selected as the final lower bound.

To illustrate this procedure, let us consider a simplified scenario with $M = 3$ destination nodes and where $L = 2$. For this example, the tree corresponding to the proposed branching procedure is depicted in Fig. 9.1. Each node in the tree corresponds to setting a a_{m,l_m} to one according to the legend in the figure. Whenever the lower bound corresponding to a node in the tree is above the upper bound P_{UB}, we conclude that this combination cannot be optimal and does not need to be considered further, i.e., the corresponding branch is pruned. A pruned branch is indicated by a crossed out branch in the figure. The algorithm starts from top left of Fig. 9.1 and ends at bottom right. Redundant branches and branches that already have been pruned elsewhere are depicted with a dashed line. For each of the three remaining nodes at the third level, a lower bound is computed and the smallest of these three lower bounds is selected as the final lower bound.

9.3.3 Proposed Initialization

In this subsection, we propose an initialization for the BnC method. First, we derive an upper bound on the optimal value of the original problem (9.2) which is used as P_{UB} in the definition of B_{m,l_m} in (9.5). Afterwards, we propose an efficient preprocessing stage.

The initialization yielding P_{UB} consists of the following two stages. In the first stage, all users and all decoding delays are considered one by one. When the decoding delay l_m of the mth user is considered, we approximate the original problem (9.3) by ignoring all QoS constraints but the one corresponding to decoding delay l_m of the mth user yielding the following optimization problem:

$$\min_{\tilde{\boldsymbol{w}}} \quad \|\tilde{\boldsymbol{w}}\|^2 \tag{9.9a}$$

$$\text{s.t.} \quad \tilde{\boldsymbol{w}}^H(P_d\tilde{\boldsymbol{\vartheta}}_{d,m,l_m}\tilde{\boldsymbol{h}}_{m,l_m}^H - \gamma_m\tilde{\boldsymbol{Q}}_{d,m,l_m})\tilde{\boldsymbol{w}} \geq \gamma_m\sigma_\nu^2. \tag{9.9b}$$

Since problem (9.9) contains only one QoS constraint, it is very similar to the QoS-constrained power minimization problem in the SU scenario considered in [52] where $K = M = 1$. It has been shown in [52] that a simple closed-form solution based on the principal eigenvector of the matrix $P_d\tilde{\boldsymbol{\vartheta}}_{d,m,l_m}\tilde{\boldsymbol{\vartheta}}_{d,m,l_m}^H - \gamma_m\tilde{\boldsymbol{Q}}_{d,m,l_m}$ exists for this SU problem and that its optimal value can be expressed as

$$P_{\min,m,l_m} = \gamma_m\sigma_\nu^2/\mathcal{L}_{\max}\{P_d\tilde{\boldsymbol{\vartheta}}_{d,m,l_m}\tilde{\boldsymbol{\vartheta}}_{d,m,l_m}^H - \gamma_m\tilde{\boldsymbol{Q}}_{d,m,l_m}\}. \tag{9.10}$$

For each user m, we select the decoding delay l_m corresponding to the smallest $P_{\min,m,l_m}$ of that user as follows:

$$l_{P_{\mathrm{UB}},m} = \mathrm{argmin}_{l_m\in\mathcal{L}_m} P_{\min,m,l_m},\ \forall m \in \mathcal{M}. \tag{9.11}$$

Note that the decoding delay $l_{P_{\mathrm{UB}},m}$ defined in (9.11) is likely to yield a low total transmitted relay power for the original problem (9.2) as well. In the second stage of the proposed initialization, the original problem (9.2) is solved approximately for $\{\mathcal{L}_m = \{l_{P_{\mathrm{UB}},m}\},\ \forall m \in \mathcal{M}\}$. Note that hence, there is only one QoS constraint per destination and in this case, problem (9.2) has the same mathematical structure as the QoS-constrained power minimization problem (3.30). We can thus use the iterative SOCP method proposed in Chapter 5 to approximately solve it. The approximate solution obtained in this way is used as P_{UB} in (9.5). Since P_{UB} is a suboptimal solution of problem (9.2), it is an upper bound on the objective function value at the optimal solution of problem (9.2). The algorithm is summarized in Table 9.1.

We propose the following preprocessing stage for the BnC algorithm to reduce its computational complexity. The preprocessing stage precedes the first level described

for $m = 1, \ldots, M$
  for $l_m = 0, \ldots, L-1$
    Compute $P_{\min,m,l_m}$ via (9.10).
  end
end
Solve problem (9.2) for $\mathcal{L}_m = \{l_{P_{\mathrm{UB}},m}\}$, $\forall m \in \mathcal{M}$ where $l_{P_{\mathrm{UB}},m}$ is obtained by (9.11). (Solve it approximately using the iterative SOCP scheme of Chapter 5.)
Output: P_{UB}.

Table 9.1. Proposed initialization

Set $\mathcal{L}_m^{(1)} = \mathcal{L}_m$, $\forall m \in \mathcal{M}$.
for $m = 1, \ldots, M$
  for $l_m = 0, \ldots, L-1$
    Compute $P_{\min,m,l_m}$ via (9.10).
    if $P_{\min,m,l_m}$ infeasible **or** $P_{\min,m,l_m} > P_{\mathrm{UB}}$
      Set $\mathcal{L}_m^{(1)} = \mathcal{L}_m^{(1)} \setminus l_m$.
    end
  end
end

Table 9.2. Proposed preprocessing stage

in Section 9.3.2. Recall that fixing one binary variable to one and then solving problem (9.8) provides a lower bound for the original problem for this variable fixed to one. However, we propose to use an additional alternative lower bound for this case which is easier to obtain: A lower bound for $a_{m,l_m} = 1$ is provided by (9.10) for the following reasons. Due to the multiple choice constraint in (9.4e), if $a_{m,l_m} = 1$, then $a_{k,\tilde{l_m}} = 0, \forall \tilde{l_m} \neq l_m \in \mathcal{L}_m$, i.e., only one QoS constraint needs to be considered for the mth destination. Moreover, the QoS constraints of all other destinations are ignored in (9.10). It is important to note that this is a way to relax the original problem (9.3) which is different from applying the continuous relaxation and the SDR. However, it is a valid relaxation as well and thus, also provides a lower bound on the optimal value of problem (9.3) under the condition that $a_{m,l_m} = 1$. This lower bound is easier to obtain since it is given by a closed-form expression. Thus, we use these lower bounds, which are a byproduct of the initialization, to fix all a_{m,l_m} to zero for which $P_{\min,m,l_m} > P_{\mathrm{UB}}$. Using the preprocessing stage, a considerable number of binary variables is set to zero with a low computational effort and thereby, the number of combinations of binary variables, which have to be considered later in the BnC algorithm, is substantially reduced. The algorithm is summarized in Table 9.2 where the resulting $\mathcal{L}_m^{(1)}$ replaces $\mathcal{L}_m$ in problem (9.8) in the subsequent BnC method described in Section 9.3.2.

9.3.4 Special Cases and Relation to State-of-the-Art

Let us discuss state-of-the-art schemes and special cases here. In [52], the special case of $K = M = 1$, i.e., the SU scenario, has been considered and the first element of vector $\boldsymbol{s}_1[n]$ has been assumed to be the desired symbol. This scheme has been extended to the MUP2P scenario (i.e., $K = M > 1$) in [54] where the center element in the vector $\boldsymbol{s}_k[n]$ has been selected as the decoded symbol for all destinations. Thus, the approaches in [52] and [54] do not make use of adaptive decoding delays. In contrast to these approaches, it has been proposed in [56] for the SU relaying scenario of [52], i.e., $K = M = 1$, to employ an adaptive decoding delay at the destination node. The adaptive decoding delay at the destination and the adaptive FIR filter coefficients at the relays have been jointly optimized. The scheme in [56] enjoys a simple closed-form solution which is, however, restricted to the SU relaying scenario and cannot be generalized to the MUP2P scenario or the MGM scenario where the joint optimization problem is substantially more complex. In this work, we propose a MIP schemes to enable adaptive decoding delays in the more general case of a MUP2P relay network. In the MUP2P and MGM relay networks, individual adaptive decoding delays at the destinations offer tremendous performance improvements due to the synchronization issues mentioned above. It is important to note that in the special case of $K = M = 1$, i.e., for a SU scenario, the initialization of Table 9.1 simplifies to the following closed-form optimal solution for the original problem (9.3):

$$P_{\text{opt}} = \min_{l_m} P_{\min,1,l_m}. \tag{9.12}$$

This is due to the fact that there is no other user whose QoS constraint is to be ignored and hence, no approximation is involved in this case. Note that in [56], for a max-min fair beamforming problem, a closed-form solution similar to the one in (9.12) has been identified (for $K = M = 1$).

9.4 Proposed Deflation Method

Since the computational complexity of the proposed BnC scheme is still prohibitively high for real-time implementation, we propose a computationally more efficient deflation method in this section. It yields a solution to problem (9.2) which is suboptimal but close to optimal as we show in our simulations.

The idea is to approximately solve the original problem (9.6) by solving a sequence of its continuously relaxed versions where the number of solved problems grows only linearly

with the number of users M and the number of decoding delays L. The continuously relaxed versions of problem (9.6) can be written as

$$\min_{\tilde{\boldsymbol{w}},\{a_{m,l_m}\}} \|\tilde{\boldsymbol{w}}\|^2 \tag{9.13a}$$

$$\text{s.t. } (9.4b),\ (9.4c),\ (9.6b),\ (9.7e),\ (9.4e). \tag{9.13b}$$

Like the original problem (9.2) for fixed binary variables, problem (9.13) can also be solved approximately using the the iterative SOCP scheme of Chapter 5. Recall that P_{UB} has to be defined for problem (9.13). We use the same P_{UB} as for the BnC method, i.e., we initialize our deflation method using P_{UB} of Section 9.3.3. Our goal is then to find a suboptimal solution for the original problem (9.2) yielding a lower total transmitted relay power than P_{UB} as follows. We propose a deflation approach where in each iteration, one decoding delay is removed from a set of candidate decoding delays considered in problem (9.13). We propose to initialize the set of candidate decoding delays as follows. We use the proposed preprocessing stage of the BnC method of Table 9.2, i.e., we select an initial set of candidate decoding delays containing all decoding delays which have not been identified as suboptimal by the preprocessing scheme. We then proceed with the proposed iterative scheme where in each iteration, we perform the following steps: We first solve problem (9.13) approximately for the current set of candidate decoding delays using the method of Chapter 5. For the relay beamforming weights obtained in this way, we then determine the worst SINR of all users and all current candidate decoding delays. Finally, the decoding delay corresponding to this SINR is removed from the current set of candidate decoding delays. As soon as only one decoding delay remains for a particular destination, an appropriate decoding delay has been found for this destination and it is therefore no longer considered when determining the worst SINR. This procedure is repeated until a decoding delay has been found for each destination. A summary of the algorithm is provided in Table 9.3.

Note that removing decoding delays from the set of candidate decoding delays is equivalent to fixing relaxed binary variables to zero. Hence, problem (9.13) is tightened from iteration to iteration and the total transmitted relay power increases from one iteration to the next. Fixing the binary variable corresponding to the worst SINR to zero is likely to keep this increase as low as possible. Thus, when all binary variables are fixed, it is likely that a better solution than P_{UB} is obtained. Due to the heuristic nature of the iterative method, this can unfortunately not be guaranteed analytically and the total transmitted relay power might increase beyond P_{UB} from one iteration to the next. If this is the case, problem (9.13) becomes infeasible due to the constraint (9.4c). We propose to use the result of the initialization of Table 9.1 if infeasibility

Initialization: Perform the algorithms of Tables 9.1 and 9.2.
Yields P_{UB}, B_{m,l_m}, and $\mathcal{L}_m^{(1)}$. Set $i = 1$.
while $|\mathcal{M}^{(i)}| > 0$
Solve problem (9.13) with $\mathcal{L}_m = \mathcal{L}_m^{(i)}$ yielding $\tilde{\boldsymbol{w}}_{\mathrm{opt}}^{(i)}$.
$\tilde{m}, \tilde{l_m} = \mathrm{argmin}_{m \in \mathcal{M}^{(i)}, l_m \in \mathcal{L}_m^{(i)}} \mathrm{SINR}_{m,l_m}(\tilde{\boldsymbol{w}}_{\mathrm{opt}}^{(i)})$
Set $\mathcal{L}_{\tilde{m}}^{(i+1)} = \mathcal{L}_{\tilde{m}}^{(i)} \setminus \tilde{l_m}$, $\mathcal{L}_m^{(i+1)} = \mathcal{L}_m^{(i)}$, $\forall m \neq \tilde{m} \in \mathcal{M}$.
if $|\mathcal{L}_{\tilde{m}}^{(i+1)}| = 1$
Set $\mathcal{M}^{(i+1)} = \mathcal{M}^{(i)} \setminus \tilde{m}$
else
Set $\mathcal{M}^{(i+1)} = \mathcal{M}^{(i)}$
end
Set $i = i + 1$.
end
Solve problem (9.13) with $\mathcal{L}_m = \mathcal{L}_m^{(i)}$.

Table 9.3. Proposed deflation procedure

occurs. During our extensive simulations, however, infeasibility occurred only in about 10% of the cases.

9.5 Complexity Reduction

In this section, we develop a scheme to reduce the complexity of the proposed deflation method. First of all, we note that the number of candidate decoding delays taken into account in the first iteration can be substantially reduced without performance loss as follows. Recall that the initialization of Section 9.3.3 yields $P_{\min,m,l_m}$ for each decoding delay which is a lower bound on the optimal value of the original problem (9.2) for decoding delay l_m of the mth destination. Decoding delays corresponding to those $P_{\min,m,l_m}$ of the mth destination which are significantly above the smallest $P_{\min,m,l_m}$ of the mth destination are very unlikely to effectively mitigate ISI and MUI. Therefore, it is reasonable not to consider them as candidates for optimum decoding delays and we propose the following extension to the initialization in Table 9.3. We only select the decoding delays corresponding to the $\tilde{L}$ smallest $P_{\min,m,l_m}$ of the mth destination as candidates for the optimum decoding delay of the mth destination. A mathematical description of this extended initialization is given in Table 9.4 where we have assumed that $|\mathcal{L}_m^{(1)}| > \tilde{L}$, $\forall m \in \mathcal{M}$, where $\mathcal{L}_m^{(1)}$ is the result of the preprocessing stage of Table 9.2. Using it, the number of iterations of the proposed iterative method can be reduced by $\sum_{m=1}^{M}(|\mathcal{L}_m^{(1)}| - \tilde{L})$ while maintaining its good performance.

$P_{\min,m,\kappa_1} \leq P_{\min,m,\kappa_2} \leq \ldots \leq P_{\min,m,\kappa_L},\ \forall m \in \mathcal{M}$ where $\kappa_l \in \mathcal{L}_m$ and $\cup_l \kappa_l = \mathcal{L}_m,\ \forall m \in \mathcal{M}$ $\mathcal{L}_m^{(1)} = \{\kappa_1, \ldots, \kappa_{\tilde{L}}\},\ \forall m \in \mathcal{M}$

Table 9.4. Proposed extended initialization

Let us now turn our attention to a further means to reduce the overall complexity of the proposed deflation method inspired by the complexity reduction proposed in Chapter 8. As mentioned earlier, problem (9.13) is solved approximately in each iteration using the iterative SOCP method of Chapter 5. To make them distinguishable, let us refer to the deflation iterations of the proposed method indexed by (i) as *outer iterations* and to those of the iterative SOCP method as *inner iterations*. In a particular outer iteration, every inner iteration yields an approximate solution to problem (9.13) where the approximation is improved from inner iteration to inner iteration. Performing inner iterations to convergence yields the best approximate solution to problem (9.13) achievable with the iterative SOCP method. However, in the next outer iteration, a binary variable is fixed to zero which practically means that a constraint is removed from problem (9.13) resulting in a new problem that is solved using the iterative SOCP method. Hence, much like in Chapter 8, processing the inner iterations up to convergence is in vain and a waste of computations since in every outer iteration, a new problem is solved anyway. Like in Chapter 8, we therefore propose to perform only a single inner iteration per outer iteration, thus avoiding unnecessarily high accuracy of intermediate solutions.

Recall that in the ith iteration of the iterative SOCP method, problem (9.13) is approximated by the following SOCP problem

$$\min_{\tilde{\boldsymbol{w}},\{a_{m,l_m}\}} \ \|\tilde{\boldsymbol{w}}\|^2 \tag{9.14a}$$

$$\text{s.t. } \mathrm{Re}\{\tilde{\boldsymbol{w}}^H \tilde{\boldsymbol{\vartheta}}_{d,m,l_m}^{(i)}\} + (1 - a_{m,l_m})\sqrt{B_{m,l_m}} \geq \sqrt{\frac{\gamma_m}{P_d}(\tilde{\boldsymbol{w}}^H \tilde{\boldsymbol{Q}}_{d,m,l_m} \tilde{\boldsymbol{w}} + \sigma_\nu^2)},\ \forall l_m \in \mathcal{L}_m, \forall m \in \mathcal{G}_d, \forall d \in \mathcal{K}, \tag{9.14b}$$

$$\mathrm{Re}\{\tilde{\boldsymbol{w}}^H \tilde{\boldsymbol{\vartheta}}_{d,m,l_m}^{(i)}\} \geq a_{m,l_m}\sqrt{\frac{\gamma_m}{P_d}\sigma_\nu^2},\ \forall l_m \in \mathcal{L}_m, \forall m \in \mathcal{G}_d, \forall d \in \mathcal{K} \tag{9.14c}$$

$$(9.4c),\ (9.7e),\ (9.4e) \tag{9.14d}$$

and its solution $\tilde{\boldsymbol{w}}_{\text{opt}}^{(i)}$ is obtained using interior point methods. Afterwards, the feasible set of problem (9.14) is updated for the next iteration via the following channel rotation

$$\tilde{\boldsymbol{\vartheta}}_{d,m,l_m}^{(i+1)} \triangleq \tilde{\boldsymbol{\vartheta}}_{d,m,l_m}^{(i)} \exp\left(-j\angle\left(\tilde{\boldsymbol{w}}_{\text{opt}}^{(i)H} \tilde{\boldsymbol{\vartheta}}_{d,m,l_m}^{(i)}\right)\right). \tag{9.15}$$

Initialization: Perform the algorithms of Tables 9.1 and 9.4.
Yields P_{UB}, B_{m,l_m}, $\mathcal{L}_m^{(1)}$, and $\tilde{\boldsymbol{\vartheta}}_{P_{\mathrm{UB}},d,m,l_m}$. Set $\tilde{\boldsymbol{\vartheta}}_{d,m,l_m}^{(1)} = \tilde{\boldsymbol{\vartheta}}_{P_{\mathrm{UB}},d,m,l_m}$.
for $i = 1, \ldots, M(\tilde{L}-1)$
Solve problem (9.14) with $\mathcal{L}_m = \mathcal{L}_m^{(i)}$.
$\tilde{m}, \tilde{l_m} = \mathrm{argmin}_{m\in\mathcal{M}^{(i)}, l_m \in \mathcal{L}_m^{(i)}} \mathrm{SINR}_{m,l_m}(\tilde{\boldsymbol{w}}_{\mathrm{opt}}^{(i)})$
Set $\mathcal{L}_{\tilde{m}}^{(i+1)} = \mathcal{L}_{\tilde{m}}^{(i)} \setminus \tilde{l_m}$, $\mathcal{L}_m^{(i+1)} = \mathcal{L}_m^{(i)}$, $\forall m \neq \tilde{m} \in \mathcal{M}$.
if $|\mathcal{L}_{\tilde{m}}^{(i+1)}| = 1$
Set $\mathcal{M}^{(i+1)} = \mathcal{M}^{(i)} \setminus \tilde{m}$
else
Set $\mathcal{M}^{(i+1)} = \mathcal{M}^{(i)}$
end
Perform the rotation of (9.15)
end
Solve problem (9.2) with $\mathcal{L}_m = \mathcal{L}_m^{(i)}$ and $\tilde{\boldsymbol{\vartheta}}_{d,m,l_m} = \tilde{\boldsymbol{\vartheta}}_{d,m,l_m}^{(i)}$.

Table 9.5. Proposed efficient deflation procedure

In every outer iteration, the feasible set is updated as well by removing a set of constraints as described in Table 9.3. We propose to transform the two-time-scale algorithm, where inner and outer iterations are separated, into a one-time-scale algorithm where in every iteration, the feasible set is updated both via rotating the channels and removing a set of constraints. Note that to be precise, the algorithm of Table 9.3 is actually a three-time-scale algorithm since each SOCP problem is solved using an interior-point method which is an iterative method itself. Using the complexity reduction proposed in Chapter 8 in addition to the complexity reduction proposed in this section, the three-time-scale algorithm can be turned into a much more efficient one-time-scale algorithm.

The more efficient algorithm with the two modifications described above is summarized in Table 9.5. Note that in the initialization of Table 9.1, P_{UB} is obtained performing the iterative SOCP procedure until convergence. Hence, besides P_{UB}, it yields a set of rotated channel vectors which we denote by $\tilde{\boldsymbol{\vartheta}}_{P_{\mathrm{UB}},d,m,l_m}$ in Table 9.5. We need to initialize the efficient deflation scheme of Table 9.5 with $\tilde{\boldsymbol{\vartheta}}_{P_{\mathrm{UB}},d,m,l_m}$ in order to guarantee feasibility of problem (9.14) in the first iteration of the algorithm in Table 9.5. Further note that once a decoding delay has been determined for every destination in Table 9.5, the original problem (9.2) has to be solved approximately performing the iterative SOCP method until convergence which we initialize using the set of rotated channel vectors $\tilde{\boldsymbol{\vartheta}}_{d,m,l_m}^{(i)}$ obtained previously. This final step is summarized in the last line of Table 9.5.

Let us now discuss the computational complexities of the proposed schemes and existing ones. Only the major FLOPs are taken into account to keep the analysis simple. Since the BnC scheme proposed in this paper is only used as a benchmark and not proposed for implementation in practice, we exclude the BnC method from the complexity analysis. Using the complexity results of Section 5.7, one can straightforwardly derive the worst-case complexities of the state-of-the-art methods and the proposed schemes. We consider the case that the iterative SOCP method of Chapter 5 is used to approximately solve problem (9.2) for fixed decoding delays and problem (9.13). State-of-the-art methods, which solve problem (9.2) approximately for fixed non-adaptive decoding delays, as well as the proposed initialization procedure of Table 9.1 require a complexity of $\mathcal{O}\left(I(NL_w)^3M^{1.5}\right)$. Recall that I denotes the maximum number of iterations after which the iterative SOCP method achieves convergence which is usually very low, e.g., $I = 5$. The computational complexity of the initialization procedure is comparable to that of the state-of-the-art methods as the overhead for computing the initial decoding delays is negligible as compared to performing the iterative SOCP method. The complexity of the proposed deflation method of Section 9.4 is $\mathcal{O}\left(I(NL_w)^3(ML)^{2.5}\right)$ while that of the efficient deflation method proposed in this section amounts to $\mathcal{O}\left((NL_w)^3(M\tilde{L})^{2.5}\right)$ where usually $\tilde{L} \ll L$. Note that the deflation schemes additionally require the complexity of the initialization scheme. We conclude that the complexity of the proposed deflation method can be substantially reduced using the complexity reduction proposed in this section. Making use of the complexity reduction which we have proposed in Chapter 8, the complexity of all methods can be further reduced. Compared to the initialization scheme, the efficient deflation scheme offers improved performance at an increased computational complexity. If this increase in computational complexity is not affordable in practice, one can resort to the initialization scheme. As we show in our simulations, the initialization scheme already yields significant performance improvements in terms of total transmitted relay power and feasibility at only slightly increased computational complexity as compared to state-of-the-art methods without adaptive decoding delays.

9.6 Practical Considerations and Discussion

Note that we want to keep the amount of processing required at the relays as small as possible. This is a strong motivation for using the simple FF protocol rather than more complex protocols such as the decode-and-forward protocol described in [22]. In the FF protocol, the relays only need to perform FIR filtering on the received signal which can also be implemented in analogue domain using tunable analogue filters. The advantage

of the decode-and-forward protocol is that no transmitted power at the relays is wasted by forwarding the relay noise to the destinations. However, in the interference limited MUP2P and MGM scenarios with frequency selective channels, the decode-and-forward protocol is not applicable for the following reason: In the considered distributed FF beamforming scenario, the relays do not exchange data among themselves while filtering and forwarding the signals from the sources to the destinations. Hence, a reliable signal detection is only possible at the destination nodes, not at the relays.

We remark that, like in the previous chapters and in [28, 52–56], we assume centralized processing, i.e., one node in the network acts as a processing node which collects all CSI of the network, solves the optimization problem and distributes the resulting FIR filter coefficients to the relays. The resulting decoding delays, however, do not need to be distributed to the destinations for the following reason. Once the decoding delays and $\boldsymbol{w}$ are optimized jointly, the mth destination can estimate the vector $\boldsymbol{w}^H \boldsymbol{H}_{d,m}$ using standard channel estimation where $\boldsymbol{w}^H \boldsymbol{H}_{d,m}$ is considered as the vector of filter taps of a frequency selective channel of an equivalent point-to-point link between the dth source and the mth destination. Then, the decoding delay can be determined at the mth destination based on the strongest element in vector $\boldsymbol{w}^H \boldsymbol{H}_{d,m}$. Hence, the destination nodes do not need to be informed about the decoding delays to use and no additional signaling overhead compared to the scheme in [54] is required.

Note that in the literature, mainly two different but closely related optimization problems are considered as design criteria for the relay filter coefficients: a max-min fair beamforming problem, where the minimum SINR of all destinations is maximized subject to a total or individual relay power constraint, and the QoS constrained power minimization problem considered in this dissertation. In [28] and [52], both problems have been considered, while in [54], [55], and [56], only the former has been studied. In the MUP2P scenario, the max-min fair beamforming problem is usually more difficult to solve and our investigations have revealed that it is easier to handle the power minimization problem with our proposed method. Although it might also be applicable to the max-min fair problem, we have decided to focus on the power minimization problem.

9.7 Simulation Results

Throughout our simulations, unless noted otherwise, we consider a MUP2P relay network, i.e., $K = M > 1$, with $N = 10$ relay nodes, choose $L_f = L_w = L_g = 5$, assume that the relay and destination noise powers are equal to each other and 10 dB below

the power transmitted by the source nodes, set $\tilde{L} = 3$ for the deflation method (see Section 9.5), and average the results over 300 Monte Carlo runs. For simplicity, we only demonstrate the performance of the proposed schemes using the example of the MUP2P relay network. However, note that, as shown above, the proposed methods are not restricted to MUP2P relay networks but also work in MGM relay network scenarios. For the deflation method, we have set $\tilde{L} = 3$ (see Section 9.5). We investigate three different scenarios: An asynchronous MUP2P network is investigated using a simple channel model and a beyond-3G channel model in Sections 9.7.1 and 9.7.2, respectively. A synchronized SU network is considered in 9.7.3.

9.7.1 Simple Channel Model

In this first scenario, we extend the channel model considered in Section 5.8.2 and [52–56] such that it can be used to model an asynchronous network where the different links have different link delays: Like in the latter references, the FIR filter coefficients of the CIRs are modeled as independent quasi-static Rayleigh fading following the exponential power delay profile $p[n] = \frac{1}{\sigma_t} \sum_{l=0}^{L_x-1} e^{-n/\sigma_t} \delta[n-l]$ where σ_t characterizes the delay spread and $L_x \in \{L_f, L_g\}$. The extension consists in using zero padding at the beginning and the end of the CIR vectors to model the different link delays. I.e., we first randomly generate an $L_x \times 1$ vector of independent Rayleigh coefficients and then multiply this vector element-wise with the modified exponential power delay profile vector

$$[\mathbf{0}_{1\times L_\mathrm{o}}, \frac{1}{\sigma_t}, \frac{1}{\sigma_t} e^{-1/\sigma_t}, \ldots, \frac{1}{\sigma_t} e^{-(L_y-1)/\sigma_t}, \mathbf{0}_{1\times L_x - L_y - L_\mathrm{o}}]^T \tag{9.16}$$

to form the CIR vector $[f_{k,i}[0], \ldots, f_{k,i}[L_f - 1]]^T$ or $[g_{m,i}[0], \ldots, g_{m,i}[L_g - 1]]^T$, respectively. L_o and L_y are supposed to randomly model the different link delays and CIR lengths of the different links, respectively. Therefore, L_o and L_y are uniformly distributed integer random variables drawn independently for each channel from the intervals $[0, L_x - 1]$ and $[1, L_x - L_\mathrm{o}]$, respectively. Note that the fully synchronized network of [52–56] and Section 5.8.2 can be modeled using $L_\mathrm{o} = 0$ and $L_y = L_x$ rather than random L_o and L_y.

Recall that we solve the QoS-constrained power minimization problem rather than the max-min fair beamforming problem considered in [54]. When we refer to the approach of [54], we mean that the center symbols are selected as the desired symbols like in [54] and as described in Section 3.3. Then, the QoS-constrained power minimization problem for this choice of fixed decoding delays is solved approximately as described

in Chapter 5. The performance of the approach of [52], i.e., selecting the first symbol as the desired symbol, is worse than that of the approach of [54] in most cases. We therefore omit the approach of [52] when displaying the results. In addition to the lower bound of Section 9.3 and the result of the deflation method of Sections 9.4 and 9.5, we show the result of the initialization of Table 9.1 yielding P_{UB}.

In Fig. 9.2, the total transmitted relay power P_{T} versus the number of source-destination pairs K is shown for an SINR threshold $\gamma_m = -2$ dB $\forall m \in \mathcal{M}$. The computation of the lower bound using the proposed BnC procedure requires a long simulation time. Therefore, K is only increased up to four and the results are averaged over 200 Monte Carlo runs. We show both, the results of the two-time-scale deflation scheme of Section 9.4 and those of the more efficient one-time-scale version of Section 9.5. The result clearly demonstrates that, compared to the state-of-the-art methods which do not make use of individual adaptive decoding delays, the required total transmitted relay power can be significantly reduced using the proposed initialization scheme and can be substantially further reduced using the proposed deflation method. The results also show that the proposed deflation method is very close to the lower bound und hence, close to optimal. Surprisingly, the one-time-scale deflation scheme outperforms the two-time-scale version in terms of total transmitted relay power even though the one-time-scale version is also computationally more efficient. The results of the two-time-scale deflation scheme are no longer shown for the remaining simulation results since it is anyway outperformed by the one-time-scale version.

Next, we consider the same scenario for up to $K = 6$ source-destination pairs where the lower bound can no longer be computed in affordable simulation time and is not shown. The results are averaged over 300 Monte Carlo runs, we consider $N = 20$ relays and the QoS threshold is increased to $\gamma_m = 0$ dB $\forall m \in \mathcal{M}$. Note that higher SINR thresholds are possible for a smaller K. However, we keep the threshold at 0 dB in order to show results for a wide range of K. The results are shown in Fig. 9.3. We observe that the trend commenced for up to $K = 4$ source-destination pairs continues when K is increased beyond four. Surprisingly, the one-time-scale deflation scheme outperforms the two-time-scale version in terms of total transmitted relay power even though the one-time-scale version is also computationally more efficient.

For the same scenario, Fig. 9.4 displays the percentage of feasible Monte Carlo runs versus the number of source-destination pairs K. Note that in this case, a distinction between the one- and the two-time-scale deflation scheme is not required since they are equivalent in terms of feasibility. It shows that significantly more feasible solutions than with the approach of [54] are obtained using the proposed method. When a feasible solution cannot be obtained using the initialization procedure of Table 9.1, then the

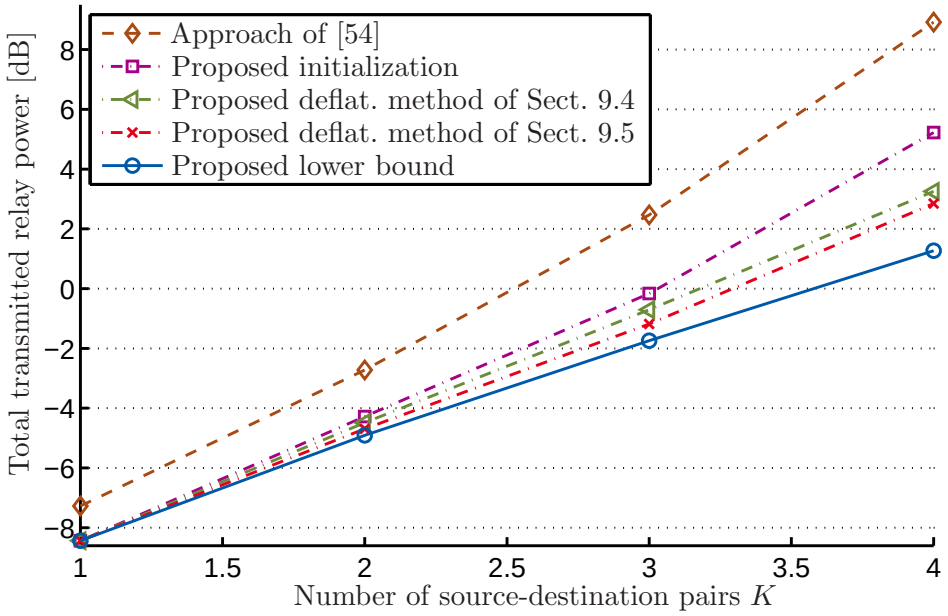

Figure 9.2. Total transmitted relay power vs. K, simple channel model, with lower bound.

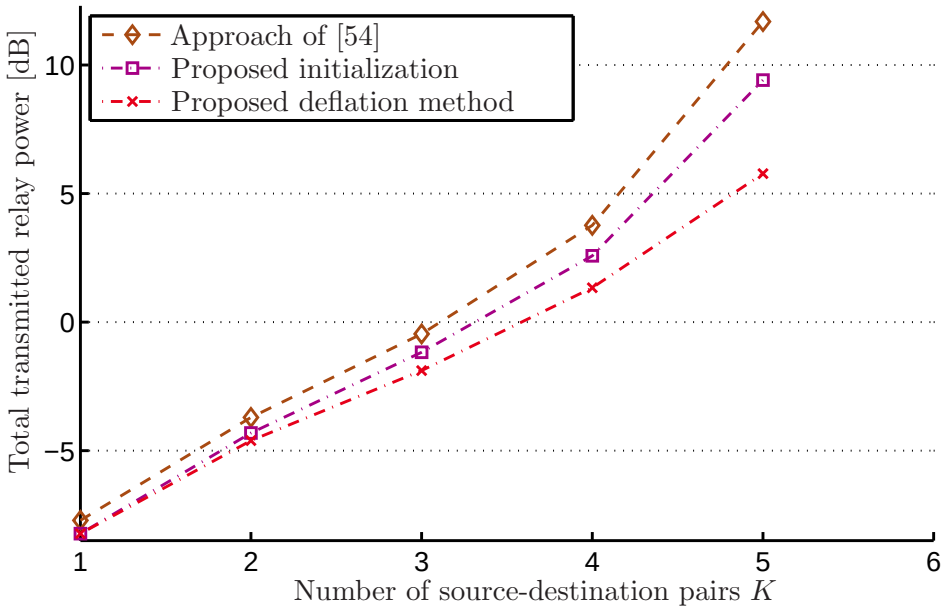

Figure 9.3. Total transmitted relay power vs. K, simple channel model.

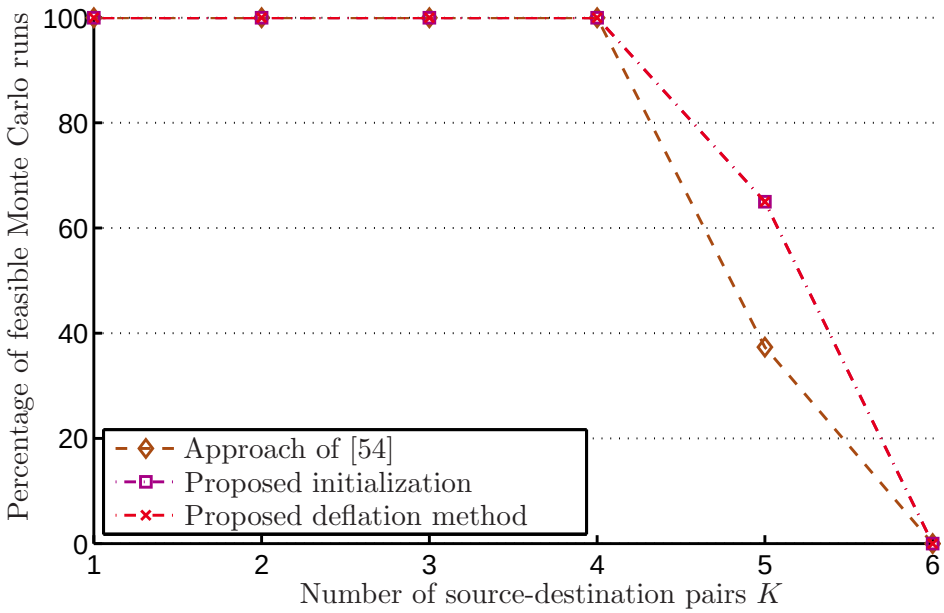

Figure 9.4. Percentage of feasible Monte Carlo runs vs. K, simple channel model.

deflation method cannot be carried out either. On the other hand, when the solution obtained with the initialization scheme is feasible but the deflation method becomes infeasible, we resort to the result of the initialization scheme. This is why the curves of the two proposed methods coincide in terms of feasibility in Fig. 9.4.

We observe from the above figures that the gap between the schemes without and the ones with adaptive decoding delays is relatively small for a single source-destination pair but increases with the number of source-destination pairs K. This can be explained as follows. The more source-destination pairs are comprised in the network, the more likely it is that they have different link delays and, as a consequence, the less likely it is that a common decoding delay for all source-destination pairs is optimal.

In Fig. 9.5, the histogram of the distribution of decoding delays selected by the proposed deflation method for 300 Monte Carlo runs is displayed for the case of $K = 2$ source-destination pairs. On the x- and y-axis, the decoding delays selected at the first and at the second destination are plotted, respectively, while the z-axis shows the number of Monte Carlo runs in which a combination of selected decoding delays occurred. We can observe from this histogram that a wide range of combinations of decoding delays is selected by the proposed method depending on the channel realization. This range is apparently wider than that demonstrated for the SU scenario in [56]. This illustrates that it is suboptimal to select pre-fixed decoding delays for all channel realizations.

To demonstrate the effectiveness of the BnC method, in Table 9.6, the number of

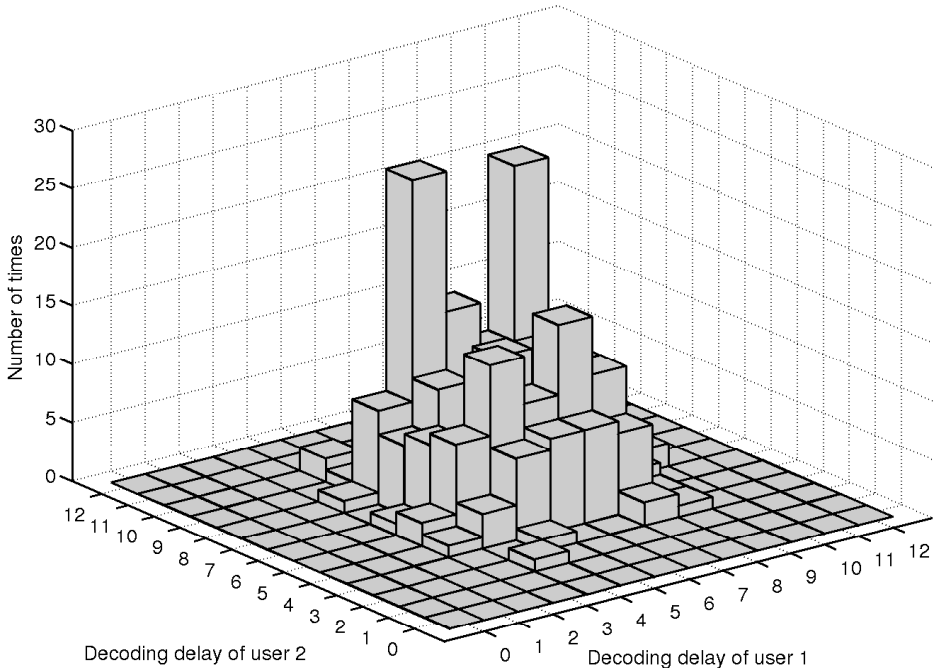

Figure 9.5. Histogram of the distribution of selected decoding delays for $L = 13$ and $K = 2$.

combinations that need to be considered in an exhaustive search are compared to the number of instances of problem (9.8) that were solved in the proposed BnC scheme (averaged over the 200 Monte Carlo runs). Obviously, only a fraction of the computational effort of an exhaustive search is required using the proposed BnC method. To get an impression of the computational complexity of the deflation method, the number of instances of problem (9.14) that were solved in the deflation method is also displayed. We remark that two instances of problem (9.2) have to be solved in addition, one during the initialization and one to obtain the final solution. The number of instances of problem (9.14) that need to be solved in the deflation method grows only linearly with K rather than exponentially as in the BnC scheme and the exhaustive search.

9.7.2 Beyond-3G Channel Model

The state-of-the-art channel model for simulation-based evaluation of Beyond-3G systems is the SCME [59], [60] which is widely accepted to be realistic. The SCME has been developed by the Wireless World Initiative New Radio (WINNER) project of the European Union's 6th Framework Program and has been adopted by the Third Generation Partnership Project (3GPP) standardization for LTE and LTE-A. To prove the

No. of source-destination pairs K	1	2	3	4
No. of possible combinations	13	$13^2 = 169$	$13^3 = 2197$	$13^4 = 28561$
Average no. of solved instances of problem (9.8) in BnC method	0	43	358	2436
Percentage	0 %	25 %	16 %	9 %
No. of solved instances of problem (9.14) in deflation method	0	4	6	8

Table 9.6. Comparison of complexity.

applicability of the proposed scheme in practice, we also test our method in a scenario where the SCME is used to model the CIRs between the nodes. The SCME yields a CIR in analogue baseband consisting of six dirac impulses each of which corresponds to one multipath via a scatterer. Each impulse has a delay τ_i, that is equal to the physical time it takes the signal to travel from the source to the destination via the scattered path, and a complex coefficient b_i that models the attenuation and phase shift of this multipath. According to [18], the relation between a CIR in analogue baseband and its counterpart in complex digital baseband is given by

$$c[l] \triangleq \sum_{i=1}^{J} b_i \mathrm{sinc}[l - \tau_i \frac{1}{T_s}]. \tag{9.17}$$

The SCME yields the coefficients b_i and delays τ_i in (9.17) where $J = 6$. The required FIR filter coefficients of the causal channel are obtained by truncating and shifting $c[l]$ such that the FIR filter coefficients are zero for $l < 0$ and $l > L_x - 1$.

We simulate the asynchronicity in the network as follows. We randomly generate the locations of the nodes and calculate the distances between them. Based on these distances, we calculate the time it takes the signal to travel from one node to the next via the direct, non-scattered path and use it as τ_1 in (9.17). The SCME is then used to compute the delays $\tau_2, \ldots, \tau_6$ corresponding to the scattered paths. To make the SCME applicable in the considered relaying scenario, based on the COST 231 pathloss model [68], we have adapted the way the path loss induced by the scattered paths is modeled in the SCME.

We have generated random locations of all nodes in the network as follows. Three areas of size 30 meters by 30 meters, 30 meters by 30 meters, and 30 meters by 45 meters, respectively, have been generated which we have placed next to each other with a

separation of 20 meters in which no nodes are placed. Then, all source nodes are distributed randomly across the area on the left with a uniform distribution. Similarly, all relay nodes and all destination nodes are uniformly distributed across the areas in the center and on the right, respectively. The area on the right is the largest area.

Recall that we consider SC transmission which is also used in the uplink of LTE. To obtain realistic values, we therefore set the transmitted power at the source nodes and the relay and destination noise powers equal to the maximum transmitted power at the user terminal and the receiver noise power in an LTE uplink, respectively. That is, we set the transmitted powers at the source nodes to 24 dBm and the relay and destination noise powers to -116.4 dBm, see [69]. The SINR threshold is set to $\gamma_m = -7$ dB $\forall m \in \mathcal{M}$ which is a realistic threshold for LTE, see, e.g., [61] and references therein. The lengths of the FIR filters of the channels are determined by the SCME. In most of the cases, $L_f = L_g = 28$. Due to these long CIRs, we have set the number of FIR filter coefficients at the relays to $L_w = 20$ and use $\tilde{L} = 6$ candidate decoding delays per destination in the deflation method. Since the resulting number of possible decoding delays is very large ($L = L_f + L_w + L_g - 2 = 76$), computing the lower bound is not affordable in our simulations. Further, we have limited the maximum number of source-destination pairs K to four. Figures 9.6 and 9.7 display the total transmitted relay power P_{T} and the percentage of feasible Monte Carlo runs, respectively, versus the number of source-destination pairs K. It can be observe that the performance improvements of the proposed method over the state-of-the-art method are even more significant than in Section 9.7.1. Thus, the proposed methods show good performance even in this very realistic scenario and again outperform the existing methods. Hence, under the assumption that perfect CSI is available at the processing node(s), the proposed scheme may well be applicable in practice.

9.7.3 Synchronized SU Network

In this section, we investigate a scenario with only one source-destination pair and a perfectly synchronized network. Note that, unlike in the MUP2P or the MGM scenario, perfect synchronization can be achieved in this SU network, as mentioned earlier. Recall that the equalization scheme of [55] is applicable in this SU network which is not the case in the MUP2P network. We investigate this scenario to compare the adaptive decoding delay scheme with the equalization scheme of [55] which has not yet been done in [56]. The authors in [55] propose to additionally employ a linear or decision feedback equalizer at the destination node. For our simulations, we choose a decision feedback equalizer optimized based on a minimum mean square error (MMSE)

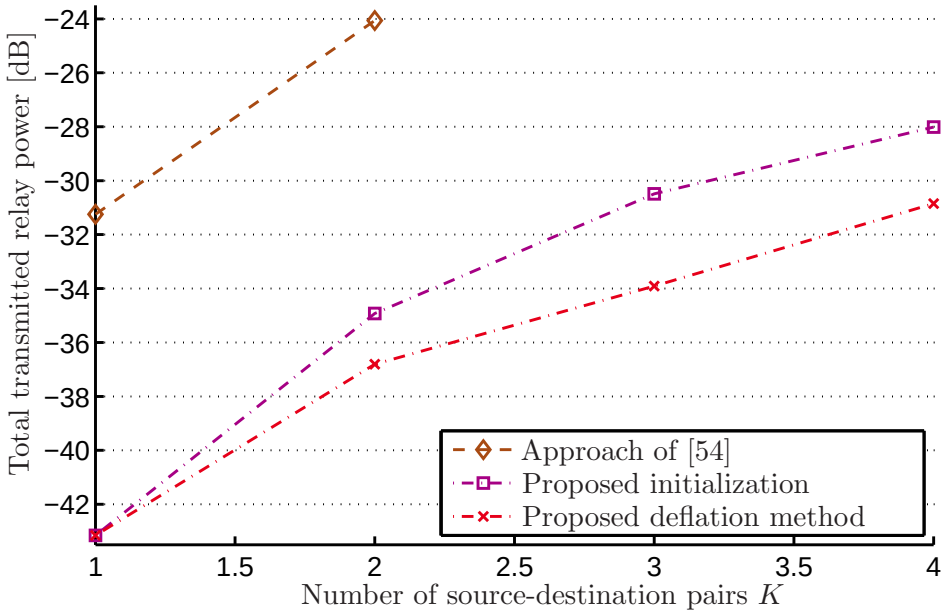

Figure 9.6. Total transmitted relay power vs. K, SCME.

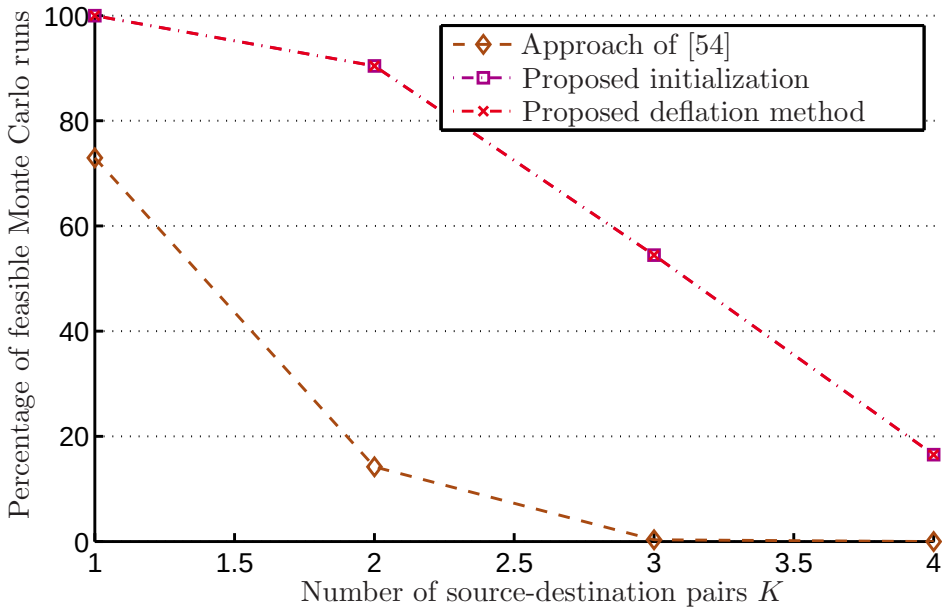

Figure 9.7. Percentage of feasible Monte Carlo runs vs. K, SCME.

criterion which usually achieves the best performance among the available equalization schemes according to [55]. The equalizer is only used for the scheme of [55] and not for the other methods considered in the simulations. In [55], the SINR is maximized subject to a constraint on the total transmitted relay power rather than minimizing this power subject to an SINR constraint as in problem (9.1). To incorporate the method of [55] into the comparison, we solve the SINR maximization problem as proposed in [55]. Then, we scale the power of the obtained beamforming weight vector such that the SINR constraint is satisfied with equality. The scaled power can then be compared to the power obtained by the other methods. This is possible since in the SU scenario, optimizing the beamforming weight vector $\boldsymbol{w}$ can be separated into optimizing its direction and optimizing its norm. The latter optimization can simply be achieved via scaling.

We use the simple channel model of Section 9.7.1 but this time its synchronous version like in Section 5.8.2 and [52–56], i.e., $L_{\mathrm{o}} = 0$ and $L_y = L_x$ in (9.16). The SINR threshold is set to $\gamma = 3$ dB and the number of relays is varied from $N = 1$ to $N = 10$. The results are averaged over 50 Monte Carlo runs. Figs. 9.8 and 9.9 show the total transmitted relay power and the percentage of feasible Monte Carlo runs versus the number of relays N, respectively. It can be concluded that both the equalization scheme of [55] and the adaptive decoding delay scheme substantially outperform the method of [52]. Note that, rather than selecting the first symbol as the desired symbol, like in [52], we select the center symbol as the desired symbol for the method of [52], like in Section 3.3 and [54], because the results for selecting the first symbol are even worse. Since the performance in terms of both total transmitted relay power and feasibility is very similar for the equalization scheme of [55] and for the adaptive decoding delay scheme, the latter scheme, which neither requires a gradient algorithm nor a complex equalizer at the destination node, is to be preferred to the equalization scheme in this scenario.

9.8 Summary

In this chapter, we have considered asynchronous MUP2P and MGM relay networks with FF relays and frequency selective channels. We have proposed to use individual adaptive decoding delays at the destinations which allow to adapt to different link delays in the asynchronous network and thereby to effectively mitigate ISI and MUI. The joint optimization of the FIR filter coefficients at the relays and the decoding delays at the destinations has been considered. This joint optimization problem is a nonconvex MIP problem which cannot be solved optimally in affordable time. Therefore, we have proposed a customized BnC method offering a lower bound as a benchmark and a

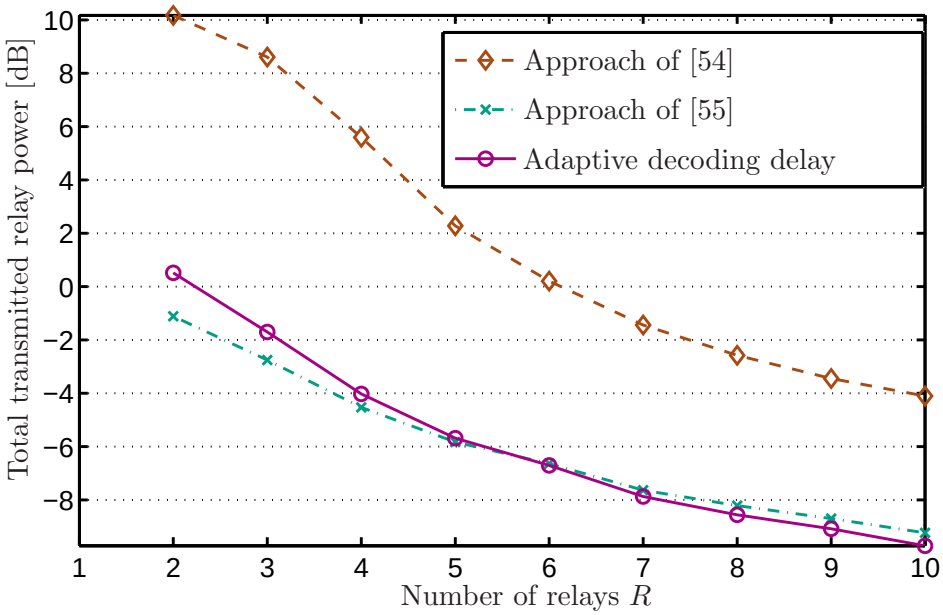

Figure 9.8. Total transmitted relay power vs. N, SU scenario.

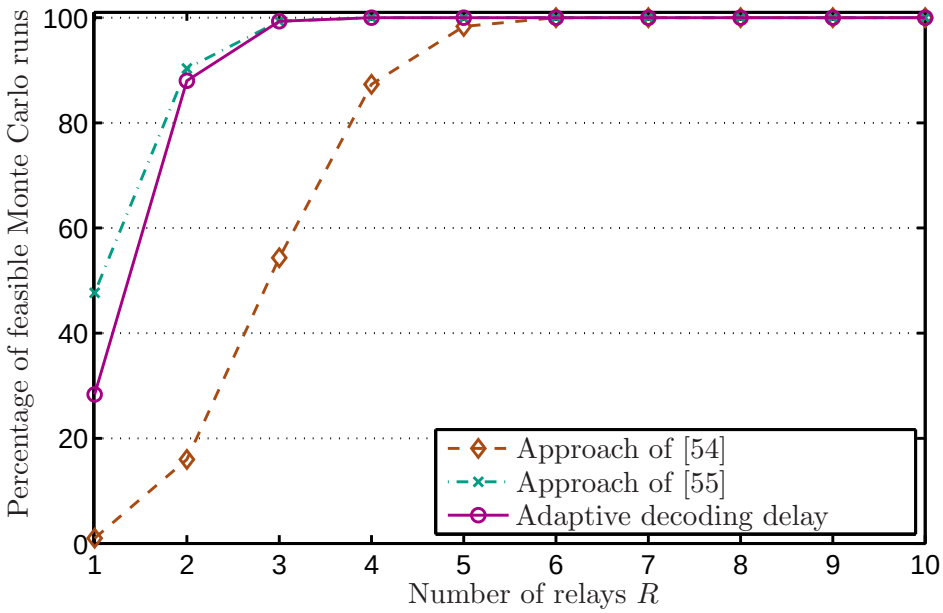

Figure 9.9. Percentage of feasible Monte Carlo runs vs. N, SU scenario.

deflation method yielding an approximate solution at a low computational complexity. For the BnC method, an efficient preprocessing stage has been proposed which uses an alternative relaxation of the original problem to obtain lower bounds on the optimal value of the original problem. With this preprocessing stage, the number of candidate combinations of decoding delays, which need to be considered in the BnC method, can be effectively reduced. Our simulation results have demonstrated that the proposed method performs close to optimal and outperforms state-of-the-art approaches which do not make use of adaptive decoding delays.

Chapter 10

Conclusions and Outlook

In this dissertation, we have considered the problem of minimizing the total transmitted power subject to QoS constraints at the receivers for various beamforming scenarios in which this problem is nonconvex and NP-hard: We have studied the MGM downlink beamforming scenario and its special case, the broadcast beamforming scenario. Furthermore, we have investigated the MUP2P AF relay network scenario which is then generalized to the MGM AF relay network scenario. In addition to the MUP2P AF relay network, the MGM AF relay network also contains the broadcasting AF relay network as a special case. The latter network topologies have also been studied for the case that the FF protocol rather than the AF protocol is implemented at the relays.

The QoS-constrained power minimization problem is nonconvex and NP-hard in all of the beamforming scenarios considered in this dissertation. This problem is therefore approximated either by a convex SDP problem or a convex SOCP problem in state-of-the-art methods to obtain a suboptimal solution. Both, the SDP and the SOCP problem, are efficiently solvable by interior-point methods. However, the approximations may become inaccurate, especially when the number of QoS constraints is large. In Chapters 5 and 6, we have therefore proposed a novel iterative convex approximation framework within which the above problems are collectively addressed. In each iteration of our iterative approach, the original nonconvex problem is approximated by a convex SOCP problem. Then, the SOCP problem is efficiently solved using interior-point methods and the SOCP approximation of the next iteration is adapted to the solution of the SOCP approximation of the current iteration. We have modified the iterative procedure such that instead of minimizing the total transmitted power, an infeasibility indicator is minimized. The modified iterative procedure has been used as a feasibility search method to find a feasible initial SOCP approximation with which the iterative power minimization procedure is initialized. We have shown analytically that the approximate solution is improved in each iteration of our iterative method which proves that the proposed method converges locally. Furthermore, we have extended the iterative feasibility search to an admission control scheme where the goal is to serve the maximum amount of users with the minimum amount of transmitted power. A detailed analytic complexity analysis of the proposed and the state-of-the-art methods has also been carried out. This complexity analysis has revealed that, as the number of users increases, the complexity of the proposed method decreases relative to that of the SDP approach. Our simulations have demonstrated that the proposed scheme

substantially outperforms state-of-the-art methods in terms of total transmitted relay power and percentage of feasible Monte Carlo runs in relay beamforming scenarios with a large number of destination users. The proposed combination of the SDP approach and the SOCP approach achieves the best results which are near-optimal. The simulations have revealed that in MGM downlink scenarios, the proposed scheme performs similar to existing schemes. However, as it has been shown in the complexity analysis, the proposed method achieves a similar performance at a significantly reduced computational complexity when the number of users in the MGM downlink beamforming scenario is large.

In Chapter 7, a non-trivial extension of the proposed iterative SOCP method has been proposed to make it applicable even when only statistical CSI in terms of the channel covariance matrices is available. Our simulation results have shown that the proposed extended iterative SOCP scheme outperforms the existing SDP-based approaches for downlink beamforming and relay beamforming scenarios with a realistic amount of scattering.

We have also proposed a complexity reduction based on incorporating the updates of the SOCP approximation into the iterations of an interior-point method in Chapter 8. Our simulation results have demonstrated that the algorithm with the reduced complexity achieves roughly the same performance in terms of total transmitted power and feasibility as the original algorithm of Chapters 5 and 6 at a substantially reduced computational complexity.

In Chapter 9, we have extended the FF relaying scheme by employing individual adaptive decoding delays at the destination nodes in relay networks with multiple destination nodes. We have again considered the QoS-constrained power minimization problem. Our goal has been to optimize the filter coefficients at the relays, which are continuous optimization variables, jointly with the decoding delays at the destinations, which are discrete (binary) decision variables. The QoS-constrained power minimization problem is thus a MIP problem in this case. Furthermore, it is a nonconvex MIP problem which is generally hard to solve optimally. For implementation in practice, we have proposed a low-complexity deflation algorithm providing an approximate solution for the latter problem. To evaluate the performance of the deflation method, we have also proposed a customized BnC method yielding a lower bound on the total transmitted relay power as a benchmark. Note that the deflation method is based on the proposed iterative SOCP approach of Chapter 5. Our simulation results have demonstrated that the approximate solution obtained by the proposed deflation scheme is close to the lower bound obtained by the proposed BnC procedure. We are thus able to conclude that it is close to optimal. Furthermore, the simulation results

have shown that the proposed deflation scheme outperforms the solutions obtained by state-of-the-art schemes which do not make use of adaptive decoding delays.

The variety of different problems to which the proposed iterative methods have been applied demonstrates that the proposed iterative convex inner approximation framework is a powerful tool which is potentially applicable for a number of other problems.

The main impediment for implementing the proposed schemes in practice, especially those proposed for relay networks, is the signaling overhead associated with the proposed schemes. It might still not be low enough for practical implementation: Once the beamforming weights are computed, the beamforming itself is performed in a distributed fashion, i.e., without any exchange of information between the relays. However, the computation of the beamforming weights is still performed in a centralized way with a central processing node. This node has to collect the CSI of the whole network, solve the optimization problem, and inform the relays about the weighting coefficients to apply. The resulting signaling overhead might not be low enough for a practical scenario. Therefore, follow-up research should be carried out aiming at a reduction of the required signaling overhead. This goal can be tackled from different angles. The proposed algorithms should be transformed into distributed and decentralized algorithms where, e.g., each relay is able to compute its own weighting coefficient(s) based on only local CSI as in, e.g., [25, 70, 71]. In Chapter 7, we have addressed a different way to reduce the signaling overhead by using only partial CSI in terms of channel statistics. An alternative partial CSI is quantized instantaneous CSI, also referred to as quantized feedback, see, e.g., [72, 73]. In quantized feedback, only a few bits containing the index of the channel in a discrete codebook of possible quantized channel coefficients are fed back. If quantized feedback is used, the proposed algorithms have to be adapted such that they can cope with channel uncertainties which inherently arise in quantized feedback since the channels are not exactly known. Making the proposed algorithms robust against deviations of the true channels from the assumed channels is a good idea in general. The research on robust beamforming schemes is already very mature (see, e.g., [74]) and the proposed schemes could be extended by incorporating the existing concepts for robust beamforming.

List of Acronyms

3G	Third generation
3GPP	Third Generation Partnership Project
AC	Admission control
AF	Amplify-and-forward
BC	Broadcast/broadcasting
BnC	Branch-and-cut
BS	Base station
CIR	Channel impulse response
CSI	Channel state information
FF	Filter-and-forward
FIR	Finite impulse response
FLOP	Floating-point operation
ISI	Inter-symbol interference
LTE	Long-Term Evolution
LTE-A	Long-Term Evolution Advanced
MBMS	Multimedia Broadcast Multicast Service
MGM	Multi-group multicast/multicasting
MIMO	Multiple-input-multiple-output
MIP	Mixed-integer programming
MISOCP	Mixed-integer second-order cone programming
MU	Multi-user
MUI	Multi-user interference
MUP2P	Multiuser peer-to-peer
NP-hard	Non-deterministic polynomial time hard

OFDM	Orthogonal frequency division multiplexing
QoS	Quality-of-service
QCQP	Quadratically constrained quadratic programming
QP	Quadratic programming
RF	Radio frequency
SC	Single-carrier
SCME	Spatial channel model extended
SDP	Semi-definite programming
SDR	Semi-definite relaxation
SINR	Signal-to-interference-plus-noise ratio
SNR	Signal-to-noise ratio
SOCP	Second-order cone programming
SU	Single-user
WINNER	Wireless World Initiative New Radio

Frequently Used Symbols

a_{m,l_m}	Binary variable modeling the selection of decoding delay l_m at the mth destination node
B_{m,l_m}	Upper bound on the right-hand side of the quality-of-service constraint
$\boldsymbol{c}_m$	Vector of complex channel coefficients between the antenna array and the mth user
$\boldsymbol{C}_m$	Channel (covariance) matrix of the mth user
$\boldsymbol{D}$	Matrix for computing the total transmitted relay power
$\boldsymbol{f}_k$	Vector of complex channel coefficients between the kth source node and the relays
$\boldsymbol{g}_m$	Vector of complex channel coefficients between the relays and mth destination node
$\mathcal{G}_k$	Index set of the kth multicasting group
$\boldsymbol{h}_{d,m}$	Channel vector of the overall channel bewteen the dth source node and the mth destination node
$\tilde{\boldsymbol{h}}_{d,m}$	Extended channel vector for the second-order cone programming formulation
$\tilde{\boldsymbol{h}}_{d,m}^{(i)}$	Rotated extended channel vector in the ith iteration
$\boldsymbol{H}_{d,m}$	Convolution matrix of the overall channel between the dth source node and the mth destination node
$\boldsymbol{\mathcal{H}}_{d,m}$	Auxiliary matrix for the second-order cone programming formulation
I	Maximum number of iterations
K	Number of multicasting groups
$\mathcal{K}$	Index set of all multicasting groups
l_m	Decoding delay at the mth destination node
L_f	Length of the source-to-relay channel impulse response
L_g	Length of the relay-to-destination channel impulse response
L_w	Relay filter length
$\mathcal{L}_m$	Index set of all possible decoding delays at the mth destination node
M	Number of destination users
$\mathcal{M}$	Index set of all destination users
n	Sampling time index
N	Number of antenna elements in the antenna array or number of relays
$\bar{\mathcal{N}}_{d,m}^{(i)}$	Set of eigenvectors of $\boldsymbol{R}_{d,m}$ selected in the ith iteration
$\bar{N}_{d,m}^{(i)}$	Cardinality of $\bar{\mathcal{N}}_{d,m}^{(i)}$
P_k	Transmit power of the kth source node

P_{T}	Total power transmitted by the BS/the relays
P_{UB}	Upper bound on the original mixed-integer programming problem
$P_{\min,m,l_m}$	Lower bound on the required total transmitted relay power for decoding delay l_m at the mth destination node
$\boldsymbol{Q}_{\mathrm{I},m}$	Matrix for computing the multi-user interference power at the mth destination node
$\tilde{\boldsymbol{Q}}_{\mathrm{N},m}$	Matrix for computing the total noise power at the mth destination node
$\boldsymbol{Q}_{\mathrm{ISI},d,m}$	Matrix for computing the inter-symbol interference power at the mth destination node
$\boldsymbol{Q}_{\mathrm{MUI},m}$	Matrix for computing the multi-user interference power at the mth destination node (in frequency selective fading)
$\boldsymbol{Q}_{\mathrm{N},m}$	Matrix for computing the total noise power at the mth destination node (in frequency selective fading)
$\boldsymbol{Q}_{\mathrm{ISI},d,m,l_m}$	Matrix for computing the inter-symbol interference power at the mth destination node for decoding delay l_m
$\tilde{\boldsymbol{Q}}_{d,m,l_m}$	Matrix for computing the total interference plus noise power at the mth destination node for decoding delay l_m
$\boldsymbol{Q}_m$	Matrix for computing the total interference plus noise power at the mth destination node (in the generalized problem formulation)
$\boldsymbol{R}_{d,m}$	Matrix for computing the desired/useful signal power at the mth destination node
s_k	Complex information symbol for the kth multicasting group
t	Auxiliary variable for the second-order cone programming formulation
$\boldsymbol{U}_m$	Auxiliary matrix for the second-order cone programming formulation
$\boldsymbol{V}$	Auxiliary matrix for the second-order cone programming formulation
$\bar{\boldsymbol{v}}_{d,m,n}^{(i)}$	Rotated nth eigenvector of $\boldsymbol{R}_{d,m}$ in the ith iteration
$\boldsymbol{w}$	Beamforming vector (in distributed beamforming)
$\boldsymbol{w}_k$	Beamforming vector for the kth multicasting group (in downlink beamforming)
$\tilde{\boldsymbol{w}}$	Extended beamforming vector for the second-order cone programming formulation (in distributed beamforming) or transformed beamforming vector for simplified problem reformulation in Chapter 9
$\boldsymbol{w}_{\mathrm{opt}}$	Optimal beamforming vector
$\tilde{\boldsymbol{w}}_{\mathrm{opt}}^{(i)}$	Solution to the second-order cone programming problem in the ith iteration
$\boldsymbol{w}_{\mathrm{all}}$	Extended beamforming vector for the second-order cone programming formulation (in downlink beamforming)
y_m	Signal received at the mth destination user

$\boldsymbol{X}$	New optimization variable in the semi-definite relaxation approach
$y_{\mathrm{S},m}$	Desired/useful signal component of y_m
$y_{\mathrm{I},m}$	Multi-user interference component of y_m
$y_{\mathrm{N},m}$	Total noise component of y_m
y_{S,m,l_m}	Desired/useful signal component of y_m for decoding delay l_m
y_{ISI,m,l_m}	Inter-symbol interference component of y_m for decoding delay l_m
$y_{\mathrm{ISI},m}$	Inter-symbol interference component of y_m
$y_{\mathrm{MUI},m}$	Multi-user interference component of y_m (in frequency selective fading)
$\boldsymbol{z}$	Auxiliary vector for the iterative feasibility search
$\alpha_{d,m}^{(i)}$	Phase rotation factor in the ith iteration
γ_m	QoS threshold at the mth receiver
$\boldsymbol{\vartheta}_{d,m,l_m}$	(l_m+1)th column of $\boldsymbol{H}_{d,m}$
$\tilde{\boldsymbol{\vartheta}}_{d,m,l_m}$	Transformed $\boldsymbol{\vartheta}_{d,m,l_m}$ for the simplified problem reformulation in Chapter 9
κ	Accuracy parameter in the barrier method
$\lambda_{d,m,n}$	nth eigenvalue of $\boldsymbol{R}_{d,m}$
σ_m^2	Noise power at the mth receiver (in downlink beamforming)
σ_ν^2	Noise power at the destination nodes (in distributed beamforming)

Bibliography

[1] N. Bornhorst, M. Pesavento, and A. B. Gershman, "Distributed beamforming for multiuser peer-to-peer and multi-group multicasting relay networks," in *Proc. IEEE Int. Conf. on Acoustics, Speech and Signal Process. (ICASSP)*, Prague, Czech Republic, pp. 2800-2803, May 2011.

[2] N. Bornhorst and M. Pesavento, "An iterative convex approximation approach for transmit beamforming in multi-group multicasting," in *Proc. IEEE Int. Workshop on Signal Process. Advances in Wirel. Commun. (SPAWC)*, San Francisco, CA, USA, pp. 411-415, June 2011.

[3] N. Bornhorst, M. Pesavento, and A. B. Gershman, "Distributed beamforming for multi-group multicasting relay networks," *IEEE Trans. Signal Process.*, vol. 60, no. 1, pp. 221-232, Jan. 2012.

[4] J. Zhang, N. Bornhorst, F. Römer, M. Haardt, and M. Pesavento, "Optimal and suboptimal beamforming for multi-operator two-way relaying with a MIMO amplify-and-forward relay," in *Proc. IEEE/ITG Int. Workshop on Smart Antennas (WSA)*, pp. 307-311, Dresden, Germany, March 2012.

[5] N. Bornhorst and M. Pesavento, "Beamforming for multi-group multicasting with statistical channel state information using second-order cone programming," in *Proc. IEEE Int. Conf. on Acoustics, Speech and Signal Process. (ICASSP)*, pp. 3237-3240, Kyoto, Japan, March 2012.

[6] N. Bornhorst, P. Davarmanesh, M. Pesavento, "An extended interior-point method for transmit beamforming in multi-group multicasting," in *Proc. European Signal Process. Conf. (EUSIPCO)*, Bucharest, Romania, pp. 6-10, Aug. 2012.

[7] N. Bornhorst and M. Pesavento, "Filter-and-forward beamforming in asynchronous relay networks," in *Proc. IEEE Int. Workshop on Signal Process. Advances in Wirel. Commun. (SPAWC)*, Darmstadt, Germany, pp. 375-379, June 2013.

[8] N. Bornhorst and M. Pesavento, "Filter-and-forward beamforming with adaptive decoding delays in asynchronous multi-user relay networks," accepted for publication in *Signal Process.*, Sept. 2014.

[9] E. Hossain, V.K. Bargava, and G.P. Fettweis, *Green Radio Communication Networks*. Cambridge, U.K.: Cambridge Univ. Press, Aug. 2012.

[10] J.-S. Wu, S. Rangan, and H.-G. Zhang, *Green Communications: Theoretical Fundamentals, Algorithms and Applications*. Boca Raton, FL, USA: CRC Press, Sept. 2012

[11] N.A. Ali, A.M. Taha, and H.S. Hassanein, "Quality of service in 3GPP R12 LTE-advanced," *IEEE Signal Process. Magazine*, vol. 51, no. 8, pp. 103-109, Aug. 2013.

[12] Cisco, "Cisco visual networking index: Global mobile data traffic forecast," Feb. 2014. [Online]. Available: http://www.cisco.com/c/en/us/solutions/collateral/service-provider/visual-networking-index-vni/white_paper_c11-520862.html

[13] M. Bengtsson and B. Ottersten, "Optimal downlink beamforming using semidefinite optimization," *Proc. 37th Annu. Allerton Conf. Commun., Contr., Comput.*, pp. 987-996, Sept. 1999.

[14] M. Bengtsson and B. Ottersten, "Optimal and suboptimal transmit beamforming," in *Handbook of Antennas in Wireless Communications*, Ed. L.C. Godara. Boca Raton, FL, USA: CRC Press, Aug. 2001, ch. 18.

[15] A.B. Gershman, N.D. Sidiropoulos, S. Shahbazpanahi, M. Bengtsson, and B. Ottersten, "Convex optimization-based beamforming: From receive to transmit and network designs", *IEEE Signal Process. Magazine*, vol. 27, no. 3, pp. 62-75, May 2010.

[16] N.D. Sidiropoulos, T.N. Davidson, and Z.-Q. Luo, "Transmit beamforming for physical-layer multicasting," *IEEE Trans. Signal Process.*, vol. 54, no. 6, pp. 2239-2251, June 2006.

[17] E. Karipidis, N.D. Sidiropoulos, and Z.-Q. Luo, "Quality of service and max-min fair transmit beamforming to multiple cochannel multicast groups," *IEEE Trans. Signal Process.*, vol. 56, no. 3, pp. 1268-1279, Mar. 2008.

[18] D. Tse and P. Viswanath, *Fundamentals of Wireless Communications*. Cambridge, U.K.: Cambridge Univ. Press, 2005.

[19] S. Sesia, I. Toufik, and M. Baker, *LTE - The UMTS Long Term Evolution: From Theory to Practice*, 2nd ed., Wiley-Interscience, John Wiley & Sons, New York, Aug. 2011.

[20] V. Tarokh, N. Seshadri, and A.R. Calderbank, "Space-time codes for high data rate wireless communication: Performance criterion and code construction," *IEEE Trans. Inf. Theory*, vol. 44, no. 2, pp. 744-765, Mar. 1998.

[21] Y.W. Hong, W.-J. Huang, F.-H. Chiu, and C.C.J. Kuo, "Cooperative communications in resource-constrained wireless networks," *IEEE Signal Processing Mag.*, vol. 24, pp. 47-57, 2007.

[22] J.N. Laneman, D.N.C. Tse, and G.W. Wornell, "Cooperative diversity in wireless networks: Efficient protocols and outage behavior," *IEEE Trans. Inf. Theory*, vol. 50, no. 12, pp. 3062-3080, Dec. 2004.

[23] G. Kramer, M. Gastpar, and P. Gupta, "Cooperative strategies and capacity theorems for relay networks," *IEEE Trans. Inf. Theory*, vol. 51, no. 9, pp. 3037-3063, Sept. 2005.

[24] M. Janani, A. Hedayat, T.E. Hunter, and A. Nosratinia, "Coded cooperation in wireless communications: Space-time transmission and iterative decoding," *IEEE Trans. Signal Process.*, vol. 52, no. 2, pp. 362-371, Feb. 2004 .

[25] Y. Jing and H. Jafarkhani, "Network beamforming using relays with perfect channel information," *IEEE Trans. Inf. Theory*, vol. 55, no. 6, pp. 2499-2517, June 2009.

[26] V. Havary-Nassab, S. Shahbazpanahi, A. Grami, and Z.-Q. Luo, "Distributed beamforming for relay networks based on second-order statistics of the channel state information," *IEEE Trans. Signal Process.*, vol. 56, no. 9, pp. 4306-4316, Sept. 2008.

[27] V. Havary-Nassab, S. Shahbazpanahi, and A. Grami, "Optimal distributed beamforming for two-way relay networks," *IEEE Trans. Signal Process.*, vol. 58, pp. 1238-1250, March, 2010.

[28] S. Fazeli-Dehkordy, S. Shahbazpanahi, and S. Gazor, "Multiple peer-to-peer communications using a network of relays," *IEEE Trans. Signal Process.*, vol. 57, no. 8, pp. 3053-3062, Aug. 2009.

[29] J. Joung and A. Sayed, "Multiuser two-way amplify-and-forward relay processing and power control methods for beamforming systems," *IEEE Trans. Signal Process.*, vol. 58, pp. 1833-1846, Mar. 2010.

[30] H. Chen, A.B. Gershman, and S. Shahbazpanahi, "Distributed peer-to-peer beamforming for multiuser relay networks," in *Proc. IEEE Int. Conf. on Acoustics, Speech and Signal Process. (ICASSP)*, Taipei, Taiwan, pp. 2265-2268, Apr. 2009.

[31] X. Liu, H. Li, and H. Wang, "Probability constrained robust multicast beamforming in cognitive radio network," in *Proc. ICST Int. Conf. on Commun. and Netw. in China (CHINACOM)*, Guilin, P.R. China, pp. 708-712, Aug. 2013.

[32] A. Schad and M. Pesavento, "Time division multiple access methods in bidirectional cooperative relay networks," in *Proc. IEEE Sensor Array and Multichannel Signal Process. Workshop (SAM)*, Hoboken, USA, pp. 89-92, June 2012.

[33] A.H. Phan, H.D. Tuan, H.H. Kha, "D.C. iterations for SINR maximin multicasting in cognitive radio," in *Proc. Int. Conf. on Signal Process. and Commun. Systems (ICSPCS)*, Gold Coast, Australia, pp. 1-5, Dec. 2012.

[34] X. Liu, F. Gao, G. Wang, X. Wang, "Joint beamforming and user selection in multicast downlink channel under secrecy-outage constraint," *IEEE Commun. Letters*, vol. 18, no. 1, pp. 82-85, Jan. 2014.

[35] A.H. Phan, H.D. Tuan, H.H. Kha, and D.T. Ngo, "Nonsmooth optimization for efficient beamforming in cognitive radio multicast transmission," *IEEE Trans. Signal Process.*, vol. 60, no. 6, pp. 2941-2951, June 2012.

[36] Y. Cheng and M. Pesavento, "Joint optimization of source power allocation and distributed relay beamforming in multiuser peer-to-peer relay networks," *IEEE Trans. Signal Process.*, vol. 60, no. 6, pp. 2962-2973, June 2012.

[37] H. Du and T. Ratnarajah, "Joint admission control and beamforming with adaptive modulation for cognitive radio network," in *Proc. IEEE Int. Conf. on Commun. (ICC)*, Ottowa, Canada, pp. 4648-4652, June 2012.

[38] H. Du and T. Ratnarajah, "Robust utility maximization and admission control for a MIMO cognitive radio network," *IEEE Trans. Veh. Technol.*, vol. 62, no. 4, pp. 1707-1718, May 2013.

[39] A. Abdelkader, M. Pesavento, and A.B. Gershman, "Orthogonalization techniques for single group multicasting in cooperative amplify-and-forward networks," in *Proc. IEEE Int. Workshop on Computational Advances in Multi-Sensor Adaptive Process. (CAMSAP)*, San Juan, Puerto Rico, pp. 225-228, Dec. 2011.

[40] M.R.A. Khandaker, Y. Rong, "Precoding design for MIMO relay multicasting," *IEEE Trans. Wirel. Commun.*, vol. 12, no. 7, pp. 3544-3555, July 2013.

[41] M.R.A. Khandaker, Y. Rong, "Transceiver optimization for multi-hop MIMO relay multicasting from multiple sources," accepted for publications in *IEEE Trans. Wirel. Commun.*, May 2014.

[42] Q. Li, Q. Zhang, and J. Qin, "A special class of fractional QCQP and its applications on cognitive collaborative beamforming," *IEEE Trans. Signal Process.*, vol. 62, no. 8, pp. 2151-2164, April 2014.

[43] B.K. Chalise and L. Vandendorpe, "Optimization of MIMO relays for multipoint-to-multipoint communications: nonrobust and robust designs," *IEEE Trans. Signal Process.*, vol. 58, no. 12, pp. 6355-6368, Dec. 2010.

[44] M. Fadel, A. El-Keyi, and A. Sultan, "QoS-constrained multiuser peer-to-peer amplify-and-forward relay beamforming," *IEEE Trans. Signal Process.*, vol. 60, no. 3, pp. 1397-1408, Mar. 2012.

[45] A. Schad and M. Pesavento, "Multiuser bi-directional communications in cooperative relay networks," in *Proc. IEEE Int. Workshop on Computational Advances in Multi-Sensor Adaptive Process. (CAMSAP)*, San Juan, Puerto Rico, pp. 217-220, Dec. 2011.

[46] R. Zhang, Y.-C. Liang, C.C. Chai, and S. Cui, "Optimal beamforming for two-way multi-antenna relay channel with analogue network coding," *IEEE J. Sel. Areas Commun.*, vol. 27, no. 5, pp. 699-712, June 2009.

[47] F. Roemer and M. Haardt, "Algebraic norm-maximizing (ANOMAX) transmit strategy for two-way relaying with MIMO amplify and forward relays," *IEEE Signal Process. Letters*, vol. 16, Oct. 2009.

[48] V. Havary-Nassab, S. Shahbazpanahi, and A. Grami, "Joint receive-transmit beamforming for multi-antenna relaying schemes," *IEEE Trans. Signal Process.*, vol. 58, no. 9, pp. 4966-4972, Sept. 2010.

[49] I. Hammerstrom and A. Wittneben, "Power allocation schemes for amplify-and-forward MIMO-OFDM relay links," *IEEE Trans. Wirel. Commun.*, vol. 6, no. 8, pp. 2798-2802, Aug. 2007.

[50] Y. Ma, N. Yi, and R. Tafazolli, "Bit and power loading for OFDM-based three-node relaying communications," *IEEE Trans. Signal Process.*, vol. 56, no. 7, pp. 3236-3247, July 2008.

[51] T. J. Oechtering, B. Schubert, and H. Boche, "FIR linear relay network with frequency selective channels," in *Proc. IEEE Int. Conf. on Commun. (ICC)*, Istanbul, Turkey, vol. 9, pp. 4065-4070, June 2006.

[52] H. Chen, A. B. Gershman, and S. Shahbazpanahi, "Filter-and-forward distributed beamforming in relay networks with frequency selective fading," *IEEE Trans. Signal Process.*, vol. 58, no. 3, pp. 1251-1262, Mar. 2010.

[53] H. Chen, S. Shahbazpanahi, and A. B. Gershman, "Distributed beamforming for two-way relay networks with frequency selective channels," *IEEE Trans. Signal Process.*, vol. 60, no. 4, pp. 1927-1941, April 2012.

[54] A. Schad, H. Chen, A.B. Gershman, and S. Shahbazpanahi, "Filter-and-forward multiple peer-to-peer beamforming in relay networks with frequency selective fading," in *Proc. IEEE Int. Conf. on Acoustics, Speech and Signal Process. (ICASSP)*, Dallas, TX, USA, pp. 3246-3249, Mar. 2010.

[55] Y.-W. Liang, A. Ikhlef, W. Gerstacker, and R. Schober, "Cooperative filter-and-forward beamforming for frequency-selective channels with equalization," *IEEE Trans. Wirel. Commun.*, vol. 10, no. 1, pp. 228-239, Jan. 2011.

[56] T. Wang, B.P. Ng, and M.H. Er, "Frequency-domain approach to relay beamforming with adaptive decision delay for frequency-selective channels," *IEEE Trans. Signal Process.*, vol. 61, no. 22, pp. 5563-5577, Nov. 2013.

[57] IBM, IBMLOG CPLEX optimization studio - CPLEX users manual v12.4, 2012.

[58] L. Wolsey, *Integer Programming*, Wiley-Interscience, John Wiley & Sons, New York, 1998.

[59] J. Salo, G. Del Galdo, J. Salmi, P. Kyösti, M. Milojevic, D. Laselva, C. Schneider, MATLAB implementation of the 3GPP Spatial Channel Model (3GPP TR 25.996), Jan. 2005, [Online], Available: http://www.tkk.fi/Units/Radio/scm/

[60] D. S. Baum, J. Salo, M. Milojevic, P. Kyösti, J. Hansen, MATLAB implementation of the interim channel model for beyond-3G systems (SCME), May 2005. [Online]. Available: http://www.tkk.fi/Units/Radio/scm/

[61] Y. Cheng, A. Philipp, M. Pesavento, "Dynamic rate adaptation and multiuser downlink beamforming using mixed integer conic programming," in *Proc. European Signal Process. Conf. (EUSIPCO)*, Bucharest, Romania, pp. 824-828, Aug. 2012,.

[62] S. Boyd and L. Vandenberghe, *Convex Optimization*. Cambridge, U.K.: Cambridge Univ. Press, 2004.

[63] E. Matskani, N.D. Sidiropoulos, Z.-Q. Luo, and L. Tassiulas, "Convex approximation techniques for joint multiuser downlink beamforming and admission control," *IEEE Trans. Wirel. Commun.*, vol. 7, no. 7, pp. 2682-2693, July 2008.

[64] R. Zhang, C. C. Chai, and Y.-C. Liang, "Joint beamforming and power control for multiantenna relay broadcast channel with QoS constraints," *IEEE Trans. Signal Process.*, vol. 57, no. 2, pp. 726-737, Feb. 2009.

[65] M. Fadel, A. El-Keyi, and A. Sultan, "Multiuser MIMO relaying under quality of service constraints," in *Proc. IEEE Wirel. Commun. and Netw. Conf. (WCNC)*, Cancun, Mexico, pp. 1623-1628, March 2011.

[66] M.S. Lobo, L. Vandenberghe, S. Boyd, and H. Lebret, "Applications of second-order cone programming," *Linear Algebra and Its Applications*, vol. 284, pp. 193-228, 1998.

[67] L. Vandenberghe and S. Boyd, "Semidefinite programming," *SIAM Review*, vol. 38, pp. 49-95, 1996.

[68] COST 231, Urban transmission loss models for mobile radio in the 900 and 1800 MHz bands (Revision 2), COST 231 TD(90)119 Rev. 2, The Hague, The Netherlands, Sept. 1991.

[69] LTE Encyclopedia, [Online], Available: https://sites.google.com/site/lteencyclopedia/lte-radio-link-budgeting-and-rf-planning

[70] G. Zheng and K.-K. Wong, A. Paulraj, and B. Ottersten, "Collaborative-relay beamforming with perfect CSI: Optimum and distributed implementation," *IEEE Signal Process. Letters*, vol. 16, no. 4, pp. 257-260, April 2009.

[71] Y. Hu and A. Ribeiro, "Optimal wireless networks based on local channel state information," *IEEE Trans. Signal Process.*, vol. 60, no. 9, pp. 4913-4929, Sept. 2012.

[72] E. Koyuncu, Y. Jing, H. Jafarkhani, "Distributed beamforming in wireless relay networks with quantized feedback," *IEEE J. Sel. Areas Commun.*, vol. 26, no. 8, pp. 1429-1439, Oct. 2008.

[73] E. Koyuncu and H. Jafarkhani, "Distributed beamforming in wireless multiuser relay-interference networks With quantized feedback," *IEEE Trans. Inf. Theory*, vol. 58, no. 7, pp. 4538-4576, July 2012.

[74] I. Wajid, M. Pesavento, Y.C. Eldar, and D. Ciochina, "Robust downlink beamforming with partial channel state information for conventional and cognitive radio networks", *IEEE Trans. Signal Process.*, vol. 61, no. 14, pp. 3656-3670, July 2013.

Wissenschaftlicher Werdegang

Name:	Nils Bornhorst
Geburtsdatum:	8. Juli 1982
Geburtsort:	Siegen

Studium

Seit 09/2009	Promotion in Elektrotechnik und Informationstechnik, Technische Universität Darmstadt, Fachgebiet Nachrichtentechnische Systeme
10/2003 - 06/2009	Studium der Elektrotechnik und Informationstechnik, Technische Universität Darmstadt, Studienabschluß: Diplom-Ingenieur
08/2006 - 01/2007	Auslandssemester, Institut Nationale Polytechnique de Grenoble (INPG), Ecole Nationale Supérieure d'Ingénieurs Electriciens de Grenoble (ENSIEG), Frankreich

Schulausbildung

08/1993 - 06/2002	Gymnasium am Löhrtor, Siegen, Schulabschluß: Allgemeine Hochschulreife

Berufserfahrung

09/2009 - 08/2014	Wissenschaftlicher Mitarbeiter, Technische Universität Darmstadt, Fachgebiet Nachrichtentechnische Systeme
08/2008 - 11/2008	Fachpraktikum, Fraunhofer-Institut für Graphische Datenverarbeitung, Darmstadt
08/2007 - 01/2008	Wissenschaftliche Hilfskraft, Fraunhofer-Institut für Graphische Datenverarbeitung, Darmstadt

Erklärung laut §9 der Promotionsordnung

Ich versichere hiermit, dass ich die vorliegende Dissertation allein und nur unter Verwendung der angegebenen Literatur verfasst habe. Die Arbeit hat bisher noch nicht zu Prüfungszwecken gedient.

Darmstadt, 1. Oktober 2014,